

SANDIA REPORT

SAND85—0762 • UC—70

Unlimited Release

Printed September 1987

Nevada Nuclear Waste Storage Investigations Project

Bulk, Thermal, and Mechanical Properties of the Topopah Spring Member of the Paintbrush Tuff, Yucca Mountain, Nevada

Francis B. Nimick, Barry M. Schwartz

Prepared by
Sandia National Laboratories
Albuquerque, New Mexico 87185 and Livermore, California 94550
for the United States Department of Energy
under Contract DE-AC04-76DP00789



SF2900Q(8-81)

***When printing a copy of any digitized SAND
Report, you are required to update the
markings to current standards.***

"Prepared by Nevada Nuclear Waste Storage Investigations (NNWSI) Project participants as part of the Civilian Radioactive Waste Management Program (CRWM). The NNWSI Project is managed by the Waste Management Project Office (WMPPO) of the U. S. Department of Energy, Nevada Operations Office (DOE/NV). NNWSI Project work is sponsored by the Office of Geologic Repositories (OGR) of the DOE Office of Civilian Radioactive Waste Management (OCRWM)."

Issued by Sandia National Laboratories, operated for the United States Department of Energy by Sandia Corporation.

NOTICE: This report was prepared as an account of work sponsored by an agency of the United States Government. Neither the United States Government nor any agency thereof, nor any of their employees, nor any of their contractors, subcontractors, or their employees, makes any warranty, express or implied, or assumes any legal liability or responsibility for the accuracy, completeness, or usefulness of any information, apparatus, product, or process disclosed, or represents that its use would not infringe privately owned rights. Reference herein to any specific commercial product, process, or service by trade name, trademark, manufacturer, or otherwise, does not necessarily constitute or imply its endorsement, recommendation, or favoring by the United States Government, any agency thereof or any of their contractors or subcontractors. The views and opinions expressed herein do not necessarily state or reflect those of the United States Government, any agency thereof or any of their contractors or subcontractors.

Printed in the United States of America
Available from
National Technical Information Service
U.S. Department of Commerce
5285 Port Royal Road
Springfield, VA 22161

NTIS price codes
Printed copy: A12
Microfilm copy: A01

SAND85-0762
Unlimited Release
Printed September 1987

BULK, THERMAL, AND MECHANICAL PROPERTIES OF THE
TOPOPAH SPRING MEMBER OF THE PAINTBRUSH TUFF,
YUCCA MOUNTAIN, NEVADA

by

Francis B. Nimick
and
Barry M. Schwartz
NNWSI Geotechnical Projects Division 6313
Sandia National Laboratories
P.O. Box 5800
Albuquerque, NM 87185

ABSTRACT

Experimental data on matrix porosity, grain density, thermal expansion, compressive strength, Young's modulus, Poisson's ratio, and axial strain at failure for samples from the Topopah Spring Member of the Paintbrush Tuff are compiled. Heat capacity and emissivity also are discussed. Data have been analyzed for spatial variability; slight variability is observed for matrix porosity, grain density, and thermal expansion coefficient. Estimates of in situ values for some properties (bulk density, heat capacity) are presented. Vertical in situ stress as a function of horizontal and vertical location has been calculated.

CONTENTS

	<u>Page</u>
1.0 INTRODUCTION	1
1.1 Properties Evaluated	3
1.2 Thermal/Mechanical Units	4
1.3 Sampling	6
1.3.1 Bulk Properties	12
1.3.2 Thermal Properties	13
1.3.2.1 Heat Capacity	13
1.3.2.2 Thermal Expansion	14
1.3.3 Mechanical Properties	15
1.3.3.1 Compressive Experiments	15
1.3.3.2 Tensile Experiments	16
1.4 Sample Preparation	17
1.5 Experiment Procedures	18
1.6 Statistical Analysis Technique	18
2.0 THERMAL/MECHANICAL UNIT TSw1	22
2.1 Lithology and Geometry	22
2.2 Bulk Properties	24
2.2.1 Data	24
2.2.2 Statistical Analysis and Discussion	26
2.2.2.1 Porosity	26
2.2.2.2 Grain Density	39
2.2.2.3 Bulk Density	43
2.3 Thermal Properties	46
2.3.1 Data	46
2.3.2 Statistical Analysis and Discussion	46
2.3.2.1 Thermal Expansion	46
2.3.2.2 Heat Capacity	54
2.3.2.3 Emissivity	58
2.4 Mechanical Properties	61
2.4.1 Data from Compressive Experiments	61
2.4.2 Statistical Analysis and Discussion	61
2.4.2.1 Compressive Strength	62
2.4.2.1.1 Saturation Effects	65
2.4.2.1.2 Temperature Effects	65

CONTENTS (continued)

	<u>Page</u>
2.4.2.1.3 Confining Pressure Effects	66
2.4.2.1.4 Strain Rate Effects	67
2.4.2.1.5 Sample Size Effects	68
2.4.2.1.6 Porosity-Compressive Strength Relationships	68
2.4.2.2 Young's Modulus	71
2.4.2.2.1 Saturation Effects	74
2.4.2.2.2 Temperature Effects	75
2.4.2.2.3 Confining Pressure Effects	76
2.4.2.2.4 Strain Rate Effects	76
2.4.2.2.5 Sample Size Effects	77
2.4.2.2.6 Porosity-Young's Modulus Relationship	77
2.4.2.3 Poisson's Ratio	79
2.4.2.4 Axial Strain at Failure	81
2.4.3 Data from Tensile Experiments	82
3.0 THERMAL/MECHANICAL UNIT TSW2	85
3.1 Lithology and Geometry	85
3.2 Bulk Properties	87
3.2.1 Data	87
3.2.2 Statistical Analysis and Discussion	88
3.2.2.1 Porosity	88
3.2.2.2 Grain Density	99
3.2.2.3 Bulk Density	101
3.3 Thermal Properties	101
3.3.1 Data	101
3.3.2 Statistical Analysis and Discussion	103
3.3.2.1 Thermal Expansion	103
3.3.2.2 Heat Capacity	110
3.3.2.3 Emissivity	110
3.4 Mechanical Properties	113
3.4.1 Data from Compressive Experiments	113
3.4.2 Statistical Analysis and Discussion	113
3.4.2.1 Compressive Strength	114
3.4.2.1.1 Saturation Effects	115
3.4.2.1.2 Temperature Effects	115

CONTENTS (continued)

	<u>Page</u>
3.4.2.1.3 Confining Pressure Effects	116
3.4.2.1.4 Strain Rate Effects	117
3.4.2.1.5 Sample Size Effects	123
3.4.2.1.6 Porosity-Compressive Strength Relationships	124
3.4.2.2 Young's Modulus	125
3.4.2.2.1 Saturation Effects	125
3.4.2.2.2 Temperature Effects	126
3.4.2.2.3 Confining Pressure Effects	126
3.4.2.2.4 Strain Rate Effects	128
3.4.2.2.5 Sample Size Effects	128
3.4.2.2.6 Porosity-Young's Modulus Relationship	130
3.4.2.3 Poisson's Ratio	130
3.4.2.4 Axial Strain at Failure	131
3.4.3 Data from Tensile Experiments	133
4.0 THERMAL/MECHANICAL UNIT TSw3	136
4.1 Lithology and Geometry	136
4.2 Bulk Properties	138
4.2.1 Data	138
4.2.2 Statistical Analysis and Discussion	138
4.2.2.1 Porosity	138
4.2.2.2 Grain Density	139
4.2.2.3 Bulk Density	139
4.3 Thermal Properties	140
4.3.1 Data	140
4.3.2 Statistical Analysis and Discussion	140
4.3.2.1 Thermal Expansion	140
4.3.2.2 Heat Capacity	143
4.3.2.3 Emissivity	144
4.4 Mechanical Properties	144
4.4.1 Data from Compressive Experiments	144
4.4.2 Data from Tensile Experiments	149
4.4.3 Relationships Between Porosity and Mechanical Properties	149

CONTENTS (continued)

	<u>Page</u>
5.0 MATERIAL BETWEEN UNITS TSw2 AND TSw3	150
5.1 Lithology and Geometry	150
5.2 Bulk, Thermal, and Mechanical Properties	151
5.2.1 Porosity and Density	151
5.2.2 Thermal Properties	151
5.2.3 Mechanical Properties	153
5.2.3.1 Data from Compressive Experiments	153
5.2.3.2 Data from Tensile Experiments	155
6.0 IN SITU VERTICAL STRESS	156
7.0 CONCLUSIONS	162
7.1 Bulk Properties	162
7.2 Thermal Properties	164
7.2.1 Heat Capacity	164
7.2.2 Thermal Expansion	164
7.2.3 Emissivity	166
7.3 Mechanical Properties	166
7.3.1 Compression Experiments	166
7.3.2 Tensile Experiments	170
7.4 Other Conclusions	170
8.0 REFERENCES	173
APPENDICES	
A. Experiment Procedures	A-1
A.1 Procedures for Saturating and Drying Samples	A-1
A.1.1 Saturation	A-1
A.1.2 Drying	A-6
A.1.2.1 Bulk Density Samples	A-6
A.1.2.2 Larger Samples	A-8
A.2 Bulk Density	A-9
A.2.1 Saturated Bulk Density	A-9
A.2.1.1 Operating Procedures	A-9
A.2.1.2 Calibration Checks	A-9
A.2.2 Dry Bulk Density	A-10

CONTENTS (concluded)

	<u>Page</u>
A.3 Grain Density	A-11
A.3.1 Water Pycnometer Technique	A-11
A.3.1.1 Operating Procedures	A-11
A.3.1.2 Calibration	A-12
A.3.2 Helium Gas Pycnometer Technique	A-13
A.3.2.1 Operating Procedures	A-13
A.3.2.2 Calibration	A-14
A.4 Porosity	A-14
A.5 Thermal Expansion	A-15
A.5.1 Unconfined Thermal Expansion	A-15
A.5.1.1 Operating Procedures	A-15
A.5.1.2 Calibration	A-16
A.5.2 Confined Thermal Expansion	A-17
A.6 Compressive Experiments	A-18
A.7 Tensile Experiments	A-19
B. Experiment Data	B-1
C. Effect of Saturation State on Mechanical Properties	C-1
D. Water in Unit TSw3	D-1
E. Relationship Between Porosity and Mohr-Coulomb Parameters	E-1
F. Candidate Information for Reference Information Base	F-1
G. Candidate Data for Site and Engineering Property Data Base	G-1

LIST OF FIGURES

<u>Figure</u>		<u>Page</u>
1	Location Map, Yucca Mountain and Vicinity	2
2	Relationship of Thermal/Mechanical and Formal Stratigraphy	5
3	Sampling Distribution in the Topopah Spring Member in UE-25a#1	7
4	Sampling Distribution in the Topopah Spring Member in USW G-1	8
5	Sampling Distribution in the Topopah Spring Member in USW G-2	9
6	Sampling Distribution in the Topopah Spring Member in USW GU-3	10
7	Sampling Distribution in the Topopah Spring Member in USW G-4	11
8	Isopach Map of Thermal/Mechanical Unit TSw1	25
9	Vertical Variation of Matrix Porosity of Unit TSw1 in UE-25a#1	30
10	Vertical Variation of Matrix Porosity of Unit TSw1 in USW G-1	31
11	Vertical Variation of Matrix Porosity of Unit TSw1 in USW G-2	32
12	Vertical Variation of Matrix Porosity of Unit TSw1 in USW GU-3	33
13	Vertical Variation of Matrix Porosity of Unit TSw1 in USW G-4	34
14	Thermal Expansion Behavior of Confined and Unconfined Samples of Unit TSw1	53
15	Heat Capacity of Solid Components as a Function of Temperature for Welded, Devitrified Topopah Spring Member	57
16	Estimated Average Values of In Situ Volumetric Heat Capacity as a Function of Temperature for Unit TSw1	60
17	Relationship Between Porosity and Tensile Strength for Unit TSw1	84
18	Isopach Map of Unit TSw2	86

LIST OF FIGURES (concluded)

<u>Figure</u>		<u>Page</u>
19	Vertical Variation of Matrix Porosity of Unit TSw2 in UE-25a#1	92
20	Vertical Variation of Matrix Porosity of Unit TSw2 in USW G-1	93
21	Vertical Variation of Matrix Porosity of Unit TSw2 in USW G-2	94
22	Vertical Variation of Matrix Porosity of Unit TSw2 in USW GU-3	95
23	Vertical Variation of Matrix Porosity of Unit TSw2 in USW G-4	96
24	Thermal Expansion Behavior of Confined and Unconfined Samples of Unit TSw2	109
25	Estimated Average Values of In Situ Volumetric Heat Capacity of Unit TSw2 as a Function of Temperature	112
26	Compressive Strength of Unit TSw2 as a Function of Confining Pressure	120
27	Unconfined Compressive Strength of Unit TSw2 as a Function of Strain Rate	122
28	Young's Modulus of Unit TSw2 as a Function of Confining Pressure	127
29	Young's Modulus of Unit TSw2 as a Function of Strain Rate	129
30	Relationships Between Porosity and Tensile Strength for Unit TSw2	135
31	Isopach Map of Unit TSw3	137
32	Thermal Expansion Behavior of Unit TSw3	142
33	Heat Capacity of Solid Components as a Function of Temperature for Welded, Vitric Topopah Spring Member (TSw3)	146
34	Estimated In Situ Volumetric Heat Capacity of Unit TSw3 as a Function of Temperature	148
35	Calculated Vertical Stress at the Base of Unit TSw1	158
36	Calculated Vertical Stress at the Base of Unit TSw2	159
37	Calculated Vertical Stress at the Floor of the Proposed Repository Horizon	161

LIST OF TABLES

<u>Table</u>	<u>Page</u>
1 Matrix Porosity of Unit TSw1	29
2 Abundance of Lithophysal Cavities in Unit TSw1	38
3 Grain Density of Unit TSw1	41
4 Estimated Bulk Densities for Unit TSw1	45
5 Summary of Linear Thermal Expansion Coefficients for Unit TSw1	52
6 Heat Capacity of Solid Components as a Function of Temperature for Welded, Devitrified Topopah Spring Member	56
7 Estimated In Situ Volumetric Heat Capacity of Unit TSw1	59
8 Compressive Strength of Unit TSw1	64
9 Estimates of Mohr-Coulomb Parameters of Unit TSw1 Based on Functional Porosity	72
10 Young's Modulus of Unit TSw1	73
11 Matrix Porosity of Unit TSw2	91
12 Abundance of Lithophysal Cavities in Unit TSw2	98
13 Estimated Bulk Densities for Unit TSw2	102
14 Summary of Linear Thermal Expansion Coefficients for Unit TSw2	108
15 Estimated In Situ Volumetric Heat Capacity of Unit TSw2	111
16 Mechanical Properties of Unit TSw2 as a Function of Confining Pressure	118
17 Mechanical Properties of Unit TSw2 as a Function of Strain Rate	121
18 Summary of Linear Thermal Expansion Coefficients for Unit TSw3	141
19 Heat Capacity of Solid Components as a Function of Temperature for Welded, Vitric Topopah Spring Member (TSw3)	145
20 Estimated In Situ Volumetric Heat Capacity of Unit TSw3 as a Function of Temperature	147
21 Bulk Properties of Material Between Units TSw2 and TSw3	152

LIST OF TABLES (concluded)

<u>Table</u>		<u>Page</u>
22	Results of Compressive Experiments on Material Between Units TSw2 and TSw3	154
23	Bulk Properties of Units TSw1, TSw2, and TSw3	163
24	Estimated In Situ Volumetric Heat Capacity as a Function of Temperature for Units TSw1, TSw2, and TSw3	165
25	Thermal Expansion Coefficients as a Function of Temperature for Units TSw1, TSw2, and TSw3	167
26	Mechanical Properties (Determined in Compression) for Units TSw1 and TSw2	168
27	Tensile Strength of Units TSw1 and TSw2	171

1.0 INTRODUCTION

Yucca Mountain, located near the southwest margin of the Nevada Test Site (NTS) in southern Nevada, is being evaluated as a potential site for underground disposal of nuclear wastes. At present, the physical, thermal, and mechanical properties of rocks from the Topopah Spring Member of the Paintbrush Tuff, the target horizon for waste disposal, are being determined as part of the Nevada Nuclear Waste Storage Investigations (NNWSI) Project, which is administered by the Nevada Operations Office of the U.S. Department of Energy (DOE). Figure 1 shows the geographic locations of the NTS and of Yucca Mountain.

Selection of a repository site will depend on demonstration that the site can isolate radionuclides for long periods of time, that an underground disposal facility can be operated safely, and that waste can be retrieved from emplacement holes if necessary. Such demonstration will require knowledge of rock properties such as strength, thermal expansion, porosity.

The purpose of this report is to provide a compilation of relevant properties that have been measured on the Topopah Spring Member and to summarize the results of analyses that have been made to determine data quality and variability. The culmination of the analysis process has been the determination of a set of recommended properties for use either directly in performance assessment calculations and design analyses or that contribute to the development of properties suitable for such usage. For some properties (bulk density, heat capacity), in situ values

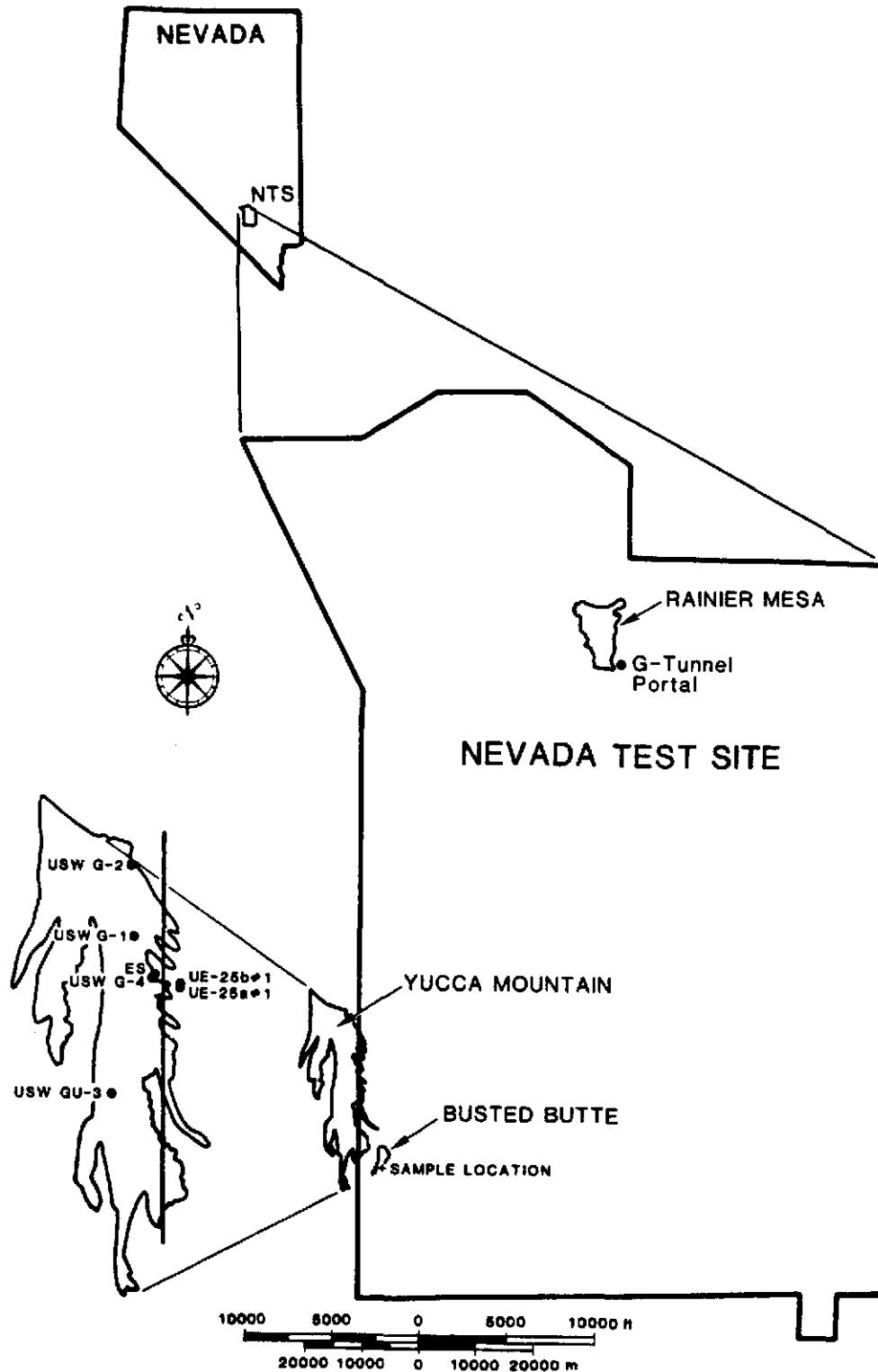


Figure 1. Location Map, Yucca Mountain and Vicinity

have been estimated. For other properties that may be affected significantly by the presence of fractures, extrapolation to in situ conditions has not been attempted.

1.1 Properties Evaluated

The rock properties that have been measured in the laboratory are divided into three categories--bulk, thermal, and mechanical. Each of the categories includes two or more properties, as follows:

Bulk: Density, porosity (intended to signify only matrix porosity unless explicitly stated otherwise)

Thermal: Heat capacity, thermal conductivity, coefficient of thermal expansion

Mechanical: Compressive strength, tensile strength, Young's modulus, Poisson's ratio.

Each of these properties except thermal conductivity is discussed in subsequent sections of this report. Analysis of existing thermal-conductivity data has been complicated by new information on saturation behavior during laboratory experiments. As a consequence, discussion of thermal conductivity is deferred to a future report. Where appropriate, supporting information (mineralogy, lithology, data from similar rock types) is included to enhance the completeness of the discussion.

Most data and analyses presented in the remainder of the report apply to matrix properties, where "matrix" is intended to exclude material that contains fractures. The properties of fractured rock, or the rock mass, of the Topopah Spring Member, will be analyzed in the future. Exceptions to the preceding statements are estimates of in situ values for bulk density and heat capacity.

1.2 Thermal/Mechanical Units

Data in this report are grouped according to thermal/mechanical units rather than by formal stratigraphic divisions. The thermal/mechanical units have been defined such that each unit has bulk, thermal, and mechanical properties that may differ from those of adjacent units. In some cases, contacts between units are gradational rather than sharp, so that differences in some properties between adjacent units also may be gradational. The units have been discussed, and their geometry has been presented in Ortiz et al. (1985). The relationship between the thermal/mechanical units and the formal stratigraphy is shown in Figure 2.

The Topopah Spring Member as a formal stratigraphic unit contains all or portions of five thermal/mechanical units: PTn, TSw1, TSw2, TSw3, and CHn1 (Figure 2). The first and last of these comprise less than 16% of the Topopah Spring Member and are not discussed in this report. In addition to TSw1, TSw2, and TSw3, a material transitional between TSw2 and TSw3 is present in some core holes. Because of its discontinuous nature, this material has not been defined as a thermal/mechanical unit. Nevertheless, any data that have been gathered on samples of the material are summarized in this report.

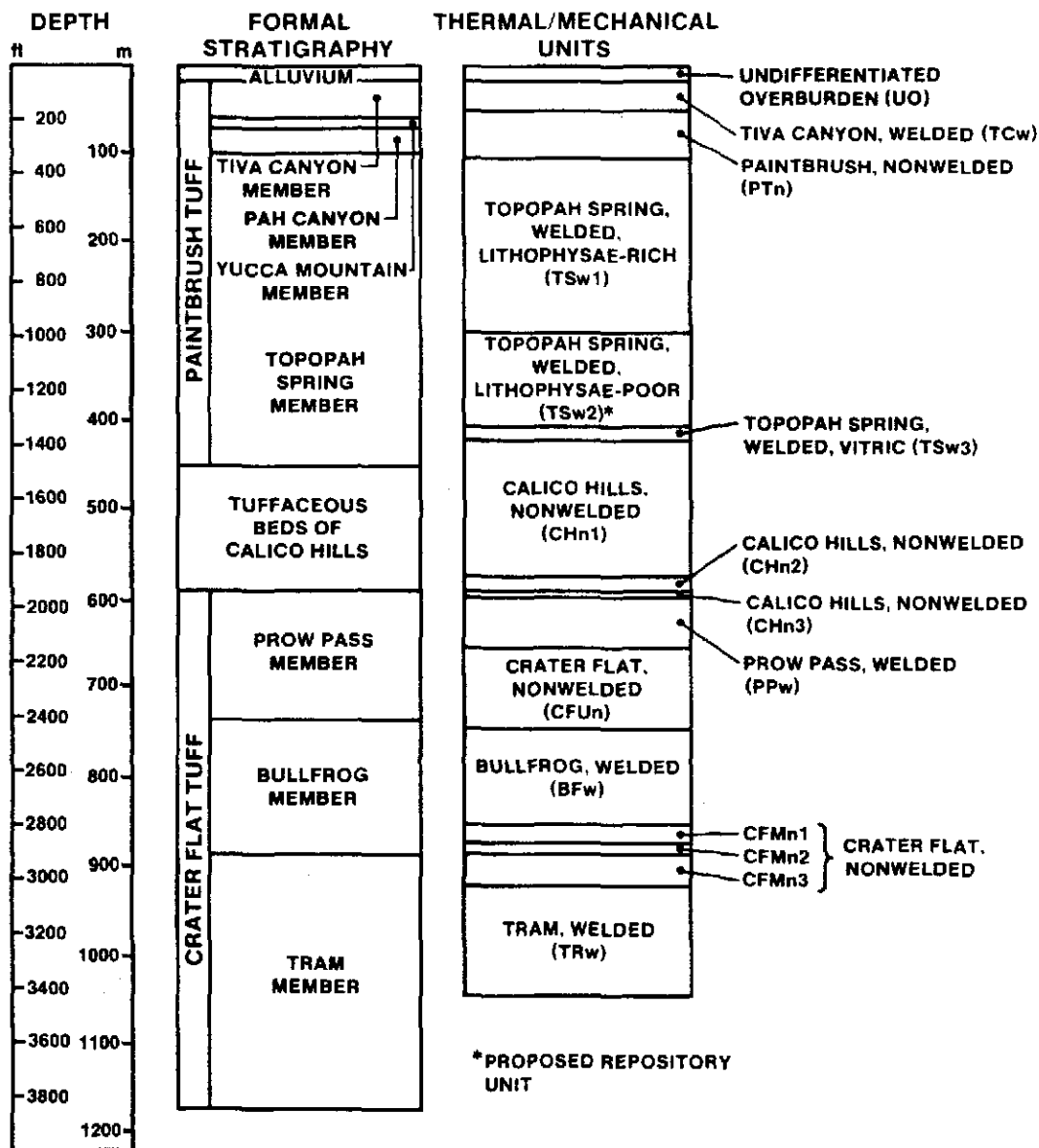


Figure 2. Relationship of Thermal/Mechanical and Formal Stratigraphy. The thicknesses are averages for the five deep core holes at Yucca Mountain (UE-25a#1, USW G-1, USW G-2, USW GU-3, and USW G-4).

An assumption was made a priori for the presentation of data in this study. Property variability within one thermal/mechanical unit in a given core hole is presented as if the vertical variability is random, (i.e., no correlation of properties with depth within a unit exists). The validity of this assumption is discussed later in the report.

1.3 Sampling

To date, the majority of samples of the Topopah Spring Member used for laboratory experiments have been obtained from core material taken from drill holes at Yucca Mountain. In addition, some samples have been obtained from surface outcrops both at Yucca Mountain and at Busted Butte, which is located southeast of Yucca Mountain. Figure 1 provides the locations of Busted Butte and the drill holes from which samples have been obtained.

As of December 1985, characterization of the bulk, thermal, and mechanical properties of the unfractured matrix of the Topopah Spring Member from the existing core holes at Yucca Mountain was essentially complete. Future laboratory measurement of properties will concentrate on samples from the exploratory shaft or from future core holes. Figures 3 through 7 provide a summary of the type of experiments performed on samples and the locations of samples from existing core holes. (Note: For all samples from core holes, sample IDs in this report include the depth, in feet, at which the sample was taken; i.e., A1-1201 is a depth of 1201 ft in UE-25a#1.)

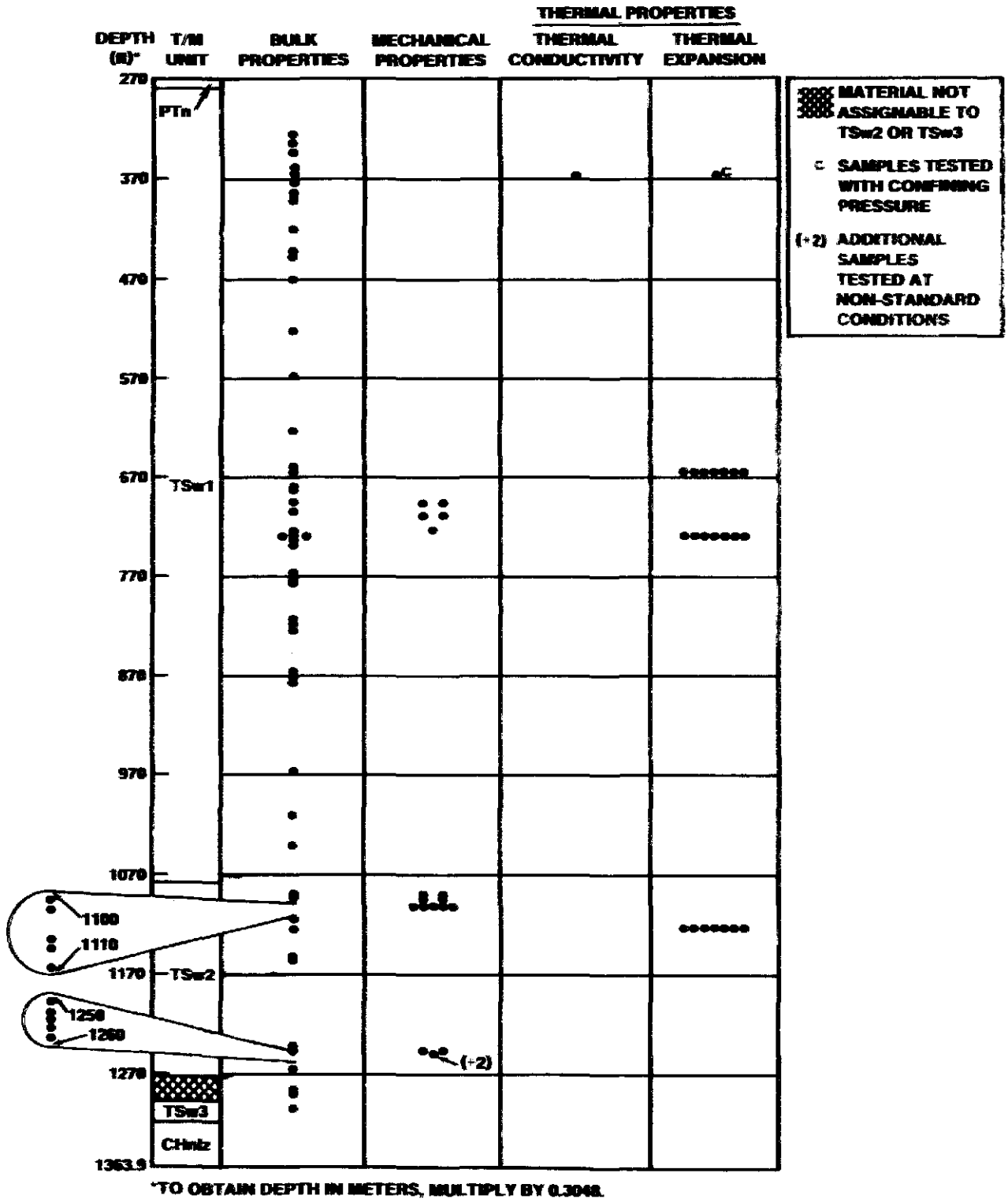


Figure 3. Sampling Distribution in the Topopah Spring Member in UE-25a#1

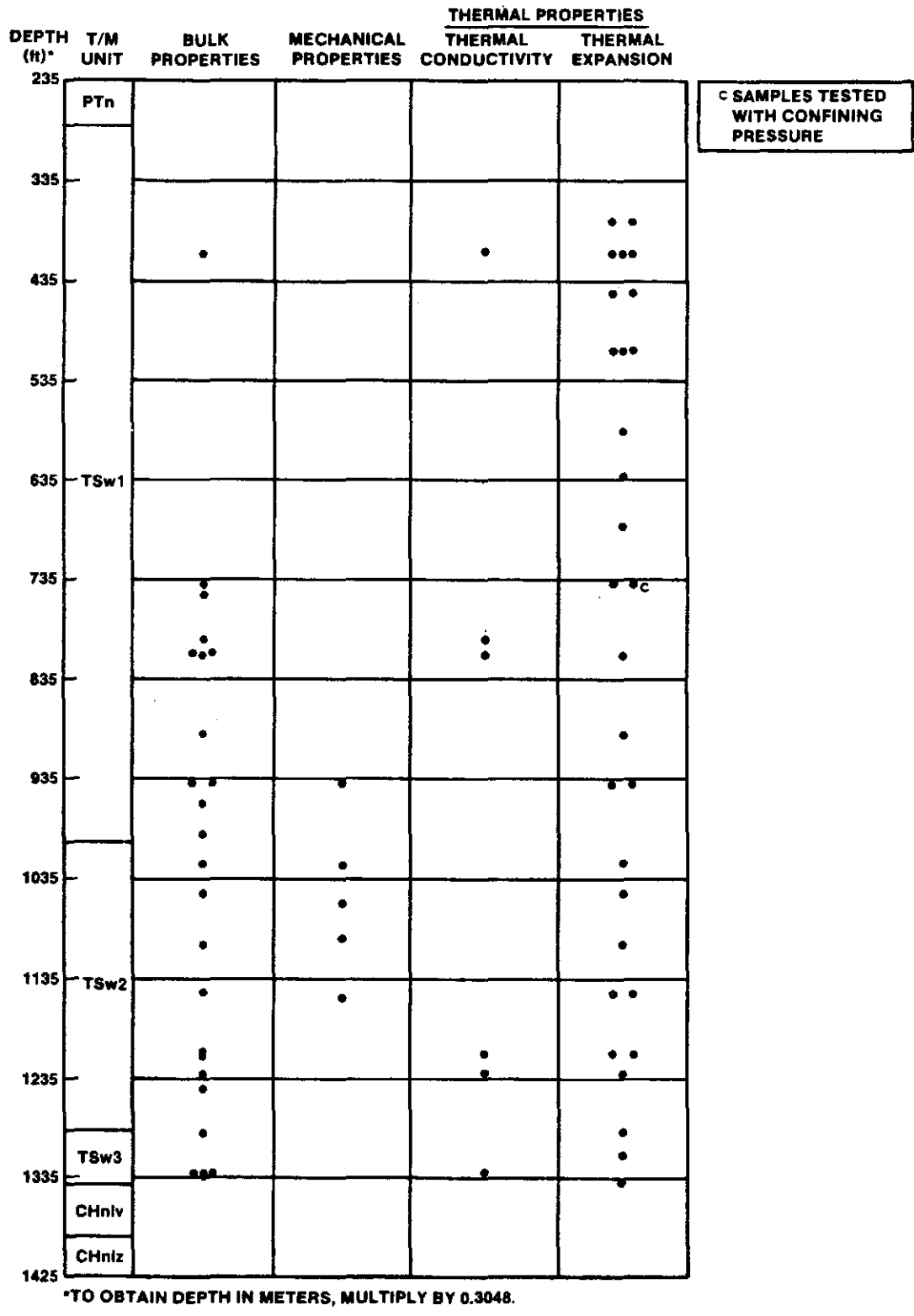


Figure 4. Sampling Distribution in the Topopah Spring Member in USW G-1

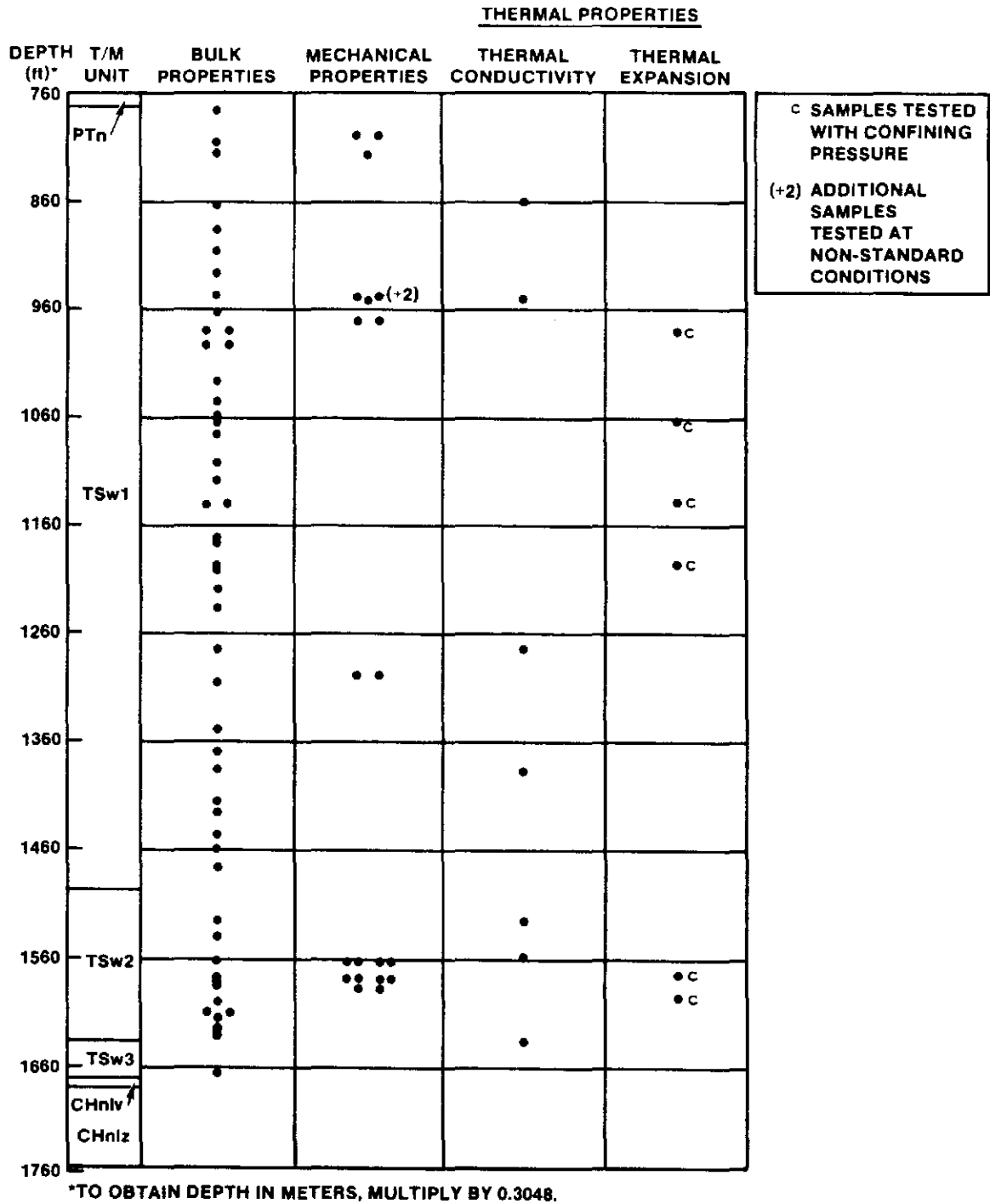


Figure 5. Sampling Distribution in the Topopah Spring Member in USW G-2

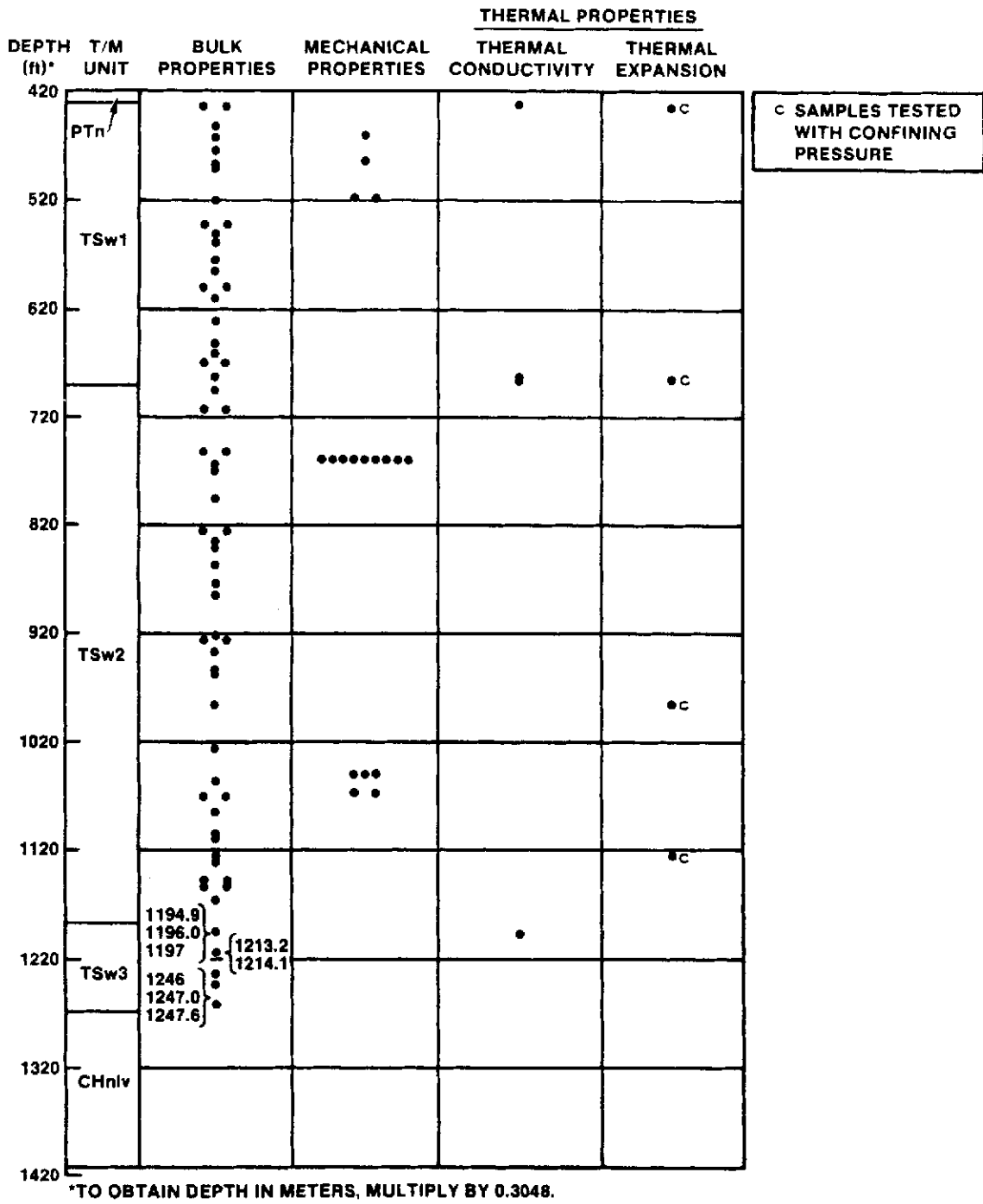


Figure 6. Sampling Distribution in the Topopah Spring Member in USW GU-3

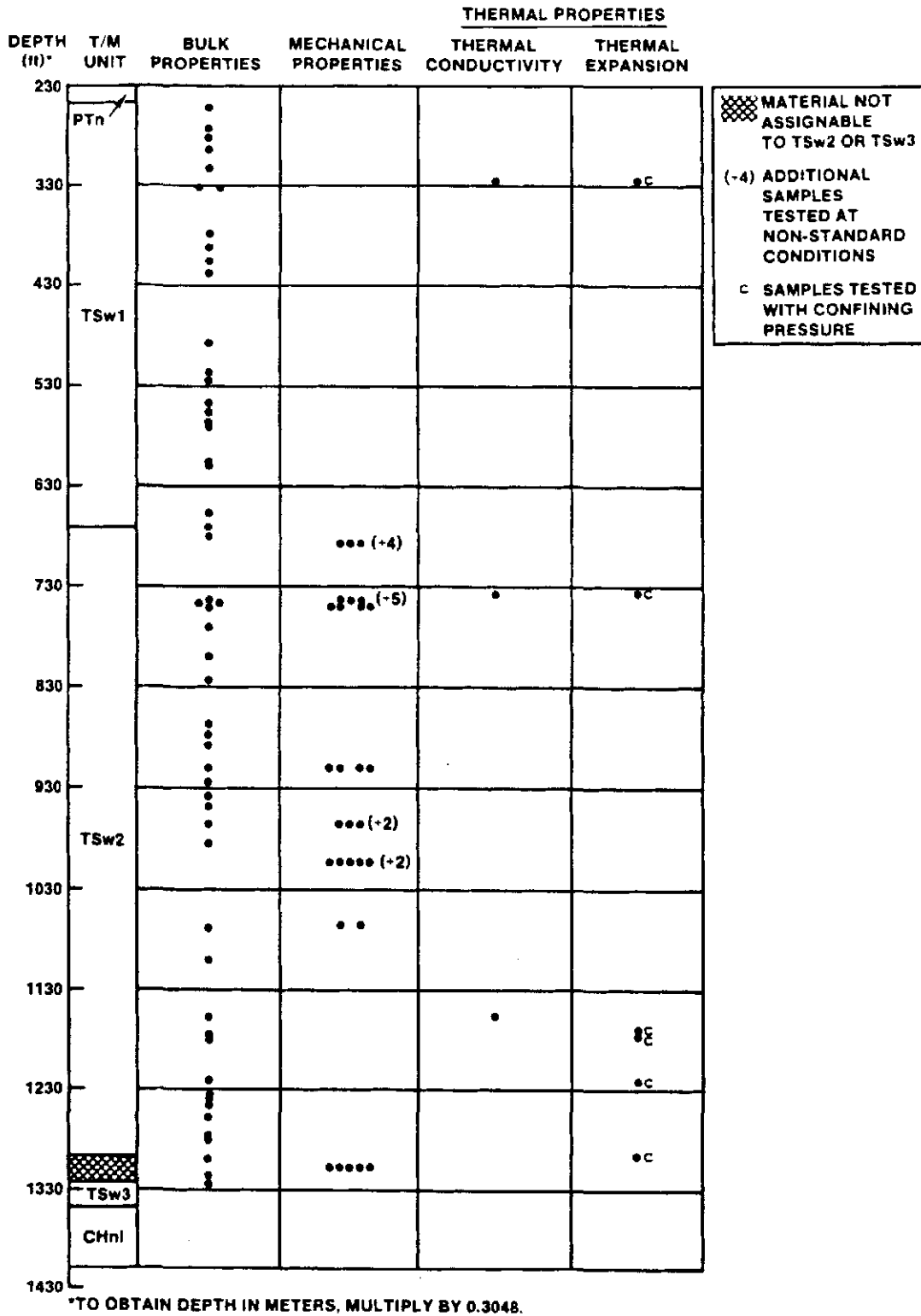


Figure 7. Sampling Distribution in the Topopah Spring Member in USW G-4

The criteria used to select samples for laboratory experiments have varied, depending on the nature of experiments and on experience gained from previous activities. An issue that has been raised frequently concerning sampling criteria is that some bias has been introduced (i.e., data measured in the laboratory are not representative of the properties of the intact material in situ). Specifically, the possibility exists that measured properties represent only "good" rock (i.e., material that did not fracture or crumble during coring operations) and therefore that properties such as compressive strength are biased toward "better" values. This concern is addressed for each category of properties in the following sections.

1.3.1 Bulk Properties

In the first two deep core holes at Yucca Mountain (UE-25a#1 and USW G-1), bulk property sampling locations were selected to examine lithologic variations (e.g., reported differences in the degree of welding or in mineralogy) as described in the lithologic logs of the holes (UE-25a#1: Spengler et al., 1979; USW G-1: Spengler et al., 1981). Although this selection rationale necessarily caused uneven sample spacing along the holes, no bias for or against "good" material was introduced. The major impact with regard to the welded, devitrified portions of the Topopah Spring Member (TSw1 and TSw2) was that relatively few samples were obtained because of the lack of lithologic variation.

In subsequent core holes (USW G-2, USW GU-3, and USW G-4), bulk property sample selection was primarily governed by an emphasis on equal

sample spacing, regardless of lithology. This criterion led to a greater number of samples from units TSw1 and TSw2 than for the two earlier holes.

In addition to the considerations mentioned above, sample size and shape may play a role in the presence or absence of sampling bias. In the case of bulk properties, relatively small amounts of material are needed, and irregular shapes are not a problem. Therefore, almost any material available for a chosen sample interval is suitable for measurement of bulk properties, and no bias should result.

1.3.2 Thermal Properties

1.3.2.1 Heat Capacity. To date, no experimental measurements of the heat capacity of the tuffs at Yucca Mountain have been made. However, samples have been obtained for experiments to be performed in late-FY88. These samples were selected at random from each lithology of interest, and are believed to be representative. All samples were irregular fragments that were subsequently ground into powder for testing.

Data for heat capacities of units TSw1, TSw2, and TSw3 are reported in Sections 2.3.2.2, 3.3.2.2, and 4.3.2.2. These data have been estimated from bulk chemical data for a number of powdered samples. Such samples require very little material, and the material can originate as fragments of any size and shape. Thus, whether heat capacities are measured directly or estimated from bulk chemical data, no sampling bias should exist for this property.

1.3.2.2 Thermal Expansion. The coefficient of thermal expansion has been measured under confining pressure and in unconfined conditions. Experiments with confining pressure used samples that were 2 in. (5 cm) in diameter and 4 in. (10 cm) long. Unlike material for bulk properties and heat capacity experiments, the material suitable for confined thermal expansion experiments was limited to pieces large enough to provide a sample.

The bias introduced by sample size requirements is that tuff rich in lithophysae* tends to break into small pieces during coring and so cannot be tested for thermal expansion (using the selected technique). However, this shortcoming has been reduced by performing unconfined experiments on larger samples obtained from outcrops of lithophysae-rich tuff.

Within the limitations imposed by sample size, sample selection for thermal expansion experiments has been based on lithologic variation between thermal/mechanical units and on evenly spaced intervals within a given unit. No additional bias should have resulted from such selection.

Unconfined thermal expansion experiments were made on samples with nominal dimensions of 1 in. x 0.125 to 0.25 in. x 0.125 in. (2.54 cm x 0.32 to 0.64 cm x 0.32 cm). Thus, samples were small enough that size did not affect which material could be used. However, the sample size often was such that a disproportionate amount of an individual sample was

*Lithophysae usually are comprised of up to three components: (1) holes or vugs that vary in size and frequency; (2) a coating of the walls of these cavities with variable thicknesses of secondary minerals; and (3) variably sized volumes of vapor-phase-altered material surrounding the cavities.

comprised of atypical material (e.g., a patch of vapor-phase-altered material or a lithic fragment). Thus, care must be taken that the effects of such atypical material on thermal expansion behavior are considered in the interpretation of data obtained for these samples.

Sample selection for unconfined thermal expansion measurement was based on lithologic variation. Within the welded, devitrified Topopah Spring Member, emphasis was placed on variations in the abundance of lithophysae and associated vapor-phase-altered material. As a result, the range in experiment results reported for units TSw1 and TSw2 (Sections 2.3.2.2 and 3.3.2.2) should be representative of the range to be expected in situ. However, some bias in the mean value of the thermal expansion coefficient may exist in the sense that the value may be representative of material richer or poorer in vapor-phase-altered material than that found at any particular location within the units. A bias of this sort is difficult to assess. Additional discussion is presented in Section 2.3.2.2.

1.3.3 Mechanical Properties

1.3.3.1 Compressive Experiments. Compressive strength, Young's modulus (taken to be the tangent modulus), and Poisson's ratio are obtained for each compressive experiment performed. Cylindrical samples with length:diameter (L:D) ratios of 2:1 are used in compressive experiments. Diameter of samples from core holes have been either 1 in. (2.54 cm) or 2 in. (5.08 cm). As with confined thermal expansion tests, sample size requirements tend to bias samples toward material that neither breaks during coring nor contains lithophysae.

Two experiment programs have been performed to eliminate this bias. Large cylindrical samples [nominal dimensions: length of 533.4 mm (21.0 in.), diameter of 266.7 mm (10.5 in.)] of lithophysae-rich tuff have been used to examine the effect of the vugs on mechanical properties (Price et al., 1985). The effect of other inhomogeneities, including some healed fractures, has been examined by using samples with diameters up to 9 in. (22.86 cm) (Price, 1986).

Within the limitation imposed by sample size, sampling of the welded, devitrified portion of the Topopah Spring Member has been designed to obtain samples at evenly spaced intervals. Because relatively more unbroken material has been available from the lithophysae-poor regions of the target horizon, the density of sampling has been biased toward unit TSw2.

1.3.3.2 Tensile Experiments. To date, tensile strength of the Topopah Spring Member has been measured using only the "Brazilian" technique, and samples have been taken only from UE-25a#1 (Blacic et al., 1982, pp. 4, 21). Sample selections "were made to provide a contrast in degree of welding. . ." (pp. 2-3). The samples for tensile strength experiments were 1 in. (2.54 cm) in diameter and 0.5 in. (1.27 cm) thick.

Additional experiments are planned in which tensile strength will be measured by both the "Brazilian" technique and by direct-pull tests. The latter require larger samples [minimum diameter of 4.76 cm (1.875 in.) and L:D of 2.0 to 2.5], and if material were to come from core holes, would suffer from the same limitations as do compressive strength and

confined thermal expansion experiments. However, outcrop material probably will be used for the experiments. Such material will be representative of only one lithologic type within the Topopah Spring Member, and experiment results may not be applicable when extrapolating to other material.

1.4 Sample Preparation

The details of sample preparation for any single type of experiments are provided in other reports. This section is intended to provide a general summary of the requirements imposed for samples discussed later in this report.

The sample history prior to being selected for experiments has varied. Most core-hole samples were separated from the remainder of the core soon after the core was removed from the hole. Some of this core was wrapped and waxed in an attempt to preserve "natural-state" moisture content. Other samples were selected from core boxes several years after completion of a core hole. The resulting variations in sample moisture content have been considered and are discussed together with the experiment results.

After selection, samples were either ground to powder of a selected mesh size (bulk properties, heat capacity) or were machined to final size. If machining was necessary, the coolant used was either water from well J-13 at Yucca Mountain, distilled water, or tap water. Dimensional tolerances for machined samples depended on the experiment to

be performed, but in all cases samples were selected to meet or exceed tolerances specified by the American Society for Testing and Materials (ASTM) and the International Society for Rock Mechanics (ISRM).

Some experiments were designed to be performed on saturated samples. Saturation of the sample usually was achieved by application of a vacuum while the samples were submerged in water from J-13. For some earlier experiments, long periods (up to 724 hr) of immersion without an applied vacuum were assumed to saturate the samples. A discussion of estimated saturation states actually achieved using different techniques is provided in Appendix A.1.

1.5 Experiment Procedures

Experiment procedures for individual properties are provided in Appendix A.

1.6 Statistical Analysis Techniques

Statistical analysis of the data tabulated in this report has been performed using a statistics package called SAS (SAS Institute, 1982a,b). SAS contains many options for data manipulation, plotting, and analysis. Two procedures were used extensively in analysis of data for the Topopah Spring Member: PROC TTEST and PROC GLM. Both procedures compare data samples and provide information about the comparability of two (TTEST) or more (GLM) sample groups.

There are three major assumptions implicit to the use of the two procedures: (1) that each sample group is the product of random sampling of a larger population; (2) that the larger population has a statistically normal distribution; and (3) that the variances of different sample groups that are being compared are equivalent. The first of these assumptions has not been tested for the data in this report, and has been assumed to be valid. The other two assumptions have been tested.

The assumption of normality has been tested at each level of comparison within analyses of each property, using box plots and normal scores plots. Thus, when results of experiments at different laboratories or for different saturation states were compared, the normality of each sample group was examined. After some or all of these small groups were lumped together, the normality of the larger group was checked. For the smaller groups, sample sizes usually were too small to adequately assess normality, in which case normality was assumed.

In some cases, sample groups appeared to have a non-normal distribution. These occurrences are noted in individual discussions later in the report. However, analyses of variance tend to be robust with regard to departures from normality (i.e., the results of the analyses are not very sensitive to moderate deviations from the assumed normal distribution of data), especially when comparison of mean values is the dominant feature as it has been for this report. Thus, statistical analysis has been continued even with the non-normal sample groups.

The third assumption--equal variances--is tested by pair-wise comparison of sample groups in PROC TTEST. Occasional differences in variance were found for the Topopah Spring Member, and are noted in discussions of individual properties.

In comparison of sample groups for this report, a null hypothesis was tested that the sample groups are representatives of populations with identical means. Another way of viewing this is that if the samples have statistically equivalent variances and means, the inference can be drawn that the samples have been taken from the same population. (Care must be taken in the interpretation of analyses such as these, however. The only definite conclusion that can be drawn is that sample groups are not the same. If an analysis does not reject the null hypothesis, there is not a certainty that the samples are from the same population.)

Two types of errors may be made in testing whether a null hypothesis is true. A Type I error is made by rejecting a null hypothesis when it is true, and a Type II error is made by accepting a null hypothesis when it is false (summarized from Iman and Conover, 1983, p. 225-226).

The probability of making a Type I error is called the "level of significance." This value is chosen by the individual performing the hypothesis testing. Given the small sample sizes characteristic of the data for this study, a level of significance that is too low (i.e., too close to zero) is more likely to cause a Type I error than would be the case if comparison were between large sample groups. For this reason a level of significance of 0.05 was chosen for use in interpretation of the results of the analyses of variance. In the remainder of this report,

the significance value is given (in the form $P = \dots$) whenever a null hypothesis has been tested.

A feature of the data analysis that is examined before comparison of sample means is the presence or absence of outliers. Outliers are data values that lie much higher or much lower than would be expected based on the distribution of the remainder of the data. Inclusion of outliers in a data set expands the standard deviation (and the variance) of the data set to an erroneously high value, and can distort the testing of null hypotheses.

There are many ways of treating the outliers, none of which are completely satisfactory. For this study, outliers have been discarded from the statistical analyses for simplicity. It is recognized that some information may be lost by doing this, but the advantages in terms of efficiency are considered to outweigh the disadvantages.

A number of independent variables were used in this study. The variable of major importance, in view of the objective to examine spatial variability of properties, was the core hole from which each sample was taken. Other independent variables that were used included saturation state, experiment environment, and testing laboratory. An analysis of covariance was made twice in which the vertical location of samples within a single thermal/mechanical unit was included in calculations in addition to core hole and testing laboratory.

The results of analyses for individual properties are discussed in subsequent sections of the report.

2.0 THERMAL/MECHANICAL UNIT TSw1

2.1 Lithology and Geometry*

In general, thermal/mechanical unit TSw1 is defined to be the lithophysae-rich portion of the welded, devitrified Topopah Spring Member (see Section 1.3.2.2 for a general description of lithophysae). Ortiz et al. (1985, p. 11) state that the unit is composed of ashflows that "locally contain more than approximately 10 percent by volume lithophysal cavities." By implication and in actuality the unit also contains ashflows that contain less than 10 volume percent lithophysal cavities. In fact, data in Spengler and Chornack (1984, p. 18) indicate the following percentages of the unit containing less than 10 percent cavities:

USW G-1:	90%
USW G-2:	96%
USW GU-3:	73%
USW G-4:	68%

Originally, the contact between units TSw1 and TSw2 was placed at the base of the lowest ashflow in the Topopah Spring Member that contained 20 percent or more lithophysae (lithophysal cavities and vapor-phase-altered

*The discussion in this section addresses the criteria used to define a contact between units TSw1 and TSw2. Definition of such a contact has been, and still is, a topic of debate. The section presents a discussion of the development of definitions for the contact, but the reader is forewarned that the debate is ongoing, so that this report is more a status report than a summary on the topic.

material), as described in the relevant lithologic logs. The contact locations defined in this way were retained by Ortiz, et al. (1985) as input data for the calculation of the geometry of the base of TSw1. These contacts have been used in the assignment of data to thermal/mechanical units for this report.

At the time that the contact between TSw1 and TSw2 was selected, the assumption was made that the lithophysal cavities account for one-half of the lithophysae; hence, the 10 percent criterion in the description of TSw1. Two points should be made about this 10 percent value. First, examination of Figure 5 of Spengler and Chornack (1984), which is based on more detailed data than are contained in lithologic logs, indicates that the use of the 10-percent-cavity content as a boundary between TSw1 and TSw2 would move the contact up 397 ft (121 m) in USW G-1, 23 ft (7 m) in USW G-2, 10 ft (3 m) in USW GU-3, and 70 ft (21 m) in USW G-4 (all changes resulting in a thinner TSw1).

The second and more important point to be made is that use of a cavity content of 10 percent as a cutoff value between the two units is an arbitrary criterion. Although such a boundary is clearly visible in plots of cavity content, and so appears to be a reasonable choice, in actuality, no analyses or experiment results have demonstrated that a specific cavity content by itself presents a problem for repository design. Also, as pointed out earlier in this section, most of TSw1 contains less than 10 percent cavities and so may be similar in properties to material in TSw2. In the future, if the two units are differentiated, the differentiation should be based on functional

porosity (the sum of matrix porosity, lithophysal cavity percentage, and clay content). The boundary between the two units should be placed at a location where the functional porosity changes significantly. The change that is necessary in order to be "significant" will be determined by sensitivity analyses conducted for repository design.

Despite the arbitrariness of the existing distinction between TSw1 and TSw2, a specific alternative has not been defined. In view of this situation, this report discusses existing data using the units as defined in Ortiz et al. (1985). Future work may require that the data be regrouped and reanalyzed.

The existing model (Ortiz et al., 1985) estimates the thickness variation of TSw1 within the repository area to be as shown in Figure 8.

2.2 Bulk Properties

2.2.1 Data

Measured bulk property data for unit TSw1 are tabulated in Appendix B (Table B-1). Data in Table B-1 have been measured by Sandia National Laboratories (SNL), Terra Tek (TT), the U.S. Geological Survey (USGS) (Anderson, 1981; 1984), Holmes and Narver (HN), and Los Alamos National Laboratory (LANL) (Blacic et al., 1982). Data for three samples from USW G-1 were obtained by either SNL, HN, or TT, but records do not indicate which one, so data for these three samples were treated initially as if they were measured by an entirely different laboratory.

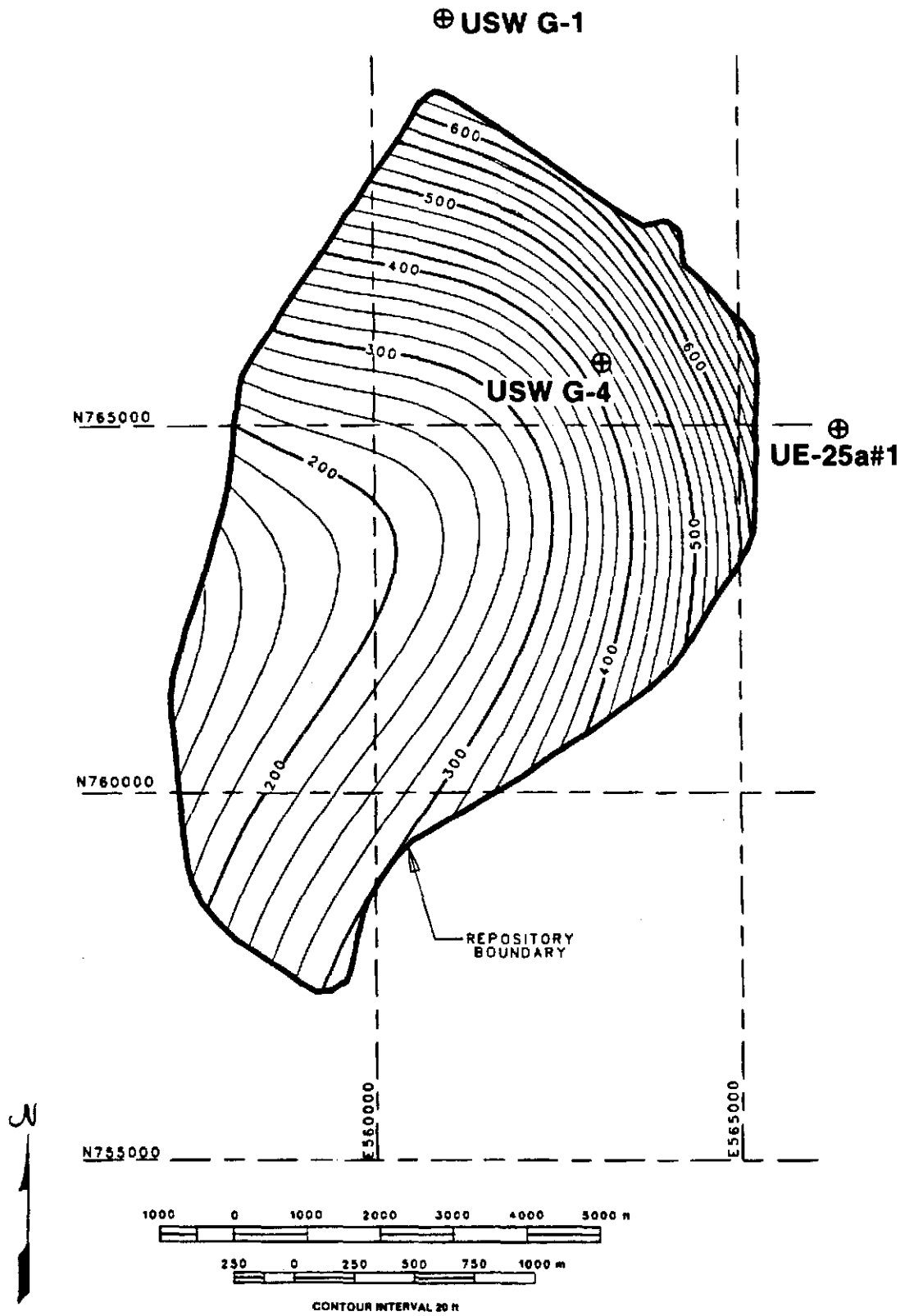


Figure 8. Isopach Map of Thermal/Mechanical Unit TSw1

Data for 26 samples from an outcrop of the lowermost, lithophysae-rich portion of unit TSw1 at Busted Butte also are listed in Table B-1. These data have not been included in the statistical analysis because of the possibility that the statistics for the total sample group would be unduly affected by the large number of samples from this single portion of the unit.

2.2.2 Statistical Analysis and Discussion

Each of the three properties, porosity, grain density, and dry bulk density, was analyzed separately. However, no results are given for dry bulk density because of component variability, as discussed in Section 2.2.2.3

2.2.2.1 Porosity. Statistical analysis of porosity with testing laboratory indicates that data obtained by LANL are significantly lower than all other data. Data from LANL are available only for samples from UE-25a#1. The following means and standard deviations were obtained for unit TSw1 in UE-25a#1: 0.102 ± 0.011 (LANL, 5 samples); 0.119 ± 0.009 (HN, 4 samples); 0.137 ± 0.043 (USGS, 15 samples); and 0.150 ± 0.027 (TT, 16 samples). Pair-wise comparison of LANL with the other three laboratories resulted in rejection of the equivalence of mean values [$P = 0.0456$ (HN-LANL), $P = 0.0090$ (USGS-LANL), $P = 0.0010$ (TT-LANL)], so the LANL data were eliminated from further consideration in this report. P-values for the other pair-wise comparisons that did not result in rejection of the null hypothesis are given below.

USGS-HN, USW GU-3: 0.1017
TT-HN, USW GU-3: 0.8240 (unequal variances)
TT-USGS, USW GU-3: 0.3506
TT-USGS, USW G-4: 0.6111
TT-unknown laboratory, USW G-1: 0.5567
USGS-HN, UE-25a#1: 0.1382 (unequal variances)
TT-USGS, UE-25a#1: 0.3230

One additional pair (TT-HN, UE-25a#1) had a P-value of 0.0351, suggesting that the null hypothesis should be rejected. However, given the small number of samples (4) for HN and the fact that the null hypothesis was not rejected in three other comparisons involving HN, the data have been retained for additional analysis.

Two of the pair-wise comparisons were made by adjusting for unequal variances, as noted above. Because one of the assumptions necessary for the valid use of ANOVA or GLM is that all samples have the same variance, such techniques cannot be applied directly in a simultaneous analysis of the data from all testing laboratories.

All other data were grouped by core hole and the core-hole groups were compared. Statistically significant differences were found, as follows:

- mean porosity in USW GU-3 greater than all other mean porosities
[P = 0.0095 (G-4, GU-3); P = 0.0001 (G-2, GU-3); P = 0.0001 (G-1, GU-3); P = 0.0002 (a#1, GU-3)].

- mean porosity in USW G-4 greater than mean porosity in USW G-2
(P = 0.0310).

In view of these differences, summary data are provided in Table 1 for each core hole individually. (P-values for those pairs without significant differences also are provided as part of Table 1).

The normality of porosity data was checked for each core hole individually and for unit TSw1 as a whole. With the exception of a few outliers, all data groups appear to have an approximately normal distribution.

The possibility that sampling differences between core holes caused the differences in porosity was examined by analyzing the covariance contributed by the vertical location of samples within unit TSw1. However, this possibility was rejected using the results of the statistical calculations. (In assessing the results of covariance calculations, an F-statistic is calculated and compared to the F value that would occur if the hypothesis were true. The latter F value for this analysis is $F = 2.447$, whereas the calculated F value is 8.383. Larger calculated values lead to rejection of the null hypothesis.)

Figures 9 through 13 illustrate the vertical variation of matrix porosity of unit TSw1 in the five core holes. The observed vertical variation is in large part attributable to porosity differences resulting from ashflow emplacement. An ashflow emplaced as a simple cooling unit

Table 1
Matrix Porosity of Unit TSw1

Core Hole	Porosity		Number of Samples	95% Confidence Interval for Mean Value
	Mean	St. Dev.		
UE-25a#1	0.141	0.034	35	0.129-0.153
USW G-1	0.122	0.027	11	0.104-0.140
USW G-2	0.126	0.036	37	0.114-0.138
USW GU-3	0.175	0.028	22	0.163-0.187
USW G-4	0.148	0.038	22	0.131-0.165
ALL CORE HOLES	0.142	0.038	127	0.135-0.149
Busted Butte	0.177	0.040	26	0.161-0.193

P-values for pairs without significant differences:

G-1, G-4: 0.0514
G-1, G-2: 0.7145
a#1, G-4: 0.4883
a#1, G-2: 0.0727
a#1, G-1: 0.0937

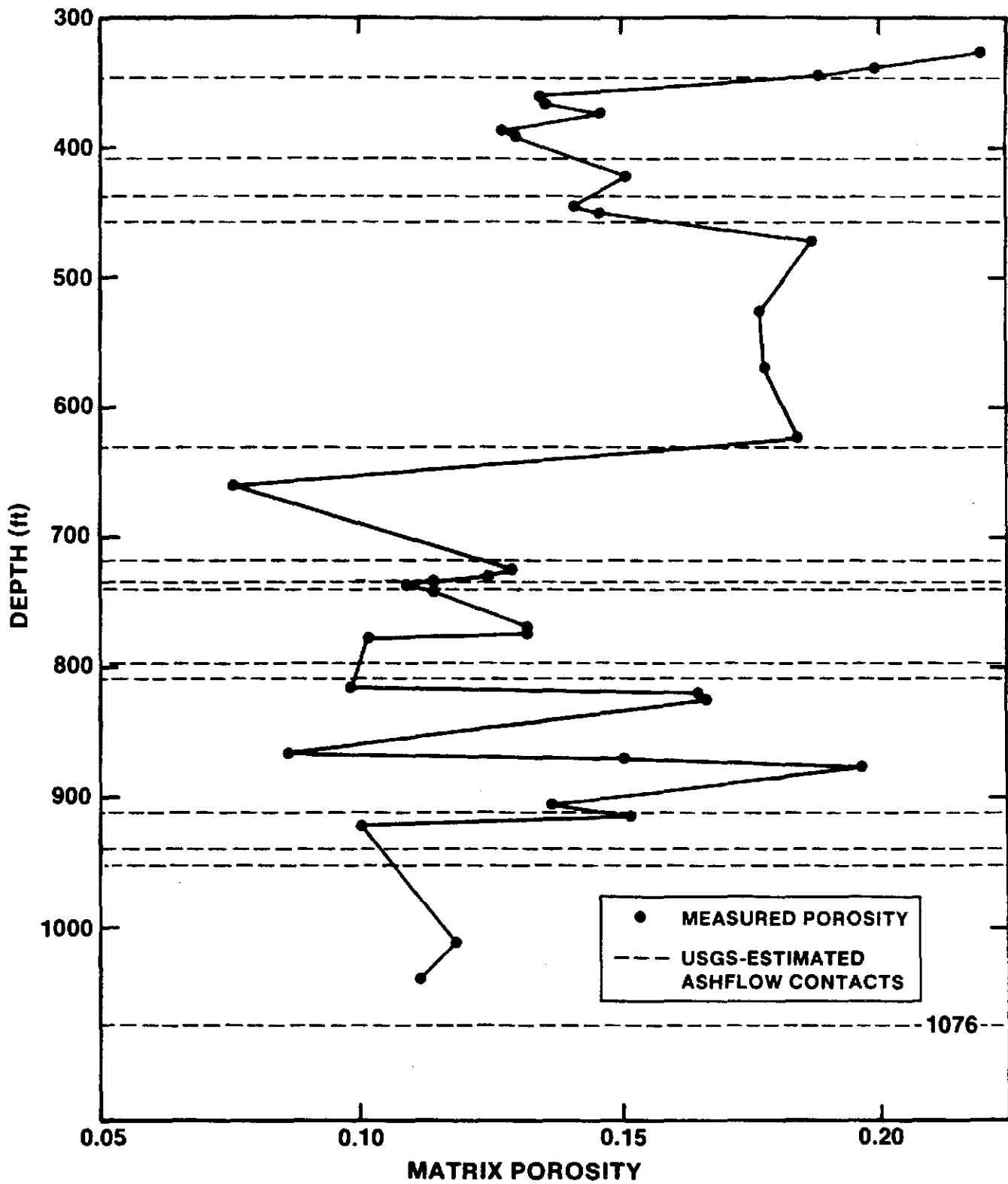


Figure 9. Vertical Variation of Matrix Porosity of Unit TSw1 in UE-25a#1. USGS-Estimated Contacts Taken From Spengler et al. (1979).

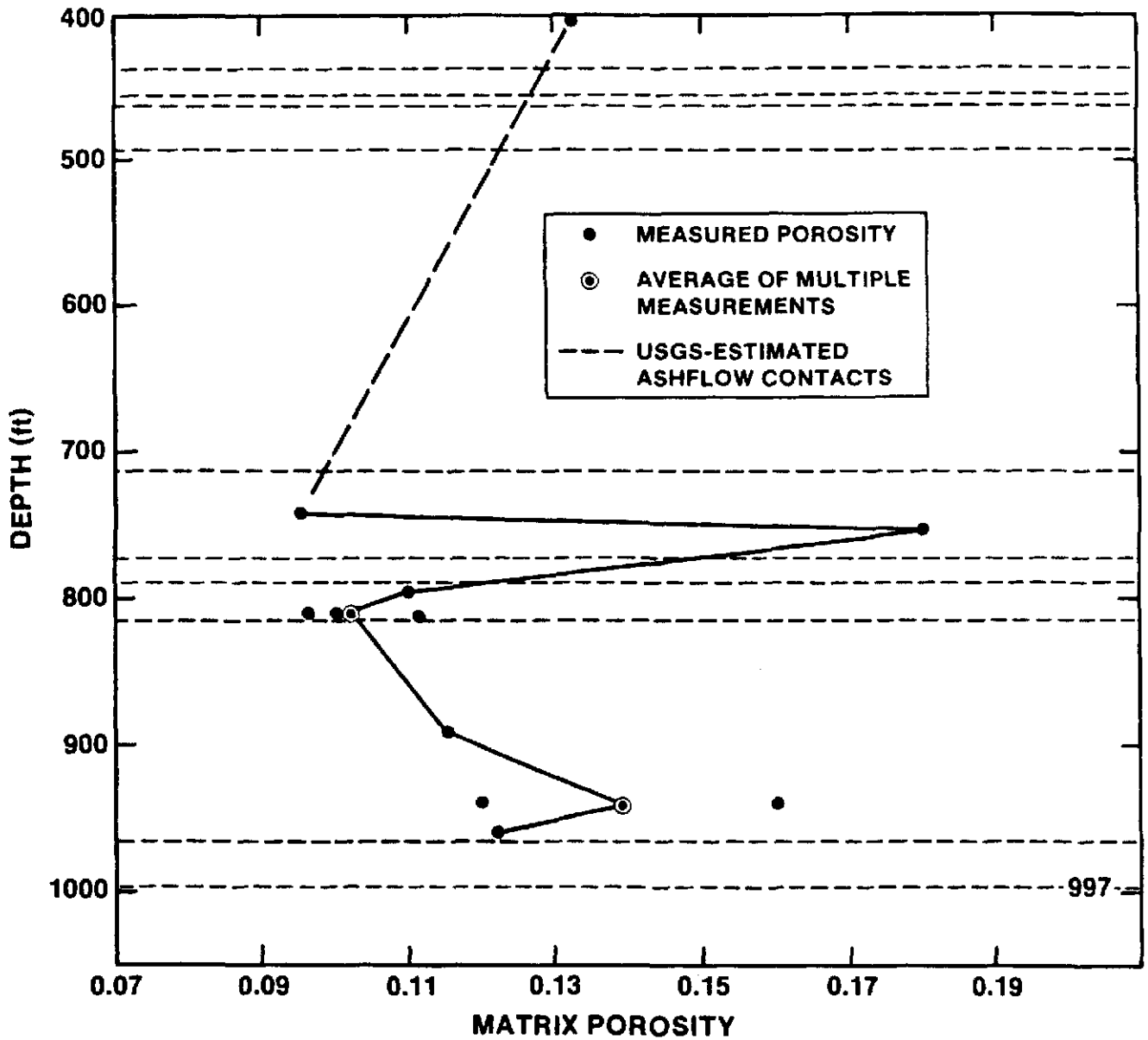


Figure 10. Vertical Variation of Matrix Porosity of Unit TSw1 in USW G-1. USGS-Estimated Contacts Taken From Spengler et al. (1981).

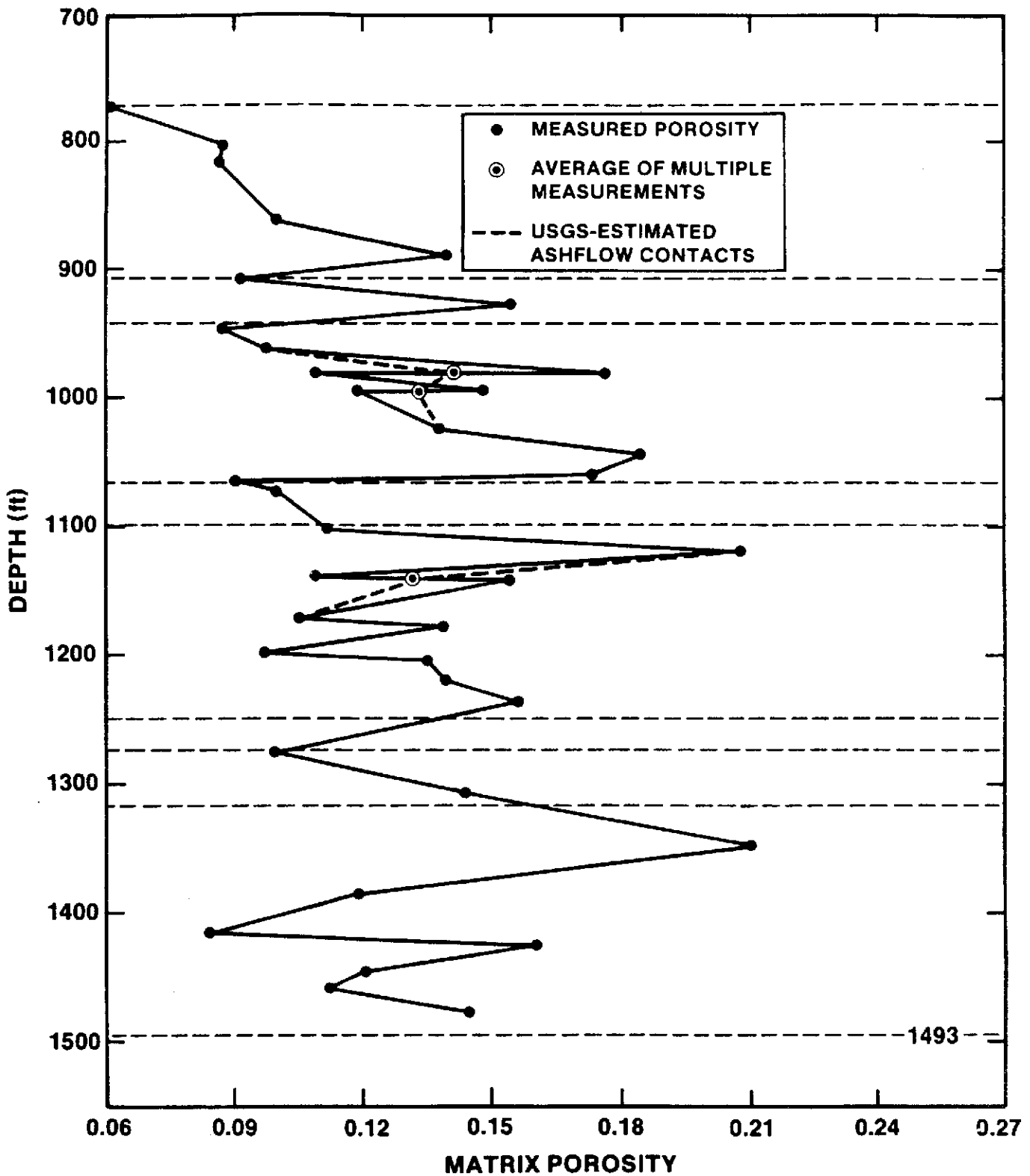


Figure 11. Vertical Variation of Matrix Porosity of Unit TSw1 in USW G-2. USGS-Estimated Contacts Taken From Maldonado and Koether (1983).

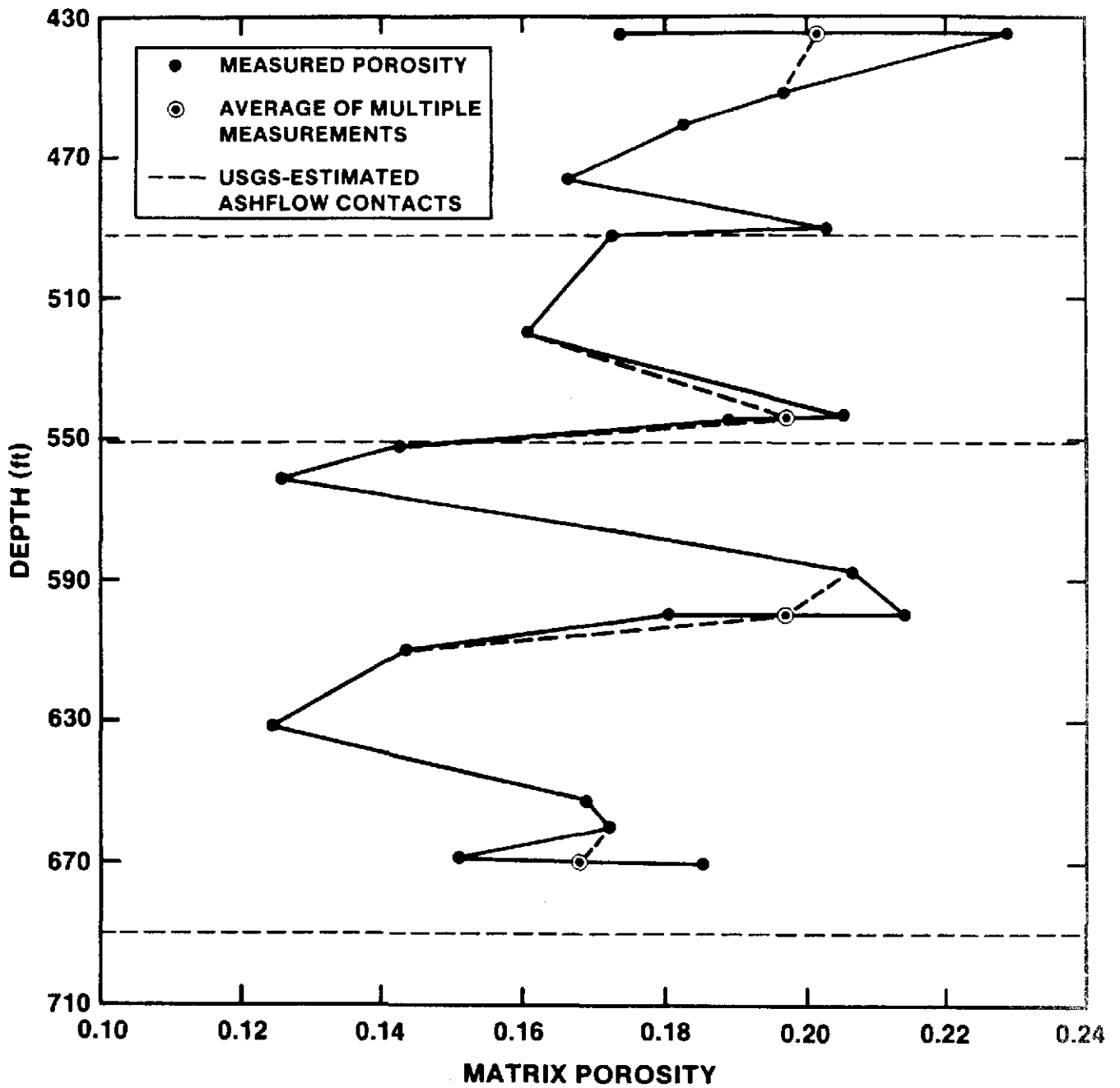


Figure 12. Vertical Variation of Matrix Porosity of Unit TSw1 in USW GU-3. USGS-Estimated Contacts Taken From Scott and Castellanos (1984).

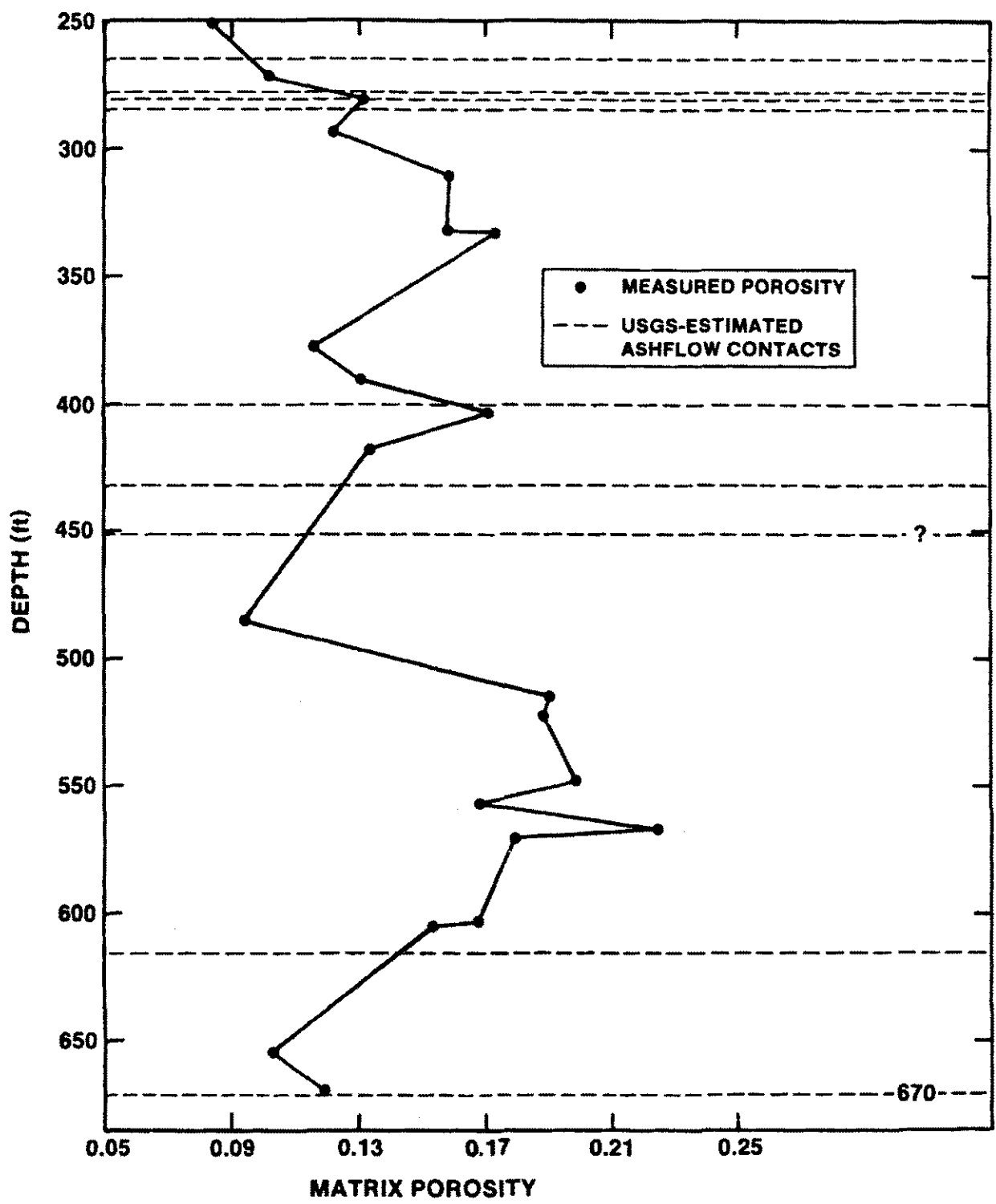


Figure 13. Vertical Variation of Matrix Porosity of Unit TSw1 in USW G-4. USGS-Estimated Contacts Taken From Spengler and Chornack (1984).

(Smith, 1960, p. 157) should have zones of high porosity at top and bottom, with decreasing porosity inward as the degree of welding increases. This simplistic pattern may be complicated by variables such as flow thickness and temperature as well as the timing between emplacement of successive ashflows (Riehle, 1973). Also, the presence or absence of lithophysal cavities and associated vapor-phase-altered material may cause local departures from the expected pattern.

Porosity data from USW GU-3 (Figure 12) suggest very clearly the presence of 4 individual ashflows in unit TSw1. In fact, of the inferred contacts (local porosity maximums), the upper 2 are very close to contacts defined by Scott and Castellanos (1984) using visual inspection of the core. The elevated porosity in Figure 12 at a depth of 652-660 ft (199-201 m) coincides with 1 of 2 zones of high lithophysae content (Spengler and Chornack, 1984; Spengler, 1985). The actual base of the ashflow containing this zone is lower in the core hole than the lowermost porosity measurement.

The correspondence between ash-flow contacts and regions of high porosity is not as clear in core holes other than USW GU-3. The good correlation at USW GU-3 is attributed to the core hole being farthest from the inferred source area. Only the largest ash flows deposited material at the USW GU-3 location, so that time intervals between successive ash flows probably were of sufficient duration to allow the development of the expected porosity profile in each ash flow. In the other core holes, more ash flows are present, implying shorter time intervals between successive ash flows, and more complex cooling and welding histories as a result.

Figures 9 through 13 demonstrate the large vertical variability of matrix porosity. This variability is a function of the number of ashflows present, their relative thickness, their emplacement timing, their degree of welding, and their gas contents (as indicated by the content of lithophysae). The effects of an individual factor cannot be isolated, so a systematic expression of vertical variability cannot be made. Therefore, matrix porosity is treated as a random variable within unit TSW1 in a single core hole, and is represented by the means and standard deviations in Table 1.

The higher matrix porosity of unit TSW1 in USW GU-3 can be explained by a comparison of the distances between each core hole and the source of the ashflows. The source is inferred to be the Claim Canyon Cauldron (Byers et al., 1976), which lies to the north of Yucca Mountain. In general, both the maximum degree of welding and the average degree of welding decrease away from the source, so that matrix porosity should increase with distance from the source. As one would expect, the highest average porosity occurs in the core hole farthest from the inferred source. However, the other four core holes do not fit this sample pattern, probably because of the complicating factors mentioned in the preceding paragraph.

The mean value and standard deviation of the matrix porosity of the 26 samples from Busted Butte are 0.177 and 0.040, respectively. Comparison with the values in Table 1 suggests similarity between the matrix porosity at the Busted Butte outcrop and that in core hole USW GU-3. All samples from Busted Butte are from tuff rich in

vapor-phase-altered material, so that the relatively high matrix porosities seem to be appropriate. The similarity to the data from USW GU-3 suggest that samples from this core hole also contain relatively large amounts of vapor-phase-altered material. Thus, differences in the matrix porosities between USW GU-3 and other core holes may result from differences in the content of vapor-phase-altered material in the sample sets rather than from variable geographic position. Whether the difference in content of vapor-phase-altered material between sample groups from different core holes is real or is an artifact of the sampling has not been determined.

In addition to matrix porosity, void space is present in unit TSw1 as lithophysal cavities. These cavities are distributed unevenly within the unit. In USW GU-3 and USW G-4, the cavities are concentrated near the base of the unit, whereas in USW G-1 and USW G-2, the distribution appears to be somewhat more random (Spengler and Chornack, 1984, p. 18). Table 2 contains data derived from Spengler and Chornack (1984) that approximate the actual distribution in four of the core holes. (Note that in many cases the standard deviation is greater than the mean value. This implies an asymmetric (non-normal) distribution.) No data are available for UE-25a#1.

In summary, the total porosity (sum of matrix porosity and lithophysal cavity content) in unit TSw1 may be quite variable. Estimates with varying degrees of precision may be made using the data in Tables 1 and 2.

Table 2

Abundance of Lithophysal Cavities in Unit TSW1

	Mean (%)	St. Dev. (%)	Range (%)	Depth Interval [ft(m)]
<u>USW G-1</u>				
	0.0	0.0	0.0	280-430 (85.3-131.1)
	10.2	7.1	0.0-27.5	430-600 (131.1-182.9)
	2.7	2.6	0.0-8.0	600-997 (182.9-303.9)
Overall	3.9	5.4	0.0-27.5	280-997 (85.3-303.9)
<u>USW G-2</u>				
	0.0	0.0	0.0	771-910 (235.0-277.4)
	5.7	4.8	0.0-16.0	910-1160 (277.4-353.6)
	2.5	2.9	0.0-10.0	1160-1493 (353.6-455.1)
Overall	3.1	4.0	0.0-16.0	771-1493 (235.0-455.1)
<u>USW GU-3</u>				
	0.0	0.0	0.0	430-560 (131.1-170.7)
	10.8	5.5	3.0-25.0	560-690 (170.7-210.3)
Overall	5.4	6.7	0.0-25.0	430-690 (131.1-210.3)
<u>USW G-4</u>				
	0.0	0.0	0.0	243-400 (74.1-121.9)
	11.9	8.3	0.0-29.0	400-670 (121.9-204.2)
Overall	7.3	8.7	0.0-29.0	243-670 (74.1-204.2)
Entire Unit	4.5	6.1	0.0-29.0	NA

NA: Not applicable
(original data are presented in Spengler and Chornack, 1984).

2.2.2.2 Grain Density. Statistical analysis of grain density with testing laboratory indicates that data obtained by LANL are significantly lower than all other data. Data from LANL are available only for samples from UE-25a#1. The following means and standard deviations were obtained for unit TSWl in UE-25a#1: $2.52 \pm 0.02 \text{ g/cm}^3$ ($157.3 \pm 1.2 \text{ lb/ft}^3$) (LANL, 5 samples); $2.57 \pm 0.01 \text{ g/cm}^3$ ($160.4 \pm 0.6 \text{ lb/ft}^3$) (HN, 4 samples); $2.54 \pm 0.03 \text{ g/cm}^3$ ($158.6 \pm 1.9 \text{ lb/ft}^3$) (USGS, 16 samples); and $2.57 \pm 0.03 \text{ g/cm}^3$ ($160.4 \pm 1.9 \text{ lb/ft}^3$) (TT, 16 samples). Pair-wise comparison of LANL with the other three laboratories resulted in rejection of the equivalence of mean values for two of the pairs [P = 0.0037 (HN-LANL) and P = 0.0009 (TT-LANL)]. Because of these inequalities and the inequalities of porosity for pair-wise comparisons involving LANL data (Section 2.2.2.1), the LANL data for grain density were eliminated from further consideration in this report.

P-values for the other pair-wise comparisons that did not result in rejection of the null hypothesis are given below.

USGS-HN, USW GU-3: 0.7108
 TT-HN, USW GU-3: 0.4223
 TT-USGS, USW GU-3: 0.8377
 TT-USGS, USW G-4: 0.1026 (unequal variances)
 TT-unknown laboratory, USW G-1: 0.4114
 USGS-HN, UE-25a#1: 0.0804
 TT-HN, UE-25a#1: 0.5905

One additional pair (TT-USGS, UE-25a#1) had a P-value of 0.0011, suggesting that the null hypothesis should be rejected. However, the fact that TT and USGS values compared favorably in two other core holes led to the decision to retain both sets of data from UE-25a#1 for additional analysis.

One of the pair-wise comparisons was made by adjusting for unequal variances, as noted above. Because one of the assumptions necessary for the valid use of ANOVA or GLM is that all samples have the same variance, such techniques cannot be applied directly in a simultaneous analysis of the data from all testing laboratories.

All other data were grouped by core hole and the core-hole groups were compared. Statistically significant differences were found between the grain density of material from UE-25a#1 and grain densities for the other four core holes. Table 3 summarizes the grain density data for each core hole individually, and gives the P-value for each pair-wise comparison.

Four of the pair-wise comparisons were made by adjusting for unequal variances, as noted in Table 3. Because one of the assumptions necessary for the valid use of ANOVA or GLM is that all samples have the same variance, such techniques cannot be applied directly in a simultaneous analysis of the data from all core holes.

The normality of grain density data was checked for each core hole individually and for unit TSW1 as a whole. Data for USW G-1 are

Table 3
Grain Density for Unit TSw1

Core Hole	Grain Density (g/cm ³) ^a		Number or Samples	95% Confidence Interval for Mean Value
	Mean	St. Dev.		
UE-25a#1	2.556	0.032	36	2.545-2.567
USW G-1	2.528	0.028	11	2.509-2.547
USW G-2	2.538	0.044	38	2.524-2.552
USW GU-3	2.526	0.029	22	2.513-2.539
USW G-4	2.520	0.052	22	2.497-2.543
ALL	2.537	0.041	129	2.530-2.544

^aTo obtain units of lb/ft³, multiply by 62.43.

<u>Pair</u>	<u>P-value</u>
a#1, G-1	0.0135
a#1, G-2	0.0496
a#1, GU-3	0.0009
a#1, G-4	0.0079 (unequal variances)
G-1, G-2	0.5059
G-1, GU-3	0.8631
G-1, G-4	0.5823 (unequal variances)
G-2, GU-3	0.2366 (unequal variances)
G-2, G-4	0.1802
GU-3, G-4	0.6455 (unequal variances)

insufficient to adequately assess normality. Data from UE-25a#1 appear to have a slightly log-normal distribution, whereas data from USW G-2, USW GU-3, and USW G-4 are normally distributed. The data set for unit TSw1 as a whole is normally distributed.

The possibility that sampling differences between core holes caused the differences in grain density was examined by analyzing the covariance contributed by the vertical location of samples within unit TSw1. However, this possibility was rejected using the results of statistical calculations. (The calculated F-value was 3.498. This value is greater than $F = 2.447$ for a true null hypothesis of equivalent mean values, so the null hypothesis was rejected). However, the validity of this conclusion may be in question because of violation of the assumption of equal variances, as discussed earlier.

Grain density is a direct function of mineralogy. Thus, a discrepancy between core holes should reflect mineralogic differences in different core holes. In the devitrified Topopah Spring Member, the dominant minerals are alkali feldspar and cristobalite, with quartz and tridymite as less important phases. The qualitative data in Figures B-3 and B-4 of Bish and Vaniman (1985) indicate that tridymite occurs relatively uniformly in the core holes except in UE-25a#1, where the thickness of the Topopah Spring Member containing tridymite is much less. Tridymite is the least dense of the four minerals common to unit TSw1, and so the relatively restricted occurrence of this phase may account for the higher mean grain density of unit TSw1 in UE-25a#1.

The mean value for the grain density of the samples from Busted Butte is 2.557 g/cm^3 (159.6 lb/ft^3). This relatively high grain density is not well-understood. As described in Section 2.2.2.1, the samples should be relatively rich in vapor-phase-altered material, a material that has a relatively low grain density based both on estimated values and on the densities of the constituent minerals.

Mineralogic variations over Yucca Mountain are probably sufficient to cause grain density variations as large as those observed between the existing core holes. Therefore, despite the difference in grain density in UE-25a#1, all measurements of grain density for samples of unit TSw1 from core holes are used to provide a recommended mean value and standard deviation of 2.537 g/cm^3 and 0.041 g/cm^3 (158.4 lb/ft^3 and 2.6 lb/ft^3). The 95% confidence interval for the mean value is 2.530 to 2.544 g/cm^3 (157.9 to 158.8 lb/ft^3).

2.2.2.3 Bulk Density. Many measurements of bulk density have been made for unit TSw1, including saturated bulk density, "natural-state" bulk density, and dry bulk density. Most measurements have been made for dry bulk density, and these are provided in Table B-1. However, neither these data nor any of the other measured bulk densities are applicable to in situ conditions in unit TSw1. There are two reasons for this. First, the mean in situ saturation of the matrix porosity is 0.65 (Montazer and Wilson, 1984, p. 13), a value perhaps approached for "natural-state" bulk density tests but not for the other experiments. Secondly, these laboratory-measured bulk densities do not account for the presence of lithophysal cavities, which will tend to lower in situ bulk density.

Table 4 summarizes estimates of mean values and standard deviations of dry and "natural-state" bulk densities for each core hole as well as for unit TSW1 as a whole. Mean values were calculated using the following equations:

$$\rho_{db} = \rho_g (1 - \phi_T) \quad (1)$$

for dry bulk density (ρ_{db}), and

$$\rho_{nb} = \rho_g (1 - \phi_T) + 0.65 \phi_m \rho_w \quad (2)$$

for "natural-state" bulk density (ρ_{nb}), where ρ_g is the grain density for unit TSW1 from Table 3, 0.65 is the saturation of the matrix porosity (lithophysal cavities are assumed to be dry when matrix porosity is not completely saturated), ϕ_T is the total porosity [the sum of the mean matrix porosity (ϕ_m) from Table 1 and the overall mean lithophysal cavity content from Table 2], and ρ_w is density of water, here assumed to be 1.0 g/cm³ (62.4 lb/ft³). Standard deviations (σ_{TOTAL}) were calculated by combining the standard deviations of the individual properties (σ_i) with partial derivatives $\left(\frac{\partial}{\partial i}\right)$ of Equations (1) and (2) in a geometric mean equation represented by

$$\sigma_{TOTAL} = \left[\prod_{i=1}^n \sigma_i^2 \left(\frac{\partial}{\partial i}\right)^2 \right]^{1/2} \quad (3)$$

In Equation (3), the partial derivatives are evaluated using the mean values of the properties present in the expressions.

Table 4

Estimated Bulk Densities for Unit TSw1

Core Hole	Bulk Density (g/cm ³) ^a			
	Dry		"Natural-State" ^b	
	Mean	St. Dev.	Mean	St. Dev.
UE-25a#1 ^c	2.052	0.201	2.144	0.194
USW G-1	2.121	0.154	2.200	0.149
USW G-2	2.140	0.142	2.221	0.130
USW GU-3	1.948	0.185	2.061	0.182
USW G-4	1.963	0.243	2.059	0.236
ALL	2.063	0.185	2.155	0.176

^aTo obtain densities in lb/ft³, multiply by 62.43.

^bAssuming that in situ saturation is 0.65 in matrix porosity.

^cAssuming that mean lithophysal cavity abundance is 5.6% (average of values for USW G-1 and USW G-4) and standard deviation is 7.0%.

2.3 Thermal Properties

2.3.1 Data

Measured data for the thermal expansion coefficient of unit TSw1 are tabulated in Appendix B (Table B-2). The data were measured by SNL (unconfined experiments) and by TT (confined experiments).

2.3.2 Statistical Analysis and Discussion

Thermal expansion coefficients have been analyzed using the TTEST and the GLM procedures. Results and discussion thereof are contained in Section 2.3.2.1. In addition, brief discussions of the heat capacity and emissivity of unit TSw1 are presented in Sections 2.3.2.2 and 2.3.2.3, respectively.

2.3.2.1 Thermal Expansion. All five core holes are represented in the nine samples on which thermal expansion measurements were made under confining pressure (Table B-2). However, data are available for only one sample each from three of the core holes. Given the paucity of data, no statistical analysis has been performed to examine spatial variability. Instead, all data have been grouped under the assumption that spatial variability is minimal. Additional analysis will be performed when more data are available.

The thermal expansion data from unconfined experiments were analyzed in two stages. The first analysis examined the samples from UE-25a#1. These samples were part of a larger program, the goal of which was to

determine whether long-term exposure ("soaking") at elevated pressures and temperatures affected the material properties of tuff (Blacic et al., 1982, 1986). Thermal expansion experiments were performed on both wet and dry samples before and after soaking for 2.5 to 6 months. Statistical comparison of the data for presoak experiments with data for postsoak experiments indicates that the soaking had no significant effect on mean thermal expansion for either wet or dry samples, a conclusion similar to that of Blacic et al. (1986). Another conclusion that can be made based on the results of the statistical comparison is that the saturation state does not affect the mean thermal expansion of welded, devitrified tuff. P-values for pair-wise comparisons are given below.

Temperature Range [°C (°F)]	Pair	P-value
25-50 (77-122)	pre-soak	0.8278
50-100 (122-212)	vs. post-soak,	0.1722
100-150 (212-302)	saturated	0.3440
150-200 (302-392)	"	0.3250
200-250 (392-482)	"	0.3673
25-100 (77-212)	"	0.1104 (unequal variances)
25-150 (77-302)	"	0.3340
25-200 (77-392)	"	0.8537
25-250 (77-482)	"	0.5110

25-50 (77-122)	pre-soak	0.7992
50-100 (122-212)	vs. post-soak,	0.6276
100-150 (212-302)	dry	0.3644
150-200 (302-392)	"	0.9272 (unequal variances)
200-250 (392-482)	"	0.7046
25-100 (77-212)	"	0.9313
25-150 (77-302)	"	0.6819
25-200 (77-392)	"	0.7929
25-250 (77-482)	"	0.8638

25-50 (77-122)	saturated	0.5625
50-100 (122-212)	vs. dry	0.9874
100-150 (212-302)	"	0.4449
150-200 (302-392)	"	0.0991
200-250 (392-482)	"	0.0673
25-100 (77-212)	"	0.6245
25-150 (77-302)	"	0.4974 (unequal variances)
25-200 (77-392)	"	0.2833 (unequal variances)
25-250 (77-482)	"	0.0662

Four of the pair-wise comparisons were made by adjusting for unequal variances, as noted above. This fact should not cause any difficulties in future analyses because the pairs of concern are not involved in more general analyses as samples that are assumed to have equal variances.

Given the results described in the preceding paragraph, and because the 7 samples from each of the two depths in UE-25a#1 were chosen to be as similar as possible, the data from the saturated samples from each depth were averaged to provide a single set of thermal expansion coefficients for each depth. In this way, comparison of data from UE-25a#1 with that from USW G-1 was not biased by overemphasizing the material chosen for the soak experiments.

A comparison of the two "samples" from UE-25a#1 with data from 11 samples of unit TSw1 from USW G-1 (data for multiple samples from a single depth in USW G-1 were combined as described for UE-25a#1) resulted in no statistically significant differences. The comparison was performed for the data as is, despite the fact that some non-normal distributions were observed for the data from USW G-1. The comparison was repeated after transforming all data for temperatures $\geq 100^{\circ}\text{C}$ (212°F) to an assumed log-normal distribution. Again, no statistically significant differences were found. The P-values for both cases are given below. Thus, all thermal expansion data from unconfined experiments can be considered to be a single sample population.

Temperature Range [°C (°F)]	Pair	P-value	
		Normal Distr.	Log-Normal Distr.
25-50 (77-122)	a#1, G-1	0.1733	0.1733
50-100 (122-212)	"	0.6499	0.6499
100-150 (212-302)	"	0.3965	0.4085
150-200 (302-392)	"	0.2858	0.1952
200-250 (392-482)	"	0.3490	0.0952
25-100 (77-212)	"	0.4927	0.4552
25-150 (77-302)	"	0.7700	0.8109
25-200 (77-392)	"	0.2970	0.2496
25-250 (77-482)	"	0.2584	0.1369

Finally, TTEST was used to compare unconfined experiment results with data from experiments under confining pressure. This comparison revealed statistically significant differences for three temperature ranges: 25° to 50°C (77° to 122°F), 25° to 100°C (77° to 212°F), and 25° to 150°C (77° to 302°F). The comparison was made for log-normal distributions for data at temperatures $\geq 100^\circ\text{C}$ (212°F). The P-values for the comparisons are given below.

Temperature Range [°C (°F)]	Pair	P-value
25-50 (77-122)	Confined vs.	0.0001
50-100 (122-212)	Unconfined	0.0560
100-150 (212-302)	"	0.7594
150-200 (302-392)	"	0.1283 (unequal variances)
200-250 (392-482)	"	0.1418
25-100 (77-212)	"	0.0002
25-150 (77-302)	"	0.0130
25-200 (77-392)	"	0.7120
25-250 (77-482)	"	0.2309

One of the pair-wise comparisons was made by adjusting for unequal variances, as noted above. This fact should not cause any difficulties in future analyses because the pair of concern is not involved in more general analyses as samples that are assumed to have equal variances.

In all three cases in which the mean expansion coefficients differ, the average coefficient of linear thermal expansion was higher when experiments were conducted with 10 MPa (1450 psi) confining pressure. This observation is consistent with the concept that partial closing of preexisting microcracks was caused by the confining pressure. As such, the confined experiments give thermal expansion results closer to those for a crack-free aggregate. The unconfined experiments, however, have reduced expansion coefficients because of mineral expansion into the preexisting open microcracks. Similar results have been reported for other rock types (Page and Heard, 1981; Bauer and Handin, 1983).

For the temperature ranges 150° to 200°C (302° to 392°F) and 200° to 250°C (392° to 482°F), thermal expansion coefficients show a large increase in both mean values and standard deviation. These changes are attributable to the polymorphic inversions of tridymite and cristobalite (increase in mean values) that are present in variable amounts (increase in standard deviations). Cristobalite is present throughout the welded, devitrified Topopah Spring Member, whereas tridymite is associated with vapor-phase alteration and so varies in abundance with the amount of vapor-phase-altered material. One sample that is essentially pure vapor-phase altered material (G1-504.1-2) has expansion coefficients consistent with those for other samples up to 150°C, but for the interval of 200° to 250°C (392° to 482°F), it has an expansion coefficient of $249.8 \times 10^{-6} \text{ } ^\circ\text{C}^{-1}$ ($138.8 \times 10^{-6} \text{ } ^\circ\text{F}^{-1}$), 5 times the average coefficient for the temperature range for unconfined conditions and 15 times the average coefficient under confining pressure.

Examination of data for the unconfined experiments indicates that a silica phase (probably tridymite) begins to invert at $161^{\circ}\text{C} \pm 12^{\circ}\text{C}$ ($322^{\circ}\text{F} \pm 22^{\circ}\text{F}$). As temperature continues to increase, the slope of the curves (i.e., the expansion coefficient) increases smoothly for approximately 100°C (180°F), then decreases smoothly until cristobalite inversion apparently is complete at $362^{\circ}\text{C} \pm 11^{\circ}\text{C}$ ($684^{\circ}\text{F} \pm 20^{\circ}\text{F}$). At temperatures higher than 362°C (684°F), the expansion coefficient is approximately constant up to 400°C (752°F).

Table 5 contains mean values and standard deviations for expansion coefficients obtained in both confined and unconfined experiments. In addition, these coefficients are translated into temperature-strain curves in Figure 14 [see subsequent paragraph for discussion of coefficients above 100°C (212°F)]. For low temperatures [up to 100°C (212°F)], both sets of coefficients are presented because both may be pertinent to thermomechanical calculations. In rock near underground openings, at least one of the principal stresses may be sufficiently low that the rock may be considered to be unconfined in one or more directions. Farther from openings, the data taken under confining pressure may be more appropriate.

Data for temperature intervals extending above 100°C (212°F) are statistically indistinguishable whether obtained with or without confining pressure. Thus, all data for these intervals have been combined into a single data set. This data set has a distribution that is more closely approximated by a lognormal distribution than by a normal distribution. As such, means and standard deviations are calculated in

Table 5

Summary of Linear Thermal Expansion Coefficients^a for Unit TSW1

	Temperature Range				
	°C 25-50 °F 77-122	50-100 122-212	100-150 212-302	150-200 302-392	200-250 392-482
<u>Unconfined</u>					
Mean	5.1	8.0	10.3	12.4	27.4
St. Dev.	1.2	1.5	(+2.2, -1.8) ^b	(+13.6, -6.5) ^b	(+27.1, -13.6) ^b
#Samples	13	13	22	22	16
<u>Confined</u>					
Mean	9.9	9.6	c	c	c
St. Dev.	1.5	2.3	c	c	c
#Samples	9	9	c	c	c

^aUnits are $10^{-6} \text{ } ^\circ\text{C}^{-1}$; to obtain units of $10^{-6} \text{ } ^\circ\text{F}^{-1}$, multiply by 5/9.

^bData for these temperature intervals are lognormally distributed, so standard deviations are in \log_e units. They are applied to the mean value in \log_e units, then converted to standard units to give the equivalent deviations in the parentheses.

^cValues listed for unconfined conditions apply for both unconfined and confined material.

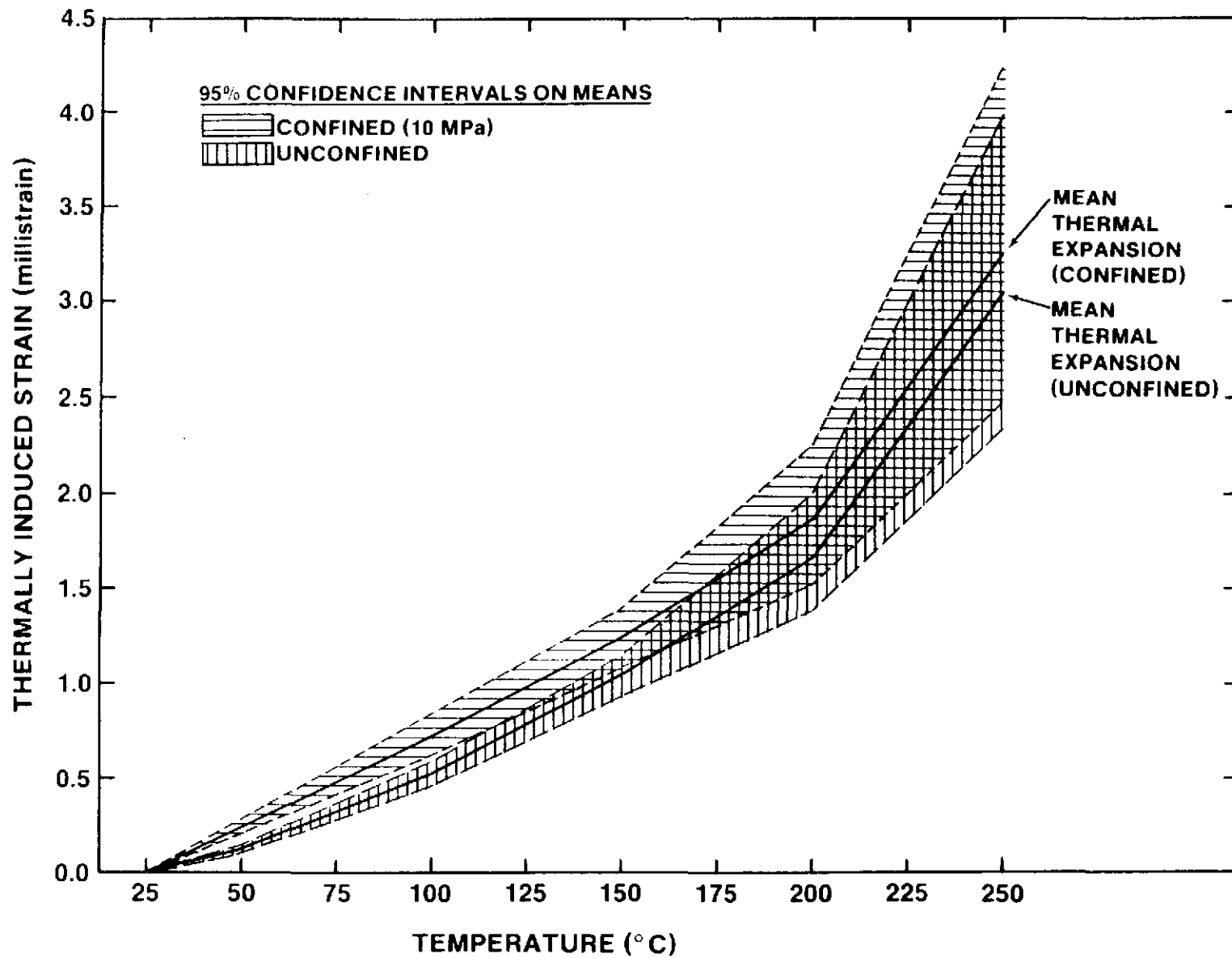


Figure 14. Thermal Expansion Behavior of Confined and Unconfined Samples of Unit TSW1

\log_e units. Upon conversion back to standard units, the "standard deviation" is no longer symmetrical about the mean, as is evident by examination of Table 5 and Figure 14. In fact, the 95% confidence limits on the mean expansion behavior that are shown in Figure 14 have been calculated in \log_e units and converted to standard units before plotting.

Thermal expansion measurements have been made on three large [5-inch (12.7-cm) diameter] samples of lithophysae-rich Topopah Spring Member (Nimick, in preparation, b). The average coefficients of linear thermal expansion for the temperature ranges 30° to 50°C (86° to 122°F) and 50° to 100°C (122° to 212°F) are $4.65 \times 10^{-6} \text{ } ^\circ\text{C}^{-1}$ ($2.58 \times 10^{-6} \text{ } ^\circ\text{F}^{-1}$) and $5.74 \times 10^{-6} \text{ } ^\circ\text{C}^{-1}$ ($3.19 \times 10^{-6} \text{ } ^\circ\text{F}^{-1}$), respectively. These values are lower than either set of coefficients in Table 5, despite the fact that the larger samples were tested under confining pressure. The lower values for the lithophysae-rich material are attributed to the presence of the lithophysal cavities. It is postulated that these open spaces absorb some of the mineral expansion in much the same way as the micro-cracks discussed earlier in this section.

2.3.2.2 Heat Capacity. No experimental data have been obtained for the heat capacity of the tuff units at Yucca Mountain. Tillerson and Nimick (1984, p. 86) assumed a constant value of 0.84 J/g°C (0.20 Btu/lb°F) for the solid portion of all of the tuff units. However, empirical estimates of the heat capacity from whole rock bulk chemistry indicate that 0.84 J/g°C (0.20 Btu/lb°F) is not a representative value and that the heat capacity has a relatively strong temperature dependence (Connolly, 1986).

The bulk chemistry of four samples of unit TSw1 and five samples of unit TSw2 was obtained with the intent of estimating heat capacities from the chemical data (Connolly, 1986). The heat capacity values that resulted were not sufficiently numerous to evaluate variability between core holes. The values were compared to examine possible differences between units TSw1 and TSw2. No statistical differences were found. P-values for the comparisons are given below.

Temperature Range [°C (°F)]	Pair	P-value
25 (77)	TSw1, TSw2	0.4433
77 (171)	"	0.4433
127 (261)	"	0.4433
177 (351)	"	0.4841
227 (441)	"	0.4664
277 (531)	"	0.4071
327 (621)	"	0.3738

Table 6 contains mean values and standard deviations of the estimated heat capacities as a function of temperature for the solid components of the welded, devitrified portions of the Topopah Spring Member. These data also are presented graphically in Figure 15. The existing estimates as discussed here do not include the effects of polymorphic inversions of cristobalite or tridymite. The delineation of these effects cannot be made until experimental data are available.

In situ volumetric heat capacity (ρC_p)_{in situ} can be estimated by using the porosity and grain density data discussed in Sections 2.2.2.1 and 2.2.2.2 with the data in Table 6 in the following equation:

Table 6

Heat Capacity^a of Solid Components as a Function of Temperature
for Welded, Devitrified Topopah Spring Member

	Temperature						
	°C 25	77	127	177	227	277	327
	°F 77	171	261	351	441	531	621
Mean	0.770	0.854	0.916	0.967	1.011	1.051	1.088
St. Dev.	0.003	0.003	0.003	0.003	0.003	0.003	0.003
# Samples	9	9	9	9	9	9	9

^aUnits are J/g°C; to obtain units of Btu/lb°F, multiply by 0.23885.

Note: Mean heat capacities (C_p^{sol}) represented by the following equation:

$$C_p^{\text{sol}} = 0.82942 + 3.397 \times 10^{-4} T + 6.0564 \times 10^{-3} T^{1/2} \\ + 4.2444 \times 10^{-8} T^2 - 1.4578 T^{-1/2} + 1.9473 \times 10^{-4} T^{-1} \\ - 1.6029 \times 10^4 T^{-2}$$

where T is in degrees Kelvin.

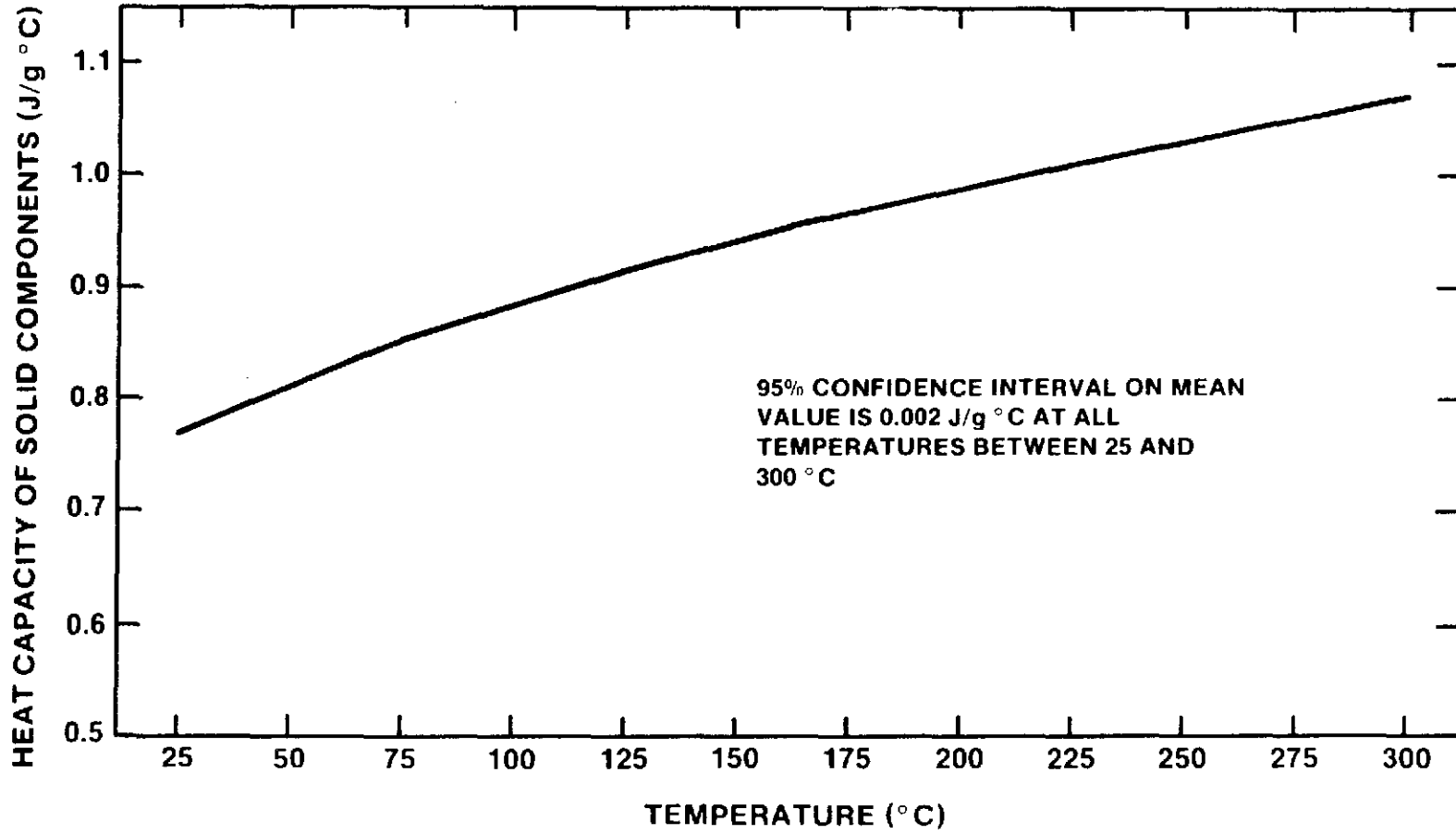


Figure 15. Heat Capacity of Solid Components as a Function of Temperature for Welded, Devitrified Topopah Spring Member

$$\begin{aligned}
(\rho C_p)_{\text{in situ}} = & \rho_g (1 - \phi_m - \phi_L) C_p^{\text{sol}} + \phi_m s \rho_{\text{H}_2\text{O}} C_p^{\text{H}_2\text{O}} \\
& + [\phi_m (1 - s) + \phi_L] C_p^{\text{air}} \rho_{\text{air}}
\end{aligned}
\tag{4}$$

where ρ_g , ϕ_m , and ϕ_L are mean values for unit TSw1, C_p^{sol} data are those given in Table 6, and $\rho_{\text{H}_2\text{O}}$ and $C_p^{\text{H}_2\text{O}}$ are as specified in the footnote to Table 7. The last term in Equation (7) is negligible because the density of air (ρ_{air}) is very small. The saturation (s) is assumed to be 0.65 at temperatures below 100°C (212°F) and 0.0 at higher temperatures. (Although the nominal boiling temperature at Yucca Mountain should be less than 100°C (212°F), the extremely low permeability of the welded Topopah Spring Member may result in elevation of boiling temperatures above the normal level in some parts of the rock. Therefore, 100°C (212°F) is used in subsequent discussions for simplicity.) The resulting estimates of in situ heat capacity are given in Table 7 and in Figure 16. These estimates do not include the enthalpy of boiling for the pore water. Note that these are estimated mean values for the unit. Values for the in situ heat capacity of lithophysae-rich portions of unit TSw1 will be somewhat higher, and values in lithophysae-poor portions will be slightly lower.

2.3.2.3 Emissivity. Although radiative heat transfer should be negligible within the rock mass, the mechanism may play a more significant role in the transfer of heat in the immediate vicinity of a waste canister. In the interest of providing a complete information base, information relevant to the emissivity of the welded, devitrified Topopah Spring Member is summarized here.

Table 7

Estimated^a In Situ Volumetric Heat Capacity^b of Unit TSw1

	Temperature							
	°C	25	50	99	101	150	200	250
	°F	77	122	210	214	302	392	482
<u>UE-25a#1</u>								
Mean		1.963	2.049	2.183	1.818	1.931	2.029	2.116
St. Dev.		0.180	0.185	0.193	0.178	0.189	0.198	0.207
<u>USW G-1</u>								
Mean		1.964	2.054	2.194	1.879	1.996	2.097	2.187
St. Dev.		0.146	0.149	0.155	0.137	0.145	0.153	0.159
<u>USW G-2</u>								
Mean		1.989	2.080	2.220	1.895	2.013	2.115	2.206
St. Dev.		0.133	0.134	0.137	0.126	0.133	0.140	0.146
<u>USW GU-3</u>								
Mean		1.974	2.055	2.179	1.725	1.832	1.926	2.008
St. Dev.		0.192	0.196	0.202	0.164	0.174	0.183	0.191
<u>USW G-4</u>								
Mean		1.913	1.995	2.122	1.739	1.847	1.941	2.024
St. Dev.		0.210	0.217	0.228	0.215	0.228	0.240	0.250
<u>Average for Entire Unit</u>								
Mean		1.973	2.060	2.194	1.827	1.941	2.039	2.126
St. Dev.		0.168	0.172	0.179	0.164	0.175	0.183	0.191

^aEquation (4) used with the following values of $C_p^{H_2O}$ and ρ_{H_2O} :

	$C_p^{H_2O}$	ρ_{H_2O}
25°C (77°F):	4.179 J/gK (0.998 Btu/lb°F)	0.9971 g/cm ³ (62.25 lb/ft ³)
50°C (122°F):	4.183 J/gK (0.999 Btu/lb°F)	0.9880 g/cm ³ (61.68 lb/ft ³)
99°C (210°F):	4.213 J/gK (1.006 Btu/lb°F)	0.9586 g/cm ³ (59.85 lb/ft ³)

^bUnits are J/cm³K; to obtain Btu/ft³°F, multiply by 14.911.

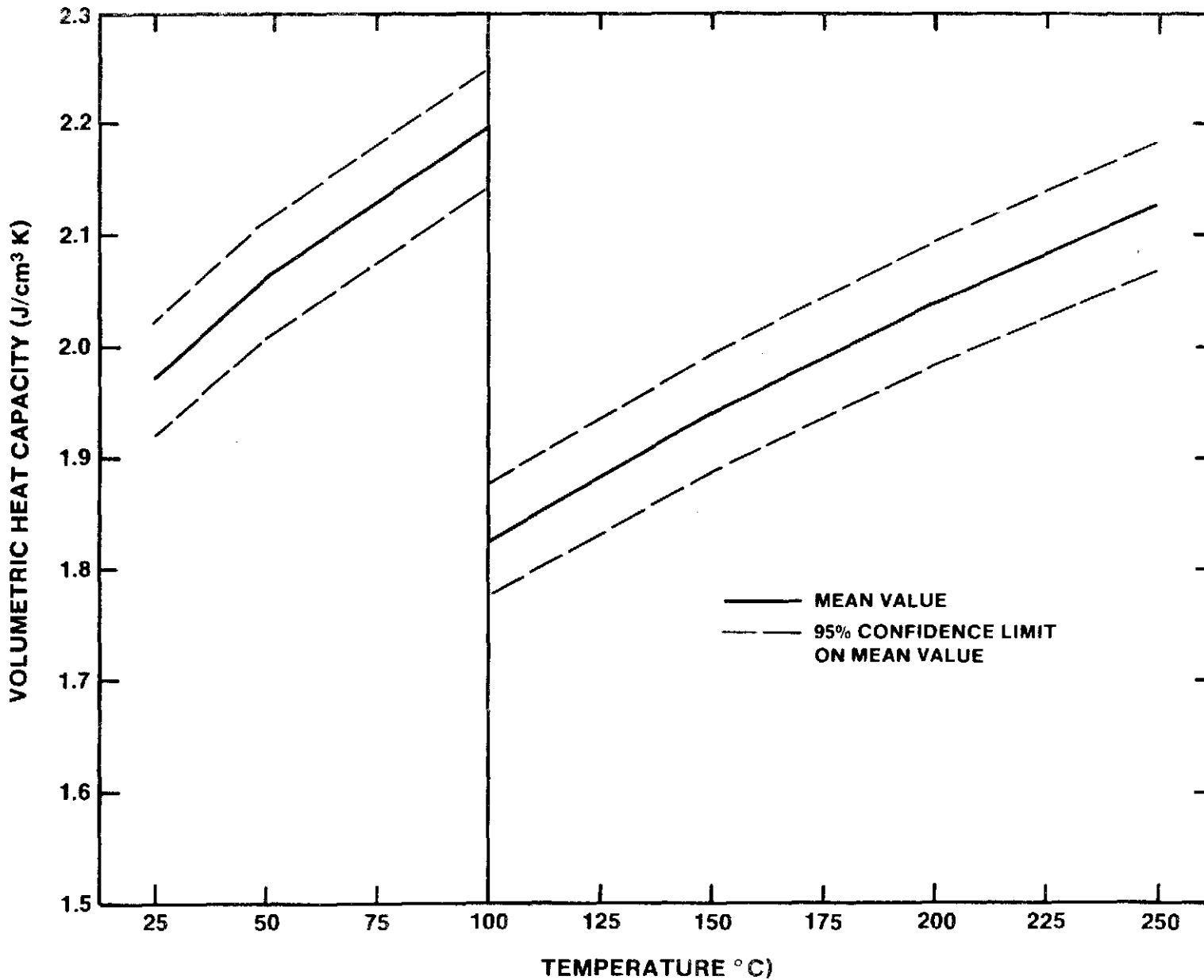


Figure 16. Estimated Average Values of In Situ Volumetric Heat Capacity as a Function of Temperature for Unit TSw1

No experimental data are available for the Topopah Spring Member, but an emissivity value of 0.89 has been measured for the Grouse Canyon Member of the Belted Range Tuff (Zimmerman et al., 1986), a welded tuff similar to the Topopah Spring Member (Zimmerman et al., 1984). This value is consistent with data in Dana (1969) for minerals common to the welded, devitrified tuffs: 0.88 for quartz and 0.93 to 0.95 for feldspar. In addition, Dana (1969) reports a value of 0.90 for granite, a coarser-grained equivalent of the tuffs. Therefore, 0.89 seems to be a reasonable value for the welded, devitrified portions of the Topopah Spring Member.

2.4 Mechanical Properties

2.4.1 Data from Compressive Experiments

Measured data for the mechanical properties (compressive strength, Young's modulus, Poisson's ratio, and axial strain at failure) determined in compression of samples of unit TSW1 are summarized in Table B-3. All data in the table were obtained from samples derived from core material (i.e., sample diameters are all \leq 5.08 cm. (2.00 in.)). Additional measurements have been made on large samples of lithophysae-rich material. Experiment results from these samples are discussed in Sections 2.4.2.1.5, 2.4.2.2.5, 2.4.2.3, and 2.4.2.4.

2.4.2 Statistical Analysis and Discussion

The data in Table B-3 were analyzed using the TTEST and GLM procedures. Most samples from any single core hole were tested at a

single testing location. Thus, the results discussed in Sections 2.4.2.1 through 2.4.2.4 must be tempered by the realization that a comparison of results between core holes is very nearly a comparison of results between laboratories and vice versa. This situation is not desirable, because the two factors cannot be treated independently. However, analysis of data for unit TSw2 (Section 3.4.2) indicates that comparison of two of the testing laboratories results in no significant differences except for Poisson's ratio (see Section 3.4.2.3). If this result is extrapolated to unit TSw1 and to the third testing laboratory, then the comparison for this unit does represent an interhole comparison.

One column in Table B-3 provides the saturation states of samples prior to measurements. Considerations discussed in Appendix C indicate that saturation by immersion alone ($s = 0.75$) should not result in any difference in compressive strength relative to saturation by immersion followed by application of a vacuum ($s = 0.95$). In contrast, room-dry saturation state ($s = 0.12$) probably will cause a difference. Therefore, the single room-dry sample in Table B-3 has been excluded from the statistical analysis.

2.4.2.1 Compressive Strength. Analysis of the assumption of normality for the data in Table B-3 indicated that the presence of two samples (G2-1297.6) caused non-normality in data for both compressive strength and Young's modulus. These two samples contained regions of abnormally high porosity relative to the more usual material (Nimick et al., 1987). These regions are inhomogeneities that are much larger relative to the overall sample dimensions than recommended by ASTM or

ISRM for obtaining valid compressive mechanical properties. The decision was made to exclude them from subsequent analyses.

Eight samples from USW G-2 were tested other than the two samples discussed in the preceding paragraph. This number was reduced to five by averaging multiple values gathered from a single depth. Statistical comparison of these data for USW G-2 and data from USW GU-3 indicated a significant difference in compressive strength ($P = 0.0009$) with the mean value higher for samples from USW G-2. This relative ranking is consistent with relative differences in porosity (Table 1) when the effect of porosity on strength (see Sections 2.4.2.1.6) is considered. Table 8 summarizes the compressive strength data for the individual core holes for which data are available. Grouping of all data into a single data set does not appear to be justified, so no values are given for unit TSw1 as a whole.

The values in Table 8 represent the compressive strength to be expected for saturated material at ambient temperatures and pressure for a strain rate of 10^{-5} s^{-1} and a cylindrical sample size of 2.54 x 5.08 cm (1 x 2 in.). In addition, the material itself is nominally free of any significant inhomogeneities (i.e., lithophysal cavities or preexisting fractures).

All of the preceding discussion on compressive strength, both in this section and in the preceding sections, has been concerned with lithophysae-poor material from unit TSw1. Ten compression experiments have been completed on large [26.67 x 53.34 cm (10.5 x 21 in.)] samples

Table 8
Compressive Strength^a of Unit TSw1

Core Hole	Compressive Strength (MPa) ^b		Number of Samples	95% Confidence Interval for Mean Value
	Mean	St. Dev.		
USW G-1	108	NA	1	NA
USW G-2	171.6	28.4	5	136.3 - 206.9
USW GU-3	67.0	5.1	3	54.3 - 79.7

^aValues obtained from experiments on saturated cylindrical samples [1 in. (2.54 cm) diameter, 2 in. (5.08 cm) length] at ambient temperature and pressure at a strain rate of $10^{-5}s^{-1}$.

^bTo obtain units of psi, divide by 6895.

NA Not available.

of lithophysae-rich material from the lower portion of TSw1 (Price et al., 1985). The unconfined compressive strength for these samples was measured to be 16.2 ± 5.0 MPa ($2,350 \pm 730$ psi). The large decrease in strength relative to the lithophysae-poor material is attributed to higher porosity. The relationship between porosity and compressive strength is discussed in Section 2.4.2.1.6.

2.4.2.1.1 Saturation Effects. As indicated in Appendix C, compressive strength is expected to increase by 20 percent to 40 percent in dry samples relative to saturated samples. This expectation is based on experimental results in other rock types as well as on data from the welded tuff of the Grouse Canyon Member of the Belted Range tuff. Unit-specific data are insufficient to confirm or reject the hypothesis for unit Tsw1. Additional experiments are planned to obtain data on saturation effects on the mechanical properties of the welded, devitrified portion of the Topopah Spring Member.

2.4.2.1.2 Temperature Effects. The only existing experimental data concerning the effect of elevated temperature on the strength of unit TSw1 come from two samples discussed by Olsson and Jones (1980, p. 19). Unfortunately, the change in temperature between the two experiments was accompanied by a change in confining pressure, so that the temperature effects alone cannot be discerned. The combination of elevated pressure and temperature resulted in little change in strength relative to ambient conditions.

Experiments in other rock types suggest that elevated temperatures have little effect on the brittle fracture of rock (Paterson, 1978, p. 29), as long as the mechanism of failure does not change. This result is to be expected in dry rocks (i.e., samples from which water is removed by dehydration at temperatures lower than experiment temperatures). However, if pressure conditions are such that the rock remains at least partially saturated at the experiment temperatures, the elevated temperature may increase the rate or intensity of any chemical interactions between the pore water and the solid framework. If this process of chemomechanical weakening occurred, the coupled interaction of temperature and saturation might decrease the strength more than would be expected as a result of changes in either parameter alone. Experiments are planned to determine the importance of this possibility in the analysis of the compressive strength of the welded, devitrified portion of the Topopah Spring Member.

2.4.2.1.3. Confining Pressure Effects. In general, the application of a confining pressure during a compressive experiment increases the strength of a material (e.g., Paterson, 1978, p. 24). The relationship between the strength ($\sigma_1 - \sigma_3$) and the confining pressure (σ_3) can be represented in several ways, grouped into two general categories as follows:

1. Linear relationship -

$$|\tau| = \tau_0 + \sigma \tan \phi \quad , \quad (5)$$

where $|\tau|$ = absolute value of shear stress acting on failure plane,

τ_0 = shear stress for failure with no normal stress
(cohesion),

σ = normal stress acting on failure plane,

$\tan \phi$ = coefficient of internal friction.

Equation (5) is known as the Coulomb failure criterion (Paterson, 1978, p. 25). The parameters τ_0 and $\tan \phi$ are empirical constants derived from experiments at different confining pressures.

2. Nonlinear relationships - these failure criteria express σ_1 as a nonlinear function of σ_3 or $(\sigma_1 + \sigma_3)$ (cf., Paterson, 1978, p. 27).

No data exist to determine confining pressure effects for unit TSw1 so that the failure criteria cannot be compared. In the past, the Coulomb criterion has been used for tuffs because of its simplicity (Olsson and Jones, 1980; Price, 1983). Even using this linear relationship, however, complications arise when the samples tested at different confining pressures have different porosities. This topic is addressed in Section 2.4.2.1.6.

2.4.2.1.4. Strain Rate Effects. In general, rocks tested at higher strain rates should have slightly higher compressive strengths (Paterson, 1978, p. 32). Within the range of strain rates of 10^{-2} to 10^{-7} s^{-1} , this trend has been observed in welded tuffs (Olsson and Jones, 1980;

Price et al., 1982; Nimick et al., 1985; Nimick et al., 1987). Although no data have been obtained for unit TSw1, experiments on samples of unit TSw2 from USW G-2 and USW G-4 suggests that strength will decrease 5 percent to 14 percent per order-of-magnitude decrease in strain rate, at least to strain rates of 10^{-7} s^{-1} (see Section 3.4.2.1.4).

Extrapolation of a linear relationship between compressive strength and strain rate to strain rates lower than 10^{-7} s^{-1} may or may not be valid. Costin (1983) has suggested that compressive strength may be constant below some threshold strain rate. This theory was shown by Costin (1983) to hold for other rock types. Planned experiments at strain rates of 10^{-8} s^{-1} and 10^{-9} s^{-1} may help to determine the nature of the strain-rate dependence at very low strain rates.

2.4.2.1.5 Sample Size Effects. Experimental data for other rock types indicate that compressive strength decreases with increasing sample size, at least up to some critical size beyond which compressive strength is a constant (Paterson, 1978, pp. 34-35). This trend has been confirmed for samples of unit TSw2. Test results are discussed in Section 3.4.2.1.5.

2.4.2.1.6 Porosity-Compressive Strength Relationships. Price (1983) analyzed the results of compression experiments on tuffs from Yucca Mountain and determined that an empirical relationship could be established between functional porosity (void volume plus clay volume) and compressive strength. Price's work was extended by Price and Bauer

(1984) to include additional experiment results. The resulting relationship is:

$$\sigma = 4.04 n^{-1.85} \quad (6)$$

where σ is the unconfined compressive strength in MPa and n is the functional porosity expressed as a volume fraction.

Equation (6) was derived using experiment results from small samples [diameters less than or equal to 5.0 cm (2.0 in.)]. Compressive strengths of the large lithophysae-rich samples in general are lower than those that would be predicted using Equation (6). The discrepancy is attributed by Price et al. (1985, p. 30) to the large ratio of inhomogeneity size to sample size.

Equation (6) may be used with porosity data for unit TSw1 to compare calculated compressive strengths with those actually measured. Data in Bish and Vaniman (1985) has been analyzed to provide the following clay contents: 0.071 ± 0.040 in USW G-2 and 0.004 ± 0.005 in USW GU-3 (Note that a standard deviation greater than a mean value is indicative of a non-normal distribution of data). In addition, the average clay content of unit TSw1 is 0.039 ± 0.041 , based on x-ray analyses of samples from USW G-2, USW GU-3, and USW G-4. This information is included with data from Tables 1 and 8 in the comparison of calculated and measured strengths.

Combining of matrix porosity data (Table 1) with the clay content data for USW G-2 yields a functional porosity of 0.197 ± 0.054 . Use of these values in Equation (6) provides estimated compressive strengths of 81.6 ± 41.4 MPa ($11,800 \pm 6,000$ psi). This range is lower than that given in Table 8. However, the eight mechanical experiment samples had matrix porosities of 0.061 ± 0.021 (Nimick et al., 1987). Using these values rather than the matrix porosity from Table 1 yields a functional porosity of 0.132 ± 0.045 and a compressive strength of 171.1 ± 107.9 MPa ($24,800 \pm 15,600$ psi). This estimated mean value is statistically indistinguishable from the mean value given in Table 8.

For USW GU-3, the functional porosity is 0.179 ± 0.028 . The compressive strength estimated using Equation (6) then is 97.4 ± 28.2 MPa ($14,100 \pm 4,100$ psi), somewhat higher than the equivalent value in Table 8. Sample-specific porosities are not available for the four samples from USW GU-3, so refinement of the comparison is not possible.

The relationship expressed as Equation (6) was derived from data for unconfined compressive strength. Intuitively, similar expressions should exist for compressive strength obtained under confining pressures. An analysis of the small number of data available has been performed (Appendix E); the results indicate that the pre-exponential "constant" in Equation (6) is in fact a function of confining pressure. In addition, both parameters in the Coulomb failure criterion can be related empirically to functional porosity:

$$\phi = \sin^{-1} \left(\frac{0.079n^{-1.856}}{2 + 0.079n^{-1.856}} \right) \quad (7)$$

and

$$\tau_o = 51.139 \tan \phi \quad (8)$$

where n is a volume fraction, ϕ is in degrees, and τ_o is in MPa. Use of the functional porosity for core holes USW G-2 and USW GU-3 in these two equations gives the results shown in Table 9.

2.4.2.2 Young's Modulus. After deletion of data for the two samples discussed in Section 2.4.2.1, data for Young's modulus from USW G-2 and USW GU-3 were compared using TTEST. The results showed a statistically significant difference ($P = 0.0019$), with material from USW G-2 having a higher mean value than material from USW GU-3. As with compressive strength, this relative ranking is consistent with the relative values of matrix porosity given in Table 1. Table 10 summarizes the data for Young's modulus for the individual core holes for which data are available. Grouping of all data into a single data set does not appear to be justified, so no values are given for unit TSw1 as a whole.

Material rich in lithophysae, however, has a much lower modulus than nonlithophysal material (Price et al., 1985). This behavior is attributed to the higher porosity of the lithophysae-rich tuffs. Following the thread of discussion in Section 2.4.2.1.1, any increase in porosity results in replacement of solid material (high modulus) with fluid (low

Table 9

Estimates of Mohr-Coulomb Parameters of Unit TSW1
Based on Functional Porosity

Core Hole	<u>Functional Porosity</u>		<u>Cohesion (MPa)^a</u>		<u>Angle of Internal Friction (°)</u>	
	Mean	St. Dev.	Mean	St. Dev.	Mean	St. Dev.
USW G-2	0.197	0.054	25.5	9.0	26.5	8.1
USW GU-3	0.179	0.028	28.8	5.6	29.4	4.8

^aTo obtain units of psi, divide by 6895.

Table 10
Young's Modulus^a of Unit TSw1

Core Hole	Young's Modulus(GPa) ^b		Number of Samples	95% Confidence Interval for Mean Value
	Mean	St. Dev.		
USW G-1	25.1	NA	1	NA
USW G-2	44.2	7.9	5	34.4 - 54.0
USW GU-3	18.6	2.7	3	11.9 - 25.3

^aValues obtained from experiments on saturated cylindrical samples [1 in. (2.54 cm) diameter, 2 in. (5.08 cm) length] at ambient temperature and pressure at a strain rate of $10^{-5}s^{-1}$.

^bTo obtain units of psi, divide by 6895.

NA Not available.

modulus), with the result of lowering the modulus of the composite material. This topic is discussed in more detail in the Section 2.4.2.2.6.

2.4.2.2.1 Saturation Effects. The state of saturation of the pores in a rock should influence the Young's modulus through the difference in the bulk moduli of air and water (0.0001 GPa (14.5 psi) and 2 GPa (0.3×10^6 psi), respectively, at atmospheric conditions). The bulk modulus of the welded tuff (K) can be calculated using 58.3 GPa (8.5×10^6 psi) as the bulk modulus of the zero-porosity material (Bauer, personal communication) and the following equations:

$$K = 58.3 (1 - \phi) + \phi K_f \quad (9)$$

$$\frac{1}{K} = \frac{1 - \phi}{58.3} + \frac{\phi}{K_f} \quad , \quad (10)$$

where K_f is the bulk modulus for the relevant fluid. It can be shown that Equation (9) gives an upper bound for the bulk modulus of the composite and Equation (10) gives a lower bound (cf., Price and Bauer, 1984, p. 91-92). Inserting the values for the bulk moduli and the average matrix porosity for unit TSw1 from Table 1 and averaging the results from the two equations for each fluid, estimates of the bulk moduli for dry and saturated rock are 25.1 GPa (3.6×10^6 psi) and 31.1 GPa (4.5×10^6 psi), respectively.

These values can then be used in an equation relating Young's modulus (E), bulk modulus, and Poisson's ratio (ν):

$$E = 3(1-2\nu)K \quad . \quad (11)$$

If ν is assumed to be independent of saturation, then the ratio of E_{dry} to E_{sat} should be identical to the ratio of K_{dry} to K_{sat} , which equals 0.8.

No experimental data are available to check the validity of this estimated ratio for unit TSwl. However, Olsson and Jones (1980) report the values of Young's moduli for the Grouse Canyon Member tested in the two saturation states. For strain rates ranging from 10^{-2} to 10^{-6} s^{-1} , the ratio $E_{\text{dry}}/E_{\text{sat}}$ ranged from 0.87 to 1.11. These values obviously do not agree with the estimated ratio. The discrepancy cannot be resolved until unit-specific data are available. Ongoing experiments should provide data for the Topopah Spring Member in the near future.

2.4.2.2.2 Temperature Effects. Lama and Vutukuri (1978, p. 80) provide a brief summary suggesting that temperature has very little, if any, effect on Young's modulus. Experiment results from Griggs et al. (1960) for granite show a marked lowering of the yield point with increasing temperature, but only a slight decrease in modulus.

Experimental data for the Topopah Spring Member are not available. Ongoing experiments will provide data for evaluation of temperature

effects; the results are expected to show little change in modulus for the temperature range 25° to 150°C (77° to 302°F).

2.4.2.2.3. Confining Pressure Effects. For most rock types, Young's modulus increases with confining pressure (Lama and Vutukuri, 1978, pp. 81-97). However, the influence is small for strong, low-porosity rocks.

The earliest experimental data for the Topopah Spring Member are given by Olsson and Jones (1980, p. 19). The experiment results indicate that Young's modulus remains nearly constant, independent of confining pressure. Later experiments (summarized by Nimick et al., 1985) also indicated that any relationship between Young's modulus of the Topopah Spring Member and confining pressure is obscured by sample variability, at least for the pressure range 0 to 10 MPa (0 to 1450 psi). Additional experiments are planned but the effect of confining pressure on modulus is not expected to be large.

2.4.2.2.4 Strain Rate Effects. Data from other rock types suggest that Young's modulus should increase with strain rate (Lama and Vutukuri, 1978, pp. 66-79). As with the effects of confining pressure, this increase is less for strong, low-porosity rocks.

Experimental data for the Grouse Canyon Member (Olsson and Jones, 1980) are equivocal. Average moduli for dry samples show no pattern with strain rate, whereas average moduli for saturated samples decrease as

strain rate increases. However, least-squares linear fits to the data give correlation coefficients that are too low to indicate the presence of any significant relationship for strain rates of 10^{-2} to 10^{-6} s^{-1} .

Experiment results for the Topopah Spring Member also show no significant relationship (Nimick et al., 1985), in this case for strain rates of 10^{-3} to 10^{-7} s^{-1} . Additional experiments at these and lower strain rates will provide more information with which to evaluate the relationship.

2.4.2.2.5. Sample Size Effects. As sample size increases, the number of inhomogeneities (i.e., preexisting fractures, lithophysae, etc.) should increase, although the number per unit volume should remain approximately constant. The influence of these features on Young's modulus will vary, depending on relative size, orientation, and abundance.

In a study summarized in Price (1986), cylindrical samples of welded devitrified material from unit TSw2 with diameters ranging from 2.54 cm (1.0 in.) to 22.86 cm (9.0 in.) were tested in compression. Resulting Young's moduli showed no relationship to sample size.

2.4.2.2.6. Porosity-Young's Modulus Relationship. Price (1983) originally established an empirical relationship between Young's modulus and functional porosity. With the availability of additional experimental data, the model was revised by Price and Bauer (1984) to the following form:

$$E = 85.5 e^{-6.96n} \quad (12)$$

where E is in GPa and n is a volume fraction.

Equation (12) was derived using experiment results from small [1 in. (2.54 cm) diameter] samples. Young's moduli of the large, lithophysae-rich samples in general are higher than those that would be predicted using Equation (12). The discrepancy is attributed by Price et al. (1985, p.30) to the presence of a stiffer matrix in these samples than is present in the sample of higher-porosity tuffs used to derive Equation (12).

Equation (12) may be used with functional porosity data for unit TSw1 to compare calculated Young's moduli with those actually measured. Using the same data for functional porosity discussed in Section 2.4.2.1.6 estimated moduli are 21.7 ± 8.2 GPa ($3.1 \times 10^6 \pm 1.2 \times 10^6$ psi) for USW G-2 and 24.6 ± 4.8 GPa ($3.6 \times 10^6 \pm 0.7 \times 10^6$ psi) for USW GU-3. The mean value for USW GU-3 is somewhat higher than that given in Table 10, but is probably not statistically different. The estimated mean value for USW G-2 is much lower than the mean value from measured data, probably because of the difference between the mean functional porosity for USW G-2 and the functional porosity of the test samples (0.132 ± 0.045). If the latter values are used in Equation (12), the estimated Young's modulus is 34.1 ± 10.7 GPa ($4.9 \times 10^6 \pm 1.6 \times 10^6$ psi), still lower than the value in Table 10, but much closer, especially when the relatively large standard deviations are considered.

2.4.2.3 Poisson's Ratio. Statistical analysis of Poisson's ratio data for unit TSw1 shows no differences resulting from comparison of core holes or testing laboratories. However, analysis of data for the Poisson's ratio of unit TSw2 (Section 3.4.2.3) indicates that data from TT are systematically higher than those for other testing laboratories. As a precaution against unwittingly biasing the data, no Poisson's ratios obtained at TT are used in subsequent discussion. The remaining two data points are used to calculate a mean value and standard deviation of 0.20 and 0.01, respectively. The 95% confidence interval for the mean value is 0.11 to 0.29; the width of the interval reflects the limited number of reliable data.

As is clear in Figure 5 of Price (1983, p. 34), the Poisson's ratio of tuffs is extremely variable even for the reference experiment conditions presented in Section 2.4.2.1. Any changes induced by variations in temperature, confining pressure, saturation, or strain rate are not expected to be significant relative to this initial variability.

Assignment of values of Poisson's ratio and Young's modulus to unit TSw1 assumes that the material deforms elastically. The relationship of axial stress and axial strain for tuffs is usually quite linear, supporting the hypothesis of elasticity. However, radial strain-axial strain and axial stress-volumetric strain relationships vary widely. Some are linear throughout an experiment, whereas others depart from linearity early in an experiment (i.e., at low stress levels).

The phenomenon responsible for this nonlinear behavior is known as dilatancy and is common in brittle rock. Dilatancy results from the opening of microcracks in a direction normal to the least principal compressive stress (Paterson, 1978, p. 119). When these microcracks begin to open, radial strain is greater than elastic deformation would permit. Also, because volumetric strain (ϵ_{vol}) is defined as

$$\epsilon_{vol} = \epsilon_{ax} + 2\epsilon_{rad} \quad (13)$$

for cylindrical samples, and ϵ_{rad} and ϵ_{ax} normally have opposite signs, ϵ_{vol} becomes less and less positive as dilatancy proceeds.

The stress at which dilatancy initiates is usually between one-third and two-thirds of the compressive strength (Paterson, 1978, p. 117). Nimick et al. (1987) analyzed data from compressive experiments on samples of units TSw1 and TSw2 from USW G-2 and estimated that dilatancy began at an average of 69 percent of the failure stress. (Note: the stress levels for which Young's modulus and Poisson's ratio are determined are always lower than the stress at which the axial stress-volumetric strain curve becomes nonlinear.

Confining pressure may cause a slight decrease in the magnitude of the dilatancy, as well as a decrease in the stress level at which dilatancy begins (Paterson, 1978, p. 116). Increased temperature and/or decreased strain rate will have the opposite effect, and saturated rocks will tend to show more dilatancy at lower stress than will dry rocks (Paterson, 1978, p. 116). Under repository conditions in which rocks are

partially saturated and are subjected to temperatures between 30° and 200°C (86° and 392°F) and initial confining pressures from 0 to 8 MPa (see Section 6.0 for in situ stress estimates), dilatant behavior is not expected to vary significantly from that observed for the USW G-2 samples.

In summary, the values provided for Poisson's ratio at the beginning of the section probably are valid only up to a stress level of approximately 70% of the expected failure stress. At greater stresses, the ratio of radial strain to axial strain will increase with increasing stress at rates depending on the rate of local microcracking. At present, numerical values cannot be assigned to this inelastic process.

2.4.2.4. Axial Strain at Failure.^{*} The strain (at failure) in the direction of the greatest principal stress is of interest because in some cases monitoring of deformation also may provide indications of rock stability. In addition, strain is more easily measured in situ than is stress. Statistical analysis of data for the axial strain at failure (ϵ_{ax}^f) for samples from unit TSw1 shows no difference resulting from comparison of core holes or testing laboratories. Thus, all data in Table B-3 (with the exception of those for the room-dry sample) are used to calculate a mean value and standard deviation of 4.47×10^{-3} and 0.99×10^{-3} , respectively. The 95% confidence interval for the mean value is 3.64×10^{-3} to 5.30×10^{-3} .

^{*}Failure for laboratory samples is taken to occur at the greatest axial stress sustained by the sample, regardless of the subsequent stress-strain behavior.

The effects of parametric variation on ϵ_{ax}^f may be estimated by combination of the effects on compressive strength (σ) and Young's modulus (E) because of the elastic relationship $\epsilon = \sigma/E$. Based on the discussions in Section 2.4.2.3, the Young's modulus of unit TSw1 is expected to be insensitive to all parameters except saturation state. For experiments in which the axial stress-axial strain relationship is linear up to the failure stress, changes in other parameters should cause ϵ_{ax}^f to have similar trends as compressive strength (i.e., increase with confining pressure and decrease with any one of increasing temperature, decreasing strain rate, or increasing sample size). Increasing sample saturation should cause compressive strength to decrease and Young's modulus to increase, so that ϵ_{ax}^f should show a marked decrease as saturation varies from 0.0 to 1.0.

Few data are available to test these expectations for the Topopah Spring Member. Experiments on samples from USW G-4 (Nimick et al., 1985) suggest that ϵ_{ax}^f indeed will decrease as strain rate decreases, although correlation coefficients for least-squares linear fits to the data suggest that the statistical significance of the trend lines is minimal. Price (1986) has determined that increasing sample size causes a decrease in ϵ_{ax}^f according to a power-law relationship.

2.4.3 Data from Tensile Experiments

All available experimental data for the tensile strength of unit TSw1 are for samples from UE-25a#1, as summarized by Blacic et al. (1982, p. 5). The "Brazilian" technique was used for all experiments. Results

from 20 experiments gave an average tensile strength of 21.1 MPa (3,060 psi), with a standard deviation of 4.6 MPa (670 psi). The 95% confidence interval for the mean value is 18.9 MPa (2,740 psi) to 23.3 MPa (3,380 psi).

Price (1983) determined that an empirical relationship exists between the tensile strengths (T_o) and porosity (P) given by Blacic et al. (1982) for all Yucca Mountain tuffs. The resulting equation is

$$T_o = 27.2 - 0.847 P \quad (14)$$

where T_o is in MPa and P is in percent. The line given by this equation is shown in Figure 17, together with a line delineating the average strength and the matrix porosity (mean value plus or minus one standard deviation). Equation (14) tends to underestimate the tensile strength of unit TSwl.

Some uncertainty exists as to whether results of the "Brazilian" technique represent the true uniaxial tensile strength of a material (e.g., Jaeger and Cook, 1979, pp. 169-173). Additional experiments are planned in which samples of the welded, devitrified Topopah Spring Member will be measured by the Brazilian indirect method as well as in direct tensile experiments.

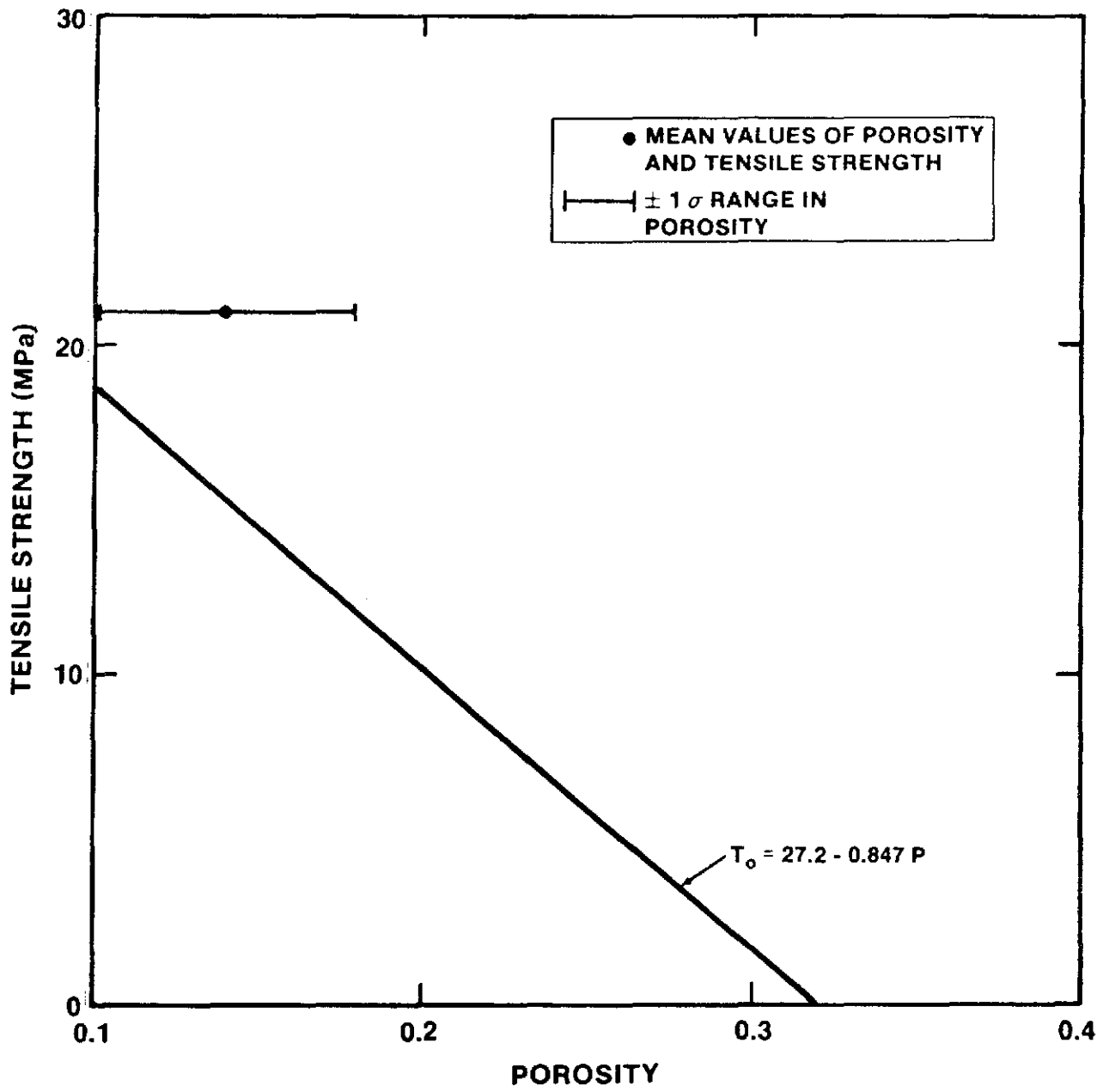


Figure 17. Relationship Between Porosity and Tensile Strength for Unit TSw1

3.0 THERMAL/MECHANICAL UNIT TSw2

3.1 Lithology and Geometry

In general, thermal/mechanical unit TSw2 is defined to be the lithophysae-poor portion of the welded, devitrified Topopah Spring Member. Ortiz et al. (1985, p. 11) state that the unit is composed of ashflows that "contain less than approximately 10 percent by volume lithophysal cavities." As discussed in Section 2.1, the selection of the 10 percent value is arbitrary but has been retained in this report for convenience.

The existing three-dimensional model of the thermal/mechanical units as presented by Ortiz et al. (1985) has been used to estimate the thickness variation of unit TSw2 within the repository area. The resulting isopach map is shown in Figure 18. The unit is thickest in the west-central portion of the repository area, thinning to the north, east, and southeast.

Unit TSw2 as depicted in Figure 18 has as its base the top of the basal vitrophyre (TSw3) as defined in the lithologic logs for the various core holes. However, data from Caporuscio et al. (1982) and Levy (1986) indicate that material in units TSw2 and TSw3 adjacent to the contact has been mildly to strongly altered. The result of this alteration varies between core holes. Rock in USW GU-3 is almost unaffected, whereas much of TSw3 in UE-25a#1 is not recognizable as vitrophyre. Material in the other three core holes falls between these extremes, showing a mixture of devitrified, vitric, and altered material in the upper portions of TSw3.

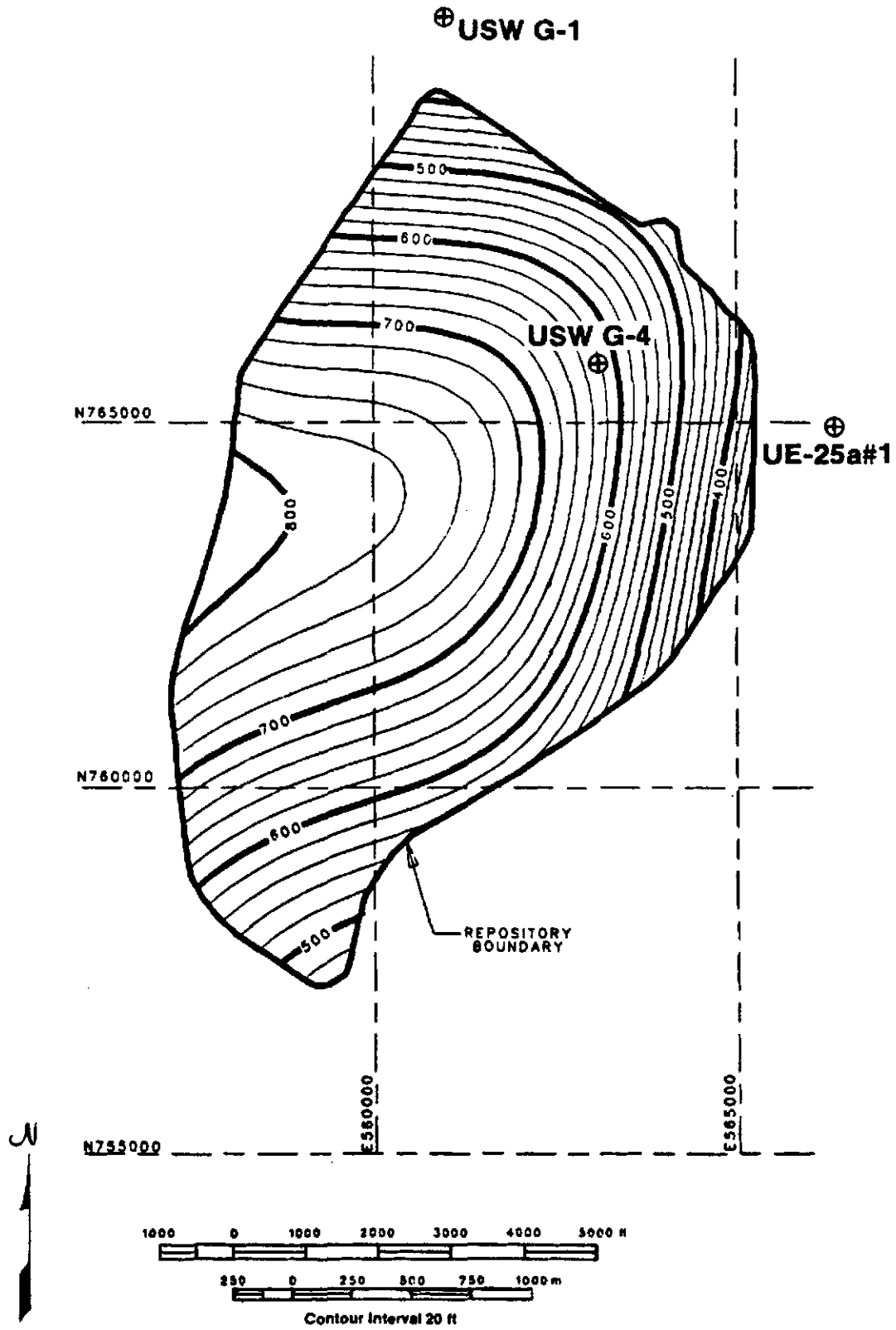


Figure 18. Isopach Map of Unit TSw2

Based on data in Caporuscio et al. (1982), Maldonado and Koether (1983, p. 63), and Levy (1986), the following depth intervals are considered to be part of neither TSw2 nor TSw3 in terms of statistical analysis of properties:

UE-25a#1: 1271.2-1297.4 ft (387.5-395.4 m)

USW G-1: 1286 ft (392.0 m)

USW G-2: 1634-1637 ft (498.0-499.0 m)

USW GU-3: Not applicable

USW G-4: 1293-1319.9 ft (394.1-402.3 m)

Discussion of the material present in the above-listed intervals is provided in Section 5.0.

3.2 Bulk Properties

3.2.1 Data

Measured bulk property data for unit TSw2 are tabulated in Appendix B (Table B-4). Data in Table B-4 have been measured by SNL, TT, USGS (Anderson, 1981, 1984), HN, and LANL (Blacic et al., 1982). Data for one sample from USW G-1 were obtained by either SNL, HN, or TT, but records do not indicate which one, so data for this sample are treated as though they had been measured by an entirely different laboratory.

Data for two samples (A1-1264.6 and A1-1266) listed in Table B-5 should be included with data for unit TSw3 if the contacts in Ortiz et al. (1985) are used to differentiate the units. However, the grain

densities of these samples are too high for vitric material. Data in Levy (1986) confirm that devitrified material is present in UE-25a#1 to a depth of 1271.2 ft (387.5 m) rather than the depth of 1262 ft (384.7 m) selected by Ortiz et al. (1985, p. 57). Thus, any data collected for samples from 1262 to 1271.2 ft (384.7 to 387.5 m) in UE-25a#1 are assigned to unit TSw2.

Data for 22 samples from an outcrop of unit TSw2 at Busted Butte are listed in Table B-4. These data have not been included in the statistical analysis because of uncertainties concerning exact location within the unit and concerning the possibility of overemphasizing a single portion of the unit within the total sample group.

3.2.2 Statistical Analysis and Discussion

Each of the three properties--porosity, grain density, and dry bulk density--was analyzed separately. However, no results are given for dry bulk density because of component variability, as discussed in Section 3.2.2.3.

3.2.2.1 Porosity. Statistical analysis of porosity with testing laboratory indicated a statistically significant difference only for the comparison of TT and HN for UE-25a#1. The P-values for all pair-wise comparisons are given below.

TT-USGS, USW G-4: 0.5057

USGS-HN, USW GU-3: 0.0533

TT-HN, USW GU-3: 0.8228
TT-USGS, USW GU-3: 0.0879
LANL-USGS, UE-25a#1: 0.3502
HN-USGS, UE-25a#1: 0.7501
TT-USGS, UE-25a#1: 0.1027
HN-LANL, UE-25a#1: 0.3317
TT-LANL, UE-25a#1: 0.1107 (unequal variances)
TT-HN, UE-25a#1: 0.0445 (unequal variances)

Because the vertical distribution of sampling in the core hole is not uniform for the two sets of samples for which a difference was found, and because porosity data obtained by TT and HN for USW GU-3 do not differ the difference has been assumed to be insignificant in the discussion that follows.

Two of the pair-wise comparisons were made by adjusting for unequal variances, as noted above. Because one of the assumptions necessary for the valid use of ANOVA or GLM is that all samples have the same variance, such techniques cannot be applied directly in a simultaneous analysis of the data from all testing laboratories.

All data for individual core holes were grouped, and the core-hole groups were compared. Statistically significant differences were found, as follows:

- mean porosity in USW G-1 greater than mean porosities in USW GU-3 and USW G-4 (P-values of 0.0391 and 0.0464, respectively)

- mean porosity in USW G-2 greater than mean porosity in USW GU-3
(P = 0.0221).

In view of these differences, summary data are provided in Table 11 for each core hole individually. P-values for pair-wise comparisons other than those mentioned above also are given in Table 11.

One of the pair-wise comparisons was made by adjusting for unequal variances, as noted in Table 11. Because one of the assumptions necessary for the valid use of ANOVA or GLM is that all samples have the same variance, such techniques cannot be applied directly in a simultaneous analysis of the data from all core holes.

The normality of porosity data was checked for each core hole individually and for unit TSw2 as a whole. The data for UE-25a#1 possibly have a negative lognormal distribution rather than a normal distribution, although the pattern is not carried over into the distribution for the unit as a whole. The data for USW G-4 suggest the presence of samples from two separate normally distributed populations. The explanation of this observation is not apparent.

Figures 19 through 23 illustrate the vertical variation of matrix porosity of unit TSw2 in the five core holes. Data from UE-25a#1, USW G-1, and USW G-2 are too sparsely distributed to infer correlations between porosity and ash-flow contents or lithophysal content. For USW GU-3 and USW G-4 (Figures 22 and 23), changes in porosity that are attributable to variations in lithophysal content are visible, but essentially no relationship to ash-flow contacts exists.

Table 11

Matrix Porosity of Unit TSw2

Core Hole	Porosity		Number of Samples	95% Confidence Interval for Mean Value
	Mean	St. Dev.		
UE-25a#1	0.109	0.028	21	0.096 - 0.122
USW G-1	0.129	0.021	7	0.110 - 0.148
USW G-2	0.130	0.035	13	0.109 - 0.151
USW GU-3	0.109	0.023	33	0.101 - 0.117
USW G-4	0.110	0.022	29	0.102 - 0.118
ALL CORE HOLES	0.113	0.026	103	0.108 - 0.118
Busted Butte	0.136	0.027	22	0.124 - 0.148

Pair	P-value
a#1, G-1	0.0968
a#1, G-2	0.0695
a#1, GU-3	0.9193
a#1, G-4	0.9058
G-1, G-2	0.9669
G-2, G-4	0.0833 (unequal variances)
GU-3, G-4	0.7897

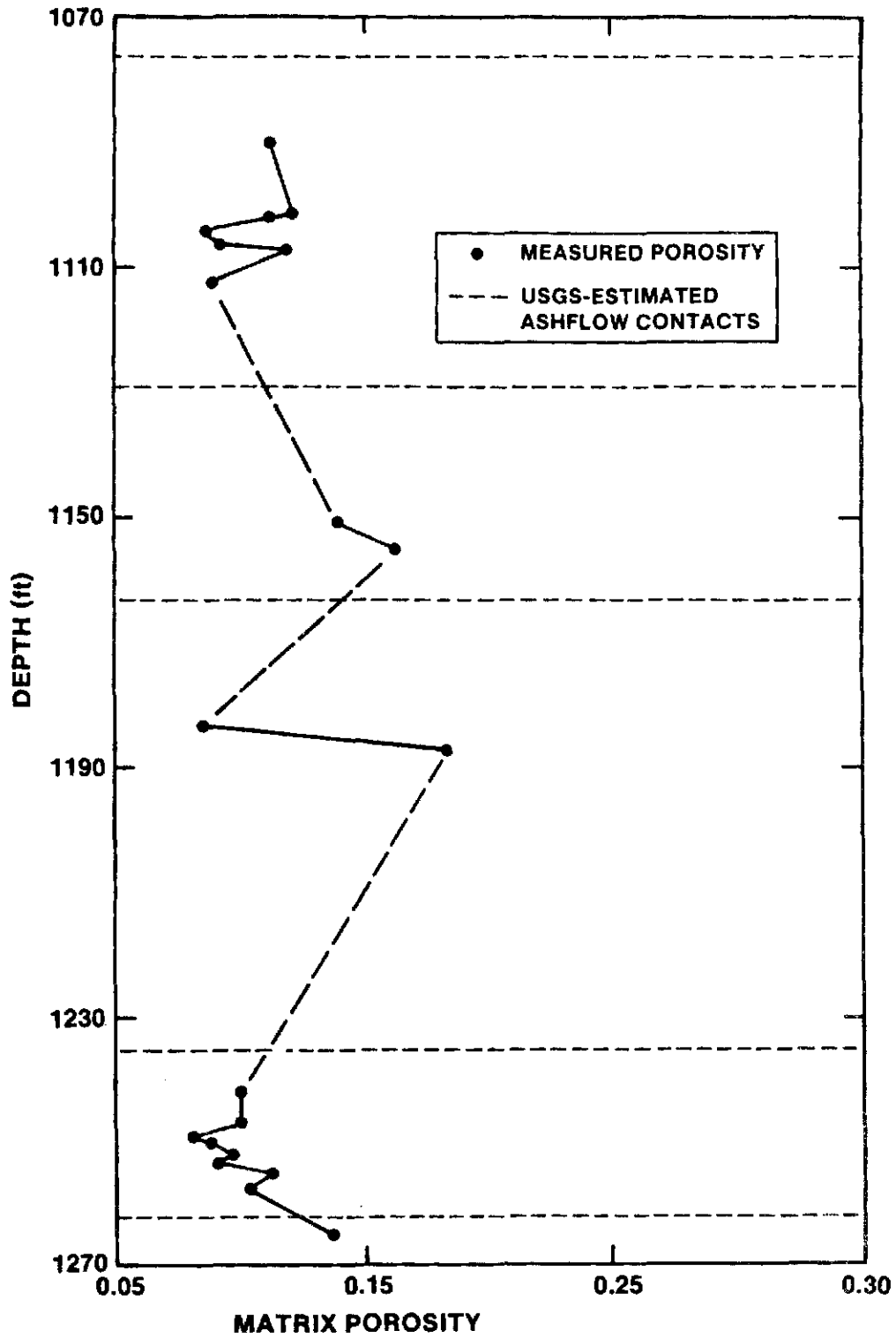


Figure 19. Vertical Variation of Matrix Porosity of Unit TSw2 in UE-25a#1. USGS-Estimated Contacts Taken From Spengler et al (1979).

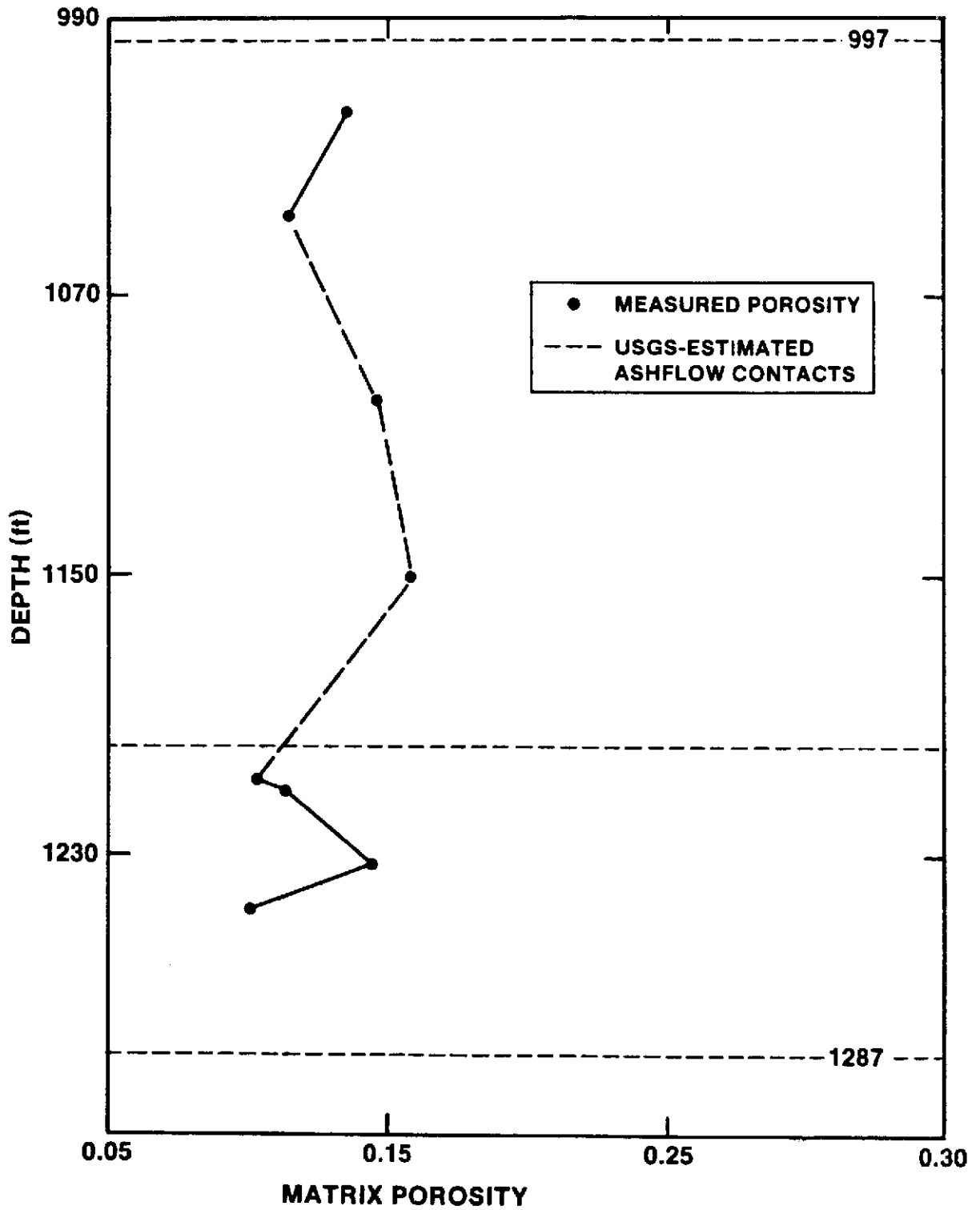


Figure 20. Vertical Variation of Matrix Porosity of Unit TSw2 in USW G-1. USGS-Estimated Contacts Taken From Spengler et al. (1981).

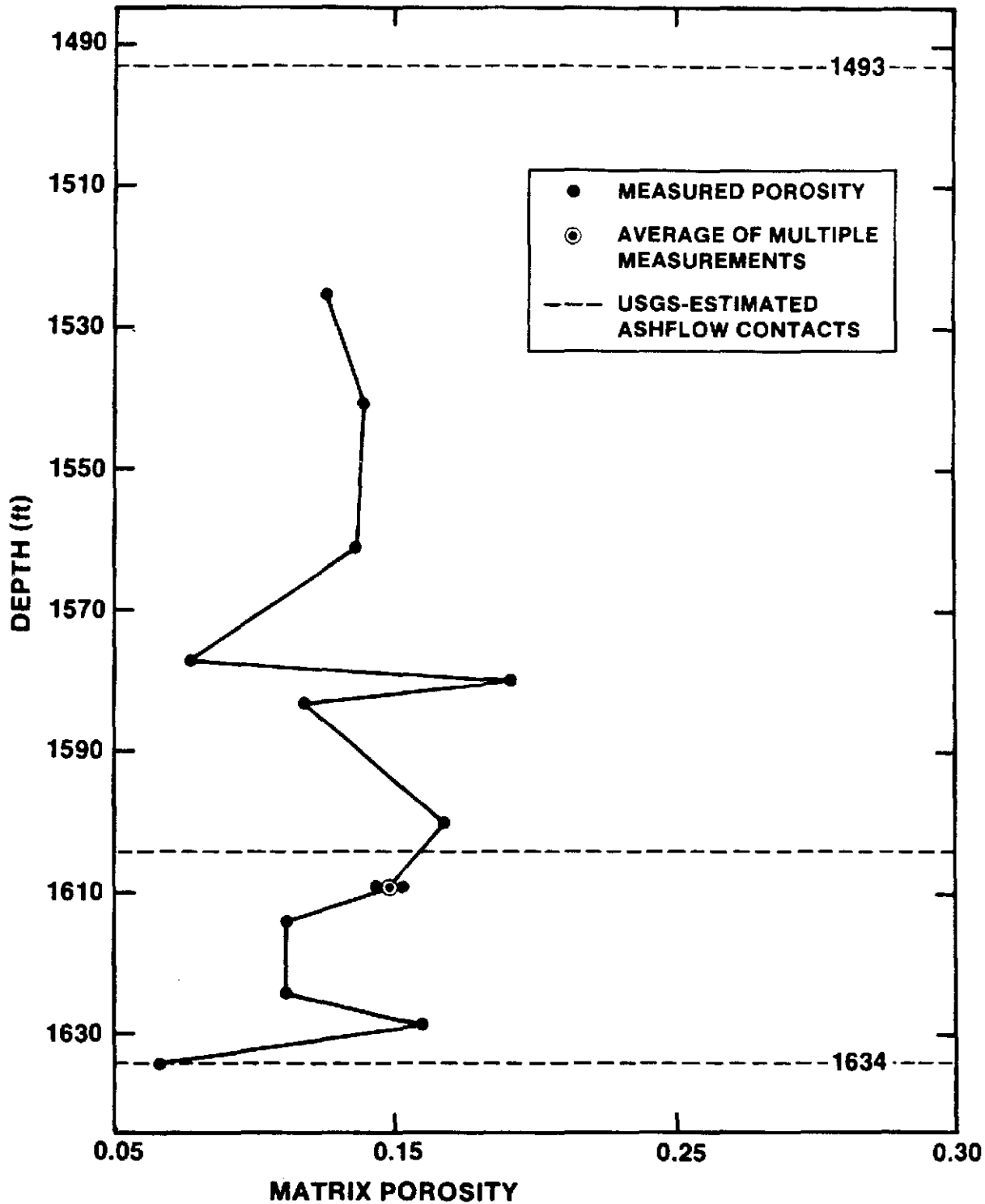


Figure 21. Vertical Variation of Matrix Porosity of Unit TSw2 in USW G-2. USGS-Estimated Contacts Taken From Maldonado and Koether (1983).

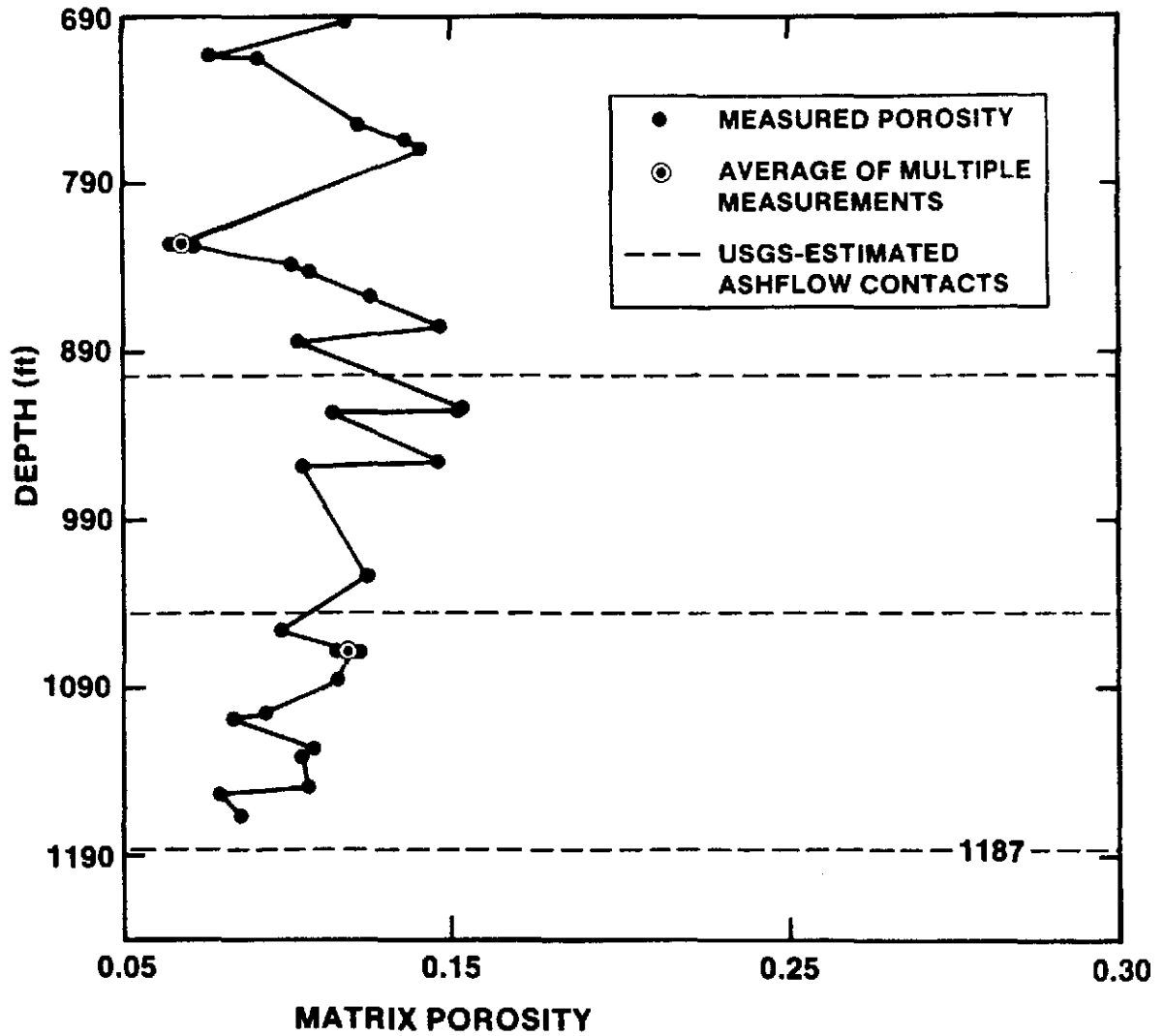


Figure 22. Vertical Variation of Matrix Porosity of Unit TSw2 in USW GU-3. USGS-Estimated Contacts Taken From Scott and Castellanos (1984).

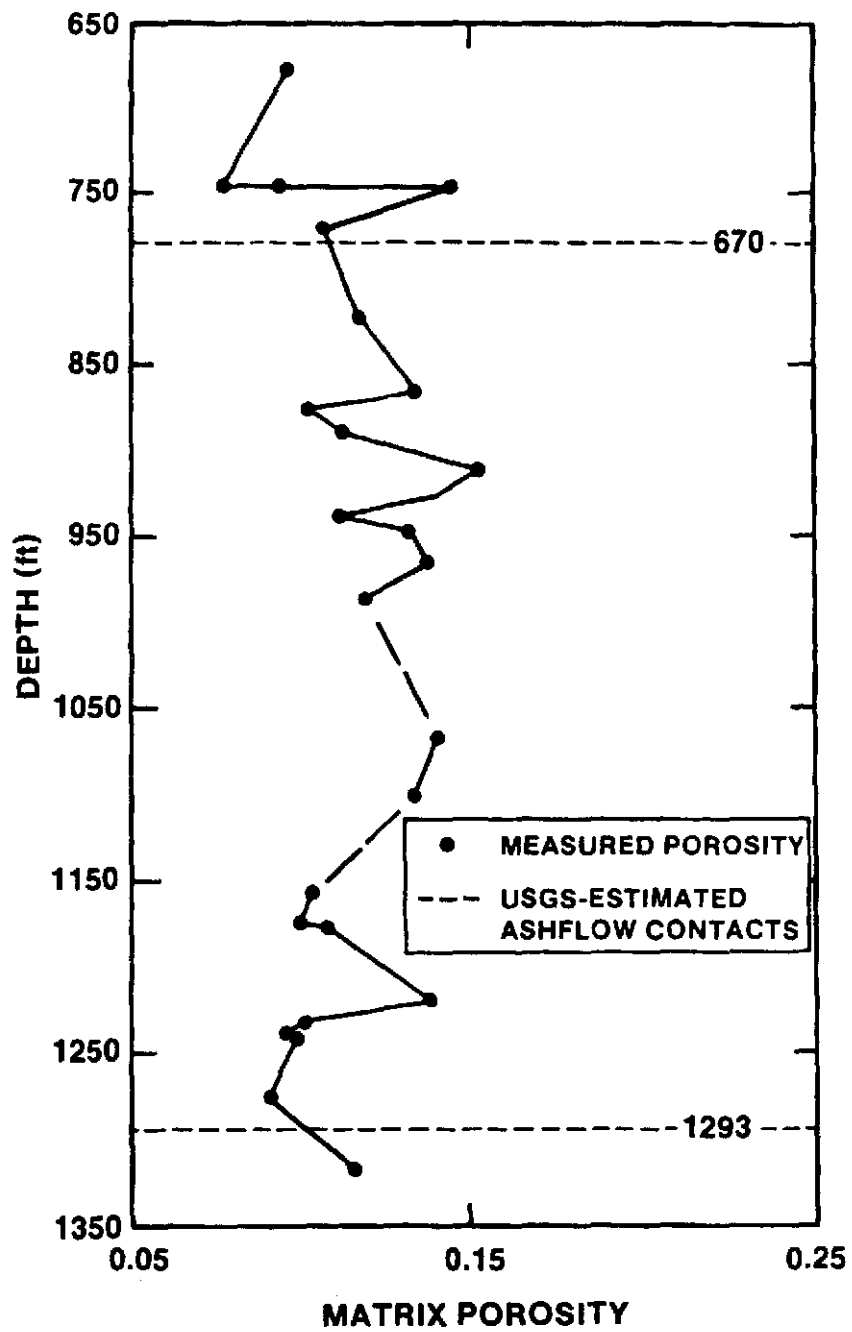


Figure 23. Vertical Variation of Matrix Porosity of Unit TSw2 in USW G-4. USGS-Estimated Contacts Taken From Spengler and Chornack (1984).

An interesting feature of Figures 22 and 23 is porosity variation in the two lowermost ashflows. The variability resulting from changes in the content of high-porosity vapor-phase-altered material (as determined by Spengler and Chornack, 1984) seems to be superimposed on a baseline porosity of 0.07 to 0.08. In USW GU-3, this observation applies to the depth interval from 884 ft to 1166 ft (269.4 to 355.4 m), and the corresponding interval in USW G-4 is 875 ft to 1317 ft (266.7 m to 401.4 m).

The mean value and standard deviation of matrix porosity of the 22 samples from Busted Butte are 0.136 and 0.027, respectively. The mean value is somewhat higher than that for data from core-hole samples (see Table 11). Comparison with data from the closest core hole (USW GU-3) suggest that the mean porosities are statistically different. The reason for the difference is not clear.

In addition to matrix porosity, void space is present in unit TSw2 as lithophysal cavities. The vertical distribution of these cavities differs in the four core holes for which data are available (Spengler and Chornack, 1984, p. 18). In USW G-1 and USW G-2, cavity percentages vary from 0 to 8 percent and are approximately evenly distributed throughout the unit. Cavities in USW GU-3 are concentrated in one interval from 900 to 1030 ft (274.3 to 313.9 m), with a maximum content of 5 percent. Up to 7 percent cavities occur in USW G-4, but cavities tend to be well-scattered and sparse. Table 12 contains data derived from Spengler and Chornack (1984) that approximate the actual distribution in the four core holes. No data are available for UE-25a#1.

Table 12

Abundance of Lithophysal Cavities in Unit TSw2

	Mean(%)	St. Dev.(%)	Range (%)	Depth Interval [ft(m)]
<u>USW G-1</u>				
	2.8	2.7	0.0-8.5	997-1200 (304-366)
	0.0	0.0	0.0	1200-1287 (366-392)
Overall	1.9	2.6	0.0-8.5	997-1287 (304-392)
<u>USW G-2</u>				
	2.9	2.4	0.0-6.0	1493-1634 (455-498)
<u>USW GU-3</u>				
	0.4	1.2	0.0-5.5	690-900 (210-274)
	1.8	1.8	0.0-6.0	900-1030 (274-314)
	0.0	0.0	0.0	1030-1187 (314-362)
Overall	0.6	1.4	0.0-6.0	690-1187 (210-362)
<u>USW G-4</u>				
	0.8	1.4	0.0-7.0	670-1090 (204-332)
	0.0	0.0	0.0	1090-1293 (332-394)
Overall	0.5	1.2	0.0-7.0	670-1293 (204-394)
Entire unit	1.0	1.9	0.0-8.5	NA
NA: Not applicable.				

3.2.2.2 Grain density. The analysis of variance of grain density with testing laboratory and core hole as independent variables indicates no significant differences. P-values for all pair-wise comparisons are given below.

TT-USGS, USW G-4: 0.9483
SNL-HN, USW GU-3: 0.7965
SNL-USGS, USW GU-3: 0.8429
SNL-TT, USW GU-3: 0.7560
USGS-HN, USW GU-3: 0.5330
TT-HN, USW GU-3: 0.4189
TT-USGS, USW GU-3: 0.7835
LANL-USGS, UE-25a#1: 1.0000
HN-USGS, UE-25a#1: 0.0565
TT-USGS, UE-25a#1: 0.2418
HN-LANL, UE-25a#1: 0.0665
TT-LANL, UE-25a#1: 0.2530
TT-HN, UE-25a#1: 0.1258

a#1, G-1: 0.0968
a#1, G-2: 0.9092 (unequal variances)
a#1, GU-3: 0.5882 (unequal variances)
a#1, G-4: 0.6139 (unequal variances)
G-1, G-2: 0.9280 (unequal variances)
G-1, GU-3: 0.6668 (unequal variances)
G-1, G-4: 0.7907
G-2, GU-3: 0.8539

G-2, G-4: 0.8708

GU-3, G-4: 0.9690

Treating all samples as originating from a single population results in calculated mean and standard deviation of 2.552 g/cm^3 (159.3 lb/ft^3) and 0.033 g/cm^3 (2.1 lb/ft^3), respectively. The 95% confidence interval for the mean value is 2.546 to 2.558 g/cm^3 (158.9 to 159.7 lb/ft^3). The data have a normal distribution.

Five of the pair-wise comparisons of data from different core holes were made by adjusting for unequal variances, as noted above. Because one of the assumptions necessary for the valid use of ANOVA or GLM is that all samples have the same variance, such techniques cannot be applied directly in a simultaneous analysis of the data from all core holes.

The mean value and standard deviation for the grain density of the 22 samples from Busted Butte are 2.61 g/cm^3 (162.9 lb/ft^3) and 0.03 g/cm^3 (1.9 lb/ft^3), respectively. These data are not only statistically different than those from the core hole samples, but only five of the core hole samples have grain densities as high or higher than 2.61 g/cm^3 (162.9 lb/ft^3). Assuming that no significant experimental error is involved, the higher grain densities for the Busted Butte samples are attributed to the relative scarcity of cristobalite and tridymite in these samples (Connolly, unpublished data, 1985) relative to other parts of unit TSw2.

3.2.2.3 Bulk density. Many measurements of bulk density have been made for unit TSw2, including saturated bulk density, "natural-state" bulk density, and dry bulk density. More measurements have been made for dry bulk density, and these are provided in Table B-4. However, neither these data nor any of the other measured bulk densities are applicable to in situ conditions in unit TSw2. There are two reasons for this. First, the mean in situ saturation of the matrix porosity is 0.65 (Montazer and Wilson, 1984, p. 13), a value perhaps approached for "natural-state" bulk density experiments but not for the other experiments. Secondly, these laboratory-measured bulk densities do not account for the presence of lithophysal cavities, which will tend to lower in situ bulk density. Because these cavities are less common in unit TSw2 than in unit TSw1, their effect on bulk density is less significant.

Use of Equations (1) and (2) with values of grain density, matrix porosity, lithophysal cavity abundance and saturation of matrix porosity allows the calculation of in situ densities. Values have been calculated for each core hole individually and for unit TSw2 as a whole, as summarized in Table 13.

3.3 Thermal Properties

3.3.1 Data

Measured data for the thermal expansion coefficient of unit TSw2 are tabulated in Appendix B (Table B-5). Table B-5 contains data measured by SNL (unconfined experiments) and by TT (confined experiments).

Table 13

Estimated Bulk Densities for Unit TSw2

Core Hole	Bulk Density (g/cm ³) ^a			
	Dry		"Natural-State" ^b	
	Mean	St. Dev.	Mean	St. Dev.
UE-25a#1 ^c	2.243	0.085	2.314	0.073
USW G-1	2.174	0.090	2.258	0.086
USW G-2	2.146	0.112	2.231	0.098
USW GU-3	2.259	0.075	2.329	0.067
USW G-4	2.259	0.070	2.330	0.063
ALL	2.238	0.087	2.312	0.078

^aTo obtain densities in lb/ft³, multiply by 62.43.

^bAssuming that in situ saturation is 0.65 in matrix porosity.

^cAssuming that mean lithophysal cavity abundance is 1.2% (average of values for USW G-1 and USW G-4) and standard deviation is 1.4%.

3.3.2 Statistical Analysis and Discussion

Thermal expansion coefficients have been analyzed using the TTEST and GLM procedures. Results and discussion thereof are contained in Section 3.3.2.1. In addition, brief discussions of the heat capacity and emissivity of unit TSw2 are presented in Sections 3.3.2.2 and 3.3.2.3, respectively.

3.3.2.1 Thermal Expansion. Three of the five core holes are represented in the nine samples on which thermal expansion measurements were made under confining pressure (Table B-5). Analysis of the resulting data using the GLM procedure suggested statistically significant differences for coefficients of thermal expansion for the following temperature ranges: 150° to 200°C (302° to 392°F) and 25° to 200°C (77° to 392°F). For both temperature ranges, the mean coefficient is highest for samples from USW G-4 and lowest for USW GU-3, with an intermediate value from USW G-2. Discussion of the differences is contained in the following paragraphs, but should be tempered by the fact that very few data are available and the differences may change as more data are gathered.

At temperatures above 150°C (302°F), the mineral phases that dominate thermal expansion behavior in the welded portion of the Topopah Spring Member are cristobalite and tridymite. Mineralogic data reported by Bish and Vaniman (1985, pp. 17-23) are consistent with the observed thermal expansion coefficients. Tridymite, the phase that undergoes polymorphic inversion beginning at approximately 160°C (320°F) (Nimick, in

preparation, a), is reported at a depth of 694 ft (212 m) in USW G-4, but not at any other depth close to the thermal expansion samples under discussion. Presumably Sample G4-737.9 also contains some tridymite, the inversion of which is responsible for the high coefficient relative to the other two core holes.

The different thermal expansion coefficients for samples from USW G-2 and USW GU-3 appear to be the result of different quantities of cristobalite. Mineralogic data for samples from depths similar to those from which thermal expansion samples were taken indicate that cristobalite abundance in USW G-2 is approximately three times that in USW GU-3. Because cristobalite begins to undergo a polymorphic inversion at 180°C (356°F) (Nimick, in preparation, a), samples containing more cristobalite would be expected to exhibit more thermal expansion in the temperature range from 150° to 200°C (302° and 392°F), as is observed.

Because of the limited number of data, the differences between core holes was ignored, and all data collected under confining pressure were grouped into a single data set. This data set has a normal distribution.

The thermal expansion data from unconfined tests were analyzed in two stages. The first analysis examined the samples from UE-25a#1. These samples were part of a larger program, the goal of which was to determine whether long-term exposure ("soaking") at elevated pressures and temperatures affected the material properties of tuff (Blacic et al., 1982; 1986). Thermal expansion experiments were performed on both wet and dry samples before and after soaking for 2.5 to 6 months.

Statistical comparison of the data for pre-soak experiments with data for post-soak experiments indicates that the soaking had no significant effect on mean thermal expansion for saturated samples, a conclusion similar to that of Blacic et al. (1986). P-values for pair-wise comparisons are given below.

Temperature Range [°C (°F)]	Pair	P-value
25-50 (77-122)	pre-soak	0.1357
50-100 (122-212)	vs post-soak,	0.8291
100-150 (212-302)	saturated	0.6889
150-200 (302-392)	"	0.6767
200-250 (392-482)	"	0.8558
250-300 (482-572)	"	0.7772
25-100 (77-212)	"	0.3492
25-150 (77-302)	"	0.3261
25-200 (77-392)	"	0.4726
25-250 (77-482)	"	0.6952
25-300 (77-572)	"	0.9243

25-50 (77-122)	saturated	0.0380
50-100 (122-212)	vs. dry	0.3824 (unequal variances)
100-150 (212-302)	"	0.5011
150-200 (302-392)	"	0.4700
200-250 (392-482)	"	0.2538
250-300 (482-572)	"	0.2415
25-100 (77-212)	"	0.3286 (unequal variances)
25-150 (77-302)	"	0.0297
25-200 (77-392)	"	0.0889
25-250 (77-482)	"	0.2517
25-300 (77-572)	"	0.6237

Two of the pair-wise comparisons were made by adjusting for unequal variances, as noted above. This fact should not cause any difficulties in future analyses because the pairs of concern are not involved in more general analyses as samples that are assumed to have equal variances.

Given the results described in the preceding paragraph, and because the seven samples from the 1122.7-ft (342.2-m) depth in UE-25a#1 were chosen to be as similar as possible, the data from the five saturated samples have been averaged to provide a single set of thermal expansion coefficients. In this way, comparison of data from UE-25a#1 with that from USW G-1 was not biased by overemphasizing the material chosen for the soak experiments.

No statistical comparison of data from UE-25a#1 and USW G-1 has been made because only one "sample" is available from UE-25a#1. Examination of the data in Table B-5 for unconfined experiments suggests that the data from UE-25a#1 may be different from those from USW G-1 for the higher temperature ranges. The lower thermal expansion of material from UE-25a#1 at temperatures above 150°C (302°F) is probably the result of lower tridymite abundances in UE-25a#1 (Bish and Vaniman, 1985, pp. 35-37).

Comparison of results from confined and unconfined experiments has been made, although the results must be tempered by the fact that no samples from a single core hole were tested in both conditions. The comparison indicates significant differences for all temperature ranges except 150° to 200°C (302° to 392°F). The P-values for the comparisons are given below.

Temperature Range [°C (°F)]	Pair	P-value
25-50 (77-122)	Confined vs.	0.0006 (unequal variances)
50-100 (122-212)	unconfined	0.0044
100-150 (212-302)	"	0.0006
150-200 (302-392)	"	0.3247 (unequal variances)
25-100 (77-212)	"	0.0010 (unequal variances)
25-150 (77-302)	"	0.0158
25-200 (77-392)	"	0.0321

Three of the pair-wise comparisons were made by adjusting for unequal variances, as noted above. This fact should not cause any difficulties in future analyses because the pairs of concern are not involved in more general analyses as samples that are assumed to have equal variances.

In all cases but one, thermal expansion coefficients are higher when obtained from experiments conducted with confining pressure. The exception is for 100° to 150°C (212° to 302°F). As discussed in Section 2.3.2.2, higher expansion coefficients under confining pressure is consistent with the partial closing of preexisting microcracks by the confining pressure of 10 MPa (1450 psi).

Table 14 contains mean values and standard deviations for expansion coefficients obtained in both confined and unconfined experiments. As was done for unit TSwl, all data for temperature intervals ranging above 100°C (212°F) are combined into a single data set. All data groups for the thermal expansion have a normal distribution.

The coefficients are translated into temperature-strain curves in Figure 24. For low temperatures [up to 100°C (212°F)] both sets of coefficients are presented because both may be pertinent to

Table 14

Summary of Linear Thermal Expansion Coefficients^a for Unit TSw2

	Temperature Range						
	°C	25-50	50-100	100-150	150-200	200-250	250-300
	°F	77-122	122-212	212-302	302-392	392-482	482-572
<u>Unconfined</u>							
Mean		2.5	7.5	9.2	13.1	20.6	36.7
St. Dev.		3.6	1.2	1.3	2.1	4.7	10.4
#Samples		7	7	14	11	7	7
<u>Confined</u>							
Mean		10.7	9.8	b	b	b	b
St. Dev.		1.2	1.3	b	b	b	b
#Samples		7	8	b	b	b	b

^aUnits are $10^{-6} \text{ } ^\circ\text{C}^{-1}$; to obtain units of $10^{-6} \text{ } ^\circ\text{F}^{-1}$, multiply by 5/9.

^bData obtained for unconfined conditions apply to both unconfined and confined experiment results.

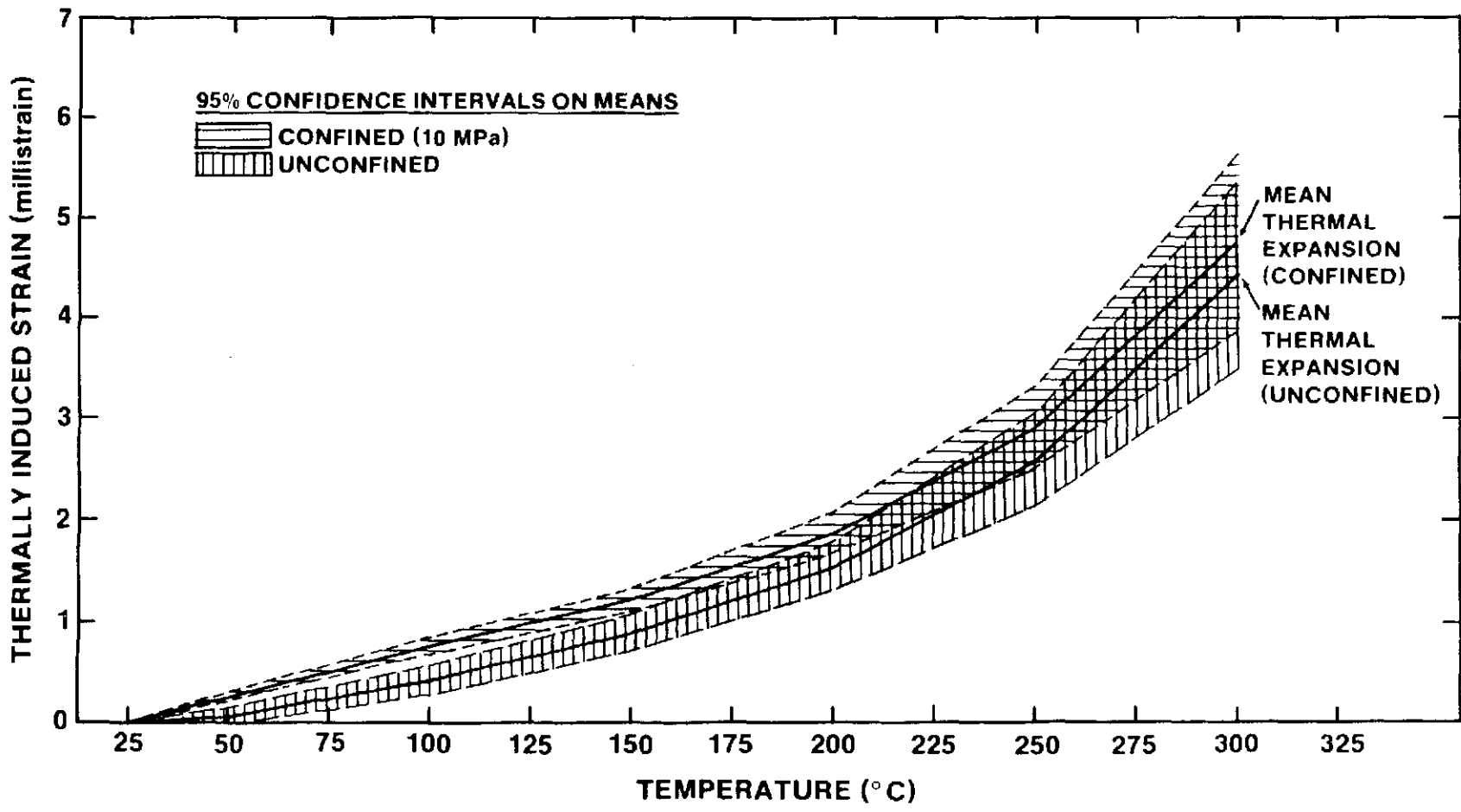


Figure 24. Thermal Expansion Behavior of Confined and Unconfined Samples of Unit TSw2

thermomechanical calculations. In rock near underground openings, at least one of the principal stresses may be sufficiently low that the rock may be considered to be unconfined in one or more directions. Farther from openings, the data taken under confining pressure may be more appropriate.

Data for temperatures above 200°C (392°F) are available only from unconfined experiments. Because the effect of preexisting microcracks should be negligible at these higher temperatures (see Section 2.3.2.2), the coefficients are believed to be representative of both experiment conditions. As such they are included on Figure 24 for both curves.

3.3.2.2. Heat Capacity. As discussed in Section 2.3.2.3, the heat capacity of the solid material is assumed to be the same for units TSw1 and TSw2. Thus, the data provided in Table 6 and Figure 15 are applicable to unit TSw2. Estimates for in situ volumetric heat capacity can be obtained in the same manner as that used for unit TSw1. The results are given in Table 15 and in Figure 25. The estimates do not include the enthalpy of boiling for the pore water.

3.3.2.3. Emissivity. Data on the emissivity of welded, devitrified tuff is summarized in Section 2.3.2.4. A value of 0.89 has been adopted for this lithology in the Topopah Spring Member.

Table 15
Estimated^a In Situ Volumetric Heat Capacity^b of Unit TSW2

		<u>Temperature</u>								
		°C	25	50	99	101	150	200	250	300
		°F	77	122	210	214	302	392	482	572
		<u>UE-25a#1</u>								
Mean		2.023	2.119	2.267	1.987	2.111	2.218	2.313	2.399	
St. Dev.		0.096	0.095	0.094	0.076	0.080	0.084	0.088	0.091	
		<u>USW G-1</u>								
Mean		2.024	2.116	2.259	1.926	2.046	2.150	2.241	2.325	
St. Dev.		0.117	0.118	0.118	0.080	0.085	0.089	0.093	0.096	
		<u>USW G-2</u>								
Mean		2.005	2.096	2.237	1.901	2.019	2.122	2.213	2.295	
St. Dev.		0.118	0.118	0.117	0.099	0.105	0.111	0.115	0.120	
		<u>USW G-3</u>								
Mean		2.035	2.131	2.281	2.000	2.125	2.233	2.328	2.415	
St. Dev.		0.095	0.095	0.094	0.066	0.071	0.074	0.077	0.080	
		<u>USW G-4</u>								
Mean		2.038	2.134	2.283	2.000	2.125	2.233	2.328	2.415	
St. Dev.		0.095	0.094	0.093	0.063	0.066	0.070	0.073	0.075	
		<u>Average for Entire Unit</u>								
Mean		2.030	2.125	2.273	1.982	2.106	2.213	2.307	2.393	
St. Dev.		0.102	0.101	0.101	0.077	0.082	0.086	0.090	0.093	

^aEquation (4) used with data for $C_p^{H_2O}$ and ρ_{H_2O} listed in Table 7.

^bUnits are J/cm³k; to obtain Btu/ft³°F, multiply by 14.911.

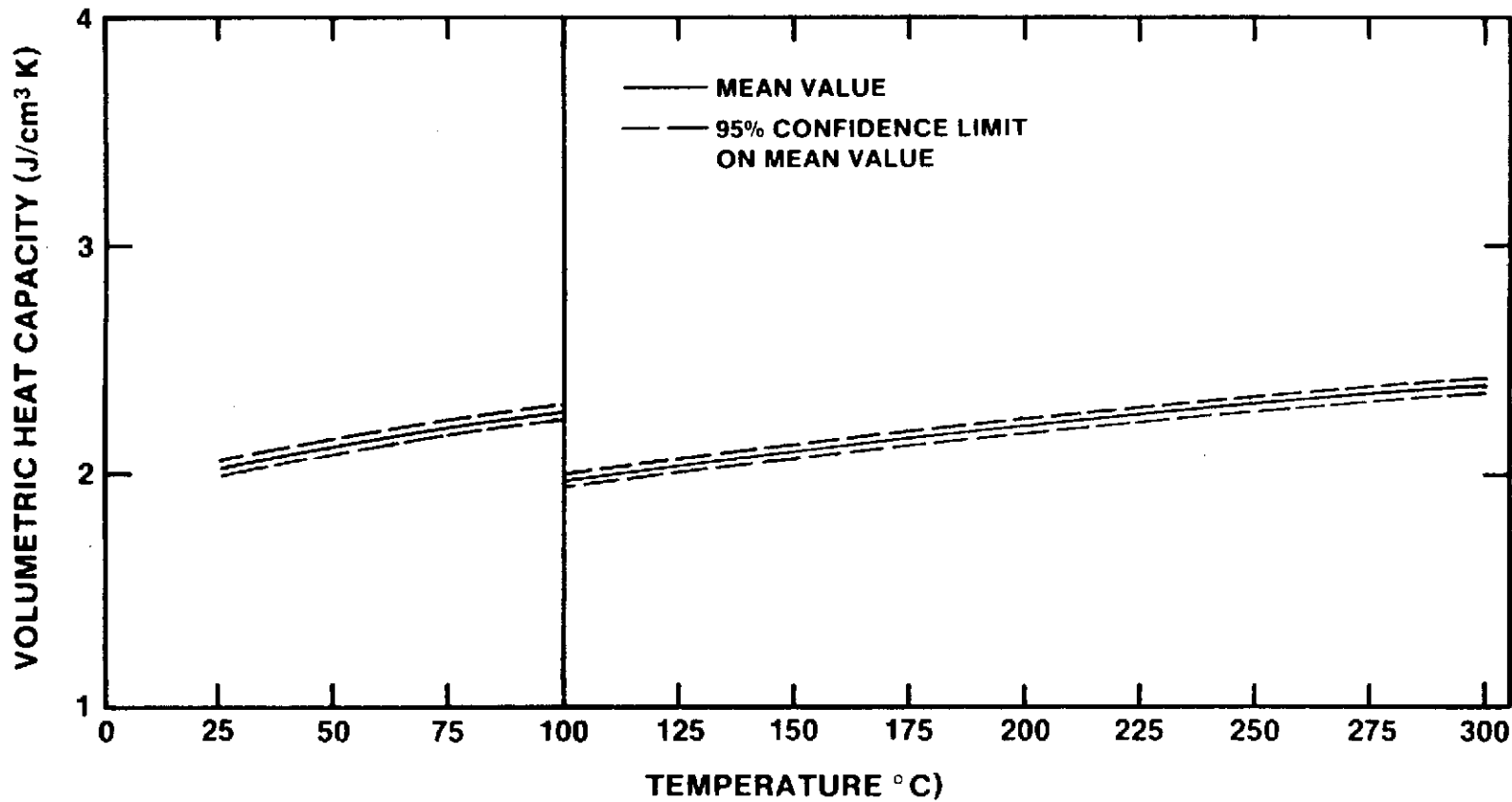


Figure 25. Estimated Average Values of In Situ Volumetric Heat Capacity of Unit TSw2 as a Function of Temperature

3.4 Mechanical Properties

3.4.1 Data from Compressive Experiments

Measured data for the mechanical properties determined in compression of samples of unit TSw2 are summarized in Table B-6. All data in the table were obtained from samples derived from core [i.e., sample diameters are all ≤ 5.08 cm (2.00 in)]. Additional measurements have been made on larger samples taken from outcrop material. Experiment results for these samples are discussed in Sections 3.4.2.1.5, 3.4.2.2.5, 3.4.2.3, and 3.4.2.4.

3.4.2 Statistical Analysis and Discussion

The data in Table B-6 were analyzed using the TTEST and GLM procedures. As was done for other properties, multiple samples from one depth in a given core hole were grouped to avoid over-emphasis of one depth interval.

Samples from a single core hole were tested at more than one laboratory only for USW G-4. Comparison of the experiment results for USW G-4 indicates that data on compressive strength, Young's modulus, and axial strain at failure are not statistically different (P-values of 0.9253, 0.9332, and 0.7520 respectively), but that data on Poisson's ratio differ between SNL and TT (P = 0.0303, with unequal variances). This difference is discussed in more detail in Section 3.4.2.3.

Assuming that all three testing laboratories are producing similar results, interhole comparisons can be made. The initial results of such a comparison indicated that, in general, the mechanical properties of unit TSw2 did not differ between core holes. The two differences that were found are discussed in later sections.

One column in Table B-6 provides the saturation states of experiment samples before testing. Considerations discussed in Appendix C indicate that saturation by immersion alone ($s = 0.75$) should not result in any difference in compressive strength relative to saturation by immersion and application of a vacuum ($s = 0.95$). In contrast, room-dry saturation state ($s \approx 0.12$) probably will cause a difference. Therefore, the single room-dry sample in Table B-6 has been excluded from the statistical analysis.

3.4.2.1 Compressive Strength. Statistical analysis of unconfined compressive strength data for unit TSw2 shows a difference only between data from USW G-1 and USW G-4, with the latter having a greater mean value. The P-values for all pair-wise comparisons are given below.

G-4, GU-3: 0.7553

G-4, G-2: 0.2073

G-2, GU-3: 0.4036

G-1, GU-3: 0.1132

G-1, G-2: 0.3999

G-1, G-4: 0.0318

Only four data values are available from USW G-1; in view of this limited sample, the difference is ignored for the present analysis. Thus, all data in Table B-6 (with the exception of the room-dry sample data) are used to calculate a mean value and standard deviation of 147.9 MPa (21,500 psi) and 57.1 MPa (8,300 psi). The 95% confidence interval for the mean value is 121.2 to 174.6 MPa (17,600 to 25,300 psi).

These values represent the compressive strength to be expected for saturated material at ambient temperature and pressure for a strain rate of 10^{-5} s^{-1} and a cylindrical sample size of 2.54 cm by 5.08 cm (1 in. by 2 in.). In addition, the material itself is nominally free of any significant inhomogeneities (i.e., lithophysal cavities or preexisting fractures). The following subsections assess the impact of changes in test parameters on the compressive strength.

3.4.2.1.1. Saturation Effects. As indicated in Appendix C, compressive strength is expected to increase by 20 percent to 40 percent in dry samples relative to saturated samples. This expectation is based on experimental results in other rock types as well as on data from the welded tuff of the Grouse Canyon Member of the Belted Range tuff. Unit-specific data are insufficient to confirm or reject the hypothesis for unit TSw2. Additional experiments are planned to obtain data on saturation effects on the mechanical properties of the welded, devitrified portion of the Topopah Spring Member.

3.4.2.1.2. Temperature Effects. No experimental data are available on the effect of elevated temperature on the compressive strength of unit

TSw2. Experiments in other rock types suggest that elevated temperatures have little effect on the brittle fracture of rock (Paterson, 1978, p. 29), as long as the mechanism of failure does not change. This result is to be expected in dry rocks (i.e., samples from which water is removed by dehydration at temperatures lower than experiment temperatures). However, if pressure conditions are such that the rock remains at least partially saturated at the experiment temperatures, the elevated temperature may increase the rate or intensity of any chemical interactions between the pore water and the solid framework. If this process of chemomechanical weakening occurred, the coupled interaction of temperature and saturation might decrease the strength more than would be expected as a result of changes in either parameter alone. Experiments are planned to determine the importance of this possibility in the analysis of the compressive strength of the welded devitrified portion of the Topopah Spring Member.

3.4.2.1.3. Confining Pressure Effects. In general, the application of a confining pressure during a compressive experiment increases the strength of a material (e.g., Paterson, 1978, p. 24). The relationship between the strength ($\sigma_1 - \sigma_3$) and the confining pressure (σ_3) can be represented by either linear or nonlinear equations, as discussed in Section 2.4.2.1.3. In the past, the Coulomb criterion has been used for tuffs because of its simplicity (Olsson and Jones, 1980; Price, 1983). Even using this linear relationship [Equation (5)], however, complications arise when the samples tested at different confining pressures have different porosities. This topic is addressed in Section 3.4.2.1.6.

Existing data taken at different confining pressures are summarized in Table 16. Compressive strength as a function of confining pressure is shown in Figure 26. Compressive strength varies more at any given confining pressure than it does between two different confining pressures. If the data at a confining pressure of 5 MPa (725 psi) (two samples) are ignored, the mean strength increases with confining pressure. However, the wide variability of the data (a linear regression of strength on confining pressure gives $r^2=0.0502$) indicates the necessity for obtaining many more data points than were available for this analysis before drawing conclusions about the validity of any particular failure criterion or calculating values for failure parameters.

3.4.2.1.4. Strain Rate Effects. In general, rocks tested at higher strain rates should have slightly higher compressive strengths (Paterson, 1978, p. 32). Within the range of strain rates of 10^{-2} to 10^{-7} s^{-1} , this trend has been observed in welded tuffs (Olsson and Jones, 1980; Price et al., 1982; Nimick et al., 1985, Nimick et al., 1987).

Relevant experiment data for unit TSw2 are summarized in Table 17 and are plotted in Figure 27. Also shown on the figure are best-fit lines for each sample set calculated by the method of least squares. The slopes of these lines correspond to decreases ranging from 5 percent to 14 percent per order-of-magnitude decrease in strain rate.

Extrapolation of a linear relationship between compressive strength and strain rate to strain rates lower than 10^{-7} s^{-1} may or may not be valid. Costin (1983) has suggested that compressive strength may be

Table 16

Mechanical Properties of Unit TSw2 as a Function of Confining Pressure

Sample ID Number	Confining Pressure (MPa) ^d	Compressive Strength (MPa) ^d	Young's Modulus (GPa) ^d	Poisson's Ratio	Axial Strain at Failure (milli)	
A1-1250 ^a	0	166	61.8	0.30	NA	
	10	412	73.0	0.23	NA	
	20	618	59.9	0.21	NA	
G4-686.6 ^b	0	270	36.2	0.18	8.7	
	0	326	40.7	0.17	10.0	
	0	180	33.1	0.21	6.4	
	5	156	40.5	0.16	13.3	
	5	87	43.6	0.30	1.8	
	10	344	38.0	0.23	10.8	
G4-964.2 ^b	10	360	35.0	0.25	11.8	
	0	187	38.0	0.21	5.6	
	0	131	31.1	0.18	4.4	
	0	148	33.1	0.19	6.0	
	10	97	14.1	0.21	11.0	
10-AE-15Z ^c	10	247	32.7	0.28	9.6	
	0	158	37.4	0.20	NA	
	-47Y ^c	0	143	36.2	0.20	NA
	-12X ^c	0	127	34.8	0.21	NA
	-6X ^c	0	107	28.6	0.14	NA
	-8X ^c	0	62	21.7	0.11	NA
	-3Y ^c	0	54	18.6	0.07	NA
	-9Z ^c	0	153	31.5	0.20	NA
	-46Z ^c	0	143	34.2	0.18	NA
	-2Z ^c	0	109	28.7	0.17	NA
	-20Z ^c	10	193	33.0	0.18	NA
	-12Z ^c	10	186	32.0	0.19	NA
	-3Z ^c	10	153	NA	NA	NA
	-42X ^c	10	152	35.5	0.19	NA
	-15Y ^c	10	117	30.5	0.18	NA
	-14Y ^c	10	220	33.0	0.14	NA
	-12Y ^c	10	182	29.7	0.15	NA
	-8Y ^c	10	40	21.7	0.11	NA
	-10Y ^c	10	181	30.8	0.19	NA
	-18Z ^c	10	161	28.1	0.12	NA
-26W ^c	10	105	32.7	0.21	NA	

Table 16 (concluded)

Mechanical Properties of Unit TSw2 as a Function of Confining Pressure

Sample ID Number	Confining Pressure (MPa) ^d	Compressive Strength (MPa) ^d	Young's Modulus (GPa) ^d	Poisson's Ratio	Axial Strain at Failure (milli)
10-AE-15W ^c	20	252	31.5	0.15	NA
-47Z ^c	20	156	19.8	0.20	NA
-9W ^c	20	212	29.6	0.20	NA
-15X ^c	20	192	28.4	0.16	NA
-42W ^c	20	160	31.2	0.21	NA

^a_c = 10⁻⁴ s⁻¹, room-dry (Olsson and Jones, 1980).

^b_c = 10⁻⁵ s⁻¹, saturated, drained (Nimick et al., 1985).

^c_c = 10⁻⁵ s⁻¹, Busted Butte samples, saturated, drained
(Nimick et al., 1987).

^dTo obtain units of psi, multiply by 1.45 x 10⁻⁴.

NA: Not available.

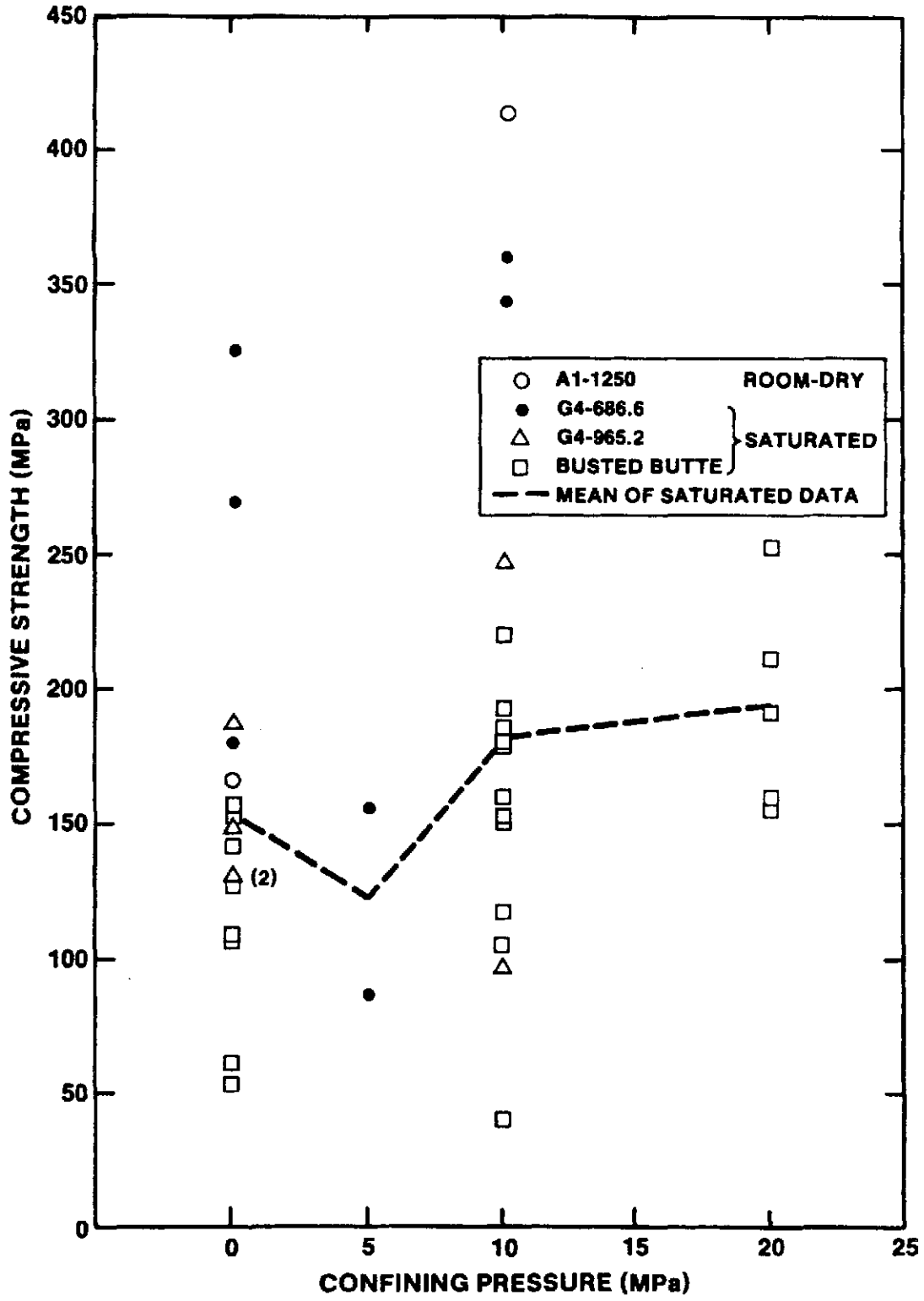


Figure 26. Compressive Strength of Unit TSw2 as a Function of Confining Pressure

Table 17

Mechanical Properties of Unit TSW2 as a Function of Strain Rate

Sample ID Number	Strain Rate (s ⁻¹)	Unconfined Compressive Strength (MPa) ^c	Young's Modulus (GPa) ^c	Poisson's Ratio	Axial Strain at Failure (milli)
G4-742.75 ^a	10 ⁻³	319	37.4	0.29	9.5
	10 ⁻³	283	34.0	0.28	9.4
	10 ⁻³	280	38.4	0.25	8.9
	10 ⁻⁵	235	35.6	0.21	7.2
	10 ⁻⁵	256	36.8	0.21	8.3
	10 ⁻⁵	279	34.6	0.21	9.3
	10 ⁻⁷	243	37.5	0.20	6.9
	10 ⁻⁷	230	33.6	0.11	7.5
G4-1002.4 ^a	10 ⁻⁵	179	33.6	0.32	5.6
	10 ⁻⁵	137	31.1	NA	4.5
	10 ⁻⁷	123	22.0	0.11	4.4
	10 ⁻⁷	138	32.8	0.20	4.5
G2-948.4 ^b	10 ⁻⁵	167	42.0	0.30	4.6
	10 ⁻⁵	157	49.0	0.26	3.3
	10 ⁻⁷	115	41.9	0.26	3.0
	10 ⁻⁷	117	42.1	0.26	3.2

^aNimick et al. (1985).

^bNimick et al. (1987).

^cTo obtain units of psi, multiply by 1.45×10^{-4} .

NA: Not available.

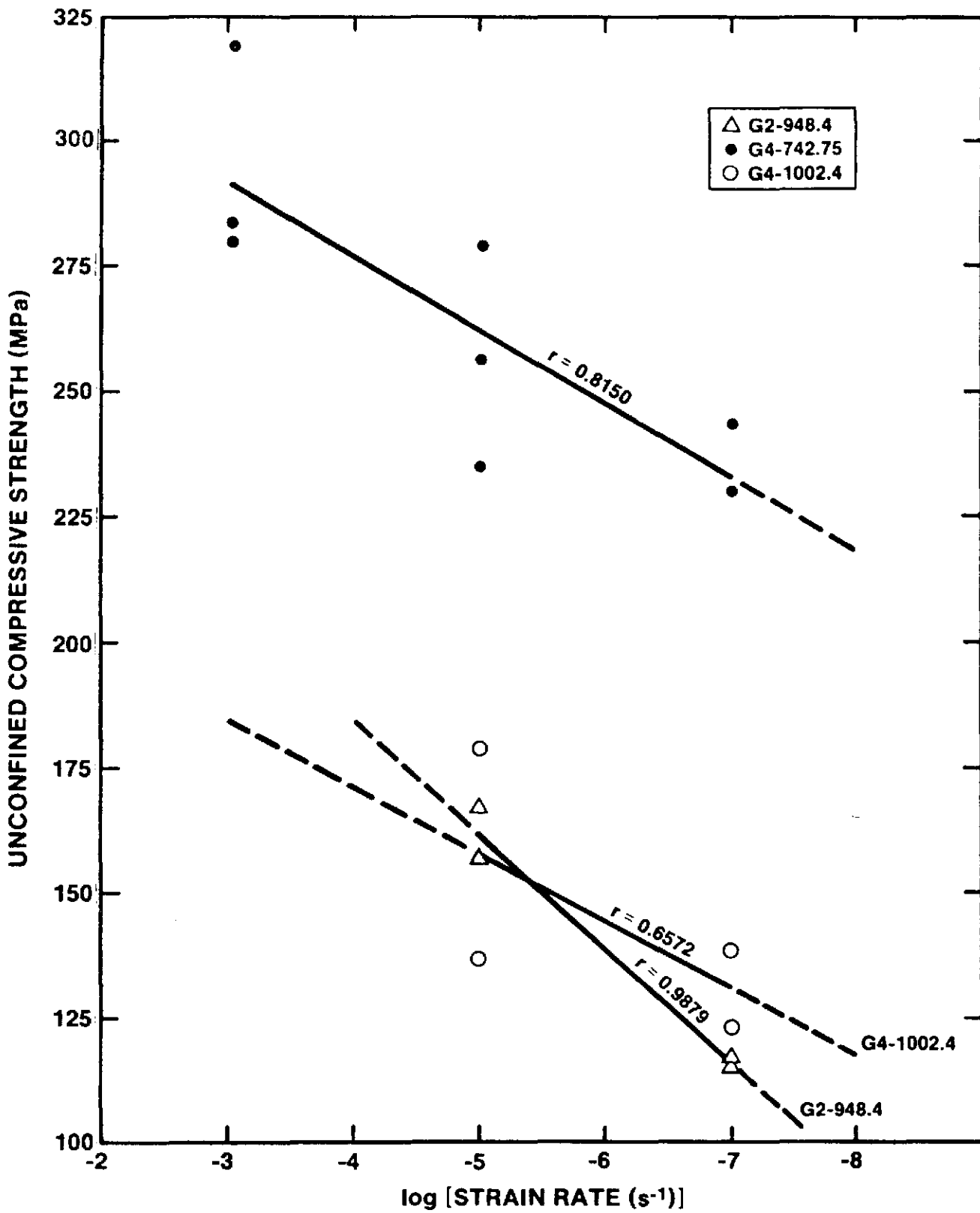


Figure 27. Unconfined Compressive Strength of Unit TSw2 as a Function of Strain Rate

constant below some threshold strain rate. This theory was shown by Costin (1983) to hold for other rock types. Planned experiments at strain rates of 10^{-8} s^{-1} to 10^{-9} s^{-1} may help to determine the nature of the strain-rate dependence at very low strain rates.

3.4.2.1.5 Sample Size Effects. Experimental data for other rock types indicate that compressive strength decreases with increasing sample size, at least up to some critical size beyond which compressive strength is a constant (Paterson, 1978, pp. 34-35). This trend has been confirmed for samples of unit TSw2. The experiment series summarized in the following paragraph is described in more detail in Price (1986).

Thirty-four samples obtained from outcrop material of unit TSw2 from Busted Butte (Figure 1) were tested in compression at a strain rate of 10^{-5} s^{-1} , ambient pressure and temperature. All samples were water-saturated. The samples ranged in diameter from 2.54 cm (1 in.) to 22.86 cm (9 in.). The compressive strengths of the samples decreased with increasing sample diameter. A least-squares fit to the data using a power-law relationship (Price, 1985) resulted in the following equation:

$$\sigma = 1944 D^{-0.846} + 69.5 \quad (15)$$

where σ is the unconfined compressive strength in MPa and D is sample diameter in millimeters.

Blacic (1985) summarized unconfined compressive strength for samples of the Topopah Spring Member with diameters of 1.27 cm (0.5 in.). The

subset of these samples taken from unit TSw2 have a mean strength of approximately 187 MPa (27,100 psi), a value not statistically different from strengths obtained for samples 2.54 cm (1 in.) in diameter. Thus, Equation (15) does not appear to be valid for samples with diameters less than 2.54 cm (1 in.).

3.4.2.1.6 Porosity-Compressive Strength Relationships. As discussed in Section 2.4.2.1.6, empirical relationships have been derived that relate compressive strength and failure parameters for the Coulomb criterion to functional porosity [see Equations (6), (7), and (8)]. Equation (6) may be used with porosity data for unit TSw2 to compare calculated unconfined compressive strengths with those actually measured. Data in Bish and Vaniman (1985) indicate that the clay content of unit TSw2 is $1.9\% \pm 3.4\%$, based on X-ray analyses of samples from USW G-2, USW GU-3, and USW G-4. The clay is not uniformly distributed, being much more prevalent in USW G-2. If data from USW G-2 are excluded, the clay content is calculated to be $1.0\% \pm 0.8\%$. These values are used with data from Tables 11 and 12 to obtain a functional porosity of 0.133 ± 0.033 . This value is used to compare calculated and measured strengths.

The functional porosity (0.133 ± 0.033) is used in Equation (6) to calculate a strength of 168.8 ± 77.5 MPa ($24,500 \pm 11,200$ psi). This value is slightly greater than the mean value determined experimentally.

Equations (7) and (8) relate the failure parameters for the Coulomb criterion to functional porosity. Calculated values of the two

parameters are $38.7^\circ \pm 7.9^\circ$ for the angle of internal friction and 41.0 ± 11.6 MPa ($5,900 \pm 1,700$ psi) for cohesion.

3.4.2.2 Young's Modulus. Statistical analysis of Young's modulus data for unit TSw2 shows no differences resulting from comparison of core holes or testing laboratories. The P-value obtained in the single comparison of testing laboratories (SNL and TT) is 0.9332. For core-hole comparisons, the relevant P-values are given below.

GU-3, G-4: 0.7447

G-2, G-4: 0.1785

G-2, GU-3: 0.3506

G-1, GU-3: 0.5621

G-1, G-2: 0.6953

G-1, G-4: 0.4812

All data in Table B-6 (with the exception of the room-dry sample data) are used to calculate a mean value and standard deviation of 31.2 GPa (4.5×10^6 psi) and 4.4 GPa (0.6×10^6 psi). The 95% confidence interval for the mean value is 29.1 to 33.3 GPa (4.2×10^6 to 4.8×10^6 psi). These values are pertinent to the same set of reference conditions as presented for compressive strength in Section 3.4.2.1. The following subsections discuss the effect of changes in experiment or environmental parameters on Young's modulus.

3.4.2.2.1. Saturation Effects. The state of saturation of the pores in a rock should influence the Young's modulus through the difference in

the bulk moduli of air and water, as discussed in Section 2.4.2.2.1. Using Equations (9) and (10) with the average matrix porosity of 0.113 for unit TSw2, estimated bulk moduli for dry and saturated rock in unit TSw2 are 25.9 GPa (3.8×10^6 psi) and 32.9 GPa (4.8×10^6 psi), respectively. Following a similar line of reasoning to that in Section 2.4.2.2.1, the ratio of E_{dry} to E_{sat} should be the ratio of these bulk moduli, or approximately 0.8.

No experimental data are available to check the validity of this estimated ratio for unit TSw2. As summarized in Section 2.4.2.2.1, experimental data for the Grouse Canyon Member (Olsson and Jones, 1980) do not agree with the estimated ratio. The discrepancy cannot be resolved until unit-specific data are available. Planned experiments should provide data for the Topopah Spring Member in the near future.

3.4.2.2.2 Temperature Effects. As discussed in Section 2.4.2.2.2, no experimental data are available for the Topopah Spring Member. Ongoing experiments covering the temperature range 25° to 150°C (77° to 302°F) are expected to indicate little change in modulus.

3.4.2.2.3 Confining Pressure Effects. For most rock types, Young's modulus increases with confining pressure (Lama and Vutukuri, 1978, pp. 81-97). Figure 28 provides a summary of the Young's modulus data listed in Table 16. The limited data do not show a monotonic dependence on confining pressure, although omitting the data for a confining pressure of 5 MPa (725 psi) (two samples) would suggest decreasing mean value of Young's modulus with increasing confining pressure. Even if

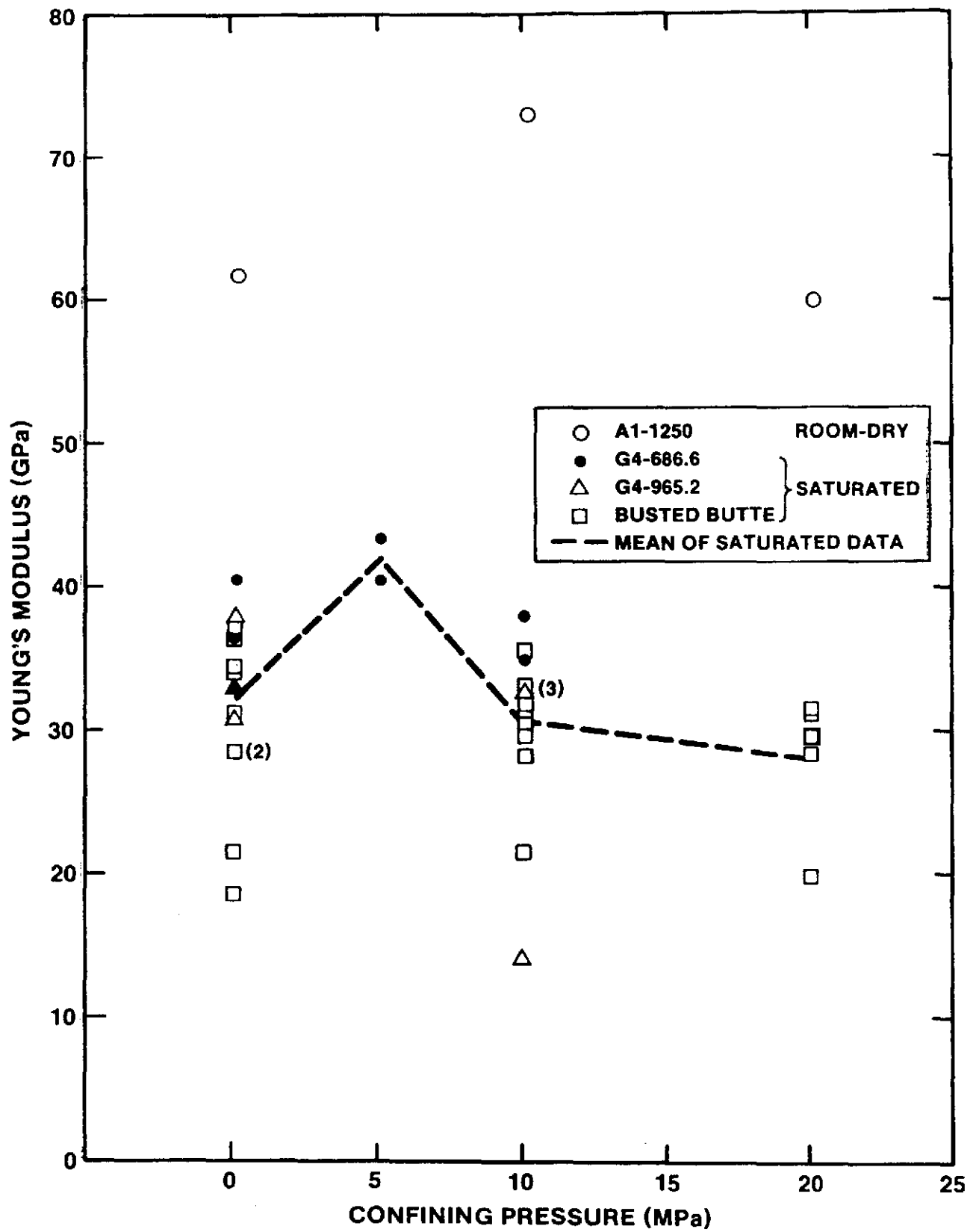


Figure 28. Young's Modulus of Unit TSw2 as a Function of Confining Pressure

this trend is real, the effect appears to be slight and actually may be insignificant relative to data variability at any single confining pressure (linear regression of modulus on confining pressure gives $r^2 = 0.0629$). Additional experiments are planned, but the effect of confining pressure on modulus is not expected to be large.

3.4.2.2.4 Strain Rate Effects. Data from other rock types suggest that Young's modulus should increase with strain rate (Lama and Vutukuri, 1978, pp. 66-79). Young's modulus data from Table 17 are plotted in Figure 29. Data from each individual depth indicate a trend consistent with that expected, but correlation coefficients are so low as to preclude attaching statistical significance to any of the least-squares-fit lines in Figure 29. In fact, if the mean values at each strain rate are compared, no trend at all is visible. Additional experiments at strain rates of 10^{-5} s^{-1} to 10^{-9} s^{-1} will provide more information with which to evaluate the relationship.

3.4.2.2.5 Sample Size Effects. As sample size increases, the number of inhomogeneities (i.e., preexisting fractures, lithophysae, etc.) should increase, although the number per unit volume should remain approximately constant. The influence of these features on Young's modulus will vary, depending on relative size, orientation, and abundance.

In a study summarized in Price (1986), cylindrical samples of welded, devitrified material from unit TSw2 with diameters ranging from 2.54 cm (1.0 in.) to 22.86 cm (9.0 in.) were tested in compression. Resulting Young's moduli showed no relationship to sample size.

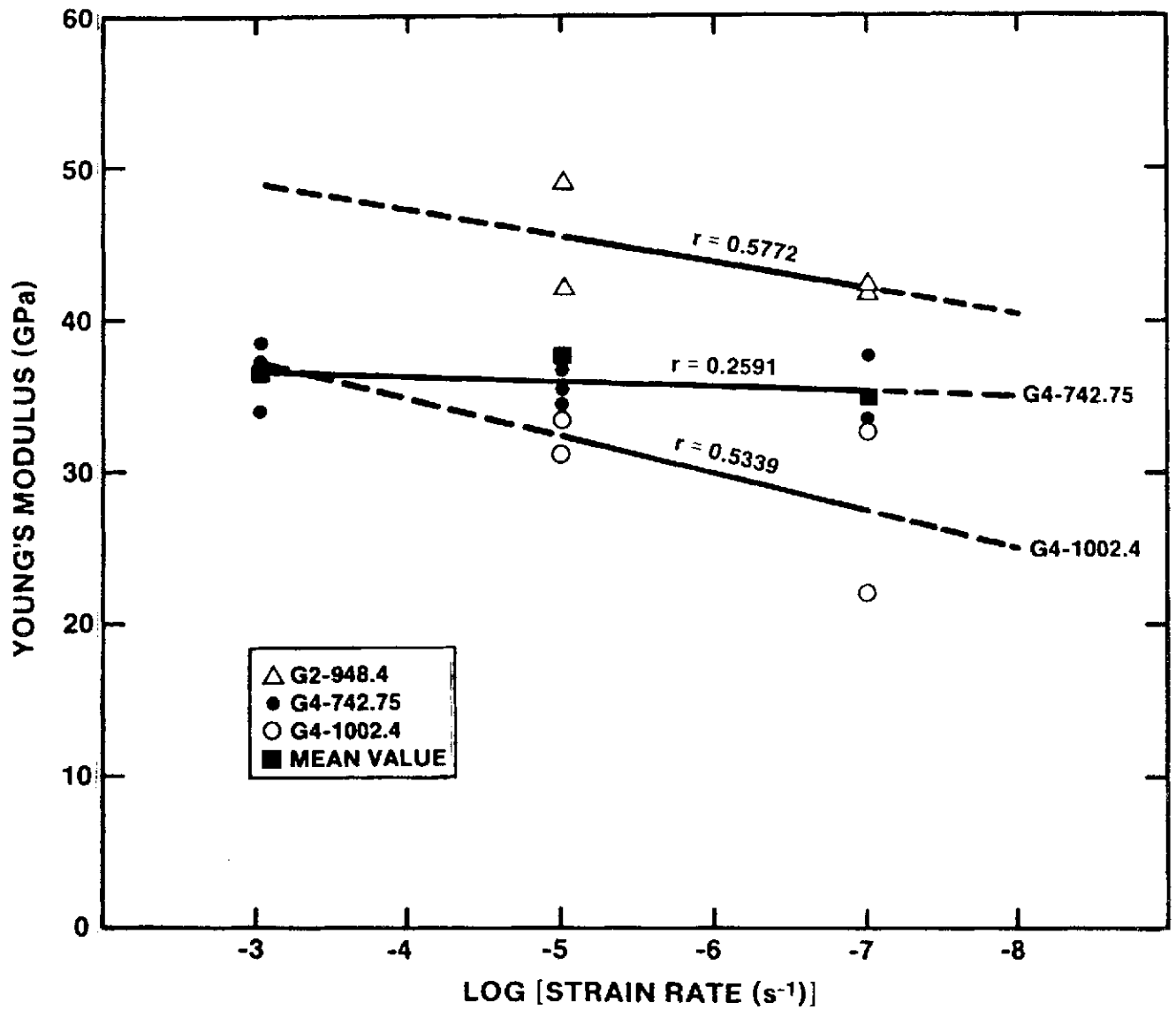


Figure 29. Young's Modulus of Unit TSw2 as a Function of Strain Rate

3.4.2.2.6 Porosity-Young's Modulus Relationship. Price (1983) originally established an empirical relationship between Young's modulus and functional porosity. With the availability of additional experimental data, the model was revised by Price and Bauer (1984). Equation (12) (Section 2.4.2.2.6) resulted, and may be used with functional porosity data for unit TSw2 to compare calculated Young's moduli with those actually measured. Using the average value of 0.133 ± 0.33 for functional porosity, Young's modulus is estimated to be 33.9 ± 7.8 GPa ($4.9 \times 10^6 \pm 1.1 \times 10^6$ psi). The estimated mean value is slightly higher than the mean value of the experimental data, but there probably is no statistical significance to the difference.

3.4.2.3 Poisson's Ratio. Initial statistical analysis of Poisson's ratio data for unit TSw2 showed that differences existed that were attributable to different testing laboratories [$P = 0.0303$ (unequal variances) for SNL-TT]. Systematically higher values of Poisson's ratio were measured at TT (Nimick et al., 1987). Subsequent analysis of only the SNL data indicated one statistical difference for data from different core holes. The P-values for pair-wise comparisons are given below.

G-1, G-4: 0.3256

G-1, GU-3: 0.3758

GU-3, G-4: 0.0174

Both USW GU-3 and USW G-4 are represented by only three samples. For preliminary analyses, the difference between the data for these two core

variability in the Poisson's ratio of unit TSw2 will be found when new data are obtained.

A data set excluding Poisson's ratios measured by TF is the one considered in the following discussion. The mean value and standard deviation for this data set (excluding the value for the single room-dry sample) are 0.27 and 0.07, respectively. The 95% confidence interval for the mean value is 0.22 to 0.32.

As discussed in Section 2.4.2.3, the effects of changes in experiment parameters (i.e., temperature, pressure, strain rate, saturation, and sample size) on Poisson's ratio are expected to be small relative to the variation at any single set of experiment conditions. Also, assuming that data in Nimick et al. (1987) on dilatancy in units TSw1 and TSw2 are correct (see Section 2.4.2.3 for discussion), the Poisson's ratio values given in the previous paragraph may be valid only up to stresses of approximately 102 MPa (14,800 psi), which is 69% of the mean compressive strength.

3.4.2.4 Axial Strain at Failure.^{*} The strain (at failure) in the direction of the greatest principal stress is of interest because in some cases monitoring of deformation also may provide indications of rock stability. In addition, strain is more easily measured in situ than is stress. Statistical analysis of data for this parameter for samples from

^{*}Failure for laboratory samples is taken to occur at the greatest axial stress sustained by the sample, regardless of the subsequent stress-strain behavior.

unit TSw2 shows a difference only for data from USW G-1 and USW G-4, with strain at failure being higher for samples from USW G-4. Only four data values are available from USW G-1. In view of this limited sample, the difference is ignored for the present analysis. Thus, all data in Table B-6 (with the exception of those for the room-dry sample) are used to calculate a mean value and standard deviation of 5.54×10^{-3} and 1.55×10^{-3} , respectively. The 95% confidence interval for the mean value is 4.81×10^{-3} to 6.27×10^{-3} .

Based on discussion in Section 2.4.2.4, ϵ_{ax}^f for experiments in which the axial stress-axial strain relationship is linear up to the failure stress is expected to mimic the response of compressive strength to all variable experiment parameters other than saturation state. Dry samples should show markedly higher values of ϵ_{ax}^f than do saturated samples. No experimental data are presently available to test this expectation. Price (1986) tested 34 samples of unit TSw2 with sample diameters ranging from 2.54 cm (1 in.) to 22.86 cm (9 in.) and found that ϵ_{ax}^f decreased as sample size (diameter) increased but that the rate of decrease was smaller at larger sample sizes. Price (1986) reports the following relationship, obtained by a least-squares fit to the data:

$$\epsilon_{ax}^f = 11.6 D^{-0.268} \quad (16)$$

where ϵ_{ax}^f is in millistrains and D is sample diameter in millimeters.

3.4.3 Data from Tensile Experiments

All available experimental data for the tensile strength of unit TSw2 are for samples from UE-25a#1, as summarized by Blacic et al. (1982, p. 5). The "Brazilian" technique was used for all experiments. Results from 15 experiments gave an average "Brazilian" tensile strength of 15.2 MPa (2204 psi). Individual experiment results are not reported by Blacic et al. (1982), so neither a standard deviation nor a 95% confidence interval can be provided.

Estimates of uniaxial tensile strength (T_o) can be made using data from triaxial compression experiments. Jaeger and Cook (1979, pp. 101-106) discuss failure criteria based on stress-concentrations at the tips of microcracks. For the plane Griffith failure criterion,

$$T_o = \frac{(\sigma_1 - \sigma_3)^2}{8(\sigma_1 + \sigma_3)} \quad \text{for } \sigma_1 + 3\sigma_3 > 0 \quad (17)$$

[from Jaeger and Cook, 1979, p. 101, Eq. (1)]. Data from Nimick et al. (1985) for samples of unit TSw2 from USW G-4 (G4-686.6 and G4-965.2) satisfy the stress requirement in Equation (17) (see Table 16). The estimated tensile strength from the relevant samples is 24.2 ± 11.6 MPa ($3,500 \pm 1,700$ psi).

Murrell (1963) extended the plane Griffith criterion to three dimensions. Jaeger and Cook (1979, pp. 103-106) summarize the extension, which results in the following calculation of T_o :

$$T_o = \frac{(\sigma_1 - \sigma_3)^2}{12 (\sigma_1 + 2\sigma_3)} \quad . \quad (18)$$

Use of Equation (18) with the same data discussed in the preceding paragraph provides an estimated tensile strength of 16.0 ± 7.7 MPa ($2,300 \pm 1,100$ psi).

Price (1983) determined that an empirical relationship exists between the tensile strengths given by Blacic et al. (1982) for all Yucca Mountain tuffs and porosity, as given by Equation (14) (Section 2.4.3). The line given by this equation is shown in Figure 30, together with a line delineating the average tensile strength as obtained by Blacic et al. (1982) and the matrix porosity (mean value plus or minus one standard deviation). Also shown are two regions outlined by mean values and standard deviations of tensile strength estimated using Equations (17) and (18). The empirical equation overestimates tensile strength relative to the experimental data. Tensile strengths estimated using Equation (18) bracket the experiment results, whereas the plane Griffith theory [Equation (17)] appears to overestimate the measured (indirect) tensile strengths.

Some uncertainty exists as to whether results of the "Brazilian" method represent the true uniaxial tensile strength of a material (e.g., Jaeger and Cook, 1979, pp. 169-173). In view of this, the comparison in Figure 30 should be interpreted with caution. Additional experiments are planned in which samples of the welded, devitrified Topopah Spring Member will be measured by the Brazilian indirect method as well as in direct tensile experiments.

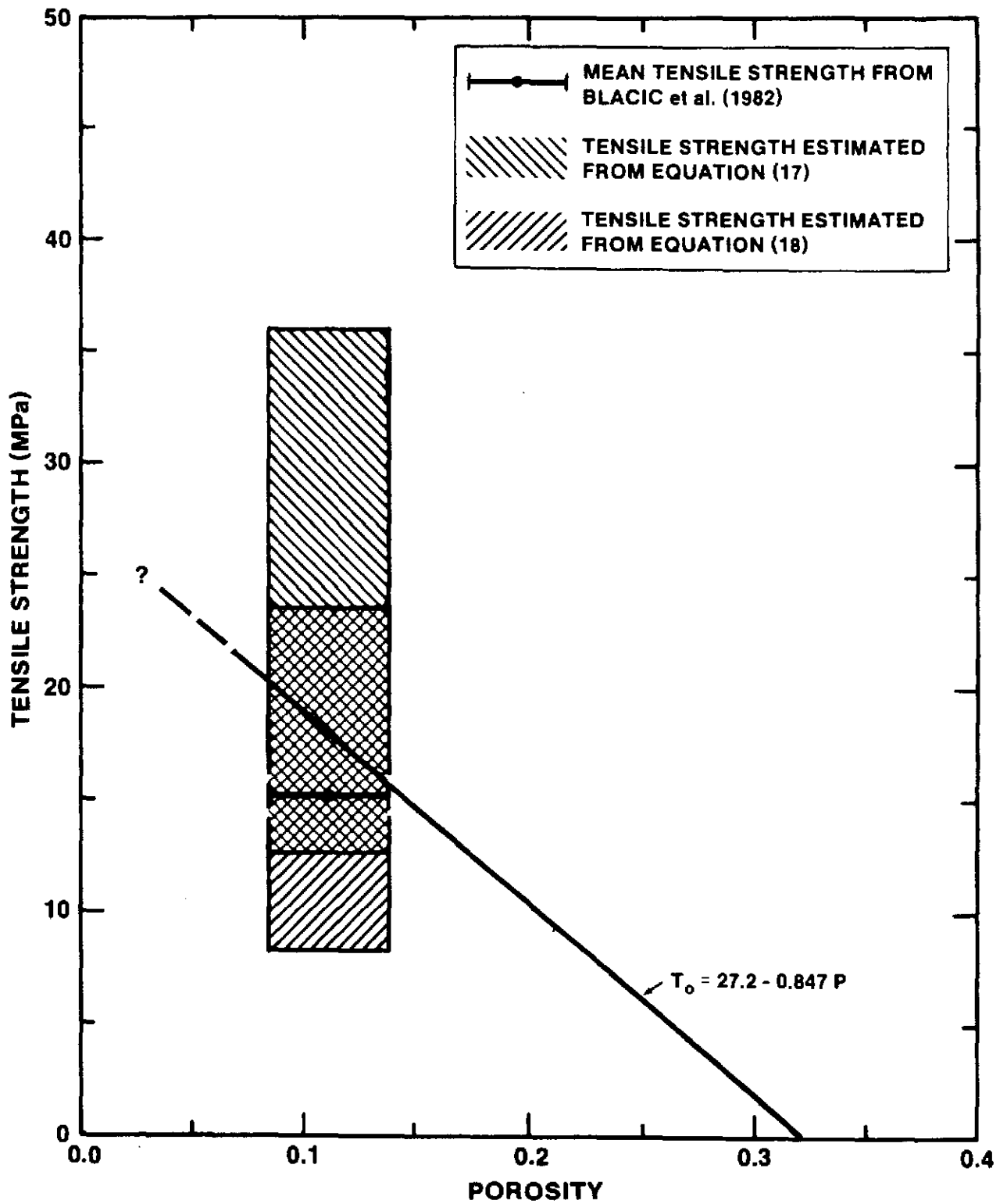


Figure 30. Relationships Between Porosity and Tensile Strength for Unit TSw2

4.0 THERMAL/MECHANICAL UNIT TSw3

4.1 Lithology and Geometry

In general, thermal/mechanical unit TSw3 is defined to be the basal vitrophyre of the Topopah Spring Member. As such, the unit comprises moderately to densely welded vitric ashflows. The existing three-dimensional model of the thermal/mechanical units has been used to estimate the thickness variation of unit TSw3 within the repository area. The resulting isopach map is shown in Figure 31. In general, the unit is thinnest in the southeastern and northeastern parts of the repository area, thickening toward the central and western parts. [Some of the thickness variability in Figure 31 may be an artifact of the modeling technique (Ortiz et al., 1985, p. 30), especially the contours of zero thickness.]

Figure 31 was derived assuming that the top of the vitrophyre was located as defined in lithologic logs. However, as discussed in Section 3.1, parts of units TSw2 and TSw3 adjacent to the contact between the units have been mildly to strongly altered. The resulting material in many cases is not considered to be representative of either unit, and depth intervals listed in Section 3.1 are not included in either unit for the purposes of property analysis.

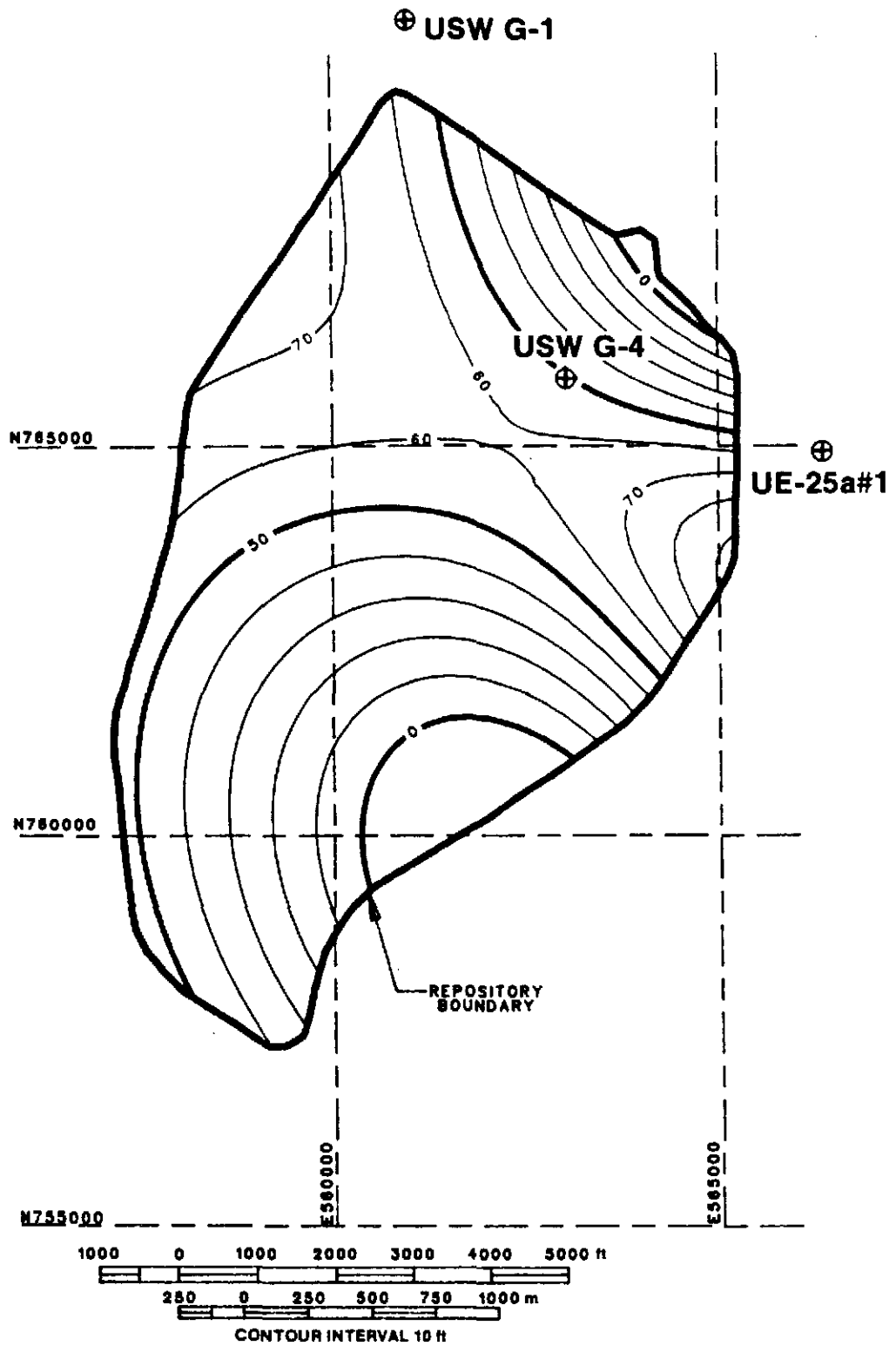


Figure 31. Isopach Map of Unit TSw3

4.2 Bulk Properties

4.2.1 Data

Measured bulk property data for unit TSw3 are tabulated in Appendix B (Table B-7). Data in Table B-7 have been measured by TT, USGS (Anderson, 1981, 1984), HN, and LANL (Blacic et al., 1982). Data from three samples from USW G-1 were obtained by either HN or by TT, but records do not indicate which one, so data for these three samples are treated as though they had been measured by an entirely different laboratory.

Data for four samples that would be treated as belonging to unit TSw3 if the depth assignments of Ortiz et al., (1985) were used have been excluded from the statistical analysis of unit TSw3. Data for these four samples (A1-1285.1, A1-1290.9, G4-1299, and G4-1317.1) are discussed in Section 5.2.1.

4.2.2 Statistical Analysis and Discussion

Each of the three properties--porosity, grain density, and dry bulk density--was analyzed separately using the TTEST procedure. However, no results are given for dry bulk density because of component variability, as discussed in Section 4.2.2.3.

4.2.2.1 Porosity. Data were sufficiently numerous only for comparison of two core holes. The mean values differ for USW G-1 and USW GU-3 ($P = 0.0238$). The mean matrix porosity at USW G-1 (0.035) is higher than that at USW GU-3 (0.025).

Because of the small size of the data set (14 samples), a mean value and standard deviation for the porosity of unit TSw3 have been calculated (0.033 and 0.014, respectively). The 95% confidence interval for the mean value is 0.026 to 0.040. Calculated porosities for samples of unit TSw3 from USW G-2 used in compressive experiments (Nimick et al., 1987) range from 0.016 to 0.040, values that are consistent with those obtained from the smaller samples used specifically for density measurements.

4.2.2.2 Grain Density. Data were sufficiently numerous only for comparison of core holes USW G-1 and USW GU-3. No significant difference was found ($P = 0.0517$). Thus, treating all samples as originating from a single population results in a calculated mean and standard deviation of 2.379 g/cm^3 (148.5 lb/ft^3) and 0.016 g/cm^3 (1.0 lb/ft^3), respectively.

4.2.2.3. Bulk Density. A number of measurements of bulk density have been made for unit TSw3, including saturated bulk density and dry bulk density. The latter measurements are provided in Table B-7. However, neither these data nor any of the other measured bulk densities are applicable to in situ conditions in unit TSw3. This is because the mean in situ saturation of the matrix porosity is 0.65 (Montazer and Wilson, 1984, p. 13), with a standard deviation of 0.19. Use of these values with the porosity and grain density data and Equation (2) results in a calculated in situ bulk density of $2.322 \pm 0.029 \text{ g/cm}^3$ ($145.0 \pm 1.8 \text{ lb/ft}^3$). The correlative value of in situ dry bulk density, calculated using Equation (1), is $2.300 \pm 0.037 \text{ g/cm}^3$ ($143.6 \pm 2.3 \text{ lb/ft}^3$).

4.3 Thermal Properties

4.3.1 Data

Measured data for the thermal expansion coefficient of unit TSw3 are provided in Table B-8. All data in Table B-8 were measured by SNL. No experimental data are available for heat capacity or emissivity.

4.3.2 Statistical Analysis and Discussion

Because only three samples have been used to obtain data for thermal expansion, no statistical analysis is warranted. Because of assumed equality of bulk properties between core holes, it is assumed that there is no spatial variability in thermal expansion of unit TSw3.

4.3.2.1 Thermal Expansion. Only three thermal expansion experiments have been performed on material from unit TSw3; all three samples are from core hole USW G-1, and all three tests were performed without confining or pore pressure. The average values of the linear thermal expansion coefficient are presented in Table 18 and the accompanying change in dimension with temperature is shown in Figure 32.

As is evident from Figure 32, and is shown by data for sample G1-1342-1, there is some tendency for material from unit TSw3 to show a decrease in the thermal expansion coefficient at temperatures above 200°C (392°F). In fact, all three samples contracted at elevated temperatures, with contraction beginning at 205°C (401°F) for one sample and at 250°C (482°F) for the other two samples.

Table 18

Summary of Linear Thermal Expansion Coefficients^a
for Unit TSw3

	Temperature Range									
	°C	25-50	50-100	100-150	150-200	200-250	25-100	25-150	25-200	25-250
	°F	77-122	122-212	212-302	302-392	392-482	77-212	77-302	77-392	77-482
Mean		1.0	6.5	6.1	4.9	2.0	4.6	5.3	5.2	4.5
St. Dev.		0.9	1.6	2.1	2.0	4.5	1.2	1.5	1.6	2.1
# Samples		3	3	3	3	3	3	3	3	3

^aCoefficients are in units of $10^{-6}^{\circ}\text{C}^{-1}$; to obtain units of $10^{-6}^{\circ}\text{F}^{-1}$, multiply by 5/9.

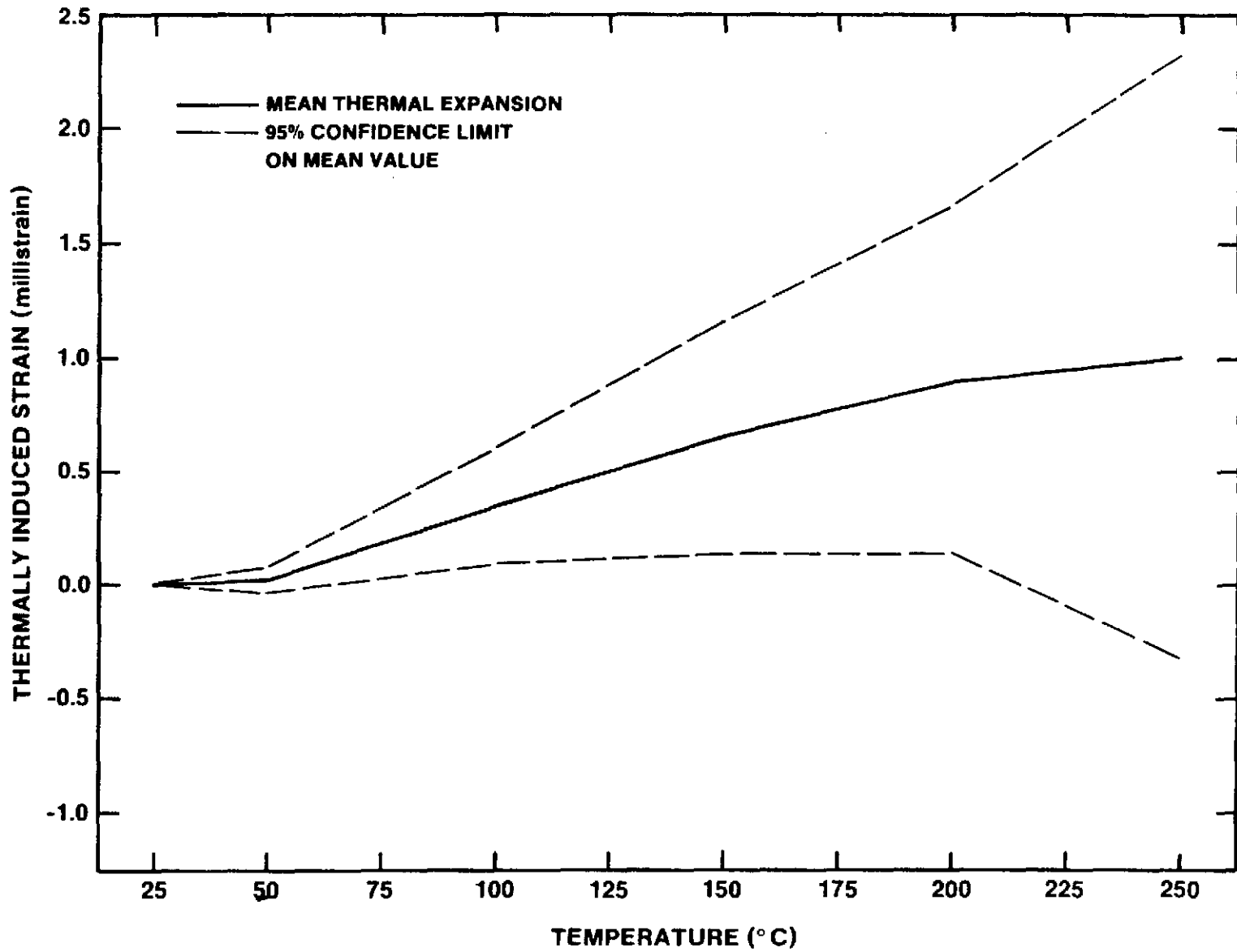


Figure 32. Thermal Expansion Behavior of Unit TSw3

The contraction mentioned in the preceding paragraph is believed to be the result of sample dehydration. The temperatures at which water is expected to be released from the material in unit TSw3 are discussed in Appendix D. Of the various possibilities, only heulandite demonstrates an increase in water loss in the vicinity of 250°C (482°F) which can be related to the increasing sample contraction mentioned previously. No data are available on the thermal expansion/contraction behavior of heulandite. However, the association of the increase in the rate of contraction of the TSw3 samples at or about 250°C (482°F) suggests a link to the conversion of heulandite to heulandite B rather than simple dehydration of the zeolites.

Data in Appendix D indicate that unit TSw3 contains water in the glass structure itself as well as in any secondary minerals. This water and some of that contained in heulandite and/or clay must be leaving the sample at temperatures much lower than 250°C (482°F). This low-temperature dehydration should be recognizable as a decrease in the expansion coefficients from those observed for anhydrous glass. The data in Table 18 are indeed lower than those measured on alkali feldspar glass [$6.6 \times 10^{-6} \text{ } ^\circ\text{C}^{-1}$ ($3.7 \times 10^{-6} \text{ } ^\circ\text{F}^{-1}$) to $7.5 \times 10^{-6} \text{ } ^\circ\text{C}^{-1}$ ($4.2 \times 10^{-6} \text{ } ^\circ\text{F}^{-1}$) (Vergano et al., 1967)] and on a porphyritic rhyolite vitrophyre [$8.4 \times 10^{-6} \text{ } ^\circ\text{C}^{-1}$ ($4.7 \times 10^{-6} \text{ } ^\circ\text{F}^{-1}$) to $11.4 \times 10^{-6} \text{ } ^\circ\text{C}^{-1}$ ($6.3 \times 10^{-6} \text{ } ^\circ\text{F}^{-1}$) (Griffin and Demou, 1972)].

4.3.2.2 Heat Capacity. No experimental data are available for the heat capacity of unit TSw3. The heat capacity of the solid materials as a function of temperature has been estimated from whole-rock oxide data

by Connolly (1986). Table 19 contains mean values and standard deviations of the estimated heat capacities as a function of temperature. These data also are presented graphically in Figure 33. The data have been combined with grain density, porosity, and saturation data in Equation (4) to calculate the in situ volumetric heat capacity. The results of the calculation are provided in Table 20 and in Figure 34.

4.3.2.3 Emissivity. Although waste canisters are not expected to be emplaced in unit TSw3, the emissivity of the welded, vitric material (essentially hydrated obsidian) is discussed here for completeness. Emissivity values for obsidian reported by Dana (1969) are 0.844 ± 0.002 for smooth surfaces and 0.919 ± 0.003 for sawed surfaces. Buettner and Kern (1965) report a value of 0.837 for a broken surface, lower than both of Dana's values, and a value of 0.862 for a polished surface, in good agreement with Dana's value for smooth surfaces. Lyon (1965) reports two values for smooth obsidian: 0.72 and 0.80. Thus, a range of emissivities from 0.72 to 0.92 appears to be applicable.

4.4 Mechanical Properties

4.4.1 Data From Compressive Experiments

Only one unconfined compression experiment has been performed on material from unit TSw3 at the standard conditions defined in Section 2.4.2.1. The strength of this single sample from USW GU-3 is 43.4 MPa (6294 psi). Four samples from USW G-2 were tested at a confining pressure of 10 MPa (1450 psi) (Nimick et al., 1987). The mean and standard deviation for the compressive strength of these four samples are

Table 19

Heat Capacity^a of Solid Components as a Function of Temperature
for Welded, Vitric Topopah Spring Member (TSw3)

	Temperature						
	°C 25	77	127	177	227	277	327
	°F 77	171	261	351	441	531	621
Mean	0.756	0.908	1.009	1.085	1.145	1.194	1.237
St. Dev.	0.010	0.011	0.013	0.015	0.017	0.019	0.021
# Samples	3	3	3	3	3	3	3

^aUnits are J/g°C; to obtain units of Btu/lb°F, multiply by 0.23885.

Note: Mean heat capacities (C_p^{sol}) represented by the following equation:

$$C_p^{\text{sol}} = 1.1742 + 1.8762 \times 10^{-4} T + 3.4857 \times 10^{-3} T^{1/2} \\ + 9.270 \times 10^{-8} T^2 - 1.3201 T^{-1/2} + 1.1208 \times 10^{-4} T^{-1} \\ - 4.1392 \times 10^4 T^{-2}$$

where T is in degrees Kelvin (Connolly, 1986).

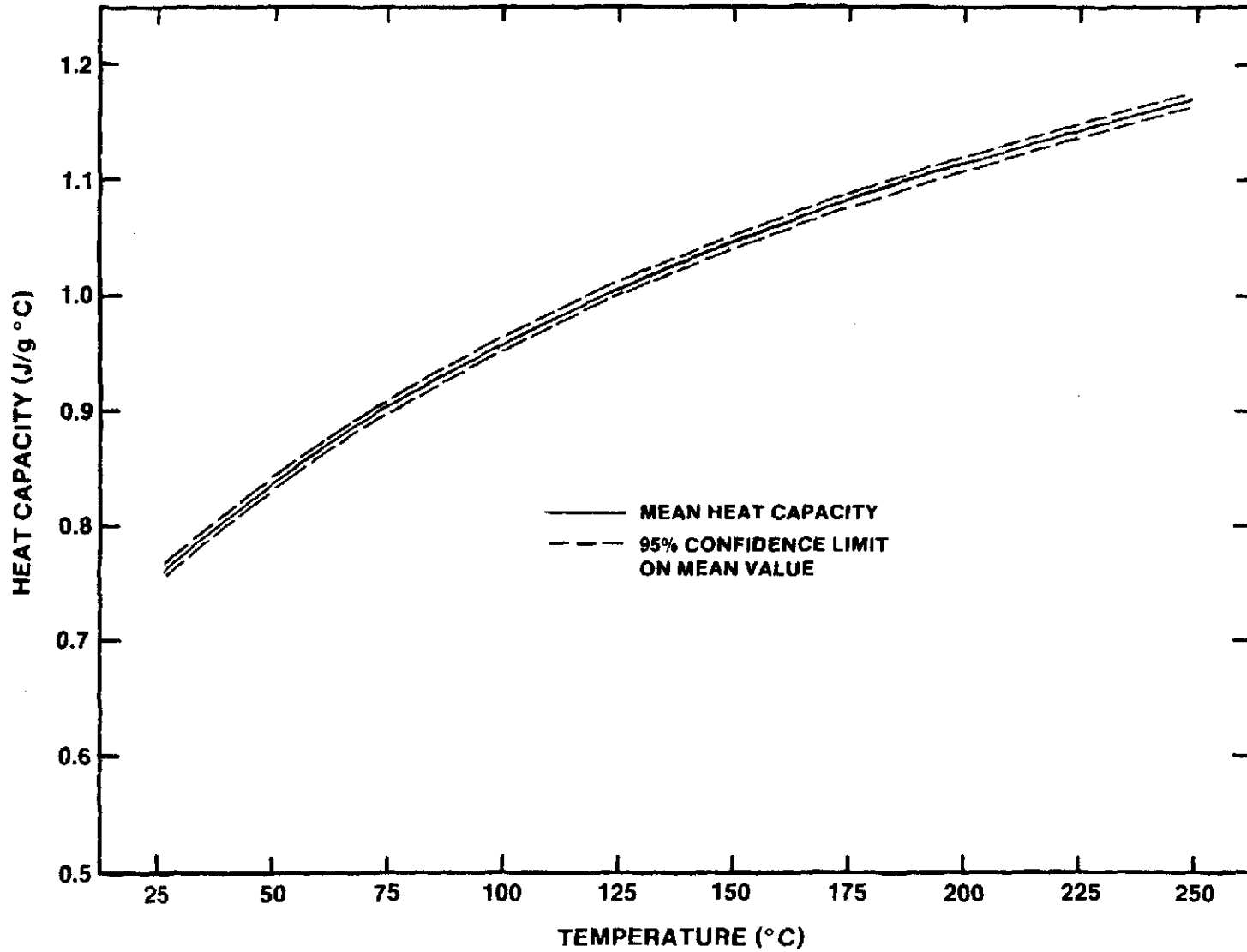


Figure 33. Heat Capacity of Solid Components as a Function of Temperature for Welded, Vitric Topopah Spring Member (TSw3)

Table 20

Estimated In Situ Volumetric Heat Capacity^a of Unit TSw3

	Temperature							
	°C	25	50	99	101	150	200	250
	°F	77	122	210	214	302	392	482
Mean		1.830	2.015	2.288	2.211	2.408	2.563	2.688
St. Dev.		0.039	0.039	0.040	0.045	0.050	0.055	0.060

^aUnits are J/cm³K; to obtain Btu/ft³°F, multiply by 14.911.

Equation (4) is used; the values of $C_p^{H_2O}$ and ρ_{H_2O} are as listed in Table 7.

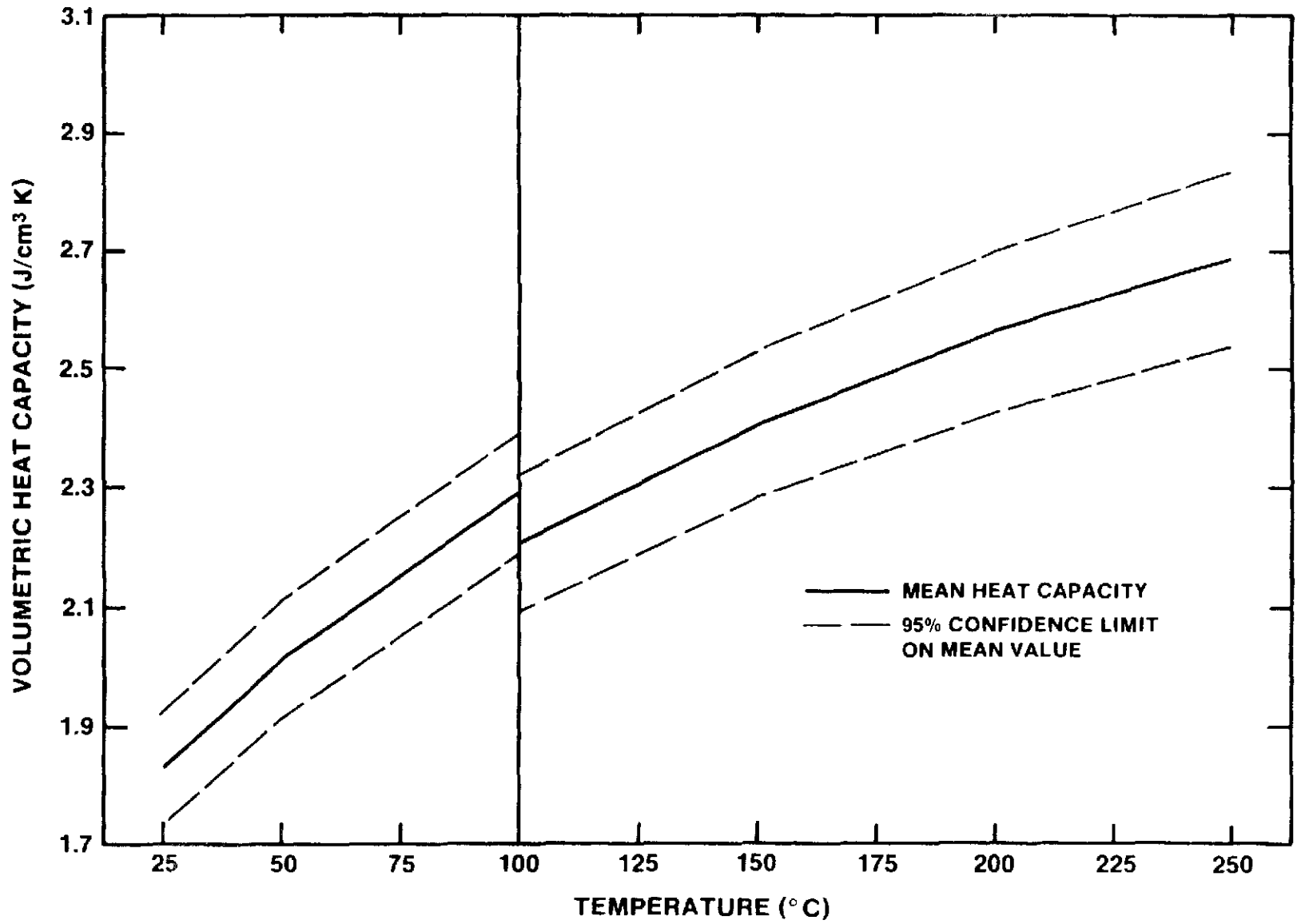


Figure 34. Estimated In Situ Volumetric Heat Capacity of Unit TSw3 as a Function of Temperature

45.0 MPa (6,526 psi) and 19.0 MPa (2,756 psi), respectively. No conclusions about the effect of confining pressure on the compressive strength of unit TSw3 are possible.

The Young's modulus of the single sample from USW GU-3 is 23.7 GPa (3.4×10^6 psi), and the Poisson's ratio is 0.15. Stress-strain and axial strain-lateral strain curves for the four samples from USW G-2 tested at a confining pressure of 10 MPa (1450 psi) did not have sufficient linearity to define Young's modulus or Poisson's ratio (Nimick et al., 1987).

No data on axial strain at failure are available for the experiment at the standard conditions discussed in Section 2.4.2.1. At a confining pressure of 10 MPa (1450 psi), the mean and standard deviation for axial strain at failure for the four samples from USW G-2 are 4.675×10^{-3} and 0.65×10^{-3} , respectively (Nimick et al., 1987).

4.4.2 Data from Tensile Experiments

No experimental data for the tensile strength of unit TSw3 are available.

4.4.3 Relationships Between Porosity and Mechanical Properties

The microstructure of welded, vitric material differs greatly from that of welded, devitrified material. As such, Equations (6), (7), (8), (12), and (14) cannot be applied to unit TSw3. Data for unit TSw3 are insufficient to establish equivalent relationships for vitric material.

5.0 MATERIAL BETWEEN UNITS TSw2 AND TSw3

5.1 Lithology and Geometry

As discussed in Section 3.1, parts of units TSw2 and TSw3 adjacent to the contact between the units have been mildly to strongly altered. This interval roughly corresponds to zeolitized Interval I of Vaniman et al. (1984, pp. 54-55). The lithology of the material ranges from welded, devitrified to welded vitric to an altered material with a mineralogy dominated by zeolites (mainly heulandite) and smectite clay.

Using the depth ranges presented in Section 3.1, this interval is thickest in UE-25a#1 and USW G-4 and is thin to absent in the other core holes. Levy (1983) suggests the possibility that the alteration is attributable to water released from the tuff above the vitrophyre during devitrification. However, this theory cannot explain thickness variations. Additional discussion of the distribution and possible origin of this material is presented in Levy (1987).

Because of the diverse lithologies of this material, the bulk, thermal, and mechanical properties should show a large amount of variability. The following section summarizes the available property data and provides a brief discussion of the variability, especially in comparison to the properties of units TSw2 and TSw3.

5.2 Bulk, Thermal, and Mechanical Properties

5.2.1. Porosity and Density

Bulk properties have been measured on four samples from this material, as summarized in Table 21. The porosity and grain density of sample A1-1285.1 are consistent with the equivalent properties for unit TSw3 (Sections 4.2.2.1 and 4.2.2.2). Samples G4-1299 and G4-1317.1 have properties similar to those of TSw2 (Sections 3.2.2.1 and 3.2.2.2). Sample A1-1290.9 has a porosity consistent with unit TSw2, but a grain density closer to the average grain density of unit TSw3. The differences in porosity and grain density of the four samples are such that calculation of mean values and standard deviations is not warranted.

5.2.2 Thermal Properties

No data on thermal conductivity, heat capacity, or emissivity are available for this material. A single sample (G4-1295) was tested for thermal expansion behavior under 10-MPa (1,450-psi) confining pressure. Linear thermal expansion coefficients for the sample are as follows:

<u>Temperature Range</u>		<u>Expansion Coefficient ($10^{-6} \text{ }^{\circ}\text{C}^{-1}$)^a</u>
<u>°C</u>	<u>°F</u>	
25-50	77-122	15.9
50-100	122-212	10.9
100-150	212-302	9.9
25-100	77-212	12.6
25-150	77-302	11.6

^aTo obtain units of $10^{-6} \text{ }^{\circ}\text{F}^{-1}$, multiply by 5/9.

Table 21

Bulk Properties of Material Between Units TSw2 and TSw3

Sample ID	Porosity (%)	Grain Density (g/cm ³) ^a	Dry Bulk Density (g/cm ³) ^a	Source of Information
A1-1285.1	1.7	2.34	NA	Blacic et al., (1982)
A1-1290.9	13.8	2.43	2.09	This report
G4-1299	9.0	2.50	NA	Peters et al. (1984)
G4-1317.1	11.63	2.58	2.28	This report

^aTo obtain units of lb/ft³, multiply by 62.43.
 NA Not available.

Although these coefficients are closer to those for unit TSw2 (Table 14) than to the coefficients for unit TSw3 (Table 18), they are slightly higher than the mean coefficients for samples of unit TSw2 measured under 10-MPa (1,450-psi) confining pressure. The reason for the difference is not apparent. Additional measurements will be made when samples are available from the ES.

5.2.3 Mechanical Properties

5.2.3.1 Data from Compressive Experiments. Five samples from a depth of 1307.2 ft (398.4 m) in USW G-4 were tested under the standard conditions described in Section 2.4.2.1. Experiment results are listed in Table 22. As described in Nimick et al. (1985, p. 26), these samples are welded vitric material with common clay alteration. Mean values and standard deviations also are given in the table.

Data from compressive experiments on samples of unit TSw3 are of insufficient quantity to compare with the data in Table 22. Comparison of the data in the table with those for unit TSw2 indicates that unit TSw2 has significantly higher unconfined compressive strength, Young's modulus, and axial strain at failure. Poisson's ratio data are similar in the two materials. The comparison should be used with caution, because the data in Table 22 can in no way be considered to be representative of all the lithologies in the transitional material.

Table 22

Results of Compressive Experiments on Material
Between Units TSw2 and TSw3^a

Sample ID	Unconfined Compressive Strength (MPa) ^b	Young's Modulus (GPa) ^b	Poisson's Ratio	Axial Strain at Failure (10 ⁻³)
G4-1307.2-A	104	30.2	0.23	5.3
G4-1307.2-C	79	22.8	0.20	3.3
G4-1307.2-D	31	20.0	0.30	1.9
G4-1307.2-E	65	16.6	0.24	7.2
G4-1307.2-F	98	34.9	0.20	3.3
Mean Value	75.4	24.9	0.23	4.2
St. Dev.	29.2	7.5	0.04	2.1

^a $\epsilon_c = 10^{-5} \text{ s}^{-1}$, saturated, drained (Nimick et al., 1985).

^bTo obtain units of psi, multiply by 1.45×10^{-4} .

5.2.3.2 Data from Tensile Experiments. All available experimental data for the tensile strength of this transitional material are for four experiments on samples from a depth of 1285.1 ft (391.7 m) in UE-25a#1, as summarized by Blacic et al. (1982, p.5). The "Brazilian" technique was used for all experiments. Results give a mean value and standard deviation of 8.6 MPa (1247 psi) and 1.8 MPa (261 psi), respectively.

6.0 IN SITU VERTICAL STRESS

Until in situ measurements are available, the vertical in situ stress at Yucca Mountain is assumed to be equivalent to the weight of the overlying material. The stress (σ_v) has been estimated using the following equation:

$$\sigma_v \approx g \sum_{i=1}^n \rho_i t_i \quad (23)$$

where g is gravitational acceleration and ρ_i and t_i are the in situ bulk density and thickness of the i th unit overlying the surface for which σ_v is being calculated. The values of ρ_i used in estimating the in situ stresses are as follows:

<u>Thermal/Mechanical Unit</u>	<u>Density^a</u>	
	<u>g/cm³</u>	<u>lb/ft³</u>
TCw (Welded Tiva Canyon Member)	2.306	144.0
PTn (Nonwelded Material between TCw and TSw1)	1.576	98.4
TSw1	2.022	126.2
TSw2	2.251	140.5

The densities used for TSw1 and TSw2 are slightly lower than those given earlier in this report. The error in the calculated in situ stresses caused by these density discrepancies is a maximum of 0.4 MPa (60 psi); the stresses provided in this section are underestimates of the true in situ stresses.

Thicknesses of the four units were obtained as a function of position within the repository area using the three-dimensional model of the thermal/mechanical units as developed by Ortiz et al. (1985) together with a digitized version of the topography at Yucca Mountain (20-ft contour interval). The error in σ_v associated with digitizing and subsequent interpolation of topographic contours is estimated to be less than 0.1 MPa (15 psi). The thicknesses of the various units and the resulting stresses were calculated at approximately 960 grid points within the repository area, and the results were contoured. Uncertainties in these thicknesses are estimated to be ± 35 ft (10.7 m) based on discussion in Nimick and Williams (1984) and Ortiz et al. (1985). The cumulative uncertainty in the vertical stress resulting from uncertainty in thicknesses is approximately ± 0.36 MPa (50 psi) at the base of TSw1 and ± 0.43 MPa (60 psi) at the base of TSw2. When combined with the uncertainty resulting from density discrepancies, the total uncertainty is a maximum of ± 0.6 MPa (90 psi).

The contribution to σ_v from Quaternary units (alluvium and colluvium) has been ignored. No appreciable error in σ_v should exist because of this because these units are thin to absent within the repository area and are low-density materials. Beneath major washes (outside the repository area), the alluvium may contribute 0.5 MPa (72.5 psi) to σ_v .

The variation of σ_v within the repository area has been calculated for three surfaces: the base of unit TSw1 (Figure 35), the base of unit TSw2 (Figure 36), and at the floor of the design repository

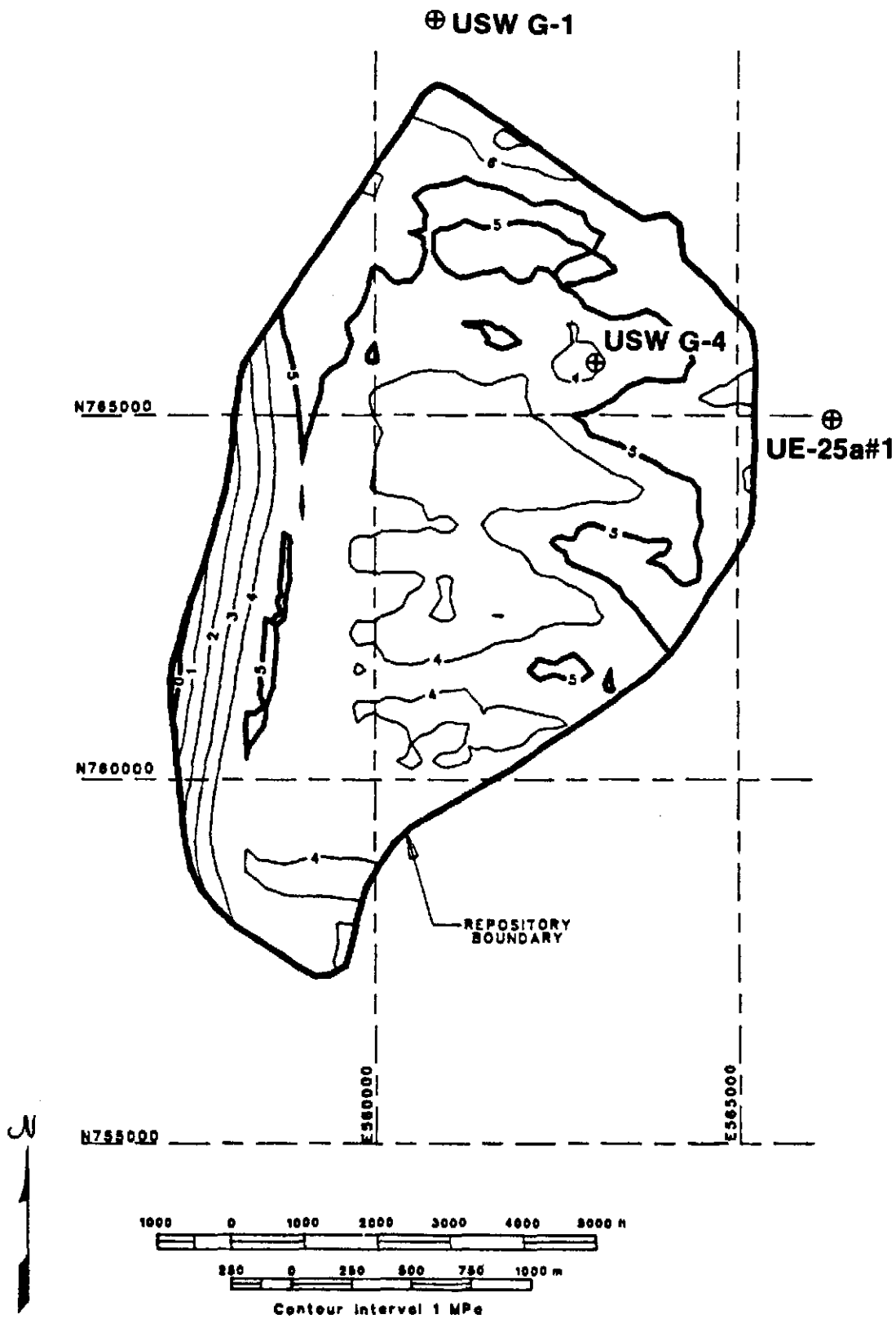


Figure 35. Calculated Vertical Stress at the Base of Unit TS1

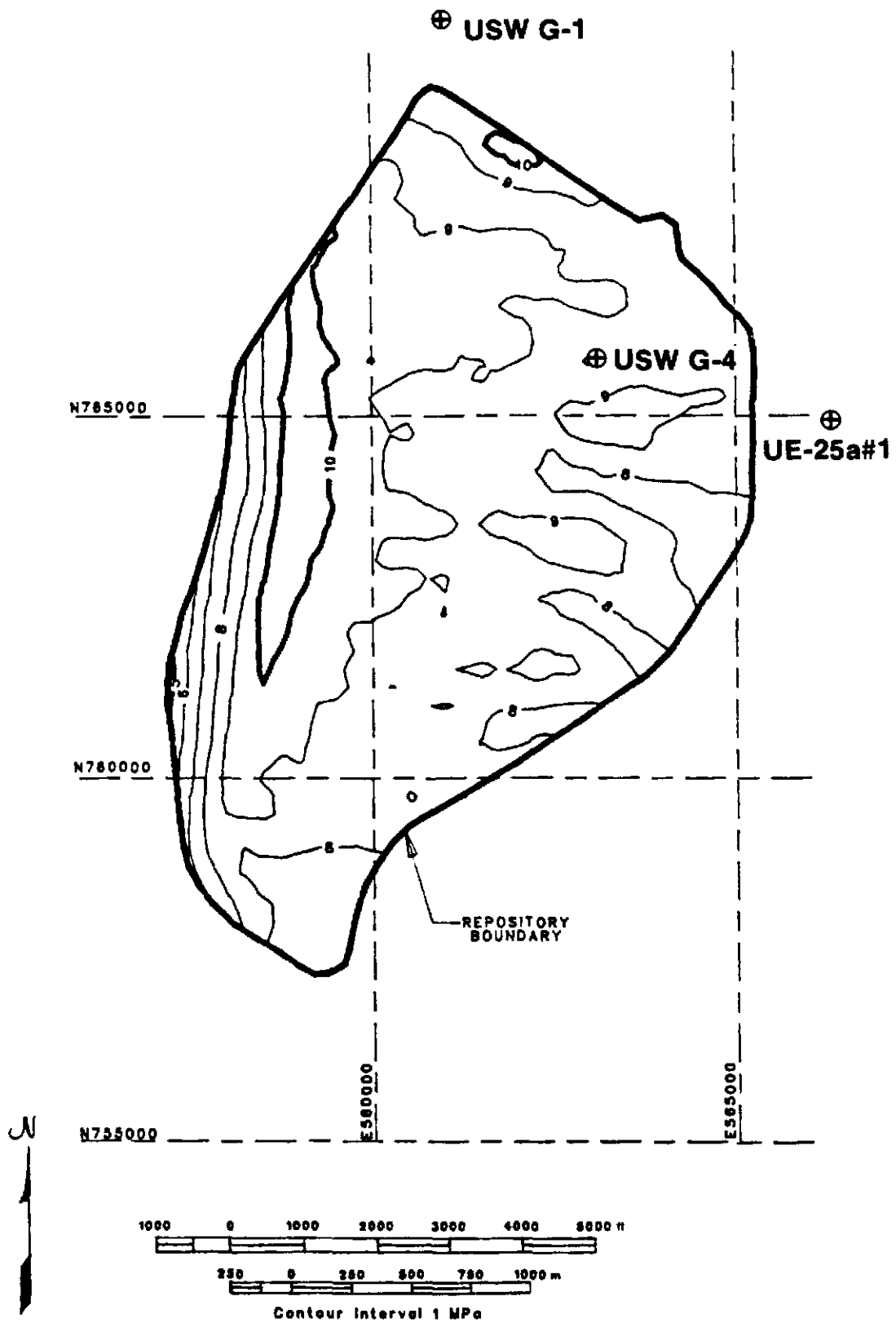


Figure 36. Calculated Vertical Stress at the Base of Unit TSw2

(MacDougall et al., 1987) (Figure 37). For the last of these surfaces, the mean vertical stress is calculated to be 7.28 MPa (1,060 psi) with a standard deviation of 0.89 MPa (130 psi).

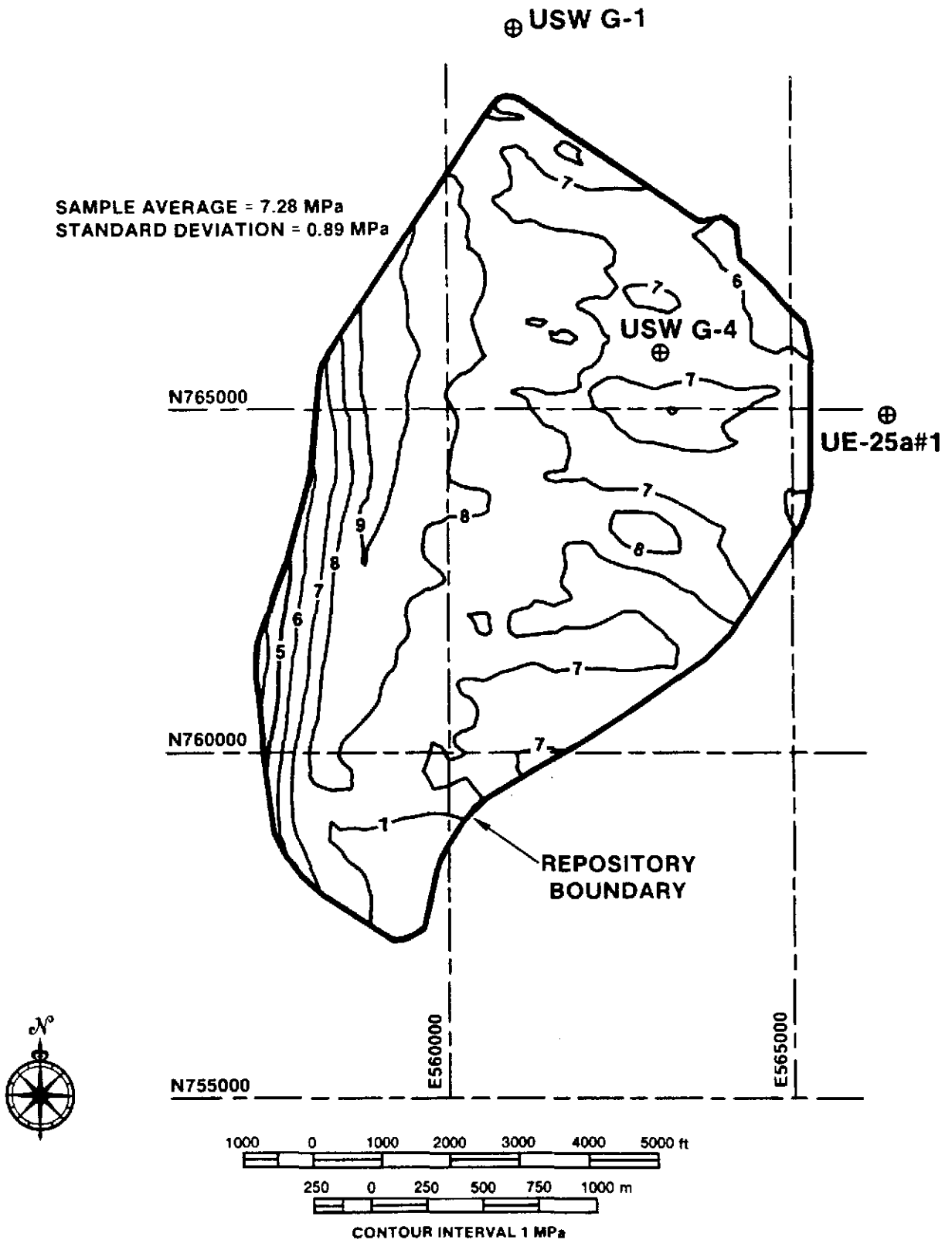


Figure 37. Calculated Vertical Stress at the Floor of the Design Repository

7.0 CONCLUSIONS

The purpose of this report is to provide a compilation of relevant properties that have been measured on the Topopah Spring Member, and to summarize the results of analyses that have been made in order to determine data quality and variability. The data compilation is presented in Appendix B. The following paragraphs and tables summarize the analyses of the data.

7.1 Bulk Properties

Porosity and grain density data were analyzed for units TSw1, TSw2, and TSw3, as well as for the material between units TSw2 and TSw3. The porosities of units TSw1 and TSw2 were found to show some spatial variability. Differences may be the result either of greater distance from the inferred source area or of greater amounts of vapor-phase-altered material in the bulk property samples.

The grain density of unit TSw1 also exhibited some spatial variability. The differences are attributed to mineralogic variation between core holes.

Table 23 contains a set of values for the bulk properties of the units under discussion. These values are considered to be the best single representation of these properties for use in computer modeling of the units.

Table 23

Bulk Properties of Units TSw1, TSw2, and TSw3

	<u>TSw1</u>	<u>TSw2</u>	<u>TSw3</u>
<u>Matrix Porosity</u>			
Mean Value	0.142 ^a	0.113 ^b	0.033 ^c
St. Dev.	0.038 ^a	0.026 ^b	0.014 ^c
No. of Samples	127	103	17
<u>Lithophysal Porosity</u>			
Mean Value	0.045	0.010	---
St. Dev.	0.061	0.019	---
No. of Samples	213 ^d	155 ^c	---
<u>Grain Density (g/cm³)^e</u>			
Mean Value	2.537 ^a	2.552	2.379
St. Dev.	0.041 ^a	0.033	0.016
No. of Samples	129	109	18
<u>"Natural-State" Bulk Density (g/cm³)^{e,f}</u>			
Mean Value	2.155 ^a	2.312 ^b	2.322 ^c
St. Dev.	0.176 ^a	0.078 ^b	0.029 ^c
No. of Samples	---	---	---
<u>Dry Bulk Density (g/cm³)^{e,f}</u>			
Mean Value	2.063 ^a	2.238 ^b	2.300 ^c
St. Dev.	0.185 ^a	0.087 ^b	0.037 ^c
No. of Samples	---	---	---

^aAssumes that spatial variability discussed in Sections 2.2.2.1 and 2.2.2.2 is not important.

^bAssumes that spatial variability in matrix porosity discussed in Section 3.2.2.1 is not important.

^cAssumes that spatial variability discussed in Section 4.2.2.1 is not important.

^dBased on assuming that a sample is a 10-ft (3 m) interval.

^eTo obtain units of lb/ft³, multiply by 62.43.

^fCalculated; assuming saturation of matrix porosity is 0.65 ± 0.19 for "natural-state" bulk density.

NA: Not available.

7.2 Thermal Properties

7.2.1 Heat Capacity

The limited amount of available data indicates that the heat capacity of solid material of single thermal/mechanical units does not vary spatially. In addition, the heat capacity of solid material in units TSw1 and TSw2 is indistinguishable. In contrast to the assumption in Tillerson and Nimick (1984) that the heat capacities of solids and pore water are constant, both are functions of temperature.

Table 24 summarizes the best single values of in situ volumetric heat capacity (ρC_p) as a function of temperature. Some spatial variability will exist because of the spatial variability in matrix porosity and lithophysal cavity abundance.

7.2.2 Thermal Expansion

The thermal expansion behavior of units TSw1 and TSw2 is complicated to interpret because of the strong dependence on mineralogy. Spatial variability of thermal expansion coefficients can be directly linked to spatial variability in mineralogy. However, until the mineralogic variation is better defined all data for a given set of experiment conditions are grouped into a single data set.

Table 24

Estimated In Situ Volumetric Heat Capacity^a as a Function
of Temperature for Units TSw1, TSw2, and TSw3

	Temperature								
	°C	25	50	99	101	150	200	250	300
	°F	77	122	210	214	302	392	482	572
TSw1		1.973	2.060	2.194	1.827	1.941	2.039	2.126	NE
TSw2		2.030	2.125	2.273	1.982	2.106	2.213	2.307	2.393
TSw3		1.830	2.015	2.288	2.211	2.408	2.563	2.688	NE

^aVolumetric heat capacity units are J/cm³K; to obtain units of
Btu/ft³°F, multiply by 14.911.

NE: Not estimated.

Table 25 summarizes the best single values of thermal expansion coefficients as a function of temperature for two conditions: unconfined and for a confining pressure of 10 MPa (1450 psi). Choice of coefficients for use in modeling of in situ thermomechanical response will depend on the expected in situ stress conditions.

7.2.3 Emissivity

Very few data on emissivity are available. A value of 0.89 has been measured on the Grouse Canyon Member of the Belted Range Tuff (Zimmerman et al., 1986) and is assumed to be valid for units TSw1 and TSw2 as well. A value in the range of 0.72 to 0.92 should apply for unit TSw3.

7.3 Mechanical Properties

7.3.1 Compression Experiments

Unconfined compression experiment results exhibited a difference in compressive strength and Young's modulus between core holes for unit TSw1. Samples from USW G-2 have greater mean values of both properties than do samples from USW GU-3. The relative values are consistent with porosity differences between the core holes. For a standard set of experiment conditions [ambient pressure and temperature, a strain rate of 10^{-5} s^{-1} , saturated 2.54 cm (1 in.) x 5.08 cm (2 in.) samples], Table 26 contains the best single values for compressive strength, Young's modulus, Poisson's ratio, and axial strain at failure for unit TSw2, as well as values of Poisson's ratio and axial strain at failure

Table 25

Thermal Expansion Coefficients^a as a Function of Temperature
for Units TSw1, TSw2, and TSw3

	Temperature					
	°C 25-50 °F 77-122	50-100 122-212	100-150 212-302	150-200 302-392	200-250 392-482	250-300 482-572
<u>TSw1 (Unconfined)</u>						
Mean Value	5.2	8.0	10.3	12.4	27.4	NA
St. Dev.	1.6	1.5	(+2.2, -1.8) ^b	(+13.6, -6.5) ^b	(+27.1, 13.6) ^b	NA
No. of Samples	13	13	22	22	16	0
<u>TSw1 (Confined)^c</u>						
Mean Value	9.9	9.6	d	d	d	NA
St. Dev.	1.5	2.3	d	d	d	NA
No. of Samples	9	9	d	d	d	0
<u>TSw2 (Unconfined)</u>						
Mean Value	2.5	7.5	9.2	13.1	20.6	36.7
St. Dev.	3.6	1.2	1.3	2.1	4.7	10.4
No. of Samples	17	7	14	11	7	7
<u>TSw2 (Confined)^d</u>						
Mean Value	10.7	9.8	d	d	d	d
St. Dev.	1.2	1.3	d	d	d	d
No. of Samples	7	8	d	d	d	d
<u>TSw3 (Unconfined)^c</u>						
Mean Value	1.0	6.5	6.1	4.9	2.0	NA
St. Dev.	0.9	1.6	2.1	2.0	4.5	NA
No. of Samples	3	3	3	3	3	0

^aUnits for thermal expansion coefficients are $10^{-6}^{\circ}\text{C}^{-1}$; to obtain units of $10^{-6}^{\circ}\text{F}^{-1}$, multiply by 5/9.

^bData in parentheses are deviations calculated from conversion of symmetrical standard deviation in \log_e units (data have lognormal distribution).

^cConfining pressure used is 10 MPa (1450 psi).

^dValues listed for unconfined conditions apply for both unconfined and confined material.

^eNo data are available for confined thermal expansion coefficients.

Table 26

Mechanical Properties (Determined in Compression)
for Units TSw1 and TSw2

	Unconfined Compressive Strength (MPa) ^a	Young's Modulus (GPa) ^a	Poisson's Ratio	Axial Strain at Failure (10 ⁻³)
<u>TSw1</u> (Lithophysae-rich ^b Values in Parentheses)				
Mean Value	NA (16.2)	NA (15.5)	0.20 ^c (0.16)	4.47 (1.23)
St. Dev.	NA (5.0)	NA (3.2)	0.01 ^c (0.03)	0.99 (0.18)
No. of Samples	NA (10)	NA (10)	2 (10)	8 (10)
<u>TSw2</u>				
Mean Value	147.9	31.2	0.27 ^d	5.54
St. Dev.	57.1	4.4	0.07 ^d	1.55
No. of Samples	20	20	10	20

^aTo obtain units of psi, multiply by 1.45×10^{-4} .

^bExperiment results were obtained on ten samples with a mean lithophysal cavity content of 0.167.

^cShould be assumed to apply only for axial stresses up to 69% of the failure stress.

^dShould be assumed to apply only for axial stresses up to 102 MPa (14,800 psi).

NA: Not applicable because of statistically significant spatial variability.

for unit TSw1. Data are insufficient to provide similar values for unit TSw3.

Data to infer changes in the values in Table 26 resulting from changes in confining pressure, temperature, strain rate, saturation state, or sample size are limited. No data are available for unit TSw1, although any trends found for unit TSw2 are expected to hold for unit TSw1 as well.

Increased confining pressure results in an indistinct increase in compressive strength, although variability at any given confining pressure is great. No single failure criterion can be justified as preferable based on the existing data. Compressive strength decreases with strain rate for rates between 10^{-3} s^{-1} and 10^{-7} s^{-1} with strength decreases from 5 percent to 14 percent per order-of-magnitude decrease in strain rate. No data are available with which to evaluate strength changes caused by changes in temperature or saturation state. Compressive strength (σ) decreases with increasing sample diameter (D) according to the following equation.

$$\sigma(\text{MPa}) = 1944 D(\text{mm})^{-0.846} + 69.5 \quad , \quad (21)$$

judged to be valid for sample diameters greater than or equal to 2.54 cm (1 in.).

Young's modulus of unit TSw2 is not significantly affected by changes in confining pressure, strain rate, or sample size. Data are unavailable

to evaluate changes in modulus resulting from changes in temperature or saturation state, although an estimate has been made that E_{dry}/E_{sat} may be of the order of 0.8.

Poisson's ratio and axial strain at failure appear to be unaffected by test parameters with one exception. Increasing sample diameter (D) results in decreasing strain to failure (ϵ_{ax}^f) according to the following equation:

$$\epsilon_{ax}^f (10^{-3}) = 11.6 D(\text{mm})^{-0.268} \quad . \quad (22)$$

Compressive strengths and Young's moduli for units TSw1 and TSw2 calculated from data for matrix porosity and clay content (functional porosity) are approximately consistent with experimental data. There is a tendency for calculated values to overestimate experimental values.

7.3.2 Tensile Tests

Tensile strength data are limited. Preliminary values for units TSw1 and TSw2 are presented in Table 27.

7.4 Other Conclusions

Material found between units TSw2 and TSw3 has properties ranging between those of the adjacent units. No attempt has been made to evaluate average properties for this material.

Table 27

Tensile Strength of Units TSw1 and TSw2

	TSw1	TSw2
Mean Value (MPa) ^a	21.1	15.2
St. Dev. (MPa) ^a	4.6	NA
No. of Samples	20	15

^aTo obtain units of psi, multiply by 1.45×10^{-4} .

NA: Not available.

Estimates of vertical in situ stress have been made assuming gravity loading. Stress contours are presented for three surfaces. For one of these, the center of the proposed repository level, vertical stress is calculated to be 7.28 ± 0.89 MPa ($1,060 \pm 130$ psi).

Acknowledgments: The authors' appreciation is extended to Bruce Whittet and Don South for assistance with development of the isopach and in situ stress data and figures; to Brian Ehgartner and Steve Bauer for careful technical reviews of the document; and to Mike Vogel for tireless work in investigation of the documentary back-up for the data in the report.

8.0 REFERENCES

- Anderson, L. A., 1981. "Rock Property Analysis of Core Samples from the Yucca Mountain UE25a-1 Borehole, Nevada Test Site, Nevada," U.S. Geological Survey Open-File Report 81-1338, Denver, CO.
- Anderson, L. A., 1984. "Rock Property Measurements on Large-Volume Core Samples from Yucca Mountain USW GU-3/G-3 and USW G-4 Boreholes, Nevada Test Site, Nevada," U.S. Geological Survey Open-File Report 84-552, Denver, CO.
- American Society for Testing and Materials, 1985a. "Standard Test Methods for Absorption and Bulk Specific Gravity of Natural Building Stone," ASTM C 97-83.
- American Society for Testing and Materials, 1985b. "Standard Test Method for Triaxial Compressive Strength of Undrained Rock Core Specimens Without Pore Pressure Measurements," ASTM D 2664-80.
- American Society for Testing and Materials, 1985c. "Standard Method for Laboratory Determination of Pulse Velocities and Ultrasonic Elastic Constants of Rock," ASTM D 2845-83.
- American Society for Testing and Materials, 1985d. "Standard Test Method for Direct Tensile Strength of Intact Rock Core Specimens," ASTM D 2936-84.
- American Society for Testing and Materials, 1985e. "Standard Test Method for Unconfined Compressive Strength of Intact Rock Core Specimens," ASTM D 2938-79.
- American Society for Testing and Materials, 1985f. "Standard Test Method for Elastic Moduli of Intact Rock Core Specimens in Uniaxial Compression," ASTM D 3148-80.
- American Society for Testing and Materials, 1985g. "Standard Test Method for Splitting Tensile Strength of Intact Rock Core Specimens," ASTM D 3967-81.
- American Society for Testing and Materials, 1985h. "Standard Test Method for Linear Thermal Expansion of Rigid Solids with a Vitreous Silica Dilatometer," ASTM E 228-71 (Reapproved 1979).
- American Society for Testing and Materials, 1985i. "Standard Test Method for Linear Thermal Expansion of Solid Materials by Thermodilatometry," ASTM E 831-81.
- Bauer, S. J., and J. Handin, 1983. "Thermal Expansion and Cracking of Three Confined, Water-Saturated Igneous Rocks to 800°C," Rock Mechanics and Rock Engineering, v. 16, p. 181-198.
- Bish, D. L., and D. T. Vaniman, 1985. "Mineralogic Summary of Yucca Mountain, Nevada," LA-10543-MS, Los Alamos National Laboratories, Los Alamos, NM.

- Blacic, J., 1985. Personal communication, 5/16/85.
- Blacic, J., J. Carter, P. Halleck, P. Johnson, T. Shankland, R. Andersen, K. Spicochi, and A. Heller, 1982. "Effects of Long-Term Exposure of Tuffs to High-Level Nuclear Waste-Repository Conditions. Preliminary Report," LA-9174-PR, Los Alamos National Laboratories, Los Alamos, NM.
- Blacic, J. D., D. T. Vaniman, D. L. Bish, C. J. Duffy, and R. C. Gooley, 1986. "Effects of Long-Term Exposure of Tuffs to High-Level Nuclear Waste-Repository Conditions: Final Report," LA-9330-MS, Los Alamos National Laboratory, Los Alamos, NM.
- Brodsky, N. S., I. C. Getting, and H. Spetzler, 1985. "An Experimental and Theoretical Approach to Rock Deformation at Elevated Temperature and Pressure," in H. J. Pincus and E. R. Hoskins (Eds.), Measurement of Rock Properties at Elevated Pressures and Temperatures, ASTM STP 869, American Society for Testing and Materials, Philadelphia, PA, p. 37-54.
- Buettner, K. J. K., and C. D. Kern, 1965. "The Determination of Infrared Emissivities of Terrestrial Surfaces," J. Geophys. Res., v. 70, p. 1329-1337.
- Byers, F. M., Jr., 1985. "Petrochemical Variation of Topopah Spring Tuff Matrix with Depth (Stratigraphic Level), Drill Hole USW G-4, Yucca Mountain, Nevada," LA-10561-MS, Los Alamos National Laboratory, Los Alamos, NM.
- Byers, F. M., Jr., W. J. Carr, P. P. Orkild, W. D. Quinlivan, and K. A. Sargent, 1976. "Volcanic Suites and Related Cauldrons of Timber Mountain - Oasis Valley Caldera Complex, Southern Nevada," U.S. Geological Survey Professional Paper 919, 70 p.
- Caporuscio, F., D. Vaniman, D. Bish, D. Broxton, B. Arney, G. Heiken, F. Byers, R. Gooley, and E. Semarge, 1982. "Petrologic Studies of Drill Cores USW-G2 and UE25b-1H, Yucca Mountain, Nevada;" LA-9255-MS, Los Alamos National Laboratory, Los Alamos, NM.
- Carlos, B. A., 1985. "Minerals in Fractures of the Unsaturated Zone from Drill Core USW G-4, Yucca Mountain, Nye County, Nevada," LA-10415-MS, Los Alamos National Laboratories, Los Alamos, NM.
- Connolly, J. R., 1982. Personal communication, 11/3/82.
- Connolly, J. R., 1986. Personal communication, June 1986.
- Costin, L. S., 1983. "A Microcrack Model for the Deformation and Failure of Brittle Rock," J. Geophys. Res., v. 88, no. B11, p. 9485-9492.
- Dana, R. W., 1969. "Measurements of 8-14 Micron Emissivity of Igneous Rock and Mineral Surfaces," University of Washington Dept. of Atmospheric Sciences Scientific Report on Contract NASA NsG-632, 78 p.

- Eichelberger, J. C., and H. R. Westrich, 1981. "Magmatic Volatiles in Explosive Rhyolitic Eruptions," Geophysical Research Letters, v. 8, no. 7, p. 757-760.
- Griffin, R. E., and S. G. Demou, 1971. "Thermal Expansion Measurements of Simulated Lunar Rocks," Third Symp., AIP Conf. Therm. Exp. Proc., p. 302-311.
- Griggs, D. T., F. J. Turner, and H. C. Heard, 1960. "Deformation of Rocks at 500°C to 800°C," Geol. Soc. Amer. Memoir 79, p. 39-104.
- Grim, R. E., 1953. "Clay Mineralogy," McGraw-Hill Book Company, Inc. (New York, NY).
- Iman, R. L., and W. J. Conover, 1983. "Modern Business Statistics," John Wiley and Sons (New York, NY).
- International Society of Rock Mechanics, 1978. "Suggested Methods for Determining Tensile Strength of Rock Materials," Int. J. Rock Mech. Min. Sci. and Geomech. Abstr., v. 15, p. 99-103.
- International Society of Rock Mechanics, 1979a. "Suggested Methods for Determining the Uniaxial Compressive Strength and Deformability of Rock Materials," Int. J. Rock Mech. Min. Sci. and Geomech. Abstr., v. 16, p. 135-140.
- International Society of Rock Mechanics, 1979b. "Suggested Methods for Determining Water Content, Porosity, Density, Absorption and Related Properties and Swelling and Slake-Durability Index Properties," Int. J. Rock Mech. Min. Sci. and Geomech. Abstr., v. 16, p. 141-156.
- International Society of Rock Mechanics, 1983. "Suggested Methods for Determining the Strength of Rock Materials in Triaxial Compression: Revised Version," Int. J. Rock Mech. Min. Sci. and Geomech. Abstr., v. 20, no. 6, p. 283-290.
- Jaeger, J. C., and N. G. W. Cook, 1979. "Fundamentals of Rock Mechanics (Third Edition)," Chapman and Hall (London, England), 593 p.
- Jezek, P. A., and D. C. Noble, 1978. "Natural Hydration and Ion Exchange of Obsidian: An Electron Microprobe Study," Amer. Miner., v. 63, p. 266-273.
- Jones, J. B., and E. R. Segnit, 1971. "The Nature of Opal. I. Nomenclature and Constituent Phases," J. Geol. Soc. Australia, v. 18, no. 1, p. 57-68.
- Klavetter, E. A., and B. M. Schwartz, 1984a. "Saturation Procedures," Internal Memorandum to Distribution, April 3, 1985.
- Klavetter, E. A., and B. M. Schwartz, 1984b. "Results of Long-Term Saturation Tests of Six Tuff Samples," Internal Memorandum to Distribution, July 31, 1984.

- Koizumi, M., 1953. "The Differential Thermal Analysis Curves and the Dehydration Curves of Zeolites," Miner. Journal., v. 1, no. 1, p. 36-47.
- Lama, R. D., and V. S. Vutukuri, 1978. "Handbook on Mechanical Properties of Rocks - Testing Techniques and Results - Volume II," Trans Tech Publications (Clausthal, Germany).
- Lappin, A. R., R. G. Van Buskirk, D. O. Enniss, S. W. Butters, F. M. Prater, C. S. Muller, and J. L. Bergosh, 1982. "Thermal Conductivity, Bulk Properties, and Thermal Stratigraphy of Silicic Tuffs from the Upper Portion of Hole USW-G1, Yucca Mountain, Nye County, Nevada," SAND81-1873, Sandia National Laboratories, Albuquerque, NM.
- Levy, S. S., 1983. "Studies of Altered Vitrophyre for the Prediction of Nuclear Waste Repository-Induced Thermal Alteration at Yucca Mountain, Nevada," LA-UR-83-3402, Los Alamos National Laboratories, Los Alamos, NM.
- Levy, S. S., 1984. "Petrology of Samples from Drill Holes USW H-3, H-4, and H-5, Yucca Mountain Nevada," LA-9706-MS, Los Alamos National Laboratory, Los Alamos, NM.
- Levy, S. S., 1986. Personal communication, 2/14/86.
- Levy, S. S., 1987. "Alteration Products and Processes in the Lower Topopah Spring Member of the Paintbrush Tuff, Yucca Mountain, Nevada," LA-10677-MS, Los Alamos National Laboratory, Los Alamos, NM.
- Lipman, P. W., 1965. "Chemical Comparison of Glassy and Crystalline Volcanic Rocks," U.S. Geological Survey Bulletin 1201-D, 24 p.
- Lyon, R. J. P., 1965. "Analysis of Rocks by Spectral Infrared Emission (8 to 25 Microns)," Econ. Geol., v. 60. p. 715-736.
- MacDougall, H. R., L. W. Scully, and J. R. Tillerson (comp.), 1987. "Site Characterization Plan Conceptual Design Report," SAND84-2641, Sandia National Laboratories, Albuquerque, NM.
- Maldonado, F., and S. L. Koether, 1983. "Stratigraphy, Structure, and Some Petrographic Features of Tertiary Volcanic Rocks at the USW G-2 Drill Hole, Yucca Mountain, Nye County, Nevada," U.S. Geological Survey Open-File Report 83-732, Denver, CO.
- Mansure, A. J., and T. S. Ortiz, 1984. "Preliminary Evaluation of the Subsurface Area Available for a Potential Nuclear Waste Repository at Yucca Mountain," SAND84-0175, Sandia National Laboratories, Albuquerque, NM.
- McTigue, D. F., R. K. Wilson, and J. W. Nunziato, 1984. "An Effective Stress Principle for Partially Saturated Media," SAND82-1977, Sandia National Laboratories, Albuquerque, NM.

- Montazer, P., and W. E. Wilson, 1984. "Conceptual Hydrologic Model of Flow in the Unsaturated Zone, Yucca Mountain, Nevada," U.S. Geological Survey Open-File Report 84-4345, Denver, CO.
- Mumpton, F. A., 1960. "Clinoptilolite Redefined," *Am. Miner.*, v. 45, p. 351-369.
- Murrell, S. A. F., 1963. "A Criterion for Brittle Fracture of Rocks and Concrete Under Triaxial Stress and the Effect of Pore Pressure on the Criterion," Proc. Fifth Rock Mechanics Symposium, University of Minnesota, p. 563-577.
- Nimick, F. B., in preparation, a. "The Thermal Conductivity of the Topopah Spring Member at Yucca Mountain, Nevada," SAND86-0090, Sandia National Laboratories, Albuquerque, NM.
- Nimick, F. B., in preparation, b. "Thermal Conductivity and Thermal Expansion of a Lithophysal Zone Within the Topopah Spring Member of the Paintbrush Tuff," SAND85-2437, Sandia National Laboratories, Albuquerque, NM.
- Nimick, F. B., R. G. Van Buskirk, and A. J. MacFarland, 1987. "Uniaxial and Triaxial Compression Test Series on the Topopah Spring Member from USW G-2, Yucca Mountain, Nevada," SAND85-0703, Sandia National Laboratories, Albuquerque, NM.
- Nimick, F. B., and A. R. Lappin, 1985. "Thermal Conductivity of Silicic Tuffs from Yucca Mountain and Rainier Mesa, Nye County, Nevada," SAND83-1711J, Sandia National Laboratories, Albuquerque, NM.
- Nimick, F. B., R. H. Price, R. G. Van Buskirk, and J. R. Goodell, 1985. "Uniaxial and Triaxial Compression Test Series on Topopah Spring Tuff from USW G-4, Yucca Mountain, Nevada," SAND84-1101, Sandia National Laboratories, Albuquerque, NM.
- Nimick, F. B., and R. L. Williams, 1984. "A Three-Dimensional Geologic Model of Yucca Mountain, Southern Nevada," SAND83-2593, Sandia National Laboratories, Albuquerque, NM.
- Olsson, W. A., and A. K. Jones, 1980. "Rock Mechanics Properties of Volcanic Tuffs from the Nevada Test Site," SAND80-1453, Sandia National Laboratories, Albuquerque, NM.
- Ortiz, T. S., R. L. Williams, F. B. Nimick, B. C. Whittet, and D. L. South, 1985. "A Three-Dimensional Model of Reference Thermal/Mechanical and Hydrological Stratigraphy at Yucca Mountain, Southern Nevada," SAND84-1076, Sandia National Laboratories, Albuquerque, NM.
- Page, L., and H. C. Heard, 1981. "Elastic Moduli, Thermal Expansion, and Inferred Permeability of Climax Quartz Monzonite and Sudbury Gabbro to 500°C and 55 MPa," Proc. of the 22nd U.S. Symposium on Rock Mechanics, Massachusetts Institute of Technology, June 28 - July 2, 1981, p. 97-104.

- Paterson, M. S., 1978. "Experimental Rock Deformation - The Brittle Field," Springer-Verlag (New York), 254 p.
- Peters, R. R., E. A. Klavetter, I. J. Hall, S. C. Blair, P. R. Heller, and G. W. Gee, 1984, "Fracture and Matrix Hydrologic Characteristics of Tuffaceous Materials from Yucca Mountain, Nye County, Nevada;" SAND84-1471, Sandia National Laboratories, Albuquerque, NM.
- Price, R. H., 1983. "Analysis of Rock Mechanics Properties of Volcanic Tuff Units from Yucca Mountain, Nevada Test Site," SAND82-1315, Sandia National Laboratories, Albuquerque, NM.
- Price, R. H., 1986. "Effects of Sample Size on the Mechanical Behavior of Topopah Spring Tuff," SAND85-0709, Sandia National Laboratories, Albuquerque, NM.
- Price, R. H., and S. J. Bauer, 1984. "Analysis of the Elastic and Strength Properties of Yucca Mountain Tuff, Nevada," Proc. 26th U.S. Symposium on Rock Mechanics, p. 89-96.
- Price, R. H., F. B. Nimick, J. R. Connolly, K. Keil, B. M. Schwartz, and S. J. Spence, 1985. "Preliminary Characterization of the Petrologic, Bulk, and Mechanical Properties of a Lithophysal Zone Within the Topopah Spring Member of the Paintbrush Tuff," SAND84-0860, Sandia National Laboratories, Albuquerque, NM.
- Price, R. H., K. G. Nimick, and J. A. Zirzow, 1982. "Uniaxial and Triaxial Compression Test Series on Topopah Spring Tuff," SAND82-1723, Sandia National Laboratories, Albuquerque, NM.
- Price, R. H., S. J. Spence, and A. K. Jones, 1984. "Uniaxial Compression Test Series on Topopah Spring Tuff from USW GU-3, Yucca Mountain, Southern Nevada," SAND83-1646, Sandia National Laboratories, Albuquerque, NM.
- Riehle, J. R., 1973. "Calculated Compaction Profiles of Rhyolitic Ash-Flow Tuffs," Geol. Soc. Amer. Bull., v. 84, p. 2193-2216.
- Ross, C. S., and R. L. Smith, 1955. "Water and Other Volatiles in Volcanic Glass," Amer. Miner., v. 40, p. 1071-1089.
- Sammis, C. G., and M. F. Ashby, 1986. "The Failure of Brittle Porous Solids Under Compressive Stress States," Acta Metall., v. 34, no. 3, p. 511-526.
- SAS Institute, Inc., 1982a. "SAS User's Guide: Basics, 1982 Edition," SAS Institute, Inc. (Cary, NC).
- SAS Institute, Inc., 1982b. "SAS User's Guide: Statistics, 1982 Edition," SAS Institute, Inc. (Cary, NC).
- Schwartz, B. M., 1981. "Unconfined Volumetric Changes in Tuff Caused by Dehydration and the Effect on Dry Bulk Densities and Porosities," Internal Memorandum to Distribution, October 23, 1981.

- Schwartz, B. M., 1985. "Grain Density Measurements of Ash Flow Tuffs: An Experimental Comparison of Water Immersion and Gas Intrusion Pycnometer Techniques," SAND83-1327, Sandia National Laboratories, Albuquerque, NM.
- Schwartz, B. M., 1986. Personal Communication.
- Scott, R. B., and M. Castellanos, 1984. "Stratigraphic and Structural Relations of Volcanic Rocks in Drill Holes USW GU-3 and USW G-3, Yucca Mountain, Nye County, Nevada," U.S. Geological Survey Open-File Report 84-491, Denver, CO.
- Smith, R. L., 1960. "Zones and Zonal Variations in Welded Ash Flows," U.S. Geological Survey Professional Paper 354-F.
- Spengler, R. W., 1985. Personal Communication.
- Spengler, R. W., F. M. Byers, Jr., and J. B. Warner, 1981. "Stratigraphy and Structure of Volcanic Rock in Drill Hole USW-G1, Yucca Mountain Nye County, Nevada," U.S. Geological Survey Open-File Report 81-1349, Denver, CO.
- Spengler, R. W., D. C. Muller, and R. B. Livermore, 1979. "Preliminary Report on the Geology and Geophysics of Drill Hole UE25a-1, Yucca Mountain, Nevada," U.S. Geological Survey Open-File Report 79-1244, Denver, CO.
- Spengler, R. W., and M. P. Chornack, 1984. "Stratigraphic and Structural Characteristics of Volcanic Rocks in Core Hole USW G-4, Yucca Mountain, Nye County, Nevada," with a section on geophysical logs by D. C. Muller and J. Kibler; U.S. Geological Survey Open-File Report 84-789, Denver, CO.
- Tillerson, J. R., and F. B. Nimick (eds.), 1984. "Geoengineering Properties of Potential Repository Units at Yucca Mountain, Southern Nevada," SAND84-0221, Sandia National Laboratories, Albuquerque, NM.
- Van Buskirk, R., D. Enniss, and J. Schatz, 1985. "Measurement of Thermal Conductivity and Thermal Expansion at Elevated Temperatures and Pressures," in H. J. Pincus and E. R. Hoskins (Eds.), Measurement of Rock Properties at Elevated Pressures and Temperatures, ASTM STP 869, American Society for Testing and Materials, Philadelphia, PA, p. 108-127.
- Vaniman, D., D. Bish, D. Broxton, F. Byers, G. Heiken, B. Carlos, E. Semarge, F. Caporuscio, and R. Gooley, 1984. "Variations in Authigenic Mineralogy and Sorptive Zeolite Abundance at Yucca Mountain, Nevada. Based on Studies of Drill Cores USW GU-3 and G-3;" LA-9707-MS, Los Alamos National Laboratories, Los Alamos, NM.
- Venugopal, J.S., B.V. Hirannaiah, and S.K. Maiumder, 1982. "Dehydroxylation and Dehydration as Parameters for Characterization of Clays - Part I: Montmorillonite, Attapulgitite and Illite," J. Geol. Soc. India, v. 23, no. 3, p. 123-128.

- Zielinski, R. A., 1980. "Stability of Glass in the Geologic Environment: Some Evidence from Studies of Natural Silicate Glasses," Nuclear Technology, v. 51, p. 197-200.
- Zimmerman, R. M., M. L. Blanford, J. F. Holland, R. L. Schuch, and W. H. Barnett, 1986. "Final Report: G-Tunnel Small-Diameter Heater Experiments," SAND84-2621, Sandia National Laboratories, Albuquerque, NM.
- Zimmerman, R. M., F. B. Nimick, and M. P. Board, 1984. "Geoengineering Characterization of Welded Tuffs from Laboratory and Field Investigations," Materials Research Society Symposia Proc., v. 44, p. 547-554.
- Zimmerman, R. M., R. L. Schuch, D. Mason, M. L. Wilson, M. E. Hall, M. P. Board, R. P. Bellman, and M. L. Blanford, 1986. "Final Report: G-Tunnel Heated Block Experiment," SAND84-2620, Sandia National Laboratories, Albuquerque, NM.

APPENDIX A

Experiment Procedures

This appendix contains summaries of the experiment procedures used by Sandia National Laboratories (SNL) or by SNL subcontractors to obtain the properties discussed in the remainder of the report. Additional detail is to be found in references cited in individual subsections of the appendix. Procedures used by non-SNL organizations can be found in the original references as cited in Appendix B.

A.1 Procedures for Saturating and Drying Samples

A.1.1 Saturation

The following is a summary of American Society for Testing Materials (ASTM) and International Society for Rock Mechanics (ISRM) procedures pertaining to the saturation of samples to be used in mechanical (compressive, tensile), thermal conductivity, and thermal expansion experiments. The procedures relating to compressive and tensile testing of rocks do not address vacuum saturation of samples or other methods of saturation that would ensure complete and/or repeatable saturation for densely welded tuff from the Topopah Spring Member. The following list synthesizes information on sample saturation:

1. ASTM D 2938-79 (Unconfined Compressive Strength) - The only reference to the moisture content of samples is found in Section 4.4, in which

it is recommended that the moisture condition of the experiment sample be either representative of field conditions or tailored to the problem at hand and well-documented.

2. ASTM D 3148-80 (Elastic Moduli) - The only reference to the moisture content of samples is found in Section 8.1.9 in which it is recommended that the moisture condition of the experiment sample be "precisely determined when possible and reported as either water content or degree of saturation."
3. ASTM D 2664-80 (Triaxial Compressive Strength) - The only reference to the moisture content of samples is found in Section 6.4 in which it is recommended that the moisture condition of the experiment sample be either representative of field conditions or tailored to the problem at hand and well-documented.
4. ASTM D 2845-83 (Pulse Velocities and Ultrasonic Elastic Constants) - This procedure, although not related to compressive experiments on rocks, was found to contain in Section 6.2.3 a vacuum-saturation procedure at ambient temperature. The criterion for defining constant weight is when sample weight increases do not exceed 0.1 percent within successive 24-hour periods.
5. ISRM (1979a) (Uniaxial Compressive Strength and Deformability) - Does not address specific procedures for obtaining completely saturated samples prior to testing.

6. ISRM (1983) (Strength in Triaxial Compression) - Does not address specific procedures for obtaining completely saturated samples prior to testing.
7. ASTM D 2936-84 (Direct Tensile Strength) - Does not address sample saturation.
8. ASTM D 3967-81 (Splitting Tensile Strength) - Does not address sample saturation.
9. ISRM (1978) (Tensile Strength) - Section 3.e states that following sample preparation, specimens should be stored prior to testing for 5-6 days @ 20°C (68°F) and 50 percent humidity.
10. ASTM E 831-81 (Thermal Expansion) - Does not address sample saturation.
11. ASTM E 228-71 (Thermal Expansion) - Does not address sample saturation.
12. Brodsky et al. (1985) (Compressive Strength) - Experiment specimens are to be stored at room temperature in 100 percent relative humidity air. Stable weight gain noted but not required.
13. Van Buskirk et al. (1985) (Thermal Conductivity and Thermal Expansion) - Does not address sample saturation.

In an attempt to come closer to complete saturation and at the very least to saturate tuff samples to a more precise definition of "constant weight," several changes were made to saturation procedures during the approximately 5 years the samples discussed in this report were tested.

The primary change to the saturation procedure was to change the criterion from simply a length of time to one based on percent weight gain of the sample in a certain time period. Initially, experiment samples to be run in a "saturated condition" were submerged in water at ambient temperature and pressure for at least 48 hours before testing. The criterion was later changed to a time period greater than or equal to 72 hours because of concern about incomplete saturation of samples. The actual time that the samples were exposed to these ambient conditions was usually much greater, because the samples were exposed to water during sample preparation and were shipped to the testing laboratory in jars in which the samples were submerged in water. The samples typically remained in these submerged conditions for several weeks before testing.

An attempt was made to develop more stringent requirements to address the fact that the rocks tested were of very low permeability and laboratory experiments seemed to indicate that neither ASTM or ISRM procedures were sufficient to completely saturate the types of low-permeability samples such as welded tuff samples from the Topopah Spring Member at Yucca Mountain. In addition, the ASTM and ISRM procedures listed were not thought to be rigorous enough to ensure complete saturation for the sample sizes utilized in thermal and mechanical experiments discussed in this report.

A procedure for vacuum-saturation was written to exceed the requirements of ASTM D 2845 pertaining to the definition of constant weight. Where ASTM procedure D 2845 defines constant weight as weight gain of less than 0.1 percent in a 24-hour period, the new procedure defined it as less than 0.05 percent weight gain in a 24- through 36-hour period. This new procedure has been used in all thermal, mechanical, and physical property experiments for which complete saturation was required that have been performed since July 21, 1983, the implementation date of the revised procedure.

As a result of the changes in procedures discussed above, the state of saturation cannot be generalized for all of the experiment samples in this report. However, certain ranges of saturation for the samples can be reasonably defined. The following is a summary of analyses of two carefully controlled saturation experiments. The experiments address the efficiency of obtaining complete saturation when saturating samples by ambient pressure submersion, vacuum saturation and pressure saturation, all performed at ambient temperature.

Klavetter and Schwartz (1984b) showed that two welded samples of the Topopah Spring Member from USW G-1 [nominal dimensions of 6.35 cm (2.5 in.) diameter by 1.27 cm (0.5 in.) thick] had reached approximately 75 percent of total saturation after 100 hours of submersion in water at ambient temperature and pressure. For all thermal, mechanical and physical property experiments for which instructions were to saturate at ambient pressure (and temperature) for more than 72 hours, it is reasonable to assume that the samples achieved a saturation of at least 75 percent. The saturation was probably even greater because experiment

samples were exposed to water for several hours during preparation and were submerged in water after sample preparation for several weeks before testing, including time during shipment of samples to the testing laboratory.

Klavetter and Schwartz (1984a), showed that in two cylindrical samples of the densely welded Topopah Spring Member [nominal dimensions 5.08 cm (2 in.) diameter by 10.16 cm (4 in.) long], an average 9.45 percent increase in saturation was achieved when pressure saturation (application of elevated pore pressure) was performed on samples that had been vacuum saturated previously to constant weight per ASTM D 2845-83. The data also show that in three cylindrical samples of the densely welded Topopah Spring Member [nominal dimensions 2.54 cm (1 in.) diameter by 5.08 cm (2 in.) long] an average 5.73 percent increase in saturation was achieved when pressure saturation was performed on samples that had already been vacuum saturated to constant weight per ASTM procedures.

Therefore, because all samples discussed here were either saturated via ambient pressure submersion and/or vacuum saturation, 2.54 cm (1 in.) diameter samples were approximately 75 percent to 94 percent saturated, and 5.08 cm (2 in.) diameter samples were approximately 75 percent to 91 percent saturated.

A.1.2 Drying

A.1.2.1 Bulk Density Samples. Dry bulk density data in this report were initially obtained on samples that had been dried at 105°C (221°F)

for 24 hours or more. Because of concerns that densely welded samples were not being adequately dried, the temperature was raised to 110°C (230°F), and the time requirement first was lengthened to greater than or equal to 48 hours, then was extended to 72 hours. Communication with laboratories performing the work indicated that drying times were typically exceeded (as allowed by the wording of the requirement), in part to ensure that the samples were dried and also as a way to fit the work into their schedule. An evaluation of ASTM and ISRM procedures was made in August 1983 to arrive at a more rigorous and reproduceable method to dry samples in support of obtaining a dry weight for dry bulk density measurements.

As is the case for saturation procedures, neither ASTM or ISRM procedures are adequate to ensure that constant weight is obtained during drying for low-permeability materials such as densely welded samples from the Topopah Spring Member.

ASTM C 97-83 (Absorption and Bulk Specific Gravity) - Section 4.3 requires drying for 24 hours at 105°C (221°F).

ISRM (1979b) (Water Content, Porosity, Density, Absorption and Related Properties) - recommends that a sample be dried for at least 24 hours at 105°C (221°F) to obtain a dry sample for physical property measurements.

Although it appeared that our procedures were consistent with generally accepted laboratory practice, there was some concern that the existing procedures were not adequate when the low permeability of the densely welded samples from the Topopah Spring Member was considered. To

minimize the concern, the criterion used to dry samples was modified from one based only on time to one based on percent weight loss of the sample in a certain time period. The criterion, which was formalized on March 30, 1984, defines constant weight as a weight loss of less than 0.05 percent in a 24- through 36-hour period after drying for 120 hours at 105°C (221°F).

A.1.2.2 Larger Samples. Unpublished experimental data (Schwartz, 1986) indicate that densely welded tuff from the Topopah Spring Member [5.38 cm (2.12 in.) nominal diameter and 10.16 cm (4 in.) long] retain the following saturation values:

For samples dried at 105°C (221°F) for 46 hours, the mean value and standard deviation are 9.5 percent and 7.55 percent, respectively.

For samples dried at 105°C (221°F) for 73 hours, the mean value and standard deviation are 5.2 percent and 4.85 percent, respectively.

For samples dried at 105°C (221°F) for 101 hours, the mean value and standard deviation are 2.3 percent and 2.63 percent, respectively.

The constant weight procedure requires that the sample be dried at 105°C (221°F) for at least 120 hours. Therefore, the mean saturation level for densely welded tuff samples from the Topopah Spring Member of diameter less than or equal to 5.38 cm (2.12 in.) that were dried per the drying procedure formalized on March 30, 1984, would be less than 2.3 percent.

A.2 Bulk Density

A.2.1 Saturated Bulk Density

Saturated and dry bulk density tests were run per revision A of SNL NNWSI quality assurance procedure (QAP) XI-9. The QAP was titled Quality Assurance Procedure and Standard Operating Procedures for Bulk Property Measurements. The procedure is quite detailed; only part of the procedure is summarized here.

A.2.1.1 Operating Procedures. The sample is submerged in water from Well J-13 or in distilled water until constant weight is attained (at least 72 hours at ambient temperature and pressure). The weight of the saturated sample is determined by subtracting the weight of the water and container from the total weight (water, container, and sample). The volume is determined using the principle of Archimedes by measuring the buoyant weight of the saturated sample. The weight of the saturated sample is divided by the volume of distilled water displaced by the immersed sample to yield the saturated bulk density in grams per cubic centimeter.

A.2.1.2 Calibration Checks. Calibration checks consisted of running either a magnesium bar or a stainless steel ball. The magnesium bar has been assayed at SNL by atomic absorption spectroscopy and emission spectroscopy for qualitative and semiquantitative analysis, respectively. The theoretical density of magnesium is 1.74 g/cm^3 (108.6 lb/ft^3). The stainless steel ball has been analyzed for density

by the standards group at SNL. The calibrated density is 7.644 g/cm^3 (477.2 lb/ft^3). Calibration checks are made once per week when any type of bulk density measurement is being performed, using the same analytical balance used that week for the bulk density measurements.

Limited data suggest that measured saturated bulk densities of devitrified tuff are precise to 0.010 g/cm^3 (0.62 lb/ft^3). Corresponding data are not available for other lithologies. No data on the accuracy of saturated bulk density values are available.

A.2.2 Dry Bulk Density

The same sample used to determine the saturated bulk density per Appendix A.2.1 is dried to constant weight in air at ambient pressure (see Appendix A.1.2 for a discussion of the evolution of the criterion for constant weight). The sample is then cooled in an evacuated desiccator until it is weighed. The weighing of the dried sample should take place within 1 minute of removal of the sample from the desiccator because the sample will absorb water on exposure to air with a corresponding weight gain, which can reduce the accuracy and precision of the results.

The weight of the sample is measured directly on an analytical balance. The sample volume used is the same volume measured in its saturated state because data have shown that for the tuff samples analyzed, the volume reduction resulting from dehydration is

insignificant compared to the effect on experiment results resulting from normal operator error and sample inhomogeneity (Schwartz, 1981). The weight of the dry sample is divided by the volume of the sample in the saturated state to yield the dry bulk density in grams per cubic centimeter.

Calibration checks of the equipment are identical to the procedures defined in Appendix A.2.1. Measured dry bulk densities have a precision of 0.054 g/cm^3 (3.37 lb/ft^3) for devitrified samples. No data are available for other lithologies or for the accuracy of the measurements.

A.3 Grain Density

A.3.1 Water Pycnometer Technique

Grain Density tests using a water pycnometer were run per revision A of SNL NNWSI quality assurance procedure (QAP) XI-10. The QAP was titled Quality Assurance and Standard Operating Procedures for Grain Density Measurements Using a Water Pycnometer. The procedure is quite detailed; only part of the procedure is summarized here.

A.3.1.1 Operating Procedures. The water pycnometer apparatus was assembled using commercially available laboratory 100-ml glass volumetric flasks calibrated $\pm 0.10 \text{ ml}$, glass thermometers, double-distilled water, an evacuation chamber, and a mechanical vacuum pump. The principle of operation is that a volume of powder is determined from the weight of distilled water (of known density) displaced in the pycnometer by the

powdered sample. The grain density (g/cm^3) is obtained by dividing the grain weight by the grain volume. The grain weight is measured on an analytical balance.

The test begins by weighing a dry 100-ml pycnometer. The powdered sample is then placed into the pycnometer, and the pycnometer is reweighed. Then 40 ml of deaerated distilled water is poured into the pycnometer, which then is placed in a vacuum chamber, evacuated, and swirled to remove trapped air from the powder-water slurry. The contents of the pycnometer are returned to ambient pressure and temperature. The pycnometer is then filled with previously deaerated, distilled water to the scribe line and the pycnometer reweighed. The temperature of the pycnometer contents is measured using a calibrated thermometer. The weight of the water is divided by the density of water at the measured temperature, which yields the volume of water in the pycnometer. The volume of the empty pycnometer minus the volume of water equals the grain volume of the powdered sample.

A.3.1.2 Calibration. Calibration of the water pycnometer is performed by measuring the volume of a known weight of distilled water when the water is at the fill line of the pycnometer. The actual volume of the pycnometer as so measured is used in the calculations, not the nominal value assigned during fabrication of the pycnometer. Calibration checks of the pycnometer are made using alpha-quartz powder as a reference material. For nonhygroscopic materials, water pycnometer measurements are accurate to ± 0.15 percent, with a precision of 0.19 percent (Schwartz, 1985, p. 11).

A.3.2 Helium Gas Pycnometer Technique

Grain density tests using a helium gas pycnometer were run per revision A of SNL NNWSI quality assurance procedure (QAP) XI-6. The QAP was titled Quality Assurance and Standard Operating Procedures for Grain Density Measurements Using a Micromeritics Model 1303 Helium Pycnometer. The procedure is quite detailed, and only part of the procedure is summarized here.

A.3.2.1 Operating Procedures. The gas pycnometer used was a Micromeritics Model 1303. The unit consists of a sample-holding chamber capable of holding up to 40 cm³ (2.44 in.³); a cylinder fitted with a movable piston, the relative position of which is indicated on the front panel dial to five significant figures (in units of cm³); a four-position valve; and a pressure detector.

The gas pycnometer works on the following principle: the volume of the empty sample chamber is measured by careful metering of the quantity of a nonabsorbing gas (helium) necessary to fill the chamber to a pressure level preset at the factory. Initially, the sample chamber is flushed with air and filled with powdered sample, then the sample chamber is evacuated slowly so that the powdered sample does not fluidize. The sample chamber is again filled with helium to the same present pressure level. The decrease in the volume of helium required to fill the chamber is equal to the volume of the powdered sample in the chamber, called the grain volume. The grain density (g/cm³) is obtained by dividing the

grain weight by the grain volume. The grain weight is measured on an analytical balance.

The experiment begins by first weighing a dry, empty gas pycnometer sample cup and then placing the sample cup into the sample chamber to determine the volume of helium required to fill the sample chamber to a selected level. The powdered sample then is placed into the sample cup and weighed. The sample cup is placed into the sample chamber and slowly evacuated using a vacuum pump to remove air and other contaminants. The sample chamber again is flooded with helium and the volume of helium necessary to fill the sample chamber to the same selected pressure level is determined. The grain volume of the powder is determined by the difference of the volumes of helium gas necessary to fill the empty and the partially filled sample cup.

A.3.2.2 Calibration. Calibration of the helium pycnometer is performed by measuring the volume of steel spheres in the pycnometer and comparing the value against the known volume of the sphere as determined by physical measurement. Calibration checks of the pycnometer are made using alpha-quartz powder as a reference material. For nonhygroscopic materials, accuracy of helium pycnometer measurements is ± 0.60 percent, with precision of ± 0.53 percent (Schwartz, 1985, p. 11).

A.4 Porosity

Porosity values have been calculated from grain density (ρ_g) and dry bulk density (ρ_{db}) test results using the following formula:

$$\phi (\%) = 100 \left(1 - \frac{\rho_{db}}{\rho_g} \right) . \quad (A.4-1)$$

Matrix porosities calculated using this equation have been found to be precise to 0.023 for all tuff samples, with precision for devitrified tuff of 0.027. No data on accuracy are available.

A.5 Thermal Expansion

A.5.1 Unconfined Thermal Expansion

Unconfined thermal expansion experiments were performed under revisions A, B, and C of SNL NNWSI quality assurance procedure (QAP) XI-5. The QAP was titled Quality Assurance Procedure and Standard Operating Procedures of Thermal Expansion Measurements Using a Theta Corp. Model 6020 Dilatometer. The procedure is quite detailed; only part of the procedure is summarized here.

A.5.1.1 Operating Procedures. The instrument used was a dual-pushrod apparatus in which parallel, horizontal rods of fused silica are utilized. One rod contacts a fused silica reference blank; the other rod contacts the sample being analyzed. Both rods are connected to a linear variable differential transducer (LVDT). Any change in length in the sample tested produces a voltage signal that is recorded on the ordinate of an X-Y recorder. The temperature of the sample is recorded on the abscissa of the same recorder using data from a Type K thermocouple that

is mounted very close to the sample within the furnace. The samples were initially saturated (submerged for greater than 48 hours) in J-13 well water.

A.5.1.2 Calibration. Before running a rock sample, thermal expansion tests were performed using platinum versus fused silica reference material. The thermal expansion of platinum is measured using a heating rate of less than or equal to 3°C (5.4°F) per minute up to 400°C (752°F). The theoretical thermal expansion for platinum from 25° to 400°C (77° to 752°F) is $94.56 \times 10^{-7} \text{ } ^\circ\text{C}^{-1}$ ($5.3 \times 10^{-6} \text{ } ^\circ\text{F}^{-1}$). This corresponds to a pen deflection of between 3.23×10^{-3} in. (8.20×10^{-3} cm) and 3.41×10^{-3} in. (8.66×10^{-3} cm) for the platinum calibration to be in-specification (± 2.5 percent).

These calibration checks were performed once each week that the dilatometer was used except when an experimental run lasted longer than 1 week. In these latter cases, the whole system calibration was run immediately following each test. If the results deviated from the expected theoretical platinum expansion by ± 2.5 percent or less, the results were considered valid. If the results deviated from the expected theoretical output by between ± 2.5 percent and ± 5 percent, the instrument was recalibrated by the operator and the calibration results were indicated on data gathered immediately before the calibration data. If the deviation was greater than ± 5 percent, data gathered immediately before the calibration run were marked to reflect the out-of-calibration situation.

A.5.2 Confined Thermal Expansion

Confined thermal expansion experiments were performed using the same test equipment and saturated experiment samples described in Section A.5 for thermal conductivity tests. The following discussion is based on that of Van Buskirk et al., (1985).

For the thermal expansion experiments, Invar end caps were attached to the samples and jacketing was applied. Thermocouples were inserted approximately 1 cm (0.4 in.) into both ends of the sample to obtain an average sample temperature. The sample assemblage was placed in the experiment apparatus, and experiment conditions (confining pressure, pore pressure, and temperature) were applied.

Total expansion was measured using four fused quartz LVDT rods placed at the ends of orthogonal diameters of the sample. System expansion, dominated by expansion of the LVDT rods, is obtained by measuring the total expansion of experiments on standard materials, then subtracting the known expansion of the standards. The system expansion then is subtracted from total expansion during experiments on rock samples in order to obtain the thermal expansion of the rocks.

Heating rates typically were less than or equal to 1°C/min (1.8°F/min). These rates were used to minimize microcracking that could result from overly rapid heating. In addition, several temperature hold-points were usually included in the temperature history for each sample in order to ensure that the pore pressure reached equilibrium in the low-permeability samples.

Accuracy of the experiment method was not assessed by Van Buskirk et al., (1985). Estimates of the accuracy made during data analysis for this report suggest that a value of $\pm 1.0 \times 10^{-6} \text{ } ^\circ\text{C}^{-1}$ ($\pm 0.56 \times 10^{-6} \text{ } ^\circ\text{F}^{-1}$) is representative for the thermal expansion coefficients of units TSw1, TSw2, and TSw3.

A.6 Compressive Experiments

As is evident in Appendix B, compressive strength data have been reported in a number of references. However, only two testing laboratories have obtained data for SNL; the test procedures for the two laboratories are described in Nimick et al. (1985) and are summarized below. Data in this report are for cylindrical samples with diameters of 2.5 cm (1 in.) and lengths of 5.1 cm (2 in.).

All samples were saturated before testing (see Section A.1 for a discussion of saturation techniques). Samples were jacketed in polyolefin shrink tubing or FEP teflon tubing. Axial and lateral strain gages or LVDTs were mounted on the jacketed samples, and the assembly was placed in the load cell. Samples then were loaded at a constant strain rate of 10^{-5} s^{-1} to failure.

Experiment systems were either calibrated or the calibration was checked using an aluminum sample of known properties with the same dimensions as the experiment sample. The calibration experiments were performed before, during, and after the experiment sequences of rock samples.

Except for Poisson's ratios measured at TT (see Section 3.4.2.3 for brief discussion), elastic moduli are believed to be accurate to ± 5 percent. Compressive strengths are accurate to ± 1 percent.

When compression test results were obtained for samples from similar depths in a core hole at different confining pressures, the Mohr-Coulomb parameters (cohesion and angle of internal friction) were calculated. A linear regression was performed of differential stress ($\Delta\sigma$) as a function of confining pressure (σ_3) to give a line of the form

$$\Delta\sigma = \sigma_0 + m \sigma_3, \quad (\text{A.6-1})$$

where σ_0 is the unconfined compressive strength and m is an empirical constant. Then the cohesion (C_0) and the angle of internal friction (ϕ) are given by

$$\phi = \sin^{-1} \left(\frac{m}{2 + m} \right) \quad (\text{A.6-2})$$

and

$$C_0 = \sigma_0 \left(\frac{\tan \phi}{m} \right). \quad (\text{A.6-3})$$

A.7 Tensile Experiments

All tensile experiments to date have been performed using the Brazilian or splitting tensile strength technique. The technique

consists of applying an increasing diametral stress to a thin cylinder of rock until failure occurs. Details of the experiments used to obtain the data in this report are contained in Blacic et al. (1982).

APPENDIX B

This appendix is a summary of the experimental data used in statistical analyses that are discussed in the main text. Some of the data have been published previously; these are annotated appropriately. The majority of the data are being published for the first time.

Table B-1

Bulk Property Data for Unit TSw1

Depth (ft) ^a	Grain Density (g/cm ³) ^b	Dry Bulk Density (g/cm ³) ^b	Porosity (%)	Source of Information ^c
<u>UE-25a/#1</u>				
328	2.57	2.01	21.9	A
338.3	2.595	2.081	19.8	-
346.0	2.594	2.109	18.7	-
360	2.55	2.21	13.3	A
365.1	2.564	2.221	13.4	-
372.8	2.577	2.204	14.5	-
387.7	2.54	2.221	12.6	-
391.4	2.534	2.207	12.9	-
421	2.51	2.13	15.0	A
444.2	2.534	2.178	14.0	-
450.0	2.52	2.155	14.5	-
471	2.49	2.02	18.6	A
524	2.47	2.04	17.6	A
569	2.54	2.09	17.7	A
623	2.57	2.10	18.4	A
660	2.51	2.32	7.5	A
664.5	NA	2.21	NA	-
680.0	2.55 ^e	NA	10.0 ^e	B
681.1	2.52 ^e	NA	10.0 ^e	B
696.7	2.52 ^e	NA	12.0 ^e	B
708.2	2.52 ^e	NA	9.0 ^e	B
723.2	2.56	2.23	12.9	-
729.4	2.58	2.26	12.4	-
730.3	2.50 ^e	NA	10.0 ^e	B
730.3	NA	2.21	NA	-
733	2.54	2.25	11.3	A
734.3	2.56	2.28	10.9	-
739.6	2.56	2.27	11.3	-
768.6	2.589	2.247	13.2	-
772	2.57	2.23	13.3	A
776.3	2.605	2.341	10.1	-
816	2.56	2.31	9.8	A
818.2	2.599	2.172	16.4	-
825.1	2.585	2.155	16.6	-
866	2.57	2.35	8.65	A
870.5	2.566	2.181	15.0	-
876.0	2.587	2.077	19.7	-
904.2	2.582	2.228	13.7	-
912.1	2.590	2.200	15.1	-
921	2.54	2.31	10.0	A
969	2.54	2.31	NA	A
1010	2.52	2.23	11.8	A
1040	2.53	2.25	11.2	A

Table B-1 (continued)

Bulk Property Data for Unit TSw1

Depth (ft) ^a	Grain Density (g/cm ³) ^b	Dry Bulk Density (g/cm ³) ^b	Porosity (%)	Source of Information ^c
<u>USW G-1</u>				
407.2	2.57	2.23	13.2	-
740.5	2.51	2.27	9.5	-
751.8	2.51	2.06	18.0	-
795	2.52	2.25	11.0	L
810.0	2.51	2.27	9.55	-
810.3	2.51	2.25	10.0	-
811.2	2.52	2.24	11.1	-
890.3	2.54	2.25	11.45	-
939	2.59	2.18	16.0	-
939	2.51	2.20	12.0	-
959.4	2.52	2.22	12.07	-
<u>USW G-2</u>				
773.7	2.57	2.41	6.1	-
801.7	2.58	2.36	8.6	-
818.4	2.58	2.36	8.5	-
861.2	2.57	2.32	9.8	-
888.0	2.63	2.27	13.9	-
906.4	2.54	2.31	9.1	-
928.0	2.50	2.12	15.4	-
948.4	2.55	2.33	8.6	-
960.9	2.54	2.30	9.6	-
979.6	2.53	2.09	17.5	-
980.0	2.57	2.29	10.78	-
993.0	2.57	2.19	14.7	-
994.0	2.57	2.26	11.75	-
1024.4	2.58	2.23	13.7	-
1042.9	2.61	2.13	18.4	-
1059.6	2.62	2.17	17.2	-
1063.2	2.58	2.35	8.88	-
1072.3	2.56	2.31	9.9	-
1100.7	2.59	2.30	11.1	-
1118.7	2.52	2.00	20.7	-
1139.0	2.55	2.27	10.76	-
1140.2	2.49	2.11	15.4	-
1171.0	2.47	2.21	10.43	-
1175.7	2.52	2.17	13.9	-
1198.0	2.54	2.29	9.61	-
1201.0	2.50	2.16	13.4	-
1219.0	2.48	2.14	13.8	-

Table B-1 (continued)

Bulk Property Data for Unit TSw1

Depth (ft) ^a	Grain Density (g/cm ³) ^b	Dry Bulk Density (g/cm ³) ^b	Porosity (%)	Source of Information ^c
<u>USW G-2 (continued)</u>				
1234.6	2.45	2.07	15.6	-
1274.1	2.49	2.25	9.8	-
1305.6	2.55	2.18	14.4	-
1348.0	2.52	1.99	21.0	-
1367.9	2.53	1.87	26.1 ^e	-
1385.0	2.51	2.21	11.8	-
1412.8	2.52	2.30	8.5	-
1424.1	2.50	2.10	16.0	-
1446.3	2.48	2.18	11.9	-
1458.5	2.49	2.11	11.2	-
1477.3	2.48	2.12	14.5	-
<u>USW GU-3</u>				
435.2	2.56	2.12	17.3	AA
435.8	2.58	1.99	22.87	-
452.2	2.55	2.05	19.61	-
461.1	2.55	2.09	18.2	AA
475.8	2.53	2.11	16.60	-
490.4	2.53	2.02	20.16	-
492.2	2.54	2.10	17.2	-
519.8	2.50	2.10	16.00	-
542.7	2.49	1.98	20.48	-
543.6	2.53	2.05	18.9	-
552.3	2.49	2.14	14.2	AA
561.0	2.49	2.18	12.45	-
576.0	2.49	2.06	17.3	AA
586.5	2.52	2.00	20.63	-
600.1	2.52	1.98	21.43	-
600.3	2.52	2.07	17.9	-
610.3	2.49	2.13	14.3	AA
631.1	2.51	2.20	12.35	-
652.0	2.55	2.12	16.86	-
660.3	2.58	2.13	17.2	AA
669.4	2.51	2.13	15.14	-
670.8	2.55	2.08	18.5	-
<u>USW G-4</u>				
247	NA	NA	3.0 ^e	P
251.2	2.57	2.36	8.17	-
272.0	2.41	2.17	9.96	-

Table B-1 (continued)

Bulk Property Data for Unit TSw1

Depth (ft) ^a	Grain Density (g/cm ³) ^b	Dry Bulk Density (g/cm ³) ^b	Porosity (%)	Source of Information ^c
<u>USW G-4</u> (continued)				
280.4	2.57	2.23	13.0	AA
293.2	2.51	2.21	11.95	-
309.5	2.60	2.19	15.77	-
332.3	2.56	2.16	15.7	AA
333.1	2.56	2.12	17.19	-
377.1	2.46	2.18	11.38	-
390.3	2.54	2.21	12.9	AA
403.0	2.45	2.03	17.14	-
417.5	2.41	2.09	13.28	-
485.0	2.46	2.23	9.35	-
515.0	2.53	2.05	18.97	-
523.4	2.50	2.03	18.80	-
548.4	2.51	2.00	20.3	AA
556.0	2.56	2.13	16.80	-
566.2	2.54	1.97	22.44	-
570.1	2.57	2.11	17.90	-
602.6	2.54	2.11	16.8	AA
604.7	2.54	2.15	15.35	-
655.0	2.53	2.27	10.28	-
668.6	2.53	2.23	11.9	AA
<u>Busted Butte</u> ^d				
1-B	2.47	2.03	17.8	f
1-D	2.64	1.97	25.4	f
1-D, top	2.60	2.01	22.7	f
2-A	2.58	2.03	21.3	f
2-A, top	2.45	2.13	13.1	f
3-A	2.54	2.08	18.1	f
3-A, top	2.57	2.06	19.8	f
4-1	2.58	2.24	13.18	-
4-2	2.53	2.14	15.42	-
4-3	2.58	2.01	22.09	-
4-4	2.52	2.11	16.27	-
4-5	2.59	2.11	18.53	-
4-6	2.59	2.20	15.06	-
4-7	2.56	2.11	17.58	-
4-8	2.58	2.10	18.61	-
4-9	2.60	2.19	15.77	-
4-10	2.56	2.11	17.58	-
8-A	2.57	2.11	17.9	f
8-A, top	2.57	1.99	22.6	f
8-B	2.50	2.07	17.2	f

Table B-1 (concluded)

Bulk Property Data for Unit TSw1

Depth (ft)	Grain Density (g/cm ³) ^b	Dry Bulk Density (g/cm ³) ^b	Porosity (%)	Source of Information ^c
<u>Busted Butte</u> ^d (continued)				
8-C	2.57	2.10	18.3	f
8-C, top	2.50	2.08	16.8	-
8-E	2.54	2.43	4.3	f
8-E, top	2.56	2.08	18.8	f
8-F	2.57	2.15	16.3	f
8-F, top	2.56	2.05	19.9	f

^aTo obtain units of m, multiply by 0.3048.

^bTo obtain units of lb/ft³, multiply by 62.43.

^cIf no source is listed, data have not been published previously.
Otherwise, notes are as follows:

- A - Anderson (1981)
- AA - Anderson (1984)
- B - Blacic et al. (1982)
- L - Lappin et al. (1982)
- P - Peters et al. (1984)

^dFor Busted Butte samples, sample ID is listed in place of sample depth,
with the ID consisting of the rock number followed by the sample number.

^eThese data excluded from statistical summaries at core-hole or higher
levels of grouping.

^fGrain density for this sample originally reported by Price et al.
(1985, p. 38), either directly or as an average of the several values
given in this table.

Table B-2

Linear Thermal Expansion Coefficients^a for Unit TSwl

Sample	°C °F	Temperature Range								
		25-50 77-122	50-100 122-212	100-150 212-302	150-200 302-392	200-250 392-482	25-100 72-212	25-150 77-302	25-200 77-392	25-250 77-482
Tests With 10 MPa (1,450 psi) Confining Pressure										
A1-369	9.1	9.0	11.2	12.3	NA	9.0	9.9	11.2	NA	
G1-740	10.9	10.2	13.3	11.2	NA	10.4	11.6	11.5	NA	
G2-980	9.7	9.5	11.8	24.2	NA	9.5	10.5	14.4	NA	
G2-1063	6.8	9.2	8.3	5.9	11.5	8.3	8.3	7.7	8.5	
G2-1139	9.9	8.8	9.3	7.4	NA	9.1	9.2	8.7	NA	
G2-1198	11.5	13.9	10.7	0.9	NA	13.0	12.1	8.8	NA	
GU3-431	9.2	5.6	6.5	12.6	NA	7.8	7.3	8.9	NA	
GU3-686	12.0	11.6	11.5	17.0	18.4	11.7	11.6	13.2	14.3	
G4-328	10.2	8.8	10.5	12.3	19.8	9.2	9.8	10.5	11.6	
Tests Without Confining Pressure										
A1-664.5b(1)	3.7	8.8	10.0	11.4	18.2	7.0	8.3	9.2	11.2	
A1-664.5b(1)	8.9	7.8	9.0	11.2	17.6	8.1	8.5	9.3	11.1	
A1-664.5b(2)	7.3	8.8	10.0	11.2	14.6	8.0	8.6	9.3	10.5	
A1-664.5b(2)	4.9	9.8	9.2	10.4	15.0	8.1	8.6	9.1	10.4	
A1-664.5b(3)	4.1	6.8	8.8	10.8	20.2	5.8	7.1	8.1	10.8	
A1-664.5b(3)	9.3	9.0	10.6	11.6	26.4	9.0	9.7	10.3	13.8	
A1-664.5b(4)	7.7	8.8	10.6	12.4	19.4	8.4	9.3	10.2	12.2	
A1-730.3b(1)	4.5	8.8	9.6	10.0	12.8	7.3	8.3	8.8	9.7	
A1-730.3b(1)	7.3	6.2	9.6	10.2	12.0	6.5	7.8	8.5	9.3	
A1-730.3b(2)	6.5	8.6	8.4	9.4	12.0	7.8	8.1	8.5	9.3	
A1-730.3b(2)	6.9	8.6	9.0	9.4	12.0	8.0	8.4	8.7	9.5	
A1-730.3b(3)	6.5	8.8	9.2	11.4	14.2	8.0	8.4	9.3	10.4	
A1-730.3b(3)	8.1	8.6	9.0	11.2	14.6	8.4	8.7	9.4	10.6	
A1-730.3b(4)	5.3	8.6	9.6	9.8	14.6	7.4	8.4	8.8	10.1	
G1-377.OA	4.9	6.6	8.6	13.2	33.2	6.0	7.1	8.8	14.3	
G1-377.OB	6.5	6.4	8.2	12.8	23.4	6.4	7.2	8.8	12.0	
G1-407.1-1A	4.5	7.6	9.2	38.6	57.0	6.5	7.6	16.5	25.5	
G1-407.1-1B	6.5	7.8	8.6	14.2	50.0	7.3	7.9	9.7	18.6	
G1-407.1-2	7.7	8.4	8.6	13.6	43.4	8.1	8.4	9.9	17.3	
G1-446.8-1	5.7	8.6	13.4	19.6	82.6	7.6	10.0	12.7	23.8	
G1-446.8-2	1.3	1.6	16.0	64.8	51.0	1.4	7.3	23.7	29.8	
G1-504.1-1 ^c	4.1	10.8	12.6	16.0	80.6	8.5	10.2	11.9	27.1	
G1-504.1-2	7.3	11.4	14.6	49.0	249.8	10.0	11.9	22.5	50.9	
G1-504.1-3	3.7	9.2	14.4	15.8	109.0	7.3	10.2	11.8	33.4	

Table B-2 (concluded)

Linear Thermal Expansion Coefficients^a for Unit TSw1

Sample	°C °F	Temperature Range								
		25-50 77-122	50-100 122-212	100-150 212-302	150-200 302-392	200-250 392-482	25-100 77-212	25-150 77-302	25-200 77-392	25-250 77-482
G1-586.4-1	3.7	7.6	11.4	12.8	32.6	6.1	8.3	9.6	14.7	
G1-631.6-1	5.7	6.6	9.0	29.2	60.0	6.2	7.4	13.6	23.9	
G1-682.6-1	4.5	7.0	12.2	11.6	21.4	6.2	8.8	9.6	12.3	
G1-740.4-1	4.9	9.6	9.0	10.4	15.6	8.0	8.4	9.0	10.5	
G1-811.1-1	7.0	10.0	10.0	12.8	20.2	9.1	9.5	9.9	12.4	
G1-890-1	3.2	8.0	11.8	13.0	29.4	6.5	8.7	10.0	14.2	
G1-939-1	4.0	8.2	9.8	12.0	22.2	6.9	8.2	9.3	12.0	
G1-939-2	5.7	8.4	9.4	13.0	23.2	7.4	8.3	9.6	12.6	

^aCoefficients are in units of $10^{-6}^{\circ}\text{C}^{-1}$; to obtain units of $10^{-6}^{\circ}\text{F}^{-1}$, multiply by 5/9.

^bSoak-test sample, number in parentheses indicates pre-test condition of sample as follows:

- (1) Pre-soak test, saturated
- (2) Post-soak test, saturated
- (3) Pre-soak test, dry
- (4) Post-soak test, dry

^cTested dry; not included in data analysis.

Table B-3

Mechanical Properties of Unit TSw1
(Unconfined, ambient-temperature experiments at $\dot{\epsilon} = 10^{-5} \text{ s}^{-1}$)

Sample ID	Saturation State ^a	Uniaxial Compressive Strength (MPa) ^b	Young's Modulus (GPa) ^b	Poisson's Ratio	Axial Strain to Failure (10 ⁻³)	Source of Data ^c
A1-723	r	138	40.4	0.22	NA	O
G1-939	su	108	25.1	0.27 ^d	5.2	-
G2-797.0	sv	162	43.5	0.25 ^d	3.80	N
G2-797.0	sv	130	39.6	0.26 ^d	3.60	N
G2-818.4	sv	160	37.8	0.24 ^d	5.30	N
G2-948.4	sv	167	42.0	0.30 ^d	4.60	N
G2-948.4	sv	157	49.0	0.26 ^d	3.30	N
G2-949.6	sv	220	38.6	0.19 ^d	6.20	N
G2-969.0	sv	130	68.3	0.38 ^d	2.60	N
G2-969.0	sv	210	46.3	0.21 ^d	4.80	N
G2-1297.6	sv	3.3	3.3	0.41 ^d	1.40	N
G2-1297.6	sv	6.8	3.8	0.26 ^d	2.40	N
GU3-462.4	s	63.1	16.6	0.18	NA	P
GU3-484.7	sv	72.8	17.6	0.19	4.27	P
GU3-519.4	sv	67.7	21.2	0.13	3.72	P
GU3-519.4	sv	62.6	22.2	0.27	3.11	P

^a s = saturated by immersion.

r = room-dry.

su = saturated; technique unknown.

sv = saturated by immersion and application of a vacuum.

^bTo obtain units of psi, multiply by 1.45×10^{-4} .

^c N - Nimick et al. (in preparation).

O - Olsson and Jones (1980)

P - Price et al. (1984).

(G1-939 data appear for the first time in this report).

^dData measured at Terra Tek; not used in calculation of mean value and standard deviation. See Section 2.4.2.3 for discussion.

NA: Not available.

Table B-4

Bulk Property Data for Unit TSw2

Depth (ft) ^a	Porosity (%)	Grain Density (g/cm ³) ^b	Dry Bulk Density (g/cm ³) ^b	Source of Information ^c
<u>UE-25a#1</u>				
1089.7	11.0	2.54	NA	B
1091.2	25.0	2.53	NA	B
1100.6	12.0	2.46	NA	B
1101.6	11.0	2.56	NA	B
1104.4	8.3	2.56	2.35	-
1105.8	9.0	2.56	NA	B
1107.2	11.7	2.60	2.29	-
1112	8.7	2.53	2.31	A
1122.7	NA	NA	2.29	-
1150.8	13.8	2.579	2.223	-
1154.8	16.2	2.565	2.149	-
1183	8.5	2.57	2.36	A
1186.7	18.2	2.564	2.098	-
1191.2	20.1	2.568	2.052	-
1242.9	10.1	2.547	2.289	-
1247.3	9.9	2.536	2.284	-
1249	8.03	2.54	2.33	A
1250.2	8.7	2.56	2.34	-
1252.1	7.6	2.527	2.336	-
1253.1	9.0	2.57	2.34	-
1255.0	11.2	2.57	2.28	-
1257.5	10.2	2.55	2.29	-
1264.6	13.6	2.52	2.18	-
1266	12.7	2.48	2.16	A
<u>USW G-1</u>				
1017.6	13.22	2.54	2.20	-
1047.1	11.25	2.55	2.26	-
1100.1	14.42	2.54	2.17	-
1151.1	15.73	2.56	2.16	-
1210.7	11.28	2.54	2.25	-
1232.1	14.4	2.57	2.20	-
1245	10	2.58	2.33	-
<u>USW G-2</u>				
1524.8	12.3	2.58	2.26	-
1540.2	13.7	2.58	2.23	-
1560.7	13.5	2.54	2.20	-
1577.2	7.5	2.46	2.28	-

Table B-4 (continued)

Bulk Property Data for Unit TSw2

Depth (ft) ^a	Porosity (%)	Grain Density (g/cm ³) ^b	Dry Bulk Density (g/cm ³) ^b	Source of Information ^c
<u>USW-G-2</u> (continued)				
1580.4	19.1	2.602	2.106	-
1582.6	11.6	2.594	2.294	-
1600.0	16.7	2.528	2.107	-
1608.7A	14.2	2.553	2.191	-
1608.7B	15.2	2.542	2.156	-
1613.9	11.1	2.587	2.301	-
1624.1	11.1	2.515	2.236	-
1628.5	16.0	2.627	2.206	-
1633.7	6.5	2.48	2.31	-
<u>USW GU-3</u>				
693.7	11.65	2.49	2.20	-
712.4	7.57	2.51	2.32	-
713.8	9.0	2.53	2.30	AA
753.0	11.95	2.51	2.21	-
753.4	12.00	2.50	2.20	-
765.0	13.4	2.50	2.17	AA
770.0	13.94	2.51	2.16	-
795.0	10.36	2.51	2.25	-
825.6	6.8	2.52	2.35	AA
826.3	6.43	2.49	2.33	-
837.3	10.16	2.56	2.30	-
841.0	10.40	2.53	2.31	-
857.1	12.26	2.61	2.29	-
873.6	14.62	2.60	2.22	-
884.1	10.2	2.60	2.34	AA
921.5	15.18	2.57	2.18	-
923.7	15.00	2.52	2.14	-
925.0	11.2	2.53	2.25	AA
938.4	18.08	2.60	2.13	-
953.7	14.62	2.60	2.22	-
957.7	10.4	2.55	2.28	AA
986.6	16.54	2.54	2.12	-
1023.6	12.20	2.54	2.23	-
1055.8	9.8	2.59	2.34	AA
1069.3	11.58	2.59	2.29	-
1069.8	12.20	2.55	2.24	-
1084.8	11.49	2.61	2.31	-
1104.4	9.34	2.57	2.33	-
1108.9	8.3	2.56	2.35	AA
1124.4	10.77	2.60	2.32	-

Table B-4 (continued)

Bulk Property Data for Unit TSw2

Depth (ft) ^a	Porosity (%)	Grain Density (g/cm ³) ^b	Dry Bulk Density (g/cm ³) ^b	Source of Information ^c
<u>USW GU-3 (continued)</u>				
1131.1	10.40	2.59	2.32	-
1132	8.0	2.54	NA	P
1149	NA	2.54	NA	-
1149.2	10.59	2.55	2.28	-
1152	NA	2.55	NA	-
1152.3	7.87	2.54	2.34	-
1165.9	8.5	2.57	2.35	AA
<u>USW G-4</u>				
678.2	9.20	2.50	2.27	-
742.5	7.4	2.50	2.31	AA
744.9	9.16	2.51	2.28	-
746.4	14.2	2.521	2.162	-
750.0	20.8	2.506	1.984	-
769.0	10.36	2.51	2.24	-
809.3	27.59	2.61	1.89	-
821.2	11.5	2.53	2.24	AA
864A	9.0	2.54	2.31	P
864B	NA	NA	2.22	P
864C	NA	NA	2.23	-
864.0	13.10	2.52	2.19	-
875.5	9.9	2.58	2.33	AA
888.0	10.94	2.56	2.28	-
909.7	15.02	2.53	2.15	-
923.8	13.78	2.54	2.19	-
937.6	10.8	2.56	2.28	AA
946.5	13.13	2.59	2.25	-
963.5	13.62	2.57	2.22	-
983.4	11.67	2.57	2.27	-
1064.5	13.8	2.55	2.19	AA
1099.0	13.28	2.56	2.22	-
1155.4	10.2	2.56	2.30	-
1158	11.0	2.58	2.30	P
1171.8	9.8	2.55	2.30	-
1176.5	10.7	2.58	2.30	-
1220.0	13.7	2.56	2.21	-
1232.2	10.0	2.61	2.35	-
1239.2	9.4	2.59	2.34	AA
1241.0	9.69	2.58	2.33	-
1256	10.0	2.53	2.28	P
1274.8	8.9	2.58	2.35	-

Table B-4 (concluded)

Bulk Property Data for Unit TSw2

Depth (ft) ^a	Porosity (%)	Grain Density (g/cm ³) ^b	Dry Bulk Density (g/cm ³) ^b	Source of Information ^c
<u>USW G-4</u> (continued)				
1278	6.0	2.50	NA	P
<u>Busted Butte</u> ^d				
10-A	12.1	2.56	2.25	-
10-A, top	11.6	2.58	2.28	-
10-C	17.1	2.63	2.18	-
10-D	14.0	2.64	2.27	-
10-E	13.1	2.67	2.32	-
11-A	15.4	2.66	2.25	-
11-B	13.6	2.58	2.23	-
11-C	13.6	2.64	2.28	-
11-D	15.0	2.66	2.26	-
12A-2	12.0	2.66	2.34	-
10-1Z	12.0	2.59	2.28	-
10-2X	10.2	2.56	2.30	-
10-5W	11.2	2.59	2.30	-
10-11W	13.1	2.60	2.26	-
10-17W	10.4	2.59	2.32	-
10-17Z	10.8	2.59	2.31	-
10-21Y	20.0	2.60	2.08	-
10-26Z	11.5	2.61	2.31	-
10-33Y	16.2	2.60	2.18	-
10-42Z	14.7	2.59	2.21	-
10-46X	19.1	2.62	2.12	-
10-52X	13.0	2.61	2.27	-

^aTo obtain units of m, multiply by 0.3048.

^bTo obtain units of lb/ft³, multiply by 62.43.

^cIf no source is listed, data are being presented for the first time in this report. Otherwise:

A - Anderson (1981).

AA - Anderson (1984).

B - Blacic et al. (1982).

P - Peters et al. (1984).

^dFor Busted Butte samples, sample ID is listed in place of sample depth, with the ID consisting of the rock number followed by the sample number.

Table B-5

Linear Thermal Expansion Coefficients^a for Unit TSw2

Sample	Temperature Range											
	°C °F	25-50 77-122	50-100 122-212	100-150 212-302	150-200 302-392	200-250 392-482	250-300 482-572	25-100 77-212	25-150 77-302	25-200 77-392	25-250 77-482	25-300 77-572
Tests With 10 MPa (1,450 psi) Confining Pressure												
G2-1577	11.6	9.8	8.3	14.2	NA	NA	10.3	9.6	10.9	NA	NA	NA
G2-1594	11.0	10.5	9.1	15.3	NA	NA	10.6	10.3	11.7	NA	NA	NA
GU3-985	10.3	9.2	7.7	10.4	NA	NA	9.5	8.8	9.4	NA	NA	NA
GU3-1123	10.0	7.9	8.0	11.8	NA	NA	8.5	8.4	9.4	NA	NA	NA
G4-737.9	15.8	12.1	13.3	18.0	30.5	NA	13.1	13.2	14.6	17.7	NA	NA
G4-1172 ^b	10.9	9.1	8.4	NA	NA	NA	9.6	9.2	NA	NA	NA	NA
G4-1177	12.5	8.6	7.7	NA	NA	NA	9.8	9.0	NA	NA	NA	NA
G4-1222	8.6	10.8	7.8	NA	NA	NA	9.6	8.9	NA	NA	NA	NA
G4-1295 ^c	15.9	10.9	9.9	NA	NA	NA	12.6	11.6	NA	NA	NA	NA
Tests Without Confining Pressure												
A1-1122.7 ^{d(1)}	7.7	8.8	9.2	11.4	13.0	18.6	8.4	8.8	9.5	10.3	11.8	NA
A1-1122.7 ^{d(1)}	7.3	7.8	9.4	9.4	12.0	16.2	7.6	8.4	8.7	9.4	10.6	NA
A1-1122.7 ^{d(2)}	6.9	8.6	9.0	10.0	14.2	19.0	8.0	8.4	8.9	10.1	11.7	NA
A1-1122.7 ^{d(2)}	4.9	7.6	8.4	9.4	11.2	16.0	6.6	7.4	8.0	8.7	10.0	NA
A1-1122.7 ^{d(2)}	4.1	9.2	9.8	10.6	12.8	18.6	7.4	8.4	9.1	9.9	12.2	NA
A1-1122.7 ^{d(3)}	0.5	3.0	10.0	10.2	15.2	21.4	2.1	5.3	6.7	8.6	10.9	NA
A1-1122.7 ^{d(4)}	3.7	7.4	9.0	11.2	12.8	17.8	6.1	7.3	8.4	9.4	10.9	NA
G1-1017.6-1	2.5	8.8	11.4	13.2	24.2	38.8	6.6	8.6	9.9	13.1	17.8	NA
G1-1047.1-1	4.5	7.8	10.6	12.8	21.2	38.2	6.6	8.3	9.6	12.2	16.9	NA
G1-1100.1-1	-3.9	6.2	9.6	12.2	23.8	49.4	2.8	5.6	7.5	11.1	18.1	NA
G1-1151.1-1	3.7	8.0	10.8	12.8	33.0	48.4	6.5	8.3	9.6	14.8	20.9	NA
G1-1151.1-2	6.9	8.0	9.4	12.4	19.2	38.2	7.6	8.4	9.5	11.7	16.5	NA
G1-1208.7-A	2.5	8.2	11.6	12.4	19.2	40.0	6.2	8.4	9.6	11.7	16.9	NA
G1-1208.7-B	4.1	7.2	11.2	12.0	19.6	41.6	6.1	8.2	9.3	11.6	17.0	NA
G1-1232.1-1	-0.7	5.6	8.8	11.6	16.6	29.0	3.4	5.6	7.3	9.4	13.0	NA

^aCoefficients are in units of $10^{-6}^{\circ}\text{C}^{-1}$; to obtain units of $10^{-6}^{\circ}\text{F}^{-1}$, multiply by 5/9.

^bSample partially (rather than completely) saturated at beginning of test.

^cSample in material neither TSw2 nor TSw3; not included in data analysis.

^dSoak-test sample. Number in parentheses indicates pre-test condition of sample as follows:

- (1) Pre-soak test, saturated
- (2) Post-soak test, saturated
- (3) Pre-soak test, dry
- (4) Post-soak test, dry

NA: Not available.

Table B-6

Mechanical Properties of Unit TSw2
(Unconfined, ambient-temperature experiments at $\dot{\epsilon} = 10^{-5} \text{ s}^{-1}$)

Sample ID	Saturation State ^a	Uniaxial Compressive Strength (MPa) ^b	Young's Modulus (GPa) ^b	Poisson's Ratio	Axial Strain to Failure (10 ⁻³)	Source of Data ^c
A1-1250	r	166	61.8	0.30	NA	O
G1-1021.8	sv	75.2	25.5	0.25	3.8	PNZ
G1-1060.8	sv	142.8	38.1	0.32	5.0	PNZ
G1-1096.0	sv	59.8	24.9	0.15	3.4	PNZ
G1-1154.9	sv	106.2	32.5	0.33	3.7	PNZ
G2-1561.3	sv	85	22.1	0.11 ^d	4.70	N1
G2-1561.3	sv	73	22.0	0.17 ^d	4.10	N1
G2-1561.3	sv	86	22.7	0.33 ^d	4.10	N1
G2-1561.3	sv	61	23.6	0.26 ^d	3.70	N1
G2-1579.1	sv	170	33.9	0.17 ^d	5.60	N1
G2-1579.1	sv	97	18.8	0.18 ^d	6.30	N1
G2-1579.1	sv	175	31.8	0.17 ^d	6.10	N1
G2-1579.1	sv	96	20.5	0.19 ^d	5.80	N1
G2-1587.8	sv	165	35.9	0.20 ^d	6.10	N1
G2-1587.8	sv	155	35.5	0.16 ^d	5.50	N1
GU3-760.9	sv	210.3	30.2	0.19	7.76	PSJ
GU3-760.9	sv	234.4	28.6	0.29	8.48	PSJ
GU3-760.9	sv	215.5	29.0	0.22	8.01	PSJ
GU3-760.9	sv	221.4	30.2	0.22	8.04	PSJ
GU3-760.9	sv	245.2	30.6	0.23	9.19	PSJ
GU3-760.9	sv	222.2	30.8	0.21	8.05	PSJ
GU3-760.9	sv	205.2	29.3	0.19	7.54	PSJ
GU3-760.9	sv	183.5	28.1	0.16	7.24	PSJ
GU3-760.9	sv	229.7	30.7	0.22	8.57	PSJ
GU3-760.9	sv	226.4	30.0	0.21	8.41	PSJ
GU3-1050.4	sv	131.3	35.5	0.18	4.17	PSJ
GU3-1050.4	sv	147.7	36.1	0.19	4.56	PSJ
GU3-1050.4	sv	152.1	36.3	0.19	5.01	PSJ
GU3-1067.8	sv	115.3	32.7	0.24	4.46	PSJ
GU3-1067.8	sv	120.1	32.1	0.24	5.32	PSJ
G4-686.6	sv	270	36.2	0.18 ^d	8.7	N2
G4-686.6	sv	326	40.7	0.17 ^d	10.0	N2
G4-686.6	sv	180	33.1	0.21 ^d	6.4	N2
G4-742.75	sv	235	35.6	0.21 ^d	7.2	N2
G4-742.75	sv	256	36.8	0.21 ^d	8.3	N2
G4-742.75	sv	279	34.6	0.21 ^d	9.3	N2
G4-748.6	sv	196	32.2	0.16 ^d	6.6	N2

Table B-6 (concluded)

Mechanical Properties of Unit TSW2
(Unconfined, ambient-temperature experiments at $\dot{\epsilon} = 10^{-5} \text{ s}^{-1}$)

Sample ID	Saturation State ^a	Uniaxial Compressive Strength (MPa) ^b	Young's Modulus (GPa) ^b	Poisson's Ratio	Axial Strain to Failure (10^{-3})	Source of Data ^c
G4-748.6	sv	190	32.3	0.21 ^d	7.0	N2
G4-749.0	sv	268	33.5	0.29	8.7	N2
G4-749.0	sv	188	34.1	0.27	6.7	N2
G4-910.7	sv	131	30.1	0.18 ^d	5.5	N2
G4-911.3	sv	160	37.6	0.36	4.8	N2
G4-911.3	sv	88	24.8	0.15 ^d	4.8	N2
G4-911.3	sv	118	26.0	0.19 ^d	5.1	N2
G4-965.2	sv	187	38.0	0.21 ^d	5.6	N2
G4-965.2	sv	131	31.1	0.18 ^d	4.4	N2
G4-965.2	sv	148	33.1	0.19 ^d	6.0	N2
G4-1001.9	sv	99	22.8	0.19 ^d	5.1	N2
G4-1001.9	sv	170	32.7	0.20 ^d	5.5	N2
G4-1001.9	sv	147	31.8	0.18 ^d	4.8	N2
G4-1002.4	sv	179	33.6	0.32	5.6	N2
G4-1002.4	sv	137	31.1	NA	4.5	N2
G4-1065.8	sv	12	2.4	NA	18.5	N2
G4-1065.8	sv	124	26.7	0.21 ^d	4.3	N2

^a s = saturated by immersion.

r = room-dry.

sv = saturated by immersion and application of a vacuum.

^bTo obtain units of psi, multiply by 1.45×10^{-4} .

^c O = Olsson and Jones (1980)

PHZ = Price, et al. (1982).

N1 = Nimick et al. (in preparation).

PSJ = Price et al. (1984).

N2 = Nimick et al. (1985).

^dData measured at Terra Tek; not used in calculation of mean value and standard deviation. See Section 3.4.2.3 for discussion.

NA: Not available.

Table B-7

Bulk Property Data for Unit TSw3

Depth (ft) ^a	Grain Density (g/cm ³) ^b	Dry Bulk Density (g/cm ³) ^b	Porosity (%)	Source of Information ^c
<u>UE-25a#1</u>				
1304	2.36	2.21	6.28	A1
<u>USW G-1</u>				
1288.4	2.41	2.32	3.66	-
1330	2.38	2.31	3	-
1330	2.38	2.30	3	-
1330	2.39	2.30	4	-
1332.8	2.40	2.31	3.67	-
<u>USW G-2</u>				
1663.9	2.39	2.25	6.1	-
<u>USW GU-3</u>				
1194.9	2.35	2.31	1.70	-
1196.0	2.40	2.32	3.20	-
1197	2.39	NA	2.0	P
1213.2	2.36	2.34	1.4	A2
1214.1	2.37	2.28	3.80	-
1234.4	2.37	2.31	2.53	-
1245	2.38	NA	7.0	P
1247.0	2.37	2.32	2.00	-
1247.6	2.37	2.31	2.53	-
1261.8	2.39	2.32	3.1	A2
<u>USW G-4</u>				
1324	2.37	NA	4.0	P

^aTo obtain units of m, multiply by 0.3048.

^bTo obtain units of lb/ft³, multiply by 62.43.

^cIf no source is listed, data have not been published previously.
Otherwise, notes are as follows:

A1 - Anderson (1981).

A2 - Anderson (1984).

P - Peters et al. (1984).

Table B-8

Linear Thermal Expansion Coefficients^a for Unit TSw3

Sample	°C °F	Temperature Range								
		25-50 77-122	50-100 122-212	100-150 212-302	150-200 302-392	200-250 392-482	25-100 77-212	25-150 77-302	25-200 77-392	25-250 77-482
G1-1288.9-1		0.5	7.8	8.4	5.6	3.2	5.3	6.6	6.3	5.6
G1-1313.0-1		2.1	7.0	5.8	6.4	5.8	5.3	5.6	5.8	5.8
G1-1342-1		0.5	4.8	4.2	2.6	-3.0	3.3	3.7	3.4	2.0

^aCoefficients are in units of $10^{-6}^{\circ}\text{C}^{-1}$; to obtain units of $10^{-6}^{\circ}\text{F}^{-1}$, multiply by 5/9.

APPENDIX C

Effect of Saturation State on Mechanical Properties

It has been established that rocks with a saturation state near 1.0 will fail at lower compressive stresses than will equivalent rocks with a saturation state near 0.0 (e.g., Paterson, 1978, pp. 76-81). This effect often has been attributed to chemical weakening of the rock by water. If the theory is valid, such a chemical effect should occur even in the presence of small amounts of water (low values of saturation).

As discussed in this appendix, there also may be mechanical effects resulting from changes in saturation state. It is these latter changes that are discussed in the remainder of the appendix.

The effect of saturation states that are not close to either 0.0 or 1.0 has not been examined, probably because of the difficulty of achieving selected values of intermediate saturation. McTigue et al. (1984) examined the effective stress principle in the presence of intermediate saturations. The principle may be stated as

$$P_{\text{eff}} = P_{\text{conf}} - P_{\text{pore}} \quad , \quad (\text{C-1})$$

where P_{eff} is the effective pressure, P_{conf} is the confining pressure, and P_{pore} is the pore pressure. If saturation is less than 1.0, then P_{pore} is negative, so that if the principle applies, P_{eff} would be greater than the applied confining pressure. McTigue et al.

(1984) conclude that the principle applies for saturations less than 1.0 (although experimental support for this conclusion is not available), but do not discuss whether there is a lower limit to the saturations at which Equation (C-1) can be used.

The pressure P_{pore} for saturations less than 1.0 is the result of surface tension at the air-water interface in the pores. Presumably, this pressure will be negligible where there is no longer enough water to maintain connection across pores, so that the remaining pore water is confined to films along grain boundaries. The saturation at which this occurs is assumed to be the residual saturation as defined by Peters et al. (1984). The data of Peters et al. (1984, p. A-23) for welded, devitrified Topopah Spring Member show a maximum residual saturation of 0.12. The value of 0.12 is assumed to be the minimum saturation for which Equation (C-1) may be used.

For saturations of 0.12 to 1.0, the relationship between saturation and P_{pore} must be defined. From McTigue et al. (1984), the following expression can be derived:

$$d\sigma = (s - s_r)d\psi \quad , \quad (C-2)$$

where $d\sigma$ is the change in stress on the solid framework resulting from change in saturation state, $d\psi$ is the equivalent change in matrix potential, s is the saturation of the rock, and s_r is residual saturation. In order to integrate this, s must be defined in terms of ψ . An equation providing such a definition is given by Peters et al. (1984, p. 31):

$$s_r - s_s = (s_s - s_r) \left[\frac{1}{1 + |\alpha\psi|^\beta} \right]^\lambda \quad (C-3)$$

where $s_s = 1.0$, and α , β , and λ are fitting parameters.

Using values of α , β , and λ from sample G4-6 of Peters et al. (1984, p. 61), the results in Table C-1 are obtained. Thus, the maximum increase in confining pressure resulting from partial saturation should be on the order of 10 MPa (1450 psi).

In terms of mechanical testing, the saturation state of the experiment samples must be defined. Samples of welded tuff saturated by immersion and application of a vacuum should be roughly 0.95, and those saturated by immersion alone should be 0.75 (Nimick, in preparation, a). Relative to complete saturation, these samples should experience pore pressures of -0.5 and -1.4 MPa (-73 and -200 psi), respectively.

Some experiment samples have been tested in a "room-dry" condition. Peters et al. (1984, p. 15) provide an equation defining the value of ψ in equilibrium with a given relative humidity as a function of temperature:

$$\psi = - \left(\frac{R}{M} \right) T \ln \left(\frac{RH}{100} \right) \quad (C-4)$$

where R = universal gas constant (g·m/K),
 M = molecular weight of water (g),
 T = absolute temperature (K), and
 RH = relative humidity (%).

Table C-1

Calculated "Pore Pressures" as a Function of Saturation

Saturation	"Pore Pressure" (MPa) ^a
1.0000	0.00
0.9977	-0.09
0.9606	-0.44
0.9496	-0.51
0.9239	-0.66
0.8825	-0.86
0.7494	-1.44
0.6560	-1.86
0.4560	-2.99
0.3608	-3.79
0.3061	-4.40
0.1438	-8.67
0.1280	-9.83
0.1168	-11.00

^aTo obtain units of psi, multiply by 1.45×10^{-4} .

In this equation, $\frac{R}{M} = 47.1 \frac{\text{m}}{\text{K}}$. Also, the relative humidity of the testing laboratory at ambient temperature is approximately 60 percent. Thus, assuming an ambient temperature of 297 K [24°C (75°F)], ψ of the "room-dry" samples is calculated to be -7146 m (-23,445 ft). Translating this to a "pore pressure" value gives -9.8 MPa (-1,400 psi). By comparison with the data in Table C-1, the conclusion may be reached that the saturation is close to the residual saturation of 0.12, and so Equation (C-1) can be used for the "room-dry" samples.

The accuracy of the result from Equation (C-4) can be assessed using data from a time-dependent thermal expansion experiment. Two samples of welded, devitrified Topopah Spring Member were initially saturated, then were allowed to sit at ambient temperature until the lengths of the samples were no longer changing. This equilibration with the ambient relative humidity required 16.5 hr for one sample and approximately 25 hr for the second sample. The total linear strains of the samples were 0.00010 and 0.00016. The strain (ϵ) can be related to existing stress (σ) by

$$\sigma = \epsilon \left(\frac{E}{1 - 2\nu} \right) , \quad (\text{C-5})$$

where E is the Young's modulus and ν is the Poisson's ratio. Taking average values of these two parameters for unit TSw1 to be 36.0 GPa (5.2×10^6 psi) and 0.21, respectively, the two values of σ are calculated to be 6.2 and 9.9 MPa (900 and 1,400 psi). These are negative stresses (i.e., compressive) because the strains are negative. The value

of 9.9 MPa (1400 psi) falls close to the higher value, suggesting that the estimated "pore pressure" of the room-dry samples is correct. Furthermore, because the saturation value corresponding to this "pore pressure" is higher than the cutoff value of 0.12, Equation (C-1) may be used for room-dry samples.

Data from Olsson and Jones (1980, p. 20) indicate that oven-drying of welded tuff samples should increase the strength by 41 percent to 45 percent of the strengths of vacuum-saturated samples. If the preceding calculations are correct, drying a sample to a residual saturation of 0.12 should cause an equivalent confining pressure of approximately 10 MPa (1450 psi). Comparison of compressive strengths of Topopah Spring Member samples measured at 0 MPa and at 10 MPa (0 psi and 1,450 psi) (Nimick et al., 1985, p. 28) shows an increase in average strength of 10.8 percent to 36.1 percent, somewhat lower than suggested by the assumption of parallel processes. Oven-drying of the samples of Olsson and Jones (1980) probably reduced the saturation to a value close to zero, thus eliminating the chemical effects on strength caused by the presence of water. The comparison with the experimental data of Nimick et al. (1985) suggests that complete removal of water results in a greater strength increase than does reduction of the saturation to cause an equivalent confining pressure of 10 MPa (1,450 psi). This conclusion, in turn, implies that the chemical weakening caused by water reduces the mechanical strengthening caused by the capillary forces. Additional data are required before more definite conclusions can be made.

APPENDIX D

Water in Unit TSw3

Unlike the other welded portions of the Topopah Spring Member, unit TSw3 contains nontrivial amounts of water in addition to the water that is present in pore space. Based on five wet chemical analyses reported by Lipman (1965, p. D6) and Connolly (1986), unit TSw3 contains 2.9 to 4.58 wt.% water, with mean and standard deviation of 3.66 and 0.64 wt.%, respectively. Although microprobe analyses are not as reliable for determination of water content, 38 such analyses reported by Levy (1984), Vaniman et al. (1984), and Byers (1985), allow calculation (by difference from 100 wt.%) of a mean value and standard deviation of 4.54 and 0.89 wt.%, respectively. These latter results are in good agreement with the results of the wet chemical analyses when allowance is made for the uncertainty in the microprobe analyses.

There are a number of possible locations of the water within the solid material of unit TSw3. A small amount [0.1 to 0.9 wt.% (Ross and Smith, 1955, p. 1077)] is probably original magmatic water and is contained within the structure of the glass itself. Additional water, up to a total of 3 wt.% (Jezek and Noble, 1978, p. 273), can be incorporated in the glass structure as part of hydration of the glass to perlite. This process results in a fine network of cracks characteristic of hydrated obsidian. Any additional hydration of the glass occurs along these cracks, tending to disrupt the glass structure and enhance the likelihood of formation of clay and zeolites (Jezek and Noble, 1978, p. 273).

Unit TSw3 contains secondary minerals such as clay and zeolites. Levy (1984) describes two samples of this material taken from USW H-5. One sample contains perlitic cracks with small amounts of associated smectite clay. The other sample has very abundant perlitic cracks with associated alteration to smectite, heulandite, and an unidentified zeolite. Carlos (1985) describes fracture fillings in vitrophyre to consist of heulandite and mordenite, with some smectite and cristobalite.

In addition to hydration, the glass may devitrify. The devitrification process at low temperatures is accelerated by hydration (Zielinski, 1980). One of the minerals commonly formed as a result of devitrification is cristobalite. X-ray analyses of samples of unit TSw3 (Connolly, 1986) suggest that the cristobalite is actually opal-CT as described by Jones and Segnit (1971). Opal-CT also may contain some of the water present in unit TSw3.

During heating of unit TSw3, the water contained in solid material will be released at different temperatures. Experimental evidence suggests that clay will dehydrate continuously between 100° to 130°C (212° to 266°F) and 210° to 300°C (410° to 572°F) (Grim, 1953; Venugopal et al., 1982), with accompanying contraction of the clay in a direction perpendicular to the interlayer sheets of water molecules. Heulandite will dehydrate continuously from approximately 50°C (122°F) to 600°C (1112°F), with approximately 65 percent of the total water loss occurring below 260°C (500°F) (Koizumi, 1953). The weight loss is especially rapid at temperatures of 250° to 300°C (482° to 572°F) (Koizumi, 1953; Mumpton, 1960), a temperature range close to the temperature at which the

heulandite structure changes to heulandite B (Mumpton, 1960). Opal-A (a less ordered form of opal than opal-CT) begins to dehydrate at approximately 110°C (230°F) and experiences continuous weight loss to temperatures greater than 700°C (1292°F). The dehydration apparently reduces the thermal expansion of the opal, so that at approximately 225° to 275°C (437° to 527°F), expansion ceases, and contraction is apparent by 350°C (662°F) (Jones and Segnit, 1971).

Dehydration of the glass itself is less well documented. Ross and Smith (1955) suggest that water loss is more dependent on the length of heating than upon actual temperatures. Data reported by Eichelberger and Westrich (1981) suggest that glass begins to lose volatiles at temperatures well below 200°C (392°F), with weight loss continuous to at least 550°C (1022°F). Comparison of densities of hydrated and nonhydrated glasses suggest that a loss of 1 wt.% water will lead to a volume decrease of approximately 1 percent (Connolly, 1982).

APPENDIX E

Relationship Between Porosity and Mohr-Coulomb Parameters

The memorandum provided in this Appendix originally was issued in 1985. Peer review comments suggested that a discussion of the mechanics of the relationship of porosity and Mohr-Coulomb parameters would be helpful. Therefore, a brief discussion is provided in the next several paragraphs. The reader may wish to scan the original memo first (starting on p. E-4).

The discussion that follows uses the physical model presented by Sammis and Ashby (1986) as a point of departure. In this model, porosity is considered to be composed of spherical pores. Compressive loading causes small cracks to grow from the pores parallel to the direction of loading (or maximum compression if loading is biaxial or triaxial). Figure E-1 is a conceptual diagram of the state of the porous solid at some intermediate stage of deformation.

After the cracks reach a critical length which depends on the pore distribution, buckling moments occur in some parts of the specimen in addition to the stresses surrounding pores during the early portions of the loading history. This buckling causes the cracks to deviate from parallelism with the direction of maximum compression (in Figure E-1, cracks from pores A and B). Eventually, the cracks begin to link together, ultimately leading to macroscopic failure.

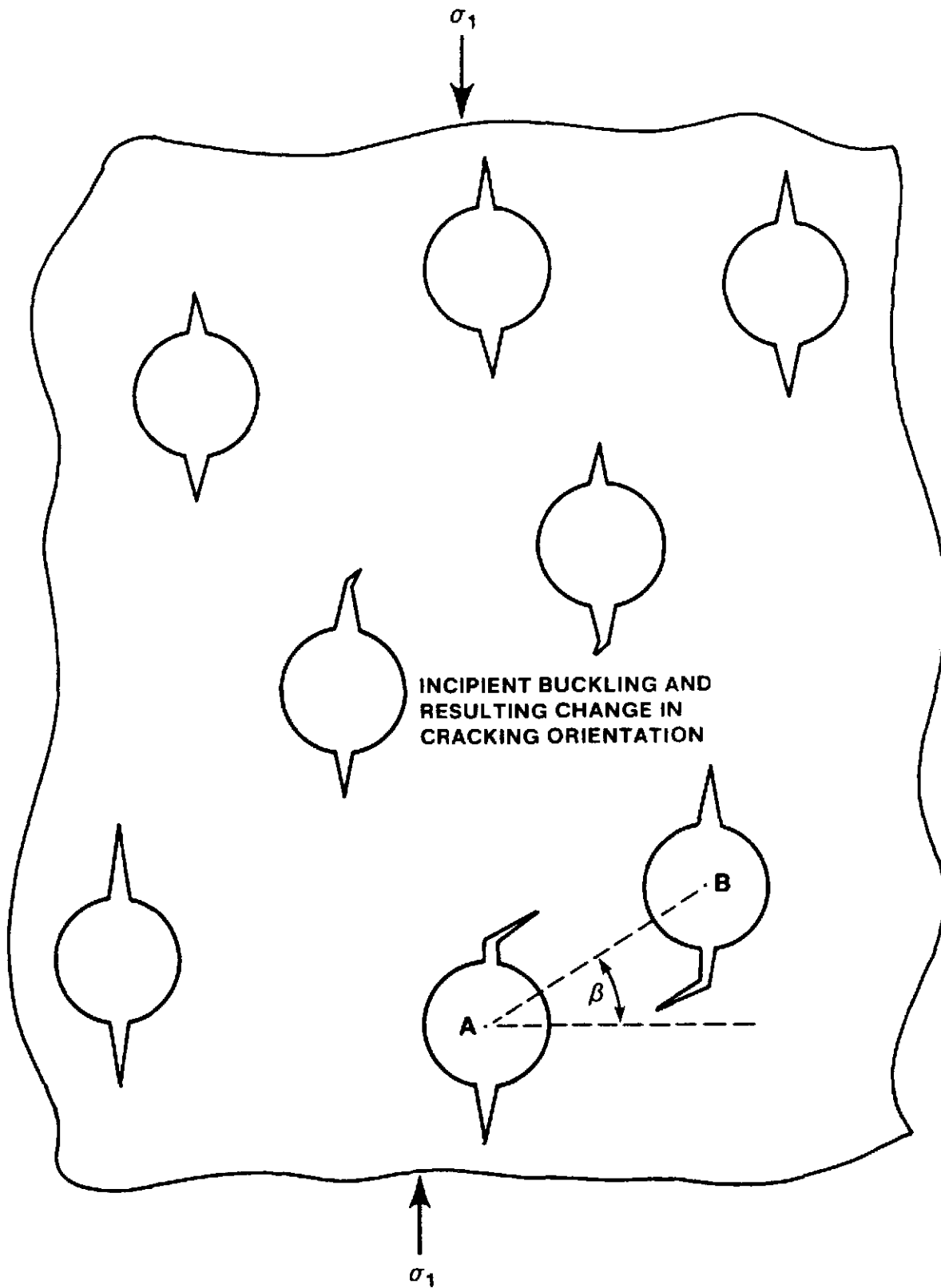


Figure E-1. Conceptual Representation of Cracking Mechanism in Porous Solid. σ_1 is maximum compressive stress.

In such a model, an increase in porosity will lead to linking of adjacent cracks at lower stress levels because individual cracks will need to extend shorter distances before the buckling moments are initiated. Thus, higher-porosity samples will tend to undergo macroscopic failure at lower stress levels, leading to the observed dependencies of cohesion and compressive strength on porosity.

The angle of internal friction ϕ is related to the angle β which the normal to the plane of fracture makes with the direction of maximum compression by

$$\beta = \frac{\pi}{4} + \frac{\phi}{2} \quad , \quad (E-1)$$

as given by Jaeger and Cook (1979, p. 97). Thus, as porosity increases, ϕ and thus β will decrease (see Section 2.4.2.1.6 and the original memo for discussions of the relationship between ϕ and porosity). Another view of this situation is that, as porosity increases, the angle that the plane of fracture makes with the direction of maximum compression will increase.

A physical explanation of this process can be seen in Figure E-1. On a microscopic scale, the plane of fracture should be one that connects individual pores, as shown between pores A and B in Figure E-1. As porosity increases, the average angle β which the line between the centers of pores makes with the normal to the direction of maximum compression will decrease because, on average, pores will be closer together in a "vertical" direction. Thus, increasing porosity should result in decreases in β and also in ϕ .

October 7, 1985

T. E. Blejwas, 6313

F. B. Nimick, 6313

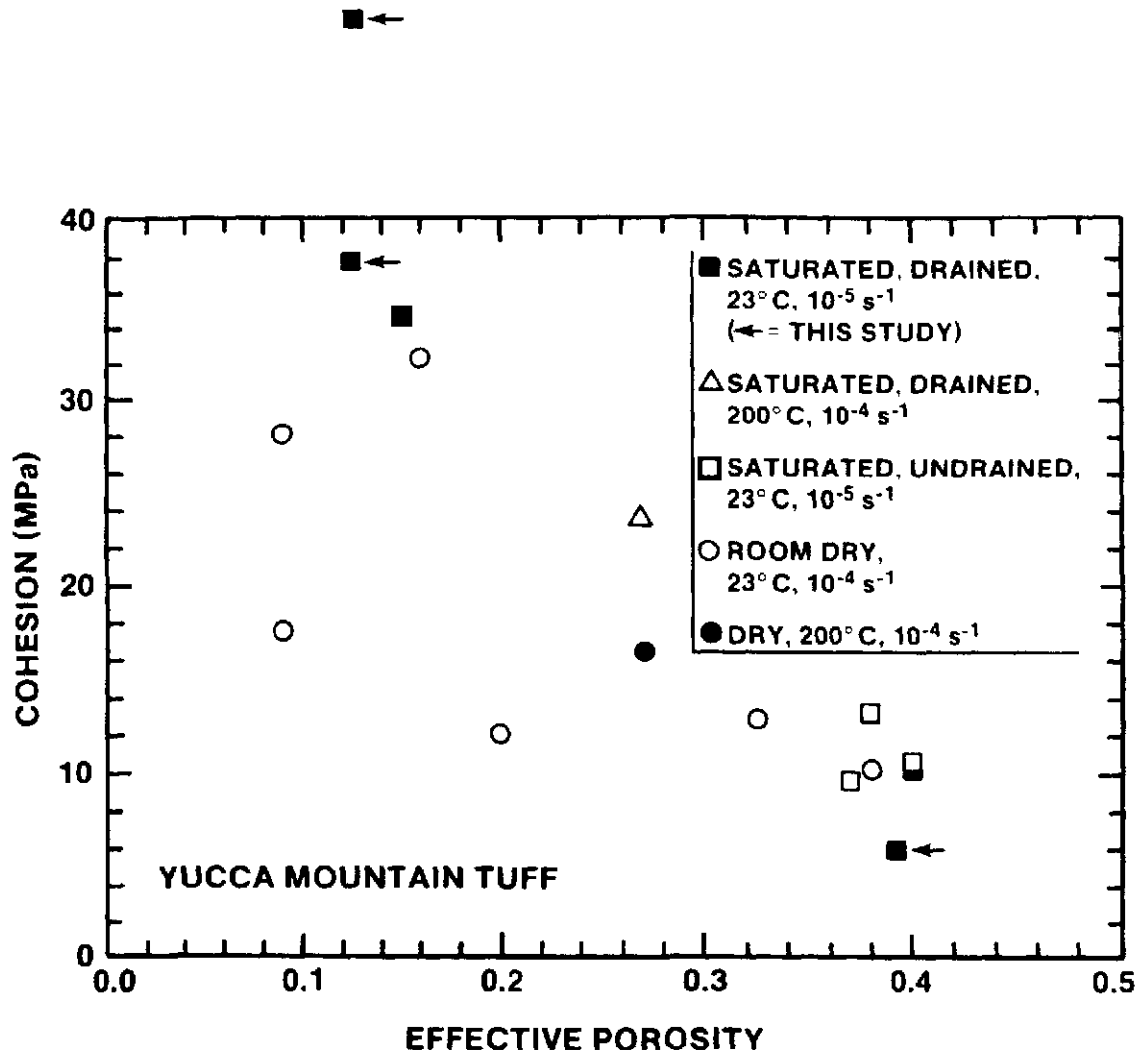
Relationship Between Mohr-Coulomb Parameters and Porosity

Empirical relationships have been established between functional porosity (n), defined as void volume plus clay volume, and several mechanical properties of tuff (Price, 1983; Price and Bauer, 1985). These properties include uniaxial compressive strength, Young's modulus, and tensile strength. The empirical relationships thus defined have been used to calculate the mechanical properties for thermal/mechanical units for which only porosity information is available (cf., Chapter 2 of the SCP).

Unfortunately, there are two mechanical properties which have not been related quantitatively to functional porosity - the Mohr-Coulomb parameters (cohesion (C_0) and angle of internal friction (ϕ)). These two parameters are often important input data for numerical calculations of the mechanical deformation of intact rock. If empirical relationships of the parameters with functional porosity could be defined with a reasonable level of confidence, they could be quite useful in adding to the existing data base of mechanical properties.

Price (1983) compiled the data on cohesion and angle of internal friction which were available at that time. His Figures 16 and 17 support his statement that "...the general inverse relationship between each of the Coulomb parameters and effective porosity is quite evident." (p. 11) ("effective porosity" has since been renamed "functional porosity" to avoid connotations deriving from the field of hydrology). These two figures in Price (1983) are reproduced here as Figures 1 and 2, with additional points for tests on samples of the Topopah Spring Member from USW G-4 added. The numerical data are summarized in Table 1.

A number of approaches can be taken to obtain a relationship between functional porosity and the two Mohr-Coulomb parameters. The two sets of data points in Figures 1 and 2 could be used to calculate linear relationships by least-squares fits. However, given that the cohesion



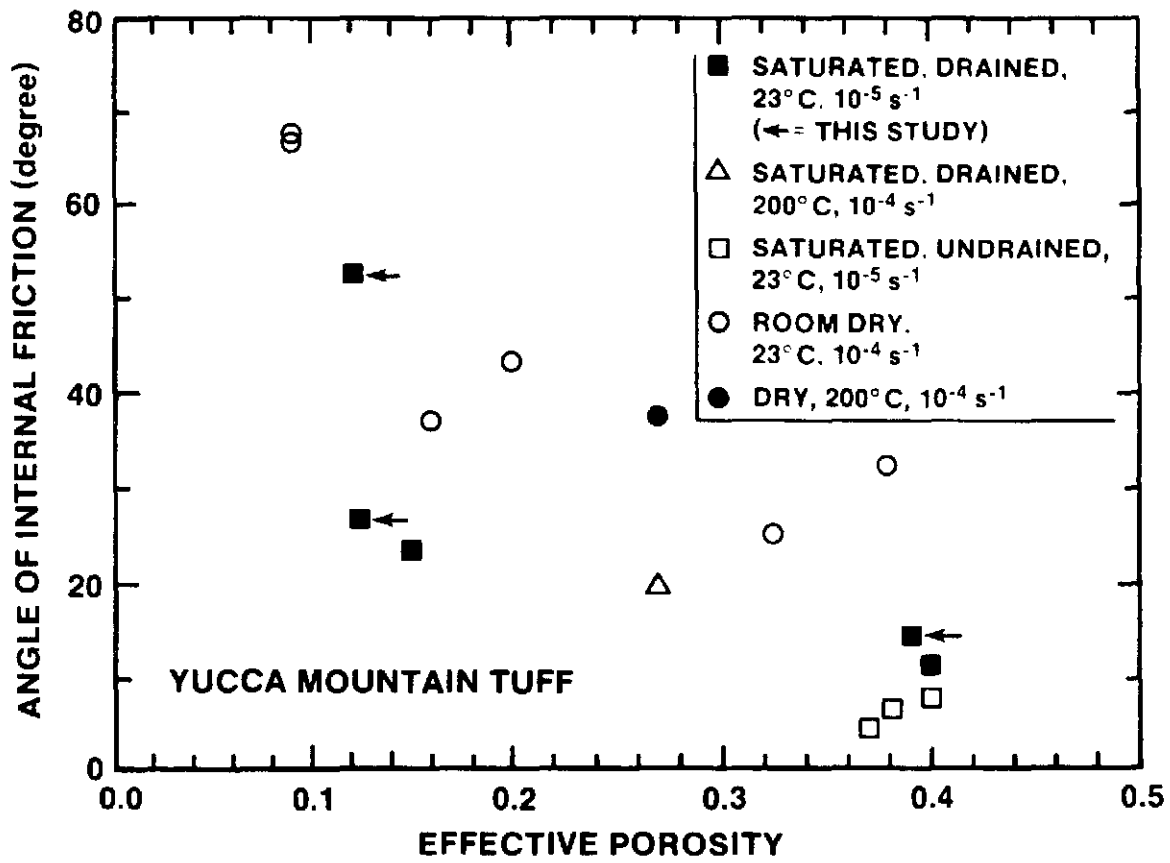


Table 1

Mohr-Coulomb Parameters for Yucca Mountain Tuffs

<u>Confining Pressures (MPa)</u>	<u>Temperature (°C)</u>	<u>Strain Rate (s⁻¹)</u>	<u>Saturation*</u>	<u>Cohesion (MPa)</u>	<u>Angle of Internal Friction (°)</u>	<u>Ref.</u>
0,10,20	23	10 ⁻⁴	R,N	28.1	68	a
0,10,20	23	10 ⁻⁴	R,N	17.5	67	a
0,5,10	23	10 ⁻⁵	S,Y	34.5	23.5	a
0,10,20	23	10 ⁻⁵	S,Y	10.2	11.1	a
0,10,20	23	10 ⁻⁵	S,N	10.6	7.81	a
0,20	23	10 ⁻⁴	R,N	12.9	25	a
0,10	23	10 ⁻⁵	R,N	10.2	32.2	a
0,10,20	23	10 ⁻⁵	S,N	13.2	6.81	a
0,10	23	10 ⁻⁵	S,N	9.67	4.78	a
0,20	23	10 ⁻⁴	R,N	32.2	37	a
0,20	23	10 ⁻⁴	R,N	12.1	43	a
5,12.5,20.7	200	10 ⁻⁴	S,Y	23.6	19.6	a
5,10,20.7	200	10 ⁻⁴	D,Y	16.5	37.4	a
0,5,10	23	10 ⁻⁵	S,Y	37.6	51.4	b
0,10	23	10 ⁻⁵	S,Y	47.5	27.1	b
0,5,10	23	10 ⁻⁵	S,Y	5.9	15.8	b

* S - saturated; R - room-dry; D - oven-dried; Y - drained; N - undrained.

Ref. a: Price (1983) compilation from earlier references.

Ref. b: This study, based on data in Nimick et al. (in preparation).

and angle of internal friction each are a function of the differential stress $\Delta\sigma = (\sigma_1 - \sigma_3)$, and that $\Delta\sigma$ itself may be a function

of environmental parameters, such as strain rate ($\dot{\epsilon}$), temperature (T), confining pressure (σ_3), saturation state, or sample size, grouping all of the experimental data regardless of test conditions is not recommended.

Another option is to obtain an empirical relationship for results obtained under common test conditions; specifically, for the baseline conditions used to obtain relationships for unconfined compressive

strength and Young's modulus: $\dot{\epsilon} = 10^{-5} \text{ s}^{-1}$, $T = 23-25^\circ\text{C}$, $\sigma_3 = 0 \text{ MPa}$, saturated and drained, with 1" x 2" right circular cylinders. Five data points each in Figures 1 and 2 are the results of tests under such conditions. Linear least-squares fits to these two sets of five points give the following:

$$\phi = 50.53 - 108.38n \quad r = 0.83 \quad (1)$$

and

$$C_0 = 57.03 - 118.15n \quad r = 0.96. \quad (2)$$

These equations appear reasonable, if the correlation coefficients are a good indicator. However, another set of correlation coefficients must be considered. In the derivation of individual values of C_0 and ϕ , a linear least-squares fit must be made for $\Delta\sigma$ and σ_3 data. Of the five sets of data for baseline conditions mentioned above, the $\Delta\sigma$ and σ_3 fits resulted in only one correlation coefficient greater than 0.6. Thus, the calculation of equations (1) and (2) is not justified because the C_0 and ϕ values are not dependable.

The method of obtaining C_0 and ϕ from $\Delta\sigma$ and σ_3 data is straightforward, as presented by Olsson and Jones (1980). If the $\Delta\sigma$ and σ_3 relationship is

$$\Delta\sigma = \sigma_0 + m \sigma_3, \quad (3)$$

where σ_0 is the unconfined compressive strength and m is a constant, then

$$\phi = \sin^{-1} \left(\frac{m}{2 + m} \right) \quad (4)$$

and

$$C_0 = \sigma_0 \left(\frac{\tan \phi}{m} \right). \quad (5)$$

Unfortunately, the derivation does not account for variability between samples. Specifically, even side-by-side samples will show some differences in functional porosity. Given that an increase in functional porosity decreases $\Delta\sigma$ (Price and Bauer, 1985), poor correlations between $\Delta\sigma$ and σ_3 may be the result of variations in n .

Therefore, the approach taken here is to take the individual test results for baseline testing conditions and group them by σ_3 . Then the data have been used to calculate a relationship of the form

$$\Delta\sigma = a n^b, \quad (6)$$

as used by Price and Bauer (1985) for $\sigma_3 = 0$ MPa. This procedure was used for $\sigma_3 = 0$ MPa and $\sigma_3 = 10$ MPa for the data sets of interest to this study. (All data used in this study and by Price and Bauer (1985) were obtained at ambient temperature, at a strain rate of 10^{-5}s^{-1} , and on saturated samples). The results are summarized in Table 2, along with the results from Price and Bauer (1985). Because the number of samples analyzed by Price and Bauer (1985) is much larger than the one for this study for $\sigma_3 = 0$ MPa (this one is a subset of the larger one), the Price and Bauer results are considered to be more representative.

Comparison of the values for a and b for the two different values of σ_3 suggests that a is a function of σ_3 , whereas b is not. Assuming an expanded form of equation (6) as

$$\Delta\sigma = (a_1 + a_2\sigma_3)n^b, \quad (7)$$

it is clear that the following parameters can be equated:

$$\sigma_0 = a_1 n^b \quad (8)$$

and

$$m = a_2 n^b \quad (9)$$

Averaging the values of b for $\sigma_3 = 0$ MPa (Price and Bauer, 1985) and $\sigma_3 = 10$ MPa (this study) from Table 2, and calculating a linear relationship between the corresponding values of a and σ_3 to obtain a_1 and a_2 , the following equation is obtained:

$$\Delta\sigma = (4.04 + 0.079 \sigma_3)n^{-1.856} \quad (10)$$

Table 2

Results of Correlations (of the Form $\Delta\sigma = a n^b$)
Between Stress Difference and
Functional Porosity

<u>Confining Pressure</u> <u>(MPa)</u>	<u>a (MPa)</u>	<u>b</u>	<u>r</u>	<u>Samples</u>	<u>Ref.</u>
0	4.921	-1.763	0.95	15	This study
0	4.04	-1.85	0.93	113	Price and Bauer (1985)
10	4.828	-1.862	0.95	9	This study

From this, using equations (4), (5), (8), and (9), expressions are obtained for cohesion and the angle of internal friction as a function of n :

$$\phi = \sin^{-1} \left(\frac{0.079n^{-1.856}}{2 + 0.079n^{-1.856}} \right) \quad (11)$$

and

$$C_0 = 51.139 \tan \phi. \quad (12)$$

Equations (11) and (12) are considered to be a better representation of the relationship between the Mohr-Coulomb parameters and functional porosity than are the linear relationships mentioned earlier in the memo. The two equations are presented in graphical form in Figures 3 and 4 with the range of functional porosity for which equations (11) and (12) apply indicated by a solid line.

The fact that equations (11) and (12) have been derived based on data from only two values of σ_3 precludes the determination as to whether correlation has been improved for the Mohr-Coulomb parameters. Ideally, data at another value of σ_3 should be obtained to examine this question.

In theory, the procedure used here to combine the effects of σ_3 and n could be extended to include the other environmental parameters as well. Unfortunately, insufficient data are available to perform such analyses. Examining the form of Equation (7) for another set of data for which $\dot{\epsilon} = 10^{-4} \text{ s}^{-1}$, $T = 23\text{-}25^\circ\text{C}$, and samples were room-dried suggest that a_1 decreases whereas a_2 increases relative to the values for baseline conditions. Whether the changes in the constants result from the higher strain rate or from the lower saturation is unclear. Hopefully, test results from the parametric sensitivity study will contribute to a better understanding of the dependence of C_0 and ϕ on environmental conditions.

References Cited

- Nimick, F. B., R. H. Price, R. G. Van Buskirk, and J. R. Goodell, in preparation, "Uniaxial and Triaxial Compression Test Series on Topopah Spring Tuff from USW G-4, Yucca Mountain, Nevada," SAND84-1101.
- Olsson, W. A., and A. K. Jones, 1980, "Rock Mechanics Properties of Volcanic Tuffs from the Nevada Test Site," SAND80-1453.

T. E. Blejwas

-7-

October 7, 1985

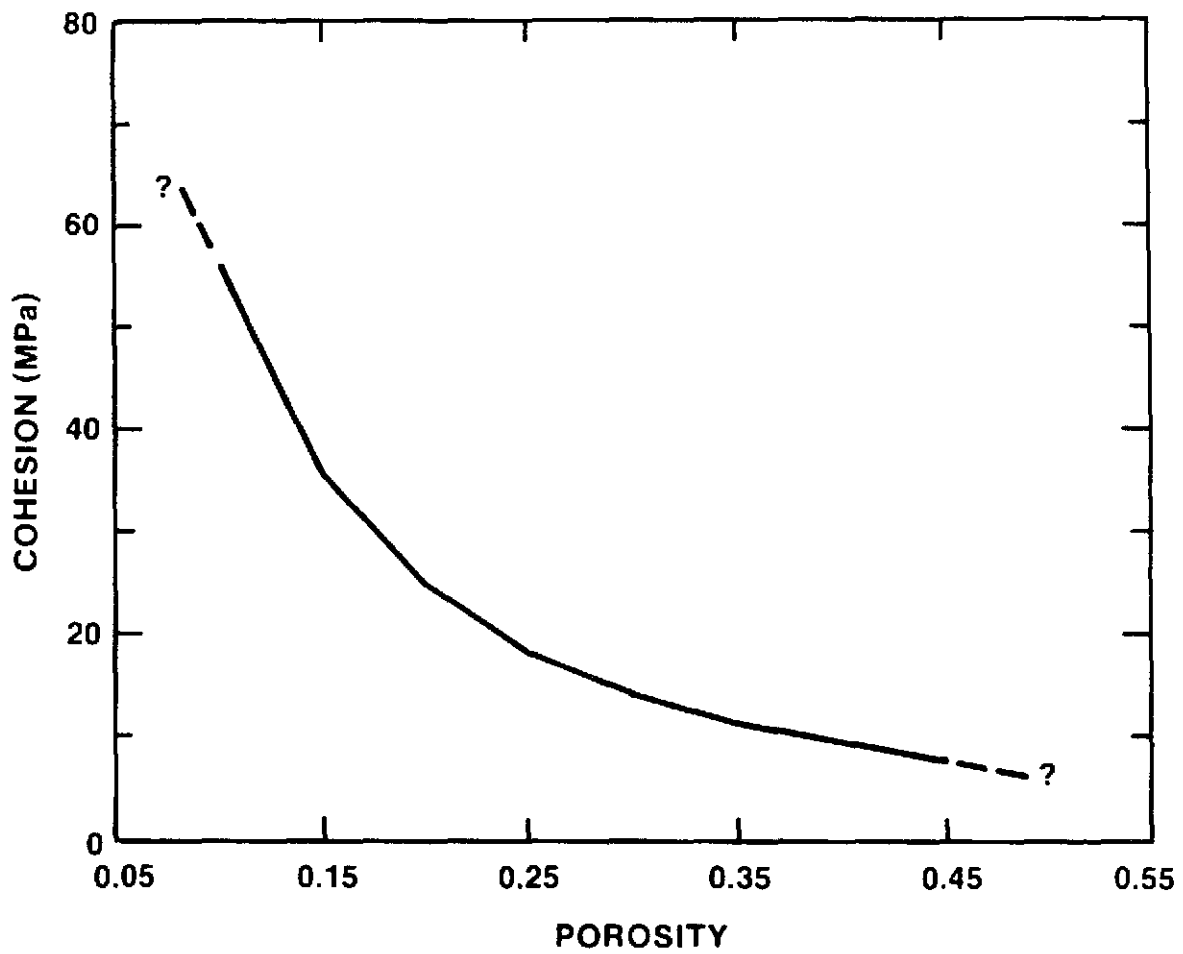
Price, R. H., 1983, "Analysis of Rock Mechanics Properties of Volcanic Tuff Units from Yucca Mountain, Nevada Test Site," SAND82-1315.

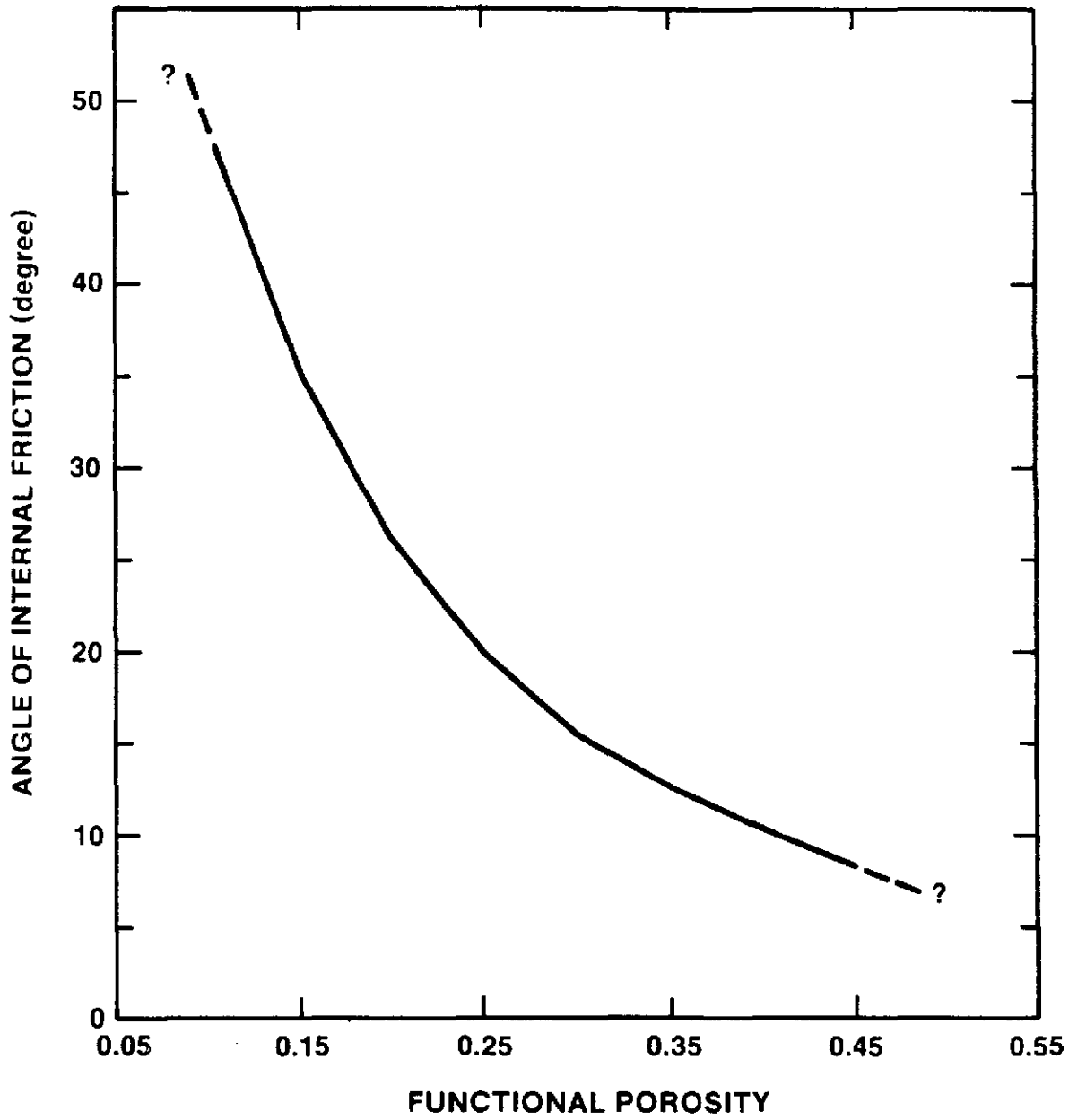
Price, R. H., and S. J. Bauer, 1985, "Analysis of the Elastic and Strength Properties of Yucca Mountain Tuff, Nevada," Proc. 26th U.S. Symposium Rock Mech., pp. 89-96.

FWB:6313:mjh

Copy to:

6310 T. O. Hunter
6310 NNWSI CF
6313 F. B. Nimick
6310 CF WBS 124213





APPENDIX F

Candidate Information for Reference Information Base

<u>Information</u>	<u>Location in Report</u>
Matrix Porosity, TSw1	Table 1, Table 23
Lithophysal Porosity, TSw1	Table 2, Table 23
Grain Density, TSw1	Table 3, Table 23
In Situ Bulk Density, TSw1	Table 4, Table 23
Thermal Expansion, TSw1	Table 5, Table 25
Thermal Expansion, Lithophysae-rich TSw1	p. 54
In Situ Heat Capacity, TSw1	Table 7, Table 24
Emissivity, TSw1 and TSw2	pp. 58, 61
Unconfined Compressive Strength, TSw1	Table 8
Compressive Strength, Lithophysae-rich TSw1	p. 65, Table 26
Porosity-Strength Relationship (Equation 6)	p. 69
Coulomb Parameter-Porosity Relationships (Equations 7, 8)	p. 71
Young's Modulus, TSw1	Table 9
Young's Modulus-Porosity Relationship (Equation 12)	p. 78
Poisson's Ratio, TSw1	p. 79, Table 26
Limiting Stress for Linear Elasticity (General and TSw1)	pp. 80-81,
Axial Strain at Failure, TSw1	p. 81, Table 26
Tensile Strength, TSw1	p. 83, Table 27

InformationLocation in Report

Boundaries of Material Neither TSw2 Nor TSw3	p. 87
Matrix Porosity, TSw2	Table 11, Table 23
Grain Density, TSw2	p. 100, Table 23
Lithophysal Porosity, TSw2	Table 12, Table 23
In Situ Bulk Density, TSw2	Table 13, Table 23
Thermal Expansion, TSw2	Table 14, Table 25
In Situ Heat Capacity, TSw2	Table 15, Table 24
Unconfined Compressive Strength, TSw2	p. 115, Table 26
Strain Rate Effects on Compressive Strength, TSw2	p. 121
Sample Size Effects on Compressive Strength (Equation 15)	p. 123
Young's Modulus, TSw2	p. 125, Table 26
Poisson's Ratio, TSw2	p. 131, Table 26
Axial Strain at Failure, TSw2	p. 132, Table 26
Tensile Strength, TSw2	p. 133, Table 27
Porosity, TSw3	p. 139, Table 23
Grain Density, TSw3	p. 139, Table 23
In Situ Bulk Density, TSw3	p. 139, Table 23
Thermal Expansion, TSw3	Table 18, Table 25
In Situ Heat Capacity, TSw3	Table 19, Table 24
Emissivity, TSw3	p. 144
In Situ Vertical Stress	Figures 35, 36, 37;

APPENDIX G

Candidate Data for Site and Engineering Property Data Base

<u>Data Category</u>	<u>Location in Report</u>
Mechanical Properties of TSw2 as a Function of Confining Pressure ^a	Table 16
Mechanical Properties of TSw2 as a Function of Strain Rate ^a	Table 17
Bulk Properties	Tables B-1, B-4, B-7
Thermal Expansion	Tables B-2, B-5, B-8
Mechanical Properties	Tables B-3, B-6
Miscellaneous:	
Mechanical Properties of Single Sample of TSw3	pp. 144, 149
Thermal Expansion of G4-1295	p. 151
Bulk Properties of non-TSw2, non-TSw3 Material	p. 152 (Table 21)
Mechanical Properties of non-TSw2, non-TSw3 Material ^a	p. 154 (Table 22)
Tensile Strength of non-TSw2, non-TSw3 Material ^a	p. 155

^aAll data in category taken from previously published references.

DISTRIBUTION LIST

B. C. Rusche (RW-1)
Director
Office of Civilian Radioactive
Waste Management
U.S. Department of Energy
Forrestal Building
Washington, DC 20585

Ralph Stein (RW-23)
Office of Civilian Radioactive
Waste Management
U.S. Department of Energy
Forrestal Building
Washington, DC 20585

J. J. Fiore, (RW-221)
Office of Civilian Radioactive
Waste Management
U.S. Department of Energy
Forrestal Building
Washington, DC 20585

M. W. Frei (RW-231)
Office of Civilian Radioactive
Waste Management
U.S. Department of Energy
Forrestal Building
Washington, DC 20585

Waste Management Project Office
U.S. Department of Energy
Post Office Box 98518
Las Vegas, NV 89193-8518

Chief, Repository Projects Branch
Division of Waste Management
U.S. Nuclear Regulatory Commission
Washington, D.C. 20555

NTS Section Leader
Repository Project Branch
Division of Waste Management
U.S. Nuclear Regulatory Commission
Washington, D.C. 20555

B. G. Gale (RW-223)
Office of Civilian Radioactive
Waste Management
U.S. Department of Energy
Forrestal Building
Washington, DC 20585

R. W. Gale (RW-40)
Office of Civilian Radioactive
Waste Management
U.S. Department of Energy
Forrestal Building
Washington, D.C. 20585

J. O. Neff, Manager
Salt Repository Project Office
U.S. Department of Energy
110 North 25 Mile Avenue
Hereford, TX 79045

V. J. Cassella (RW-222)
Office of Civilian Radioactive
Waste Management
U.S. Department of Energy
Forrestal Building
Washington, DC 20585

S. A. Mann, Manager
Crystalline Rock Project Office
U.S. Department of Energy
9800 South Cass Avenue
Argonne, IL 60439

K. Street, Jr.
Lawrence Livermore National
Laboratory
Post Office Box 808
Mail Stop L-209
Livermore, CA 94550

L. D. Ramspott (3)
Technical Project Officer for NNWSI
Lawrence Livermore National
Laboratory
P.O. Box 808
Mail Stop L-204
Livermore, CA 94550

Document Control Center
Division of Waste Management
U.S. Nuclear Regulatory Commission
Washington, D.C. 20555

V. M. Glanzman
U.S. Geological Survey
Post Office Box 25046
913 Federal Center
Denver, CO 80225

P. T. Prestholt
NRC Site Representative
1050 East Flamingo Road
Suite 319
Las Vegas, NV 89109

M. E. Spaeth
Technical Project Officer for NNWSI
Science Applications
International Corporation
Suite 407
101 Convention Center Drive
Las Vegas, NV 89109

SAIC-T&MSS Library (2)
Science Applications
International Corporation
Suite 407
101 Convention Center Drive
Las Vegas, NV 89109

W. S. Twenhofel, Consultant
Science Applications
International Corp.
820 Estes Street
Lakewood, CO 89215

A. E. Gurrola
General Manager
Energy Support Division
Holmes & Narver, Inc.
Mail Stop 580
Post Office Box 93838
Las Vegas, NV 89193-3838

D. T. Oakley (4)
Technical Project Officer for NNWSI
Los Alamos National Laboratory
N-5, Mail Stop J521
P.O. Box 1663
Los Alamos, NM 87545

L. R. Hayes (6)
Technical Project Officer for NNWSI
U.S. Geological Survey
Post Office Box 25046
421 Federal Center
Denver, CO 80225

C. H. Johnson, Technical
Program Manager
Nuclear Waste Project Office
State of Nevada
Evergreen Center, Suite 252
1802 North Carson Street
Carson City, NV 89701

ONWI Library
Battelle Columbus Laboratory
Office of Nuclear Waste Isolation
505 King Avenue
Columbus, OH 43201

W. M. Hewitt, Program Manager
Roy F. Weston, Inc.
955 L'Enfant Plaza, Southwest, Suite 800
Washington, DC 20024

H. D. Cunningham
General Manager
Reynolds Electrical &
Engineering Co., Inc.
Post Office Box 14400
Mail Stop 555
Las Vegas, NV 89114

T. Hay, Executive Assistant
Office of the Governor
State of Nevada
Capitol Complex
Carson City, NV 89710

J. A. Cross, Manager
Las Vegas Branch
Fenix & Scisson, Inc.
Mail Stop 514
Post Office Box 93265
Las Vegas, NV 89193-3265

John Fordham
Desert Research Institute
Water Resources Center
Post Office Box 60220
Reno, NV 89506

Department of Comprehensive
Planning
Clark County
225 Bridger Avenue, 7th Floor
Las Vegas, NV 89155

Lincoln County Commission
Lincoln County
Post Office Box 90
Pioche, NV 89043

Community Planning and
Development
City of North Las Vegas
Post Office Box 4086
North Las Vegas, NV 89030

City Manager
City of Henderson
Henderson, NV 89015

Timothy G. Barbour
Science Applications
International Corporation
1626 Cole Boulevard, Suite 270
Golden, CO 80401

E. P. Binnall
Field Systems Group Leader
Building 50B/4235
Lawrence Berkeley Laboratory
Berkeley, CA 94720

R. R. Loux, Jr., Executive Director (3)
Nuclear Waste Project Office
State of Nevada
Evergreen Center, Suite 252
1802 North Carson Street
Carson City, NV 89701

Dr. Martin Mifflin
Desert Research Institute
Water Resources Center
Suite 1
2505 Chandler Avenue
Las Vegas, NV 89120

Planning Department
Nye County
Post Office Box 153
Tonopah, NV 89049

Economic Development
Department
City of Las Vegas
400 East Stewart Avenue
Las Vegas, NV 89101

Director of Community
Planning
City of Boulder City
Post Office Box 367
Boulder City, NV 89005

Commission of the
European Communities
200 Rue de la Loi
B-1049 Brussels
BELGIUM

Technical Information Center
Roy F. Weston, Inc.
955 L'Enfant Plaza, Southwest, Suite 800
Washington, DC 20024

Gerald Parker (RW-241)
Office of Civilian Radioactive
Waste Management
U.S. Department of Energy
Forrestal Building
Washington, DC 20585

T. H. Isaacs (RW-20)
Office of Civilian Radioactive
Waste Management
U.S. Department of Energy
Forrestal Building
Washington, DC 20585

D. H. Alexander (RW-232)
Office of Civilian Radioactive
Waste Management
U.S. Department of Energy
Forrestal Building
Washington, DC 20585

B. J. King, Librarian (2)
Basalt Waste Isolation Project
Library
Rockwell Hanford Operations
Post Office Box 800
Richland, WA 99352

D. L. Fraser, General Manager
Reynolds Electrical & Engineering
Co., Inc.
Mail Stop 555
Post Office Box 98521
Las Vegas, NV 89193-8521

J. P. Pedalino
Technical Project Officer for NNWSI
Holmes & Narver, Inc.
101 Convention Center Drive,
Suite 860
Las Vegas, NV 89109

Eric Anderson
Mountain West Research-Southwest, Inc.
Phoenix Gateway Center
432 North 44 Street
Suite #400
Phoenix, AZ 85008-6572

Judy Foremaster (5)
City of Caliente
Post Office Box 158
Caliente, NV 89008

J. P. Knight (RW-24)
Office of Civilian Radioactive
Waste Management
U.S. Department of Energy
Forrestal Building
Washington, DC 20585

Allen Jelacic (RW-233)
Office of Civilian Radioactive
Waste Management
U.S. Department of Energy
Forrestal Building
Washington, DC 20585

J. R. Rollo
Deputy Assistant Director
for Engineering Geology
U.S. Geological Survey
106 National Center
12201 Sunrise Valley Drive
Reston, VA 22092

Vincent Gong
Technical Project Officer for NNWSI
Reynolds Electrical & Engineering
Co., Inc.
Mail Stop 615
Post Office Box 98521
Las Vegas, NV 89193-8521

S. D. Murphy
Technical Project Officer for NNWSI
Fenix & Scisson, Inc.
Mail Stop 514
Post Office Box 15408
Las Vegas, NV 89114

S. H. Kale (RW-20)
Office of Civilian Radioactive
Waste Management
U.S. Department of Energy
Forrestal Building
Washington, DC 20585

J. H. Anttonen, Deputy Assistant
Manager for Commercial
Nuclear Waste
Basalt Waste Isolation Project
Office
U.S. Department of Energy
P.O. Box 550
Richland, WA 99352

J. C. Bresee (RW-22)
Office of Civilian Radioactive
Waste Management
U.S. Department of Energy
Forrestal Building
Washington, DC 20585

J. L. Fogg (12)
Technical Information Office
Nevada Operations Office
U.S. Department of Energy
P.O. Box 98518
Las Vegas, NV 89193-8518

R. L. Bullock
Technical Project Officer for NNWSI
Fenix & Scisson, Inc.
Mail Stop 514
P.O. Box 93265
Las Vegas, NV 89193-3265

D. Eppler
Science Applications
International Corp.
101 Convention Center Dr.
Suite 407
Las Vegas, NV 89109

K. Campbell
Los Alamos National Laboratory
P.O. Box 1663
F-600
Los Alamos, NM 87545

B. Bohlke
Parsons Brinckerhoff Quade and Douglas
1625 Van Ness Ave.
San Francisco, NM 94109-3678

6300 R. W. Lynch
6310 T. O. Hunter
6310 NNWSI CF
6311 A. L. Stevens
6311 C. Mora
6311 V. Hinkel (2)
6312 F. W. Bingham
6313 T. E. Blejwas

C. L. West, Acting Director
Office of External Affairs
Nevada Operations Office
U.S. Department of Energy
P.O. Box 98518
Las Vegas, NV 89193-8518

P. K. Fitzsimmons, Director
Health Physics and Environmental
Division
Nevada Operations Office
U.S. Department of Energy
P.O. Box 98518
Las Vegas, NV 89193-8518

Prof. S. W. Dickson
Department of Geological Sciences
Mackay School of Mines
University of Nevada, Reno
Reno, NV 89557

E. Hardin
Science Applications
International Corp.
101 Convention Center Dr.
Suite 407
Las Vegas, NV 89109

D. Montan
Lawrence Livermore National
Laboratory
P.O. Box 808
MS L200
Livermore, CA 94550

D. Dawson
Science Applications
International Corp.
101 Convention Center Dr.
Suite 407
Las Vegas, NV 89109

6313 R. Finley
6313 B. Luke
6313 F. B. Nimick (5)
6313 R. H. Price
6313 B. M. Schwartz (5)
6313 L. E. Shephard
6313 R. M. Zimmerman
6314 J. R. Tillerson
6314 S. J. Bauer
6314 L. S. Costin
6314 B. L. Ehgartner
6314 J. A. Fernandez
6314 A. J. Mansure
6315 S. Sinnock
6315 C. A. Rautman
6316 R. B. Pope
6332 WMT Library (20)
6430 N. R. Ortiz
3141 S. A. Landenberger (5)
3151 W. L. Garner (3)
8024 P. W. Dean
3154-3 C. H. Dalin (28)
for DOE/OSTI
6313 B. M. Schwartz (2)
(for following DRMS files)

Physical Properties Data

51/L03.A-12/1/78
51/L03.A-6/24/80
51/L03.A-1/13/81
51/L03.A-5/21/81
51/L01A.A-7/16/81
51/L03.A-10/7/81
51/L03.A-4/28/82
51/L03.A-5/27/82
51/L03.A-5/28/82
51/L03.A-6/21/82
51/L03.C-11/1/82
51/L03.A-2/1/83
51/L03.A-7/11/83
51/L02A1.A-7/29/83
51/L03.A-9/17/84
51/L03.A-10/15/84
51/L03.A-1/18/85

Mechanical Compressive Data

51/L02A1.A-3/1/80
51/L02A1.A-6/24/80
51/L02A1.A-3/1/82
51/L02A1.A-9/7/82
51/L02A1.A-2/11/83
51/L02A1.A-6/1/83
51/L02A1.A-10/12/83
51/L02A1.A-3/30/84

Thermal Expansion Data

51/L01B1.A-6/24/80
51/L01B1.A-10/7/81
51/L01B1.A-9/7/82
51/L01B1.A-1/23/85
51/L01B2.A-5/1/80

Thermal Conductivity Data

51/L01A.A-6/24/80
51/L01A.A-7/16/81
51/L01A.A-10/7/81
51/L01A.A-9/7/82
51/L01A.A-12/2/82
51/L01A.A-1/23/85